A STUDY ON MECHANICAL, DURABILITY AND MICROSTRUCTURAL PROPERTIES OF GRAPHENE OXIDE REINFORCED CONCRETE COMPOSITE

Submitted in partial fulfilment of the requirements of the degree of

DOCTOR OF PHILOSOPHY

in

CIVIL ENGINEERING

by

V R K REDDY POTAMSETTI

Roll No: 719007

Supervisor

Dr. D RAVI PRASAD

ENGINEERING STRUCTURES

DEPARTMENT OF CIVIL ENGINEERING

NATIONAL INSTITUTE OF TECHNOLOGY WARANGAL

WARANGAL-506 004, TS, INDIA

JULY 2023

NATIONAL INSTITUTE OF TECHNOLOGY

WARANGAL

Certificate

This is to certify that the thesis entitled "**A STUDY ON MECHANICAL, DURABILITY AND MICROSTRUCTURAL PROPERTIES OF GRAPHENE OXIDE REINFORCED CONCRETE COMPOSITE"** being submitted by **V R K REDDY POTAMSETTI** for the award of the degree of **DOCTOR OF PHILOSOPY** to the faculty of engineering and technology of **NATIONAL INSTITUTE OF TECHNOLOGY, WARANGAL** is a record of bonafide research work carried out by him under my supervision and it has not been submitted elsewhere for award of any degree.

Dr. D RAVI PRASAD
Thesis Supervisor
Associate Professor
Department of Civil Engineering
National Institute of Technology
Warangal (T.S.) – INDIA

Approval sheet

This Dissertation Work entitled "**A STUDY ON MECHANICAL, DURABILITY AND MICROSTRUCTURAL PROPERTIES OF GRAPHENE OXIDE REINFORCED CONCRETE COMPOSITE"** by **V R K REDDY POTAMSETTI** is approved for the degree of Doctor of Philosophy

Examiners

_____

_____

_____

Supervisor (s)

_____

_____

_____

Chairman (Program Coordinator)

_____

Date: _____ Place: _____

Declaration

This is to certify that the work presented in the thesis entitled "**A STUDY ON MECHANICAL, DURABILITY AND MICROSTRUCTURAL PROPERTIES OF GRAPHENE OXIDE REINFORCED CONCRETE COMPOSITE"** is a bonafide work done by me under the supervision of **Dr. D RAVI PRASAD** and was not submitted elsewhere for the award of any degree.

I declare that this written submission represents my ideas in my own words and where others' ideas or words have been included, I have adequately cited and referenced the original sources. I also declare that I have adhered to all principles of academic honesty and integrity and have not misrepresented or fabricated or falsified any idea / data / fact / source in my submission. I understand that any violation of the above will be a cause for disciplinary action by the Institute and can also evoke penal action from the sources which have thus not been properly cited or from whom proper permission has not been taken when needed.

_____

V R K REDDY POTAMSETTI
Roll No.: 719007

Date: _____

Dedicated to

my beloved

father

Acknowledgements

With great pleasure and proud privilege, I manifest my heartier thankfulness to my research supervisor, **Dr. D. Ravi Prasad**, Associate Professor, Department of Civil Engineering, for his invaluable suggestions, sagacious guidance, scholarly advice, and comprehensive critical remarks in bringing out this research work with artistry.

I am perspicuous to divulge my sincere gratefulness to **Prof. T. D. Gunneswara Rao**, Professor & Head, Department of Civil Engineering and Chairman, Doctoral Scrutiny Committee for his enlightening guidance and immense help rendered in bringing out this work.

I am grateful to **Prof. D. Rama seshu**, Professor in Department of Civil Engineering, **Prof. K. Venkata Reddy**, Professor in Department of Civil Engineering and **Prof. R. Narasimha Rao**, Professor in Department of Mechanical Engineering, members of Doctoral Scrutiny Committee, for their guidance and help during the investigation.

I am also thankful to Prof. C. B. Kameshwar Rao, Prof. G. Rajesh Kumar, Prof. P. Rathish Kumar, Sri. M. Sudhakar, Dr. S. Venkateswara Rao, Dr. T. P. Tezeswi, Dr. M. V. N. Sivakumar, Dr. K. Gopikrishna, Dr. S. Anitha Priyadharshani, Dr. B. Kavitha, and Dr. B. Umesh the faculty members of Engineering Structures Division, Department of Civil Engineering, NITW for the moral support given during the period of research work.

I will be failing in my duty if I do not ventilate my gratefulness to my Parents, better half Bhagya Rekha and little princes Sadhana & Sanvika who strived for my excellence.

Finally, I thank everyone, who contributed either directly or indirectly in successful completion of this work.

V R K REDDY POTAMSETTI

ABSTRACT

Concrete is widely used construction material in all over the world. Advancements in nanotechnology have now paved the way for novel strategies for improving the performance of cement composites. Several investigations have been carried out in recent years to produce cement composites using identified nanomaterials, such as nano-titanium oxide, nano-iron, nano-alumina, nano-silica, carbon nanotubes, and recently graphene oxide (GO) was also widely employed. These nanomaterials as reinforcements in the cement matrix are much more beneficial than conventional reinforcements such as steel rebars and different types of fibres, because these nano reinforcement materials arrest the cracks at nanoscale in cement composite prior to their propagation.

The aim of the present study is to develop the GO reinforced concrete composite, with the aim to investigate the influence of GO on the static and dynamic mechanical characteristics, durability properties of concrete, the mechanism of development of crystals and to find the hydration crystals that are beneficial for the formation of distinct microstructures in the concrete composites related to the performance. The present study also focussed on the sustainable development of concrete by introducing GO and fly ash, and to investigate the combined effect of nanomaterial and supplementary cementitious materials on the performance and microstructural characterization. To achieve the aim of the present study, the experimental investigation is planned and carried out in three different phases.

In the first phase of experimental program, the static mechanical, dynamic mechanical, durability properties and microstructural characteristics of GO reinforced cement concrete were evaluated. Two different grades of concrete mixes such as standard concrete (SC) and high strength concrete (HSC). In this study, GO content varied from 0% to 0.2% with an increment of 0.05% by weight of cement was considered. This phase is divided into two main parts. The first part focused on the evaluation of static

mechanical and dynamic mechanical properties. The microstructural characterization was carried out using SEM, EDX, XRD, FTIR and TGDTA. The second part consists of assessment of durability performance of GO reinforced cement concrete. From the experimental results the mechanical and durability properties of cement concrete is significantly improved with the addition of the GO compared to the control concrete. The optimum influence of the GO addition was identified at a dosage of 0.15%. The detailed mechanism for the related improvements was developed with the results of microstructural characterisation.

Second phase of experimental program, the combined effect of GO and fly ash on the static mechanical, dynamic mechanical, durability properties and microstructural characteristics concrete was investigated. In this phase, the optimum dosage of GO attained from Phase-I experimental results and further replacement of cement with fly ash at 10%, 20%, and 30% by weight of cement was considered. This phase is also carried out in two different parts. The first part focused on the evaluation of static mechanical, dynamic mechanical and microstructural characteristics. The second part consists of evaluation of durability performance. The performance of GO reinforced fly ash concrete is compared with control concrete. From the experimental results the mechanical and durability properties of concrete is significantly improved with the addition of the GO and replacement of cement with fly ash compared to the control concrete. The detailed mechanism was identified for the improved performance with the results of microstructural characterisation.

Third phase of the investigation consists the validation of experimental findings with results obtained through finite element modelling (FEM). Commercially available finite element software was used to model 100x200mm cylinders in order to obtain the stress-strain curves analytically. Thereafter, a flexure specimen of 500x100x100mm was modelled and analysed using inputs from the 100x200mm cylindrical model. Experimental results of GO-cement concrete and GO-fly ash concrete are in good agreement with the values obtained by the finite element modelling of cylinders and prismatic beams. The percentage variation observed between experimental and analytical results is less than 15%.

Table of Contents

List of Table

List of Figures

CHAPTER 1
INTRODUCTION

1.1. General

Concrete is widely used construction material in all over the world, and continues to play a significant role in the construction of civil infrastructure. As an engineered construction material, concrete is extensively employed owing to its high compressive strength, ease of moulding, and low maintenance cost compared to other materials. However, when it comes to designing structural members subjected to complex loadings, the quasi-brittle character of concrete is a major drawback. Brittleness of concrete is due to its low tensile strength, low flexural strength, poor resistance to crack development, and low strain capacities. To overcome these drawbacks, concrete is typically reinforced with different materials (Mehta and Monteiro 2014). Because of the heavy calcium components in Portland cement, concrete is prone to acid attack. The components of cement paste degrade, with calcium hydroxide being the most noticeable when exposed to acids. Acid attacks on concrete has typically received considerable attention, even when cement composites are extensively attacked by acids, causing calcium hydroxide to dissolve and the hydrated silicate and aluminium phases to disintegrate, consequently the concrete to lose its strength and degrade promptly (Ariffin et al. 2013). Many attempts have been made to enhance the performance of concrete composite by modifying the properties of the concrete composites with different admixtures, supplementary cementitious materials and fibres. Ordinary Portland cement (OPC) is the primary binding material of the concrete ingredients which holds together the constituents to attain a solid mass. The production of OPC generates enormous amounts of carbon dioxide (CO_2) in to the atmosphere, contributing 6-7% global CO_2 emission. Cement consumption is predicted to nearly double by the year 2050, reaching 6 billion tonnes per year (Davalos 2012). The

environmental problems associated with emission of greenhouse gases along with depletion of natural resources, plays a major concern regarding the sustainability. Therefore, significant contributions to sustainable development must be made using SCMs and nanomaterials such as nano-titanium oxide, nano-iron, nano-alumina, nano-silica, carbon nanotubes, and graphene oxide to modify the properties of cement and concrete composites at micro and nano level.

1.2. Nanotechnology in cement composites

Several noteworthy attempts have been made to improve the performance of cement composites with the addition of supplementary cementitious materials, mineral admixtures, natural fibers and synthetic fibers. Advancements in nanotechnology have now paved the way for novel strategies for improving the performance of cement composites. Investigations have been carried out in recent years to produce cement composites using identified nanomaterials, such as nano-titanium oxide (Kawashima et al. 2013), nano-iron, nano-alumina, nano-silica (Oltulu and Şahin 2013), carbon nanotubes (CNTs) (Abu Al-Rub et al. 2012), and recently graphene oxide (GO) was also widely employed (Gong et al. 2015). According to Scrivener and Kirkpatrick (2008), these nanomaterials as a reinforcements in the cement matrix are much more beneficial than conventional reinforcements such as steel rebars and fibres, because these nanomaterials arrest the cracks at nanoscale in cement composite prior to their development into microscale. The biggest challenge for the researchers is attaining inherent strength characteristics through the dispersion of these nanoparticles into the cement matrix.

1.3. Graphene oxide (GO)

The Graphene nano material is most generally defined as an allotrope of carbon in the form of mono layer of atoms in 2-dimensional hexagonal lattice with one atom forming each vertex. Graphene, like CNTs, is composed of sp^2-bonded carbon atoms (Porwal, Grasso, and Reece 2013), which is responsible for outstanding mechanical characteristics.

The Young's modulus and characteristic strength of graphene around 1 TPa and 60 to 130 GPa, respectively (Chuah et al. 2014). Furthermore, the aspect ratio and the surface area of a single graphene sheet can exceed 2000 and 2600 m^2/g, respectively, both are significantly greater than that of CNTs (Chuah et al. 2014). Nevertheless, difficulty in dispersion of graphene and the expensive cost of manufacture prevents their potential applications. Graphene oxide (GO) is a derivative of graphene which comprises a single-layer of sp2-hybridized carbon atoms functionalized with the combination of hydroxyl, carboxyl, and epoxy groups (Shamsaei et al. 2018). The oxygenated functionalities, which are connected to the edges and basal planes of GO sheets, considerably modify their van der Waals bonds among the GO sheets, thus improving the dispersion in aqueous solution (Li et al. 2008). In cement matrix, GO sheets were reported to have been dispersed uniformly (Collins, Lambert, and Duan 2012). Aspect ratio, surface area, and tensile strength are other characteristics of GO that are also highly significant (Chuah et al. 2014). Furthermore, GO may be effectively produced from natural graphite flakes (a low-cost resource) through intense oxidation followed by exfoliation. GO is a promising nanomaterial for increasing the strength characteristics of cement composites because to its superior mechanical characteristics, high dispersibility in water, and low cost of production. In terms of GO surface functionality, the oxygenated functionalities may further facilitate the use of these carbon nanostructures in cement composites, since it develops covalent connections with hydrated phases. For instance, it is reported that carboxyl acid functions can develop a strong covalent connection with calcium silicate hydrate (C-S-H), significantly improving the mechanical characteristics of cement composites (Li, Wang, and Zhao 2005).

1.4. GO reinforced cement composites

Several investigation are carried out to verify the suitability of GO nanomaterial as a reinforcement for improving the mechanical characteristics of cement composites. GO employed in various methods to catalyse cement matrix using various methods such as w/c ratios and admixtures, and the significant influence of GO on mechanical characteristics was observed with small amount by weight percentage of cement (Gong

et al. 2015). Flexural and compressive strengths of cement composites with the addition of GO have been shown to improve with enhanced hydration rate and development of a dense microstructure owing to nucleation effect of GO at nanoscale into the cement matrix and better pore structure (Wang et al. 2015). However, scaling out the physical interaction of cement hydration phases with GO using microstructural characterization methods is challenging and need to be studied further. The enhanced rate of hydration, decrease in pore size, higher nucleation, and cracks bridging with GO as a reinforcement at nanoscale level have all been connected to better mechanical characteristics of cement composites (Gong et al. 2015; Pan et al. 2015; Wang et al. 2015). However, relatively limited research has focussed on the analysis of microstructure development and formation of crystals in the interfacial transition zone of the concrete matrix as governed by GO.

1.5. Motivation of research work

The aim of the present study is to develop the GO reinforced concrete composite, with the main motivation being to investigate the influence of GO on the static and dynamic mechanical characteristics, durability properties of concrete, the mechanism of development of crystals and to find the hydration crystals that are beneficial for the formation of distinct microstructures in the concrete composites related to the performance of composite. The present study also focussed on the sustainable development of concrete by introducing GO and fly ash, and to investigate the combined effect of nanomaterial and supplementary cementitious materials on the performance and microstructural characterization. These concrete composites have been evaluated systematically utilising modern characterisation techniques. The significant improvements in mechanical characteristics and durability performance caused by the formation of microstructure in these concrete composites has been observed. The likely mechanism of development of distinctive microstructure and formation of crystals has been investigated from the test results and data characterisation.

1.6. Organization of the thesis

The present thesis organized in the following way

Chapter 1 starts with a brief introduction about concrete, nanotechnology in concrete and its advantages, graphene oxide (GO) and GO reinforced cement composites. Problem statement as well as the aim of research work has also been discussed.

Chapter 2 consists of a critical review of the state of art. An overview of literature survey on performance assessment of concrete, microstructural characteristics of concrete, and GO reinforced cement composites have been presented.

Chapter 3 represents the scope and objectives of the research work. Research significance and methodology also presented.

Chapter 4 provides detailed information on the experimental program including material used and their properties, concrete mix proportions and preparation of specimens. Testing methods are also discussed.

Chapter 5 presents the detailed discussion on the effect of GO on static mechanical, dynamic mechanical, durability, and microstructural characteristics of concrete.

Chapter 6 consists the detailed discussion on hybrid effect of GO and fly ash on static mechanical, dynamic mechanical, durability, and microstructural characteristics of concrete.

Chapter 7 includes the validation of results obtained experimentally with the values through finite element modelling.

Chapter 8 represents the overall conclusions from the present investigation. The scope for further research and references are also included.

1.7. Outline of the thesis

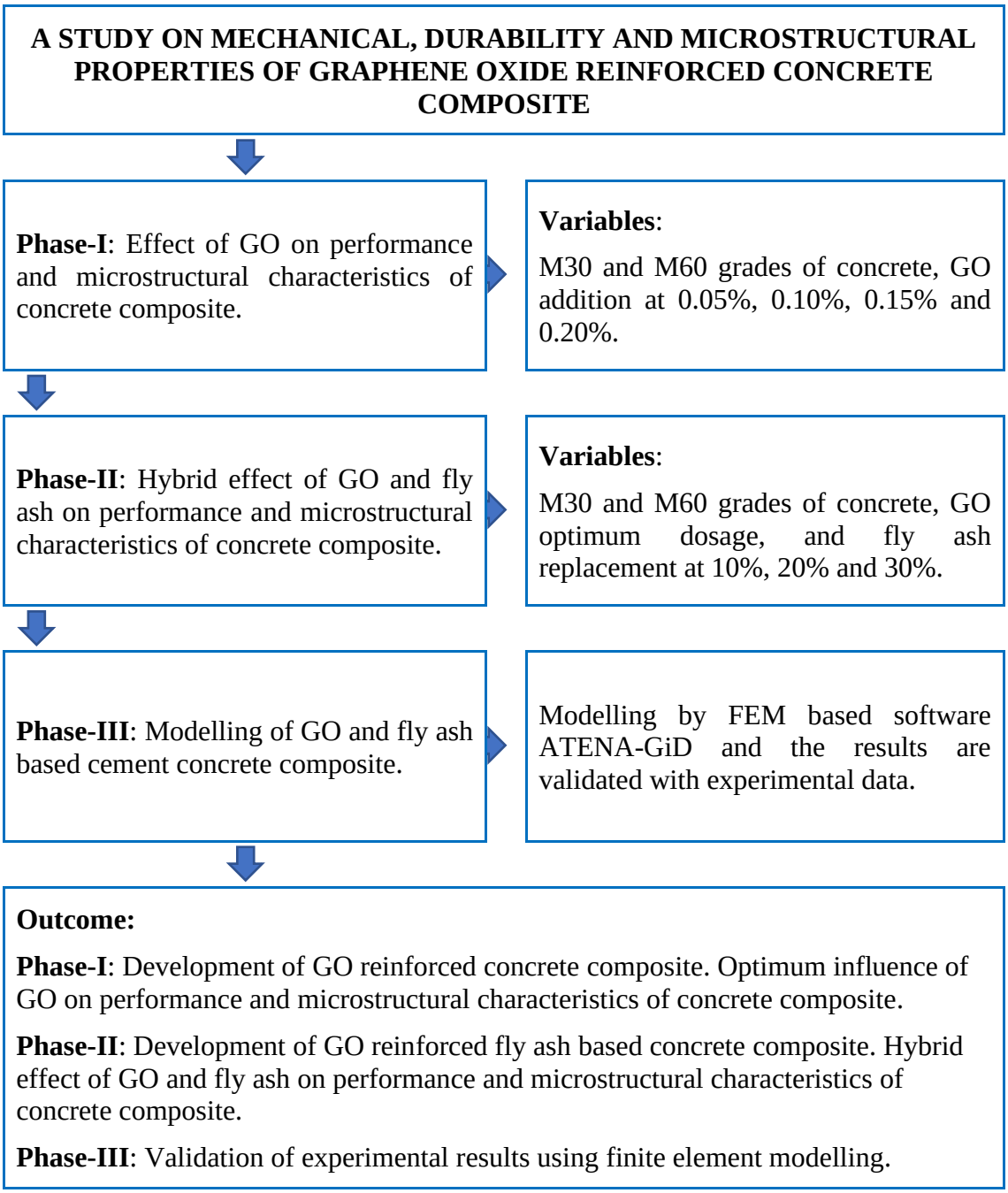

CHAPTER 2
LITERATURE REVIEW

2.1. Introduction

Concrete is the most commonly material used in civil engineering projects around the globe. It is extensively used because of its desirable characteristics, such as high compressive strength, low cost, hardening at room temperature, ability to cast in to desired shape, good bonding with steel reinforcement, resistance to high-temperature, and low maintenance requirements. Among other advantages, its compressive strength is an important factor in its acceptance as a construction material. Besides the advantages of the concrete as a construction material, the major drawbacks of the concrete are poor resistance to crack development, low tensile and flexural strengths, and low strain capacities. The key ingredient of concrete is cement which acts as a binding material and inherently transmits brittleness to the concrete through the formation of crystals and development of hydration phases in the microstructure at the interfacial transition zone (ITZ).

Many efforts have recently been made to improve the performance of cement composites with the inclusion of supplementary cementitious materials, admixtures, natural fibres and synthetic fibres. Many studies have been conducted to verify the suitability of nanomaterials such as nanosilica (nano-SiO_2), nanoiron oxide (nano-Fe_2O_3), nanotitanium dioxide (nano-TiO_2), nanoaluminum oxide (nano-Al_2O_3), carbon nanotubes (CNTs), and graphene derivatives such as reduced graphene oxide (RGO) and graphene oxide (GO) to improve the performance of cement composites. These novel nanomaterials can be classified based on their geometric dimensions and shape. As shown in Figure 2.1, silica nanoparticles are zero-dimensional (0D), CNTs and carbon nanofibers (CNFs) have one dimension (1D), and sheet like GO and GNPs have two

dimensions (2D). 1D fibres and 2D sheets, unlike 0D nanoparticles, act as reinforcing materials to bridge the cracks. Large aspect ratios and inherent strength of 1D fibres and 2D sheets are therefore significant for improving the performance of composite at nano scale.

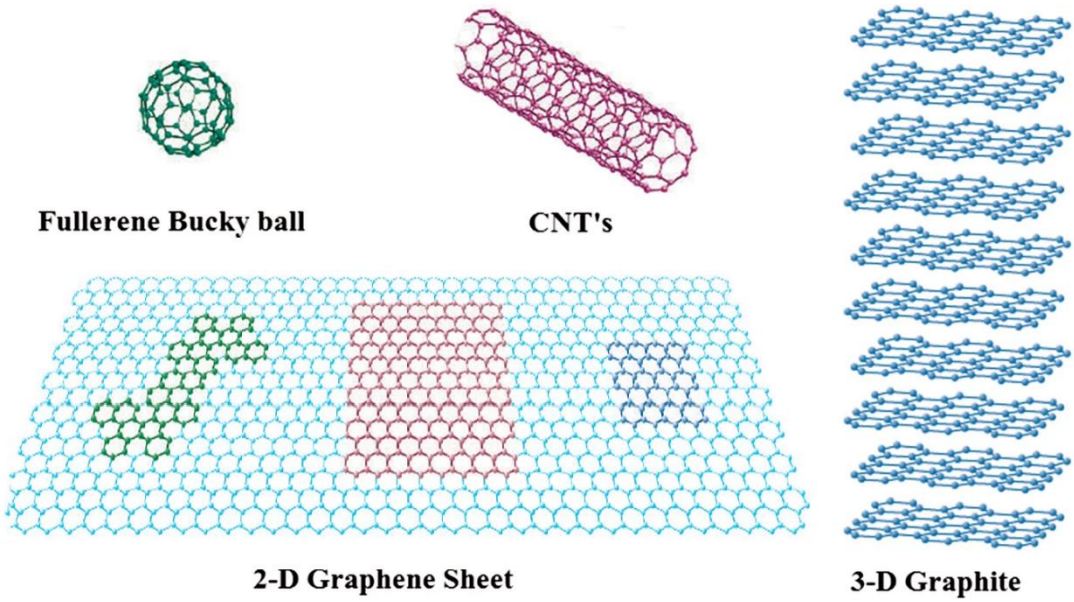

Figure 2.1 Structure of carbon-based nanomaterials (Shamsaei et al. 2018)

The comparison between proportions of different nanomaterials and the common ingredients present in cement and concrete are shown in Figure 2.2. Cement particles have been considered the principal ingredient for binding aggregates in concrete. The development of high-performance concrete in various application necessitates the use of mineral additives such as fly ash, blast furnace slag, metakaolin, and silica fume. With the advancement nanotechnology, Nanomaterials have been introduced into cement composites with an aim to reinforce the cement composites at nanoscale level, which is expected to improve the performance because of their size which is similar to that of calcium silicate hydrate (C-S-H).

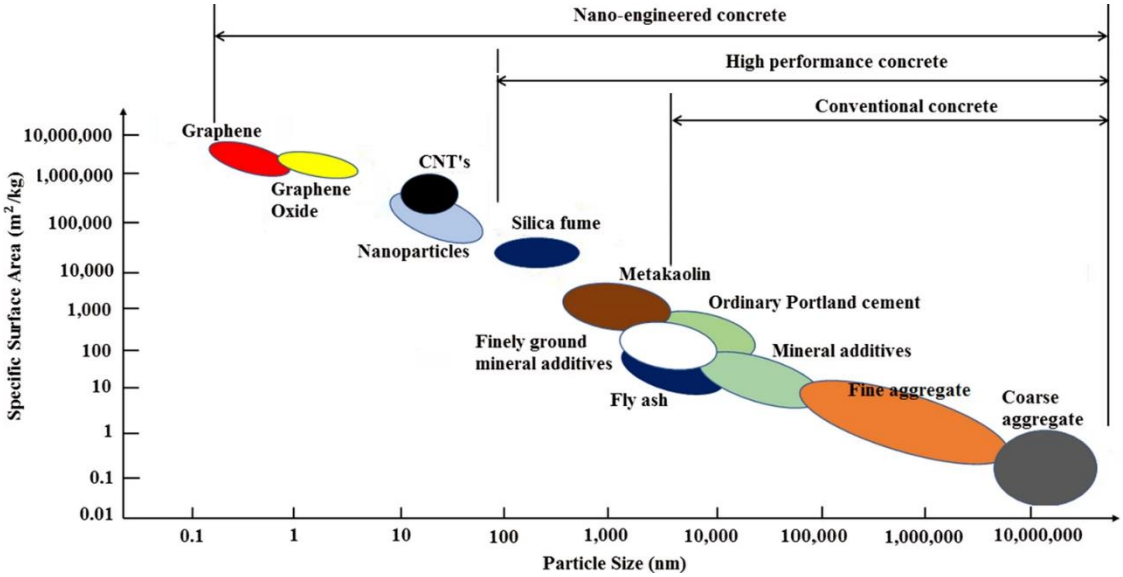

Figure 2.2 Comparison of the proportions of nanomaterials with common ingredients present in the concrete (Chuah et al. 2014)

2.2. Micro and Nano fillers based Cementitious Composites

Many reinforcing materials have been using extensively in the development of reinforced concrete for the last few decades (Brandt 2008). Table 2.1 summarizes the material characteristics of common fillers, they have a higher tensile strength and elastic modulus compared to OPC. Thus, the introduction of reinforcing material improves the tensile and flexural strengths of cement composite.

In recent times, microfibers such as carbon, polymeric, glass, and steel were widely employed to reinforce cement concrete composite. They have aspect ratios ranging between 10 and 1000, and their material characteristics are also shown in Table 2.1. Recent times, carbon fibres are widely employed in the construction field for reinforcing cement composites because of its high elastic modulus of about 200MPa and tensile strength of 3.5GPa (Zhao and Zhang 2007). Steel fibres have comparable mechanical characteristics, with the added benefit of reducing cracks generated by rebar corrosion and alkali silica reaction expansion (Grubb et al. 2007). Glass fibres can also increase the tensile and flexural strengths of cement composite due to their elastic modulus of 72.4GPa

and tensile strength of 3.45MPa (Marikunte, Aldea, and Shah 1997). To resist highly alkaline media of OPC, high zirconia glass and surface treatment can be given to achieve the high degree of performance improvement (Proctor, Oakley, and Litherland 1982). Mechanical anchoring allows even polypropylene fibres with inferior mechanical characteristics to reinforce the brittle cementitious matrix (Bentur, Peled, and Yankelevsky 1997).

An excellent inherent fibre strength and high aspect ratio are required to act as a reinforcement. Fibers improve the strength of cement matrix by supporting a portion of applied load and more importantly, by allowing the matrix to bridge the cracks (Qian and Stroeven 2000). Microfibers and its bridging mechanism improve the toughness, ductility and tensile strength of cement composite. Microfibers such as PP fibers, glass and carbon fibers can arrest plastic shrinkage cracks. However, the addition of these fibres has little effect on compressive strength (Hamoush, Abu-Lebdeh, and Cummins 2010), decrease the workability by entrapping air voids. Although polymer and carbon fibres can produce covalent connections with the cement matrix, their low surface area hinder interface strength (Wichmann, Schulte, and Wagner 2008). In this aspect, nanoparticles outperform typical microfibres since they modify the properties and act as a reinforcement at the nano level.

In recent times, powdered nanoparticles such as nanosilica (nano-SiO_2), nanoiron (nano-Fe_2O_3), and nanoalumina (nano-Al_2O_3) have been successfully used in cement composites (Oltulu and Şahin 2013). Meanwhile, nanoclays, calcium carbonate nanoparticles (nano-$CaCO_3$), and nano-titanium oxide (nano-TiO_2) are also being introduced into cement composites (Kawashima et al. 2013). The particle size of these nanomaterials varies between 10 and 70 nm, allowing for reactive and filling properties. Nanoparticles such as nanosilica have pozzolanic properties, which allow them to develop C-S-H by consuming non-strength contributing CH crystals (calcium hydroxide). Consequently, the size and orientation of CH crystals are reduced, resulting in a better interface structure (Qing et al. 2007). The physical filler effect becomes more pronounced by increasing nanoparticle dosage. For example, increasing the nanosilica content

between 3% and 6% continues to optimize the pore structure, even while CH consumption remains stable (Said et al. 2012).

CNTs, which belong to the family of nanocarbons, are one-dimensional carbon allotropes that have a cylinder-shaped nanostructure. This structure can be conceptualized as having been rolled out of a single sheet of planar graphene, as illustrated in Figure 2.1. The elastic modulus of pure graphene and carbon nanotubes approaches 1 TPa, and the tensile strength ranges from 10 to 60 GPa. Additional characteristics of nanocarbons, such as elastic properties (Walters et al. 1999), excellent thermal properties (See and Harris 2007), and electrical conductivity (Kaneto et al. 1999), provide multifunctional and efficient characteristics. High aspect ratio (1000) facilitates physical reinforcement, while the high surface area offered by the nano-size carbon allotropes in the range of 100–2600 m^2/g makes them extremely reactive. These essential properties have several applications in electronics (Yang et al. 2011), nanofiltration (Qiu et al. 2011), biologically acceptable devices (Labroo and Cui 2013; Patil et al. 2009), and nanocomposites such as polymers (Kim, Abdala, and Macosko 2010), ceramics (Tapasztó et al. 2011), and cement matrices (Nasibulin et al. 2013). The huge surface area of these nanocarbons promotes reactivity and improves the mechanical characteristics of cement composite, thus making them suitable to reinforce cementitious composites.

2.3. Graphene

Graphene is the fundamental structural unit of all graphitic materials. It is comprised of a sheet of carbon atoms arranged in a single layer that is densely packed into a honeycomb structure which is two-dimensional (2D) and has a thickness of 0.335 nanometers (Novoselov et al. 2004). Although, relatively established research on other carbon-based nanomaterials, particularly CNTs, has facilitated rapid advancement on graphene-based cement composites (Geim and Novoselov 2007), the application of graphene in concrete has certain inherent benefits over them. Graphene is 2-dimensional, is easier to synthesis in high volumes with fully reproducible characteristics, is more easily disperse in a solution, has a larger specific surface area (SSA), is less hazardous to the environment

and health (Porwal et al. 2013), and making it more attractive for various applications in cement composites.

Table 2.1 Characteristics of microfibers and nanomaterials (Chuah et al. 2014)

Material	Shape	Tensile strength (GPa)	Elastic modulus (GPa)	Density (Kg/m^3)	Diameter / thickness (nm)	Surface area (m^2/g)	Aspect ratio
Graphene	2D	~130	1000	2200	~ 0.08	2600	6000-600,000
GO	2D	~0.13	23-42	1800	~0.67	700-1500	1500-45,000
CNTs	1D	11-63	950	1330	15-40	70-400	1000-10,000
Nano-silica	0D	-	-	2400	6-15	170-200	-
Carbon fibre	3D	0.4-5	7-400	1770	6000-20,000	0.134	100-1000
PP fibre	3D	0.3-0.9	3-5	900	18,000 - 30,000	0.225	160-1000
Glass fibre	3D	3.45	72	2540	5000-10,000	0.3	600-1500
Steel fibre	3D	1.50	200	7800	50,000-900,000	0.02	45-80

2.3.1. Graphene and their derivatives

Graphene available in a variety of forms depending on its production and extraction from raw graphite. Several scientific researchers structured graphene theoretically and were able to develop graphene with 50 to 100 layers after few decades of research. However, in 2004, researchers were successful in achieving a single layer of graphene from pure

graphite using scotch tape and were awarded the Nobel Prize in 2010 (Novoselov et al. 2004). Since development of graphene in the field of nanotechnology, various kinds of graphene are commercially available and may be synthesized in laboratories. The structural representation of graphene and their derivatives is shown in Figure 2.3.

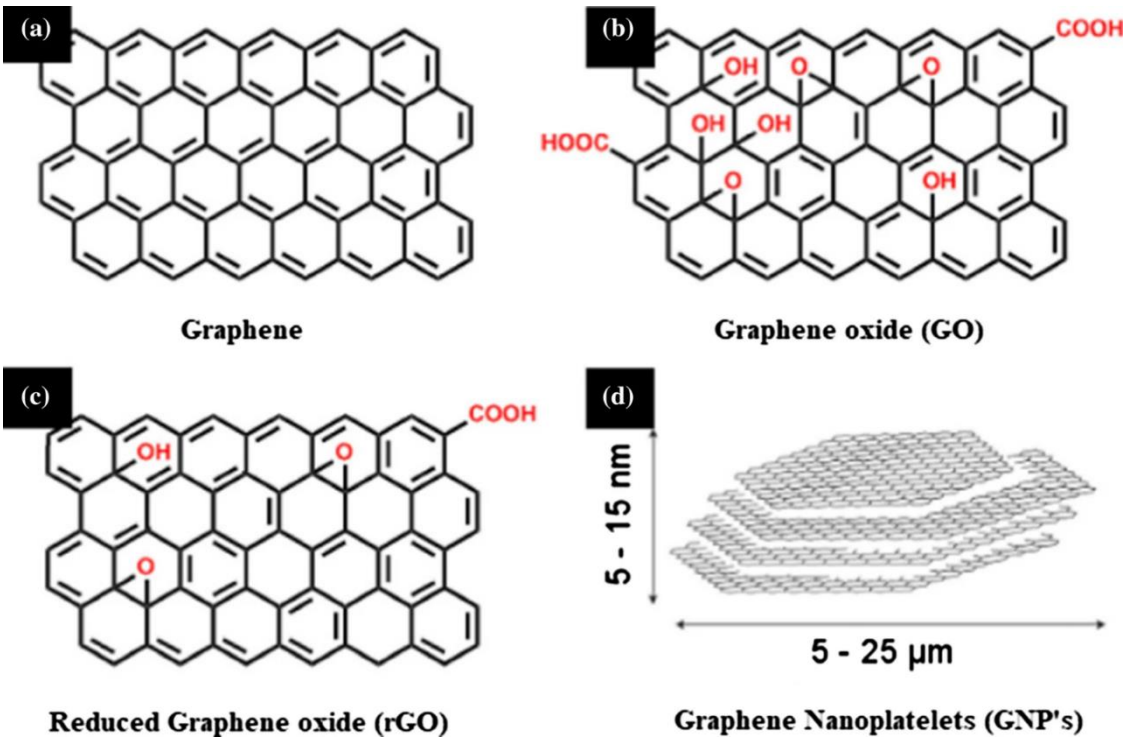

Figure 2.3 Representation of (a) graphene, (b) graphene oxide (GO), (c) reduced graphene oxide (rGO) and (d) graphene nanoplatelets (GNPs) (Shamsaei et al. 2018)

2.3.1.1. Graphene oxide (GO)

Graphene oxide, the well-known derivative of graphene, is quickly gaining attention as a promising nanomaterial to use in wide variety of electronic devices due to its unique combination of characteristics including excellent thermal and electrical conductivity. For the synthesis of GO, pure graphite is chemically oxidized, exfoliated, and dispersed in a specific solvent or water. It is composed of single layer sheets connected by a hexagonal carbon network. The basic difference between GO and graphene is that GO comprises carboxyl, carbonyl, hydroxyl, and epoxide functional groups on its surface, which results

in superior dispersion in the cement matrix and better reactivity with cement, making it more suitable to develop cement composites (Shamsaei et al. 2018).

2.3.1.2. Reduced graphene oxide (rGO)

Reduced graphene oxide (rGO) is synthesized by chemically reducing graphene oxide (GO). Upon reduction, few oxygenated functionalities remain bonded to the surface of the graphene layers, indicating that they are not the pure graphene layers. Harsh chemicals or inadequate heat treatments may cause structural damage (Shamsaei et al. 2018).

2.3.1.3. Graphene nanoplatelets (GNPs)

Graphene nanoplatelets have a structure similar to CNTs after being exfoliated, but they have the added benefit of being more susceptible to chemical modification along their edges. GNPs are typically less than 5 nm thick with a lateral dimension from 1µm to 100µm in, depending on the synthesis technique. While the utilization of exfoliated GNPs and the effect they have on the formation of microstructure in cement are still in the early stages of research, but they are frequently used in new thermal conductivity and electrical applications (Alkhateb et al. 2013).

2.3.2. Synthesis of Graphene oxide

Researchers have recognized the presence of graphene layers since the 1960s; however, in 2004, a single layer graphene was successfully extracted in a reproducible method (Novoselov et al. 2004). This finding is greatly responsible for the improved significance of this nanomaterial (Choi et al. 2010; Soldano, Mahmood, and Dujardin 2010). The initial process involved manually exfoliating highly oriented pyrolytic graphite to create a few layers of graphene. Although, graphene developed by this method has irregular forms and irregular orientation (Choi et al. 2010), it is extremely reliable for the synthesis of single-layer sheets (Choi et al. 2010; Novoselov et al. 2004; Soldano et al. 2010).

With the growing importance of graphene and its remarkable characteristics, tremendous advancement has been made from the initial method for producing graphene (Lin and Liu 2016). In general, there are two major methodologies for graphene synthesis: top-down and bottom-up. However, both the methods are employed to produce graphene sheets, the materials produced by these two fabrication methods have different properties and hence intended for various purposes. Bottom-up techniques include graphene growth with a high degree of control over layers and imperfections. This method is more expensive and is best suited for advanced industrial applications such as solar cells, anti-corrosion coatings, and electronics. In contrast, top-down techniques are more appropriate for large-scale and low-cost production when defect-free graphene is usually not essential, such as in applications of cementitious materials.

Top-down synthesis involves extracting graphene layers from graphite powder. This method depends on the stacked graphite layers are connected together with weak van der Walls bonds (Choi et al. 2010; Soldano et al. 2010; Wang et al. 2009; Zhang et al. 2010). These bonds can be separated by applying energy in one of three different forms: mechanical, chemical, or electrochemical. This will result in the production of a few layers of graphene. However, because of its low productivity and high cost, the extraction of pure graphene by a bottom-up approach is not suited for use on a large scale (Li et al. 2008). Therefore, the top-down approach that uses graphite oxide as a raw material for synthesizing GO at large-scale is most preferred so far (Lowe and Zhong 2016). GO is easier to separate than graphene, and the existence of hydrophilic functionalities makes it possible to produce nanosheets in alkaline solutions without the need of any surfactants (Li et al. 2008; Lowe and Zhong 2016).

For the synthesis of GO, initially graphite is oxidized using Hummers method in a solution containing concentrated potassium permanganate ($KMnO_4$), sodium nitrate ($NaNO_3$), and sulfuric acid (H_2SO_4) (Lowe and Zhong 2016; Soldano et al. 2010). The graphite layers are oxidized after H_2SO_4 has intercalated between them, which results in a larger volume between the layers. After that, graphite oxide is separated into individual GO sheets through ultrasonication (Li et al. 2008; Soldano et al. 2010). This is followed by a purification procedure that removes any leftover ions from the GO structure,

including K^+, H^+, Mn^{2+}, and SO_4^{2-}. Finally, GO can be converted into rGO using a variety of processes, including plasma procedures (Alotaibi et al. 2018; Lee et al. 2012), hydrazine vapours or solutions (NH_2-NH_2) (Li et al. 2008; Tung et al. 2009; Zhang et al. 2010), alkaline conditions (Soldano et al. 2010), photocatalysis (Gengler et al. 2013), and annealing (Saleem, Haneef, and Abbasi 2018). The addition of sulfonic groups can preserve rGO dispersibility in solution (Si and Samulski 2008). Figure 2.4 shows the Hummers method for producing GO.

The hummers method is well-established, and just a few changes were recently suggested. For example, instead of adding $NaNO_3$, H_3PO_4 mixed with H_2SO_4 resulted in increased oxidation efficiency (Marcano et al. 2010). Despite the fact that the GO was oxidized more intensely, the rGO produced by this approach has the same electrical conductivity as rGO produced by other approaches. This method also avoids the requirement of filter the wastewater from Na^+ and NO^{-3}, as well as the discharge of harmful gases (Emiru and Ayele 2017; Lowe and Zhong 2016). The $NaNO_3$-free Hummer's technique was enhanced by partially substituting $KMnO_4$ with K_2FeO_4, which is an environment friendly and powerful oxidant (Peng et al. 2015; Wei et al. 2016). By combining graphite and $KMnO_4$ before adding H_2SO_4, during intercalation the risks associated with exothermic reactions were minimized (Sun and Fugetsu 2013). As top-down GO manufacturing technology advances, more reproducible nanosheets with low-cost and higher quality became available in the market.

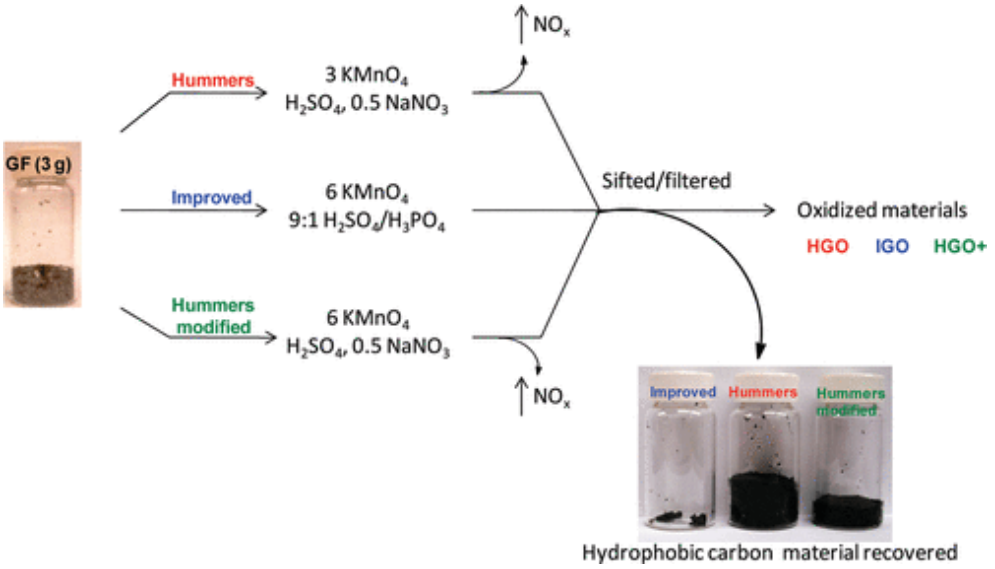

Figure 2.4 Hummer's method for producing GO (Marcano et al. 2010)

2.3.3. Characterization of Graphene oxide

Graphene is extensively investigated due to its distinctive aspect ratio, geometrical shape, lattice structure, surface morphology, and ability to attach functional groups. Although, the material properties of graphene must be established in order to fully employ its potential in a given application. The unique material characteristics of GO are determined using a variety of characterization methods.

2.3.3.1. Dimensional and Dispersion Characterization using SEM

The SEM characterisation method may be employed for a highly broad variety of examinations, including the measurement of surface dimensions, the study of surface shape, and the dispersion of nanomaterials. As can be seen in Figure 2.5, Kang et al. (2019) showed the morphology of GO and discovered that it has a wrinkled structure with many folds as a result of the oxidation of graphite.

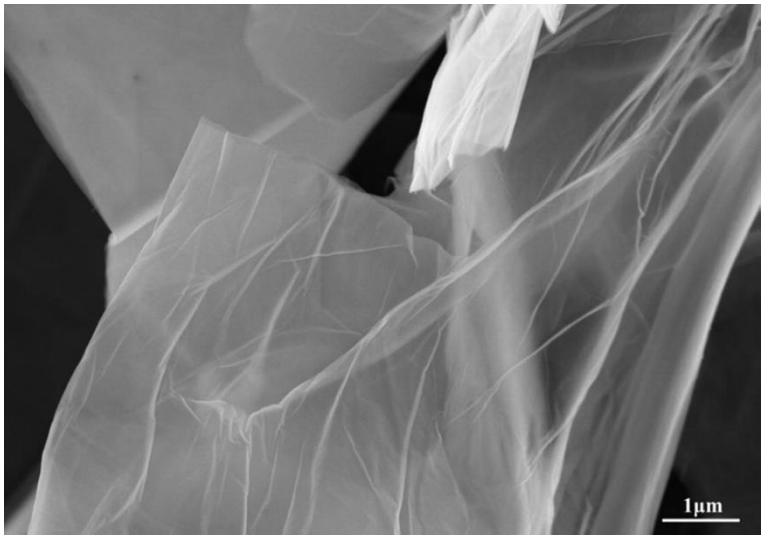

Figure 2.5 SEM image of GO (Kang et al. 2019)

2.3.3.2. Crystallographic Characterization using XRD

X-ray diffraction (XRD) is a method that is frequently applied in the study of crystal structure, crystallite size, and quantitative phase identification in the investigation of materials. The XRD patterns for GO and natural graphite are shown in Figure 2.6. In comparison to the GO peak, the pattern indicates the graphite crystal orientation with a strong and high peak intensity at an angle of $2\theta=26.5°$ with a interlayer distance of 0.337nm according to Bragg's equation (Peng et al. 2019). In the case of GO, a broadened and shifted diffraction peak was detected at $2\theta=10°$ with an interplanar distance of 0.850 nm, suggesting that during graphite oxidation the oxygenated functionalities become captured in the layer of carbon atoms. The structural morphology of graphene is changed as a result of the graphite oxidation, which causes oxygen atoms to engage with the carbon atoms through the process of covalent bonding.

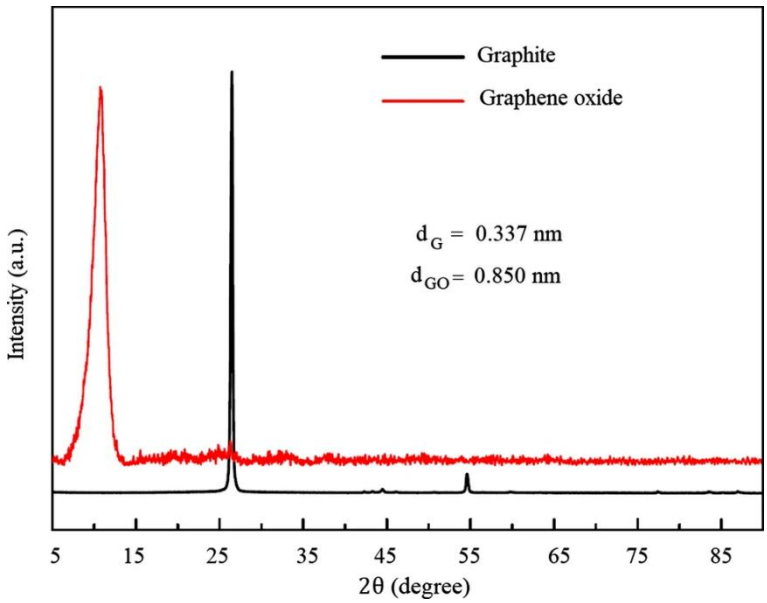

Figure 2.6 XRD patterns of graphite and graphene oxide (Peng et al. 2019)

2.3.3.3. Chemical Structure Characterization using FTIR

FTIR spectroscopy is widely employed to identify the type of bond or functional group that contains oxygen by determining the precise position of peaks. The graphite and GO FTIR spectroscopic patterns are shown in Figure 2.7. The bending and stretching vibrations of functionalities are identified using FTIR spectra, which indicate peaks at various wavenumbers. FTIR spectroscopy was performed Peng et al. (2019) on GO and graphite, identified that the -OH of water molecules have stretching vibration spectra at wavenumbers of 3396 (cm^{-1}) and 1621 (cm^{-1}), whereas -OH of hydroxyl has bending vibration peaks at wavenumbers of 1400 (cm^{-1}) and stretching vibration spectra at wavenumbers of 3140 (cm^{-1}). During GO production, the presence of the bonds at various wavenumbers demonstrates that the graphite is oxidized to its maximum level.

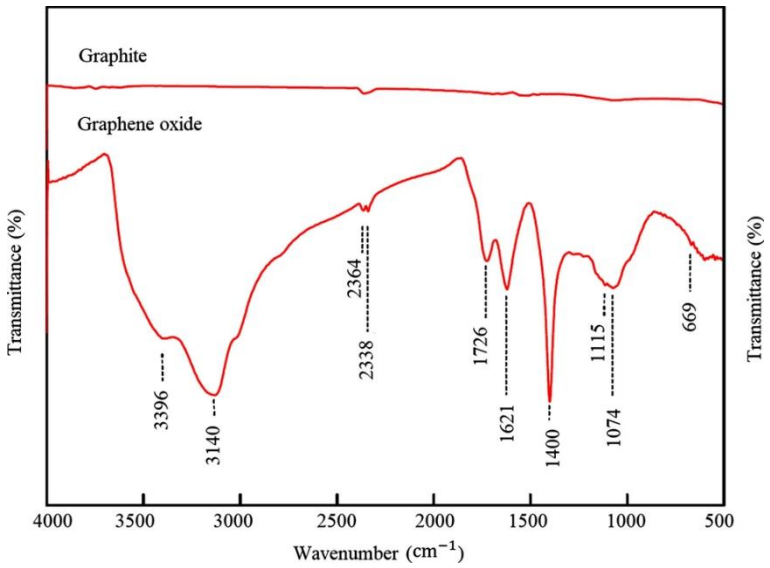

Figure 2.7 FTIR spectrum of graphite and GO (Peng et al. 2019)

2.3.4. Dispersion of Graphene oxide

Nanomaterials were recognized to modify the strength and durability properties of cementitious composite when they are well distributed. The huge specific surface area of the nanomaterials causes the Van der Waals forces to bind the nanomaterial around each other, causing them to behave as agglomerates. The formation of agglomerates results in the formation of defect sites (Li et al. 2004), which might take the shape of voids or unreacted "pockets". Rupture will occur as a result of the accumulated stress in this area. It is absolutely necessary to have all of the following methods, or some combination of them, in order to achieve a dispersion that is appropriate.

2.3.4.1. Mechanical Dispersion

There are different kinds of mechanical processes, such as ultrasonication, shear mixing, ball milling, extrusion, stirring, and calendaring, that can be used to achieve uniform dispersion (Ma et al. 2010). To achieve a homogeneous dispersion in water, ultrasonication has been commonly employed among the abovementioned mechanical processes. The ultrasonic probe transfers excitation energy, which, along with the strong local shear, causes the clusters to be broken apart (Strano et al. 2003). The CNT bundles

can be disentangled using ultrasonication; however, this results in a reduction in the aspect ratio.

2.3.4.2. Physical Surface Modification

The surface energy of CNTs is decreased by surfactants, facilitating the dispersion of nanomaterials in water. Many previous investigations have concentrated on surfactant-assisted CNT dispersion in organic and aqueous solutions, along with polymer matrices (Wang 2009). In response to growing concern regarding the possible incompatibility of surfactants with the hydration of cement, since surfactants might either delay or prevent hydration, retain a significant amount of air in the paste, or perform interactions with admixtures (Collins et al. 2012). Polyacrylic acid has been proposed to function as dispersing agent for carbon nanotubes and a plasticizing agent for cement paste (Cwirzen et al. 2009). Collins et al. (2012) investigated CNTs dispersion and the consistency of fresh CNT-cement mixes using different chemical admixtures that with an exception of polycarboxylate are incompatible with CNTs. Abu Al-Rub et al. (2012) and Tyson et al.(2011) demonstrated that high-range polycarboxylate-based water-reducing additive reduces cement mix viscosity.

2.3.4.3. Chemical Surface Modification

Chemical functionalization is a method of adding oxygen functionalities through covalent bonding to the surfaces of CNTs. The tendency of CNTs to form agglomerates is reduced, while the hydrophilic behavior of the CNTs is improved through the use of covalent surface modification. CNTs must be oxidized with acid before interacting with hydroxyl groups (-OH) or carboxylic acid (-COOH). Li et al. (2005) discovered that by combining nitric and sulfuric acids in 1:3 volume ratio, the functional group of carboxylic acid may be linked to the CNT surface. The treated CNTs were uniformly distributed with no evidence of agglomeration (Li, Wang, and Zhao 2007). However, the aggressive chemical functionalization's unavoidable side effect is the development of defects at the surface of CNT, which subsequently reduces the inherent strength (Hilding et al. 2003).

Researchers were proposed a combination of chemical treatment and ultrasonication as the best method for dispersing CNTs due to the significance of the challenge. On the other hand, GO does not require any kind of surfactants for the dispersion. GO has the morphology of a functionalized graphene and is synthesized by the oxidation of graphite through the modified process developed by Hummer (Li et al. 2008). Thus, compared to the hydrophilicity of GO, electrostatic repulsion from the functional groups allows GO to be distributed without the application of surfactants (Geng, Wang, and Kim 2009). It is difficult to distribute GO in alkaline cement pore solution (Stephens, Brown, and Sanchez 2016), despite the fact that GO can maintain its stability in aqueous solution owing to its hydrophilicity nature and electrostatic repulsion (Stankovich et al. 2007). The steric hindrance effect of polycarboxylate-based superplasticizer (PCE) has been shown in recent studies to be effective in dispersing GO in the chemical environment or saturated $Ca(OH)_2$ solution formed by cement hydration (Chuah et al. 2018; Yang et al. 2017; Zhao et al. 2017; Zhou et al. 2017). The most common solution to the issue of GO dispersion is to combine the use of surfactants, particularly PCE, with ultrasonication in an effort to reduce its intensity as shown in Table 2.2.

Table 2.2 Dispersion methods of GO in cement composites

Matrix	w/c	GO (% wt)	Dispersion method		Refs.
			Mechanical	Chemical	
Mortar	0.34	0.06	Mechanically stirring	—	(Mohammed et al. 2015)
Mortar	0.45	0.06	Mechanically stirring	—	(Mohammed et al. 2016)

Matrix	w/c	GO (% wt)	Dispersion method		Refs.
			Mechanical	Chemical	
Paste/ Mortar	0.3–0.6	0.03–3.0	Ultrasonication	—	(Li et al. 2017)
Paste	N.A.	0.1	Ultrasonication	—	(Naseri, Irani, and Dehkhodarajabi 2016)
Mortar	N.A.	1.0	Ultrasonication	—	(Kang et al. 2017)
Mortar	0.5	0.2	—	MK, SF	(Roy et al. 2018)
Paste	0.4	0.02	Ultrasonication	SF	(Li et al. 2016)
Paste	0.45	1.0	Ultrasonication	SP	(Sharma et al. 2018)
Mortar	0.2	0.05	Ultrasonication	CCS	(Lv et al. 2017)
Paste	N.A.	N.A.	—	PCE	(Mohammed, Al-Saadi, and Al-Mahaidi 2017)
Paste/ Mortar	0.3–0.66	0.05–0.5	—	PCE	(Long et al. 2018; Long et al. 2018; Lv et al. 2014; Wang et al. 2016; Wang et al. 2015)
Paste/ Mortar	0.29–0.66	0.022–2.5	Ultrasonication	PCE	(Babak et al. 2014; Li et al. 2015; Long et al. 2017; Lv et al. 2013; Wang et al. 2017; Yang et al. 2017)

w/c-water to cement ratio; wt-by weight of cement; N.A.-Not Available; MK-Metakaolin; SF-Silica Fume; SP-Superplasticizer; CCS-Carboxymethyl Chitosan; PCE-Polycarboxylate-based Superplasticizer.

2.4. Workability of GO reinforced cement composites

Workability is defined as the ease with which fresh concrete composite flow and consolidate, which is critical to the strength development and long-term performance of hardened cementitious composites. Lack of the required fluidity might cause the

entrapment of air voids and make it difficult to compact fresh cement composite, which degrades the performance (Pan et al. 2015; Yang et al. 2017).

Many researchers have been concluded that the inclusion of GO has a negative impact on workability as shown in Table 2.3. The negative impact due to hydrophilic functional groups and wide surface area of GO, and is able to absorb a significant amount of water. As a result, there is a decrease in the quantity of water required to lubricate the cement grains, and there is an increase in resistance to friction among the cement grains (Gong et al. 2015; Pan et al. 2015; Wang et al. 2016; Zheng et al. 2017). The drawback of GO on the workability of fresh cement composite becomes more pronounced because dispersed GO has a high specific surface area and thus demands more free water to be connected to GO (Zheng et al. 2017). According to several studies, the development of GO agglomeration entraps free water which reduces workability of cement composites (Li et al. 2017; Shang et al. 2015), due to van der Waals bonds among GO sheets cause cement particles to attract one another, the physical interaction between cement particles and GO also leads to the decrease in workability of cement composite at fresh state (Lu et al. 2017).

Presently, numerous solutions have been presented for detrimental effect of GO on workability. The inclusion of PCE is regarded as the most feasible and efficient solution to this problem (Long et al. 2018; Lu et al. 2017; Lv et al. 2014; Lv et al. 2013; Wang et al. 2016; Wang et al. 2015). PCE has dual functions of electrostatic repulsion and steric hindrance, which allows the scatter of cement particles and liberate the water that was entrapped in the cement flocculation (Stephens et al. 2016). A decrease in available water due to GO sheet absorption might be countered by the release of entrapped water. When graphene oxide-encapsulated silica fume (GOSF) was added to samples with the same amount of silica fume (SF), the samples became more fluid and had lower rheological parameters (Shang et al. 2015). In a related study, fly ash with the ball effect has the potential to enhance the fluidity of cement composite that contains GO (Q. Wang et al. 2017). In an effort to counteract the decreased fluidity of cement composites caused by GO, several researchers have developed GO co-polymers with chemical agents like

polyether amine (M. Wang et al. 2017), carboxymethyl chitosan (Lv et al. 2017), and monomers of PCE (Lv et al. 2016).

Table 2.3 Effect of GO on the workability of cement composites.

Matrix	w/c	GO (wt%)	Method	The change of fluidity/slump	Refs.
Paste	0.29	0.05	N.A.	The fluidity was distinctly reduced by 54.4%.	(Lv et al. 2016)
Paste	0.35	0.05	Rheometer test	The fluidity was reduced by 70.3%.	(Wang et al. 2016)
Paste	0.4	0.08	Rotary viscometer; Mini-slump tests	The diameter was reduced by 36.2% and increased the yield stress and viscosity.	(Shang et al. 2015)
Paste	0.4	0.03	Mini-slump test	The diameter of slump flow was decreased by 21%.	(Li et al. 2017)
Paste	0.5	0.03	Mini-slump test	The diameter of mini-slump was reduced by 34.6%.	(Gong et al. 2015)
Paste	0.5	0.05	Mini-slump test	The diameter of slump was decreased by 41.7%.	(Pan et al. 2015)
Paste	0.35	0.08	Mini-slump test	The fluidity, initial and final setting time was decreased by 21.4%, 24.0% and 30.7%, respectively.	(Lu et al. 2017)
Mortar	0.37	0.05	Digital rotary viscosity meter	The apparent viscosity was increased from 988.5 mPa.s to 19284.0 mPa.s and the fluidity is decreased by 15.2%.	(Wang et al. 2015)
Mortar	0.5	0.1	Mini-slump flow	The diameter of slump flow was reduced by 27.8%.	(Lu et al. 2017)

Matrix	w/c	GO (wt%)	Method	The change of fluidity/slump	Refs.
Mortar	0.66	0.2	Mini-slump test	The workability was decreased by 18.8%.	(Long et al. 2017)

Wt-by weight of cement; N.A.-Not Available.

2.5. Strength properties of GO reinforced cement composites

Strength performance of cement composites is considered as the most significant in the majority of applications. Numerous investigations have recently studied the feasibility of GO as a potential reinforcement to improve the strength characteristics of cement composites and the findings are shown in Table 2.4.

Addition of small dosage of GO were identified to remarkably enhance the compressive, flexural, and tensile strength of composite. The following are the suggested reinforcing mechanisms which have been observed from the published literature: (1) The superior mechanical characteristics of GO significantly helped in reinforcing the cement composites (Li et al. 2017; C. Lu et al. 2016); (2) Nucleation effects of GO can expedite hydration of cement (Horszczaruk et al. 2015; Long et al. 2018; Long et al. 2018); (3) GO can densify the microstructure, reduce porosity, and prevent propagation of cracks at the initiation phase (Gong et al. 2015; Pan et al. 2015); and (4) The chemical bonding at the interface of GO and cement can enhance load-transfer effectiveness (M. Wang et al. 2016). A comprehensive discussion is made in Section 2.6 on the modifications that GO has on the microstructure, which has a primary influential role in relation to strength characteristics of cement composites.

There is a significant amount of variation between these findings with regard to the growth rate of strength as well as the optimal dosage of GO. In addition to the physical properties of GO (oxygen content, number of layers, sheet size, and layer thickness) and characteristics of GO (Young's modulus and tensile strength), other factors that affect the

reinforcing efficiency of GO include type of cement, w/c ratio, superplasticizer, curing ages, curing conditions, and the process used to prepare GO-cement composites.

Agglomerated GO rather than the dispersed GO may have contributed to the gain in strength characteristic using GO solution mixing directly with cement without any modifications. Due to the high inherent strength of GO aggregation, the research conducted by Li et al. (2017), demonstrated that GO agglomerates with the addition of 0.04 weight percent could improve the compressive, tensile, and flexural strength by 14%, 67%, and 83%, respectively. According to the findings of L. Lu et al. (2018), the contribution of pre-stabilized GO by PCE to cement paste was greater than that of post-addition of PCE to GO-cement paste. Comparable findings were reported by Long, Li et al. (2018), which observed that a post-addition of PCE to GO-cement shown lesser flexural and compressive strengths than PCE modified GO mixed with cement. Hu et al. (2019) also observed that superior dispersibility of GO had efficient reinforcing capability, resulting in a considerably improvement in the mechanical characteristics of cement composites. Z. Lu et al. (2019) studied the effect of GO agglomeration size on the reinforcing potential of cement paste. The findings demonstrated that the reduction of the large specific surface area and superior mechanical characteristics of GO caused to decrease compressive strength of cement paste as GO aggregation size is increased. Accordingly, even though several studies have shown that presence of agglomerated GO increases strength of cement composites, it is feasible that GO nanosheets with a higher specific surface area can contribute more to strength characteristics by promoting hydration of cement (Long et al. 2018).

Many researchers have studied the influence of GO properties such as concentration, sheet size, and oxygen content on the reinforcing effects of cement composites.

Sharma & Kothiyal (2016) minimized the GO size in planetary ball milling to improve the efficiency of GO reinforcement on the strength improvement of cement-based materials. The increased number of small nanosheets led to a larger surface area, which can supply extra nucleation sites to accelerate the cement hydration further (Sharma and Kothiyal 2016). This tendency is comparable with the findings of S. Lv et al. (2014),

when the average GO size dropped from 430nm to 72nm, improvements in compressive and flexural strength enhanced by 29.5% and 30.7%, respectively, compared to plain cement composites. Nevertheless, Tong et al. (2016) discovered that, while GOC (generated from GNPs of grade C) had a greater ratio of surface area than GOM (generated from GNPs of grade M having higher diameter and thickness), average strength improvement with the GOC incorporation was significantly less than that of GOM. They indicated that more oxygen functionalities prefer to connect higher GOM with more flaws, resulting in more nucleation sites for cement hydration and formation of dense microstructure.

Other approaches to improve GO's ability to reinforce cement composites were also investigated. It has been observed that NH_2-functionalization increased the cohesiveness between cement matrix and GO sheets, resulting in enhanced strength properties of cement composites in comparison to those reinforced with pure GO (Abrishami and Zahabi 2016). In another investigation, microwave curing was employed in combination with the addition of GO. This resulted in an increase in compressive strength by 126.8% when compared to control sample, which was attributable to stimulated hydration of cement that was activated by the combined effects of GO and microwave curing (Qin, Wei, and Hang Hu 2017). With the addition of GO, various mechanical characteristics like elastic modulus, toughness, strain capability, and dynamic mechanical characteristics such as energy absorption, storage modulus, and loss factors of cement composites were enhanced (Horszczaruk et al. 2015; Kang et al. 2017; Long et al. 2017; Long et al. 2018; Lu and Ouyang 2017; Pan et al. 2015).

Aforementioned findings indicates that GO had potential for improving strength characteristics of cement composites. Although, existing literature has mostly focused on behaviour of GO in cement paste or mortar. No study has been reported addressing the influence of GO reinforcement in concrete performance. From the application point of view in the construction industry, detailed investigation on reinforcing effect of GO in different grades of concrete need to be carried out.

Table 2.4 Effect of GO on mechanical performance of cement composites.

Matrix	GO (%)	Water/ Binder	Improvement in performance	Mechanism	Ref
Paste	0.02	0.4	11.2% Compressive Strength.	XRD, FT-IR and ^{29}Si-NMR indicated that the structure of C-S-H was not affected by GO.	(Yang et al. 2017)
Paste	0.03	0.33	18.8% Compressive Strength; 56.6% Flexural Strength.	Proposed a 3D mechanism model for cement modified with GO nanosheets.	(M. Wang et al. 2016)
Paste	0.03	0.5	46% Compressive Strength.	GO diminished the workability of cement paste; Degree of hydration was improved by GO addition.	(Gong et al. 2015)
Paste	0.04	0.4	14% Compressive Strength.	GO decreased the workability, due to water entrapped in GO agglomeration; Pore structure of cement paste was refined due to nanofiller effect by GO agglomeration.	(Li et al. 2017)
Paste	0.04	0.4	67% Tensile Strength.	Chemical cross-linking of GO nanosheets in saturated calcium hydroxide solution produced GO aggregates with greater aspect ratios and dimensions than the initially prepared GO.	(Li et al. 2017)
Paste	0.04	0.4	46.6% Compressive Strength and 14.2% Flexural Strength.	Dormant period of cement hydration was reduced by GO. Flexural strength was significantly affected by GO agglomeration at higher GO content (more than 0.08%).	(Li et al. 2017)

Matrix	GO (%)	Water/ Binder	Improvement in performance	Mechanism	Ref
Paste	0.05	0.5	15–33% Compressive Strength; 41–59% Flexural Strength.	A substantial decrease in workability; A broader stress-strain curve in the post-peak zone, resulting in a less sudden failure; Crack tortuosity is high.	(Pan et al. 2015)
Mortar	0.02	0.5	20% Compressive Strength; 32% Flexural Strength.	Chemical reactions between the cement matrix and the GO are revealed by TG/DTG analysis. GO can control hydration phases and form compact cross-linking structures was revealed by SEM images.	(Cao, Zhang, and Zhang 2016)
Mortar	0.022	0.4	34.1% Compressive Strength; 30.4% Flexural Strength; 32.4 %Young's modulus; 33% Flexural toughness.	The increased resistance to crack development and growth was attributed to the toughening process of mortars with PC@GO.	(Zhao et al. 2017)
Mortar	0.022	0.42	27% Compressive Strength; 26% Flexural Strength.	The GO effect in decreasing the fluidity of fresh cement mortar was reduced by adding polycarboxylate superplasticizer.	(Zhao et al. 2016)
Mortar	0.03	0.4	38.9% Compressive Strength; 78.6% Tensile Strength; 60.7% Flexural Strength.	Reduced cement brittleness and increased toughness are achieved by controlling GO nanosheets to produce flower-like hydration crystals.	(Lv et al. 2013)

Matrix	GO (%)	Water/ Binder	Improvement in performance	Mechanism	Ref
Mortar	0.05	0.37	24.4% Compressive Strength; 70.5% Flexural Strength.	Accelerated hydration, reduced pore volume, improved crystallization and crystallite alignment generated by GO enhanced the strength cement composites.	(Wang et al. 2015)
Mortar	0.05	0.5	32% Compressive Strength.	The bridge effect of GO was associated with the strength improvement because it is covalently bonded with C-S-H to increase the coherence inside the matrix.	(Kang et al. 2017; Zhao et al. 2016)
Mortar	0.1	0.485	37.5% Compressive Strength; 77.7% Flexural Strength.	XRD results indicated that the GO enhances water accessibility to oxygen functional groups of GO and C-S-H, accelerating the hydration.	(Gholampour et al. 2017)
Mortar	0.5	0.3	126.6% Compressive Strength.	A regular and compact structure was produced as a result of the acceleration of cement hydration caused by the combined use of GO doping and microwave-curing.	(Qin et al. 2017)
Mortar	1.5	0.4	48% Tensile Strength	GO surfaces and the surrounding cement matrix have a strong connection. High bond strength was determined by FE-SEM and XRD analysis to be caused by the nucleation and production of C-S-H.	(Babak et al. 2014)

2.6. Microstructural characteristics of GO reinforced cement composites

2.6.1. Microstructure and hydration products

The microstructure of cement paste with the addition of GO having 29.75% oxygen at various dosages was examined using SEM images by Lv et al. (2013), as shown in Figure 2.8. The unique morphological modifications were observed with the increased GO dosages. The SEM images of the fracture surface for control sample (without GO) shown bar-like and needle like hydration crystals such as calcium hydroxide (CH), ettringite (AFt), and monosulfonate (AFm) (Figure 2.8a). When the GO dosage in the cement was increased from 0.01 to 0.03% by weight, dense flowerlike crystals developed. Only a few tiny flowerlike crystals are seen at 0.01% GO dosage, and only a few are exposed at the surface (Figure 2.8b). The hydrated crystals, when blended with the 0.02% of GO, acquired the appearance of full flower with large petals and were dispersed evenly throughout the cement matrix (Figure 2.8c). Dosage of GO 0.03%, flowerlike crystal further grows denser (Figure 2.8d). The hydrated crystal gradually takes on an irregular polyhedral structure after the dosage is increased from 0.04 to 0.05%, which remains collectively and finally develops a regular, complete polyhedral shape (Figure 2.8(e-f)). Polyhedral geometry differs from that of previously created flowerlike hydrated crystals. The crystal that looks like a flower helps to improve toughness, while the crystal that looks like a polyhedron helps to improve compressive strength (Lv et al. 2013). The mechanism of cement hydration crystals growth was also investigated. The findings suggest that GO sheets govern cement hydration crystals by producing flowerlike crystals in the cracks and pores of the cement matrix. Figure 2.9 depicts the mechanism of GO in the development of cement hydration crystals. The oxygen functionalities on the GO nanosheet surface are shown in Figure 2.9a. The hydration reaction delayed with usage of superplasticizer while the functional groups react with the cement's phases chemically, leading to the production of growth points on hydration products shown in (Figure 2.9(b-c)). At each of the numerous growing spots on the surface of GO, the hydration reaction

initiates itself once again and continues further (Figure 2.9d). In the phenomenon that is referred to as the "template effect," the quantity of GO present in a solution serves as a governing factor that controls the development of growth points. Due to the presence of GO nano-sheets, flower-shaped and column crystals developed in the presence of hydrated phases (Figure 2.9e).

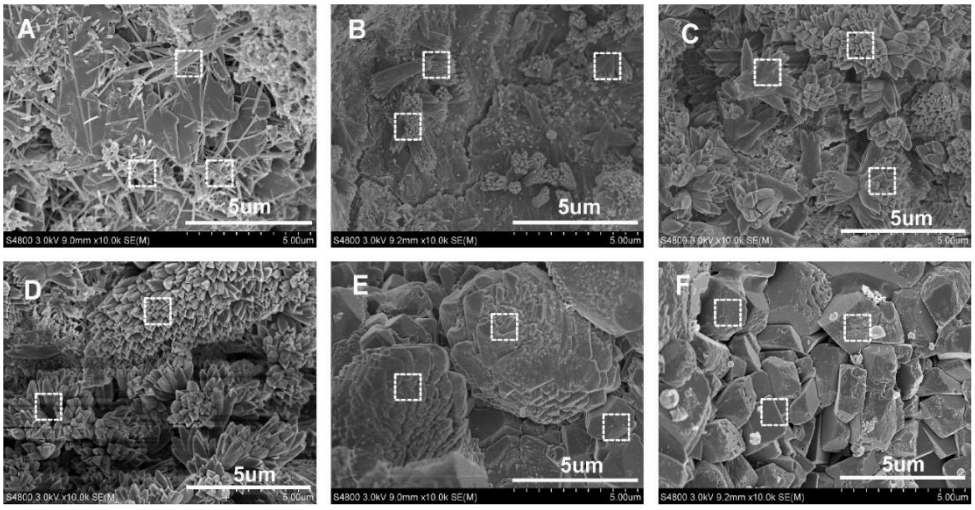

Figure 2.8 SEM images of cement composite with varying dosages of GO at 28 days: (a) control sample, (b) 0.01%, (c) 0.02%, (d) 0.03%, (e) 0.04%, and (f) 0.05% (Lv et al. 2013)

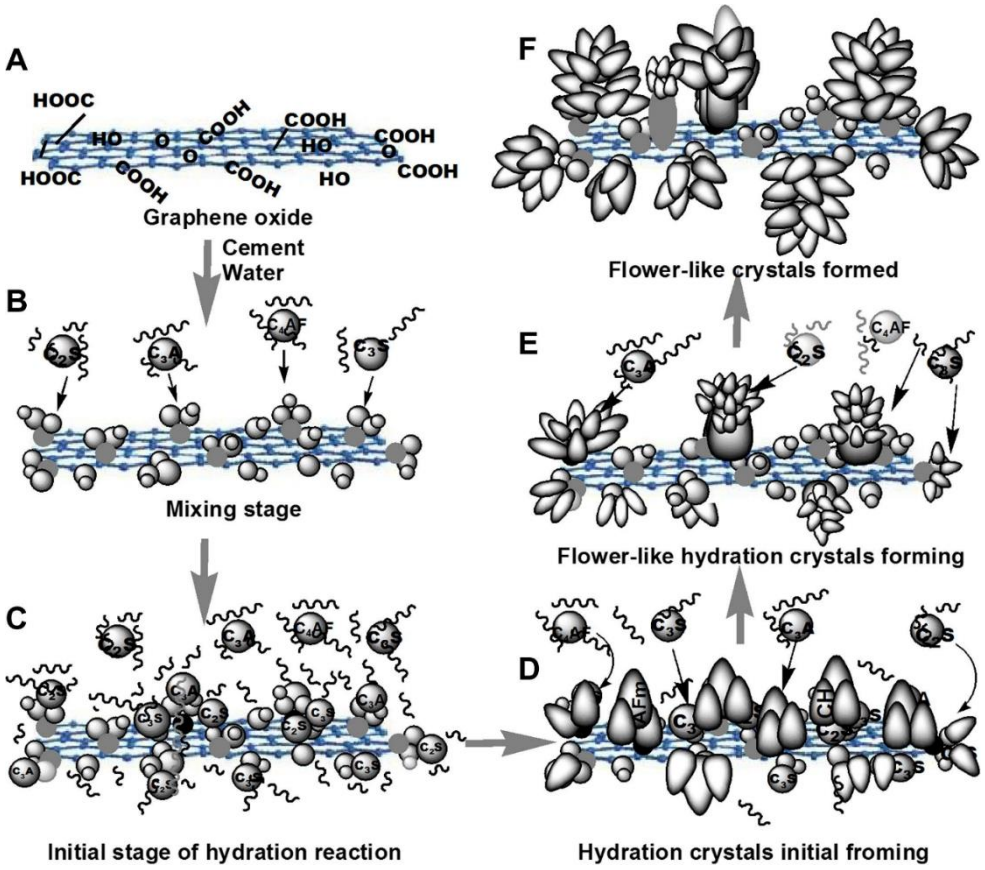

Figure 2.9 Mechanism of cement hydration crystal formation using GO at different stages. (Lv et al. 2013)

Because of the tremendous tension that exists surrounding them, these column-shaped crystals protrude outward from the surface of the GO. After the development of column-shaped crystals, fully developed flowerlike crystals formed (Figure 2.9f). These crystals that have grown into flowerlike shapes fill the fractures, loose structure, and pores, which further delays and eventually stops the crack growth. Lv et al. (2013) also studied the fact that when the dosage of GO was greater than 0.04%, shape of hydration crystals might change. It would take on the form of a polyhedron as a result of the development of a single crystal that resembled a flower. This crystal formed a compact and dense microstructure at the growth points. In order to further improve the toughness against cracking, cement-based materials generate flowerlike crystals in the pores and develop crosslinking network (Lv et al. 2014; Lv, Ma, Qiu, and Zhou 2013; Lv et al. 2013; Lv et al. 2014).

2.6.2. Cement hydration process

Qureshi & Panesar (2019) used a calorimetric technique to examine the hydration process. The rate and cumulative heat of hydration of cement with the addition of GO/rGO at various dosages were observed for the first 48 hours as shown in Figure 2.10. The primary and secondary peaks are represented by various peaks on the heat of hydration curve. The primary peak, which is also known as the main peak, is determined by the C_3S content of the cement and determines the final setting time. On the other hand, secondary peaks are determined by the alumina content of the cement (Qureshi and Panesar 2019). According to their findings, the rGO and GO both have a greater rate of heat evolution as well as a larger total heat of evolution during hydration compared to the control sample. However, in terms of heat release, when compared between GO and rGO, the rGO-based cement composite would liberate significantly higher heat of hydration than the GO-based cement composites. It can be seen in Figure 2.10b, the dispersion influence of cement composites causes the cumulative heat release to be less for rGO than it is for GO composites during the first twenty-four hours of the hydration process. The rGO plays a substantial part in the C_3A hydration process due to the fact that the total heat release after 16 hours is greater for the rGO in comparison to the GO.

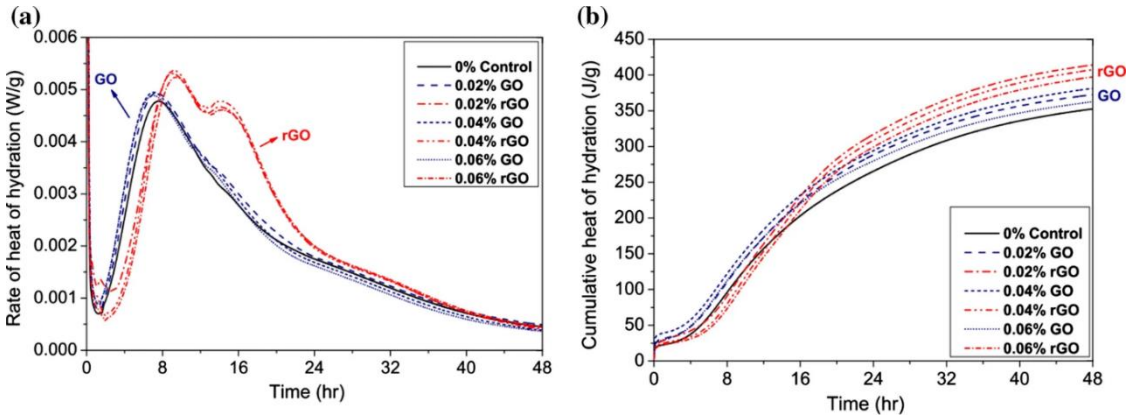

Figure 2.10 Isothermal calorimetric analysis of cement composites reinforced with different dosage of GO/rGO: (a) Rate of heat of hydration curves; (b) Cumulative heat of hydration curves. (Qureshi and Panesar 2019)

2.6.3. Hydration time on microstructure

The influence of hydration time on microstructure of GO reinforced cement composites was examined by Lv et al (2013). SEM micrographs were observed in their investigation at a GO of 0.03% by weight of cement. The SEM image shows that GO facilitates the progress of flowerlike crystals during cement hydration. The development of small, irregularly-shaped flower petals is shown in Figure 2.11a. At three days, a large number of tiny rod-shaped crystals emerge together with partially formed flowers-shaped crystals (Figure 2.11b). After seven days, several petals begin to form on the crystals that resemble incomplete flowers (Figure 2.11c). In comparison to 7 days, this flower-shaped crystal assumes a uniform shape at 28 days instead of uneven shape (Figure 2.11d). The flower-shaped crystals collected and formed a connected cluster after 60 and 90 days (Figure 2.11(e-f)). Through the development of flowerlike hydration crystals, GO can encourage the development of a highly dense and compact cross-linking structure.

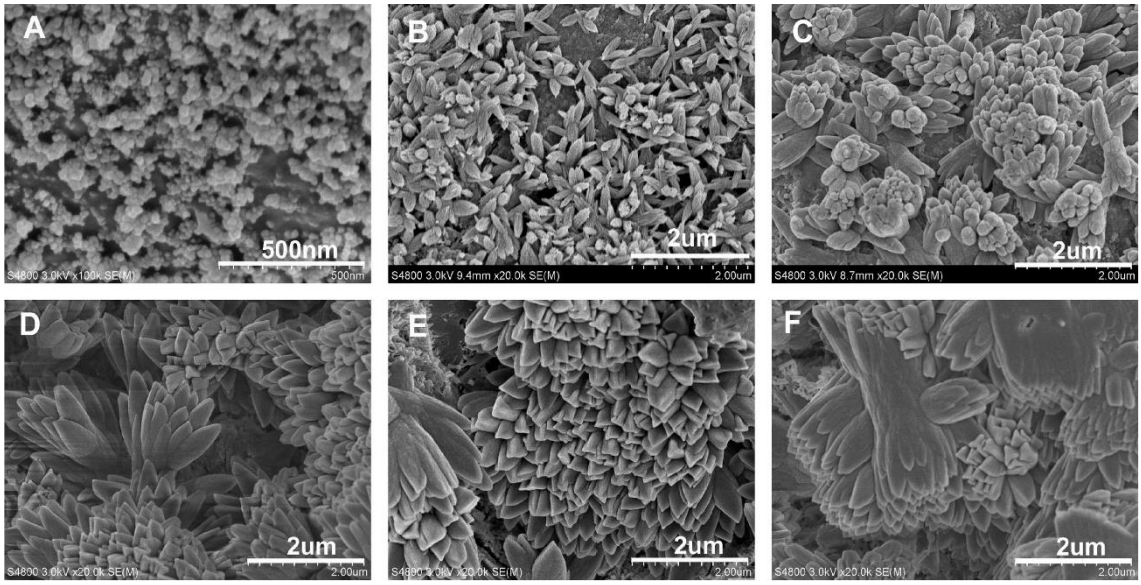

Figure 2.11 SEM images of hydration crystals of cement composite with 0.03% GO at different curing periods: (a) 1 day, (b) 3 days, (c) 7 days, (d) 28 days, (e) 60 days, and (f) 90 days (Lv et al. 2013)

2.6.4. Thermogravimetric/differential thermal analysis (TGA/DTA)

TGDTA is commonly employed to investigate weight loss and decomposition of a substance as a function of temperature. X. Kang et al. (2019) investigated the influence of GO addition on C_3S hydration. The TGA/DSC pattern indicates the degradation of CH that occurred between 400 and 500 °C as show in Figure 2.12. The CH content of the cement paste was initially 16.85%; with the introduction of GO 0.01% and 0.05%, the $Ca(OH)_2$ quantity was 20.14% and 19.58%, respectively. Using TGA and DTA, B. Wang et al. (2016) demonstrated how the behaviour of GNPs modified depending on the degree of hydration of cement. The first weight loss of $Ca(OH)_2$, $CaCO_3$ and non-evaporable water of control sample is 3.69%, 3.49%, and 4.96%, respectively, as shown in Figure 2.13. Following the incorporation of GNPs at 0.10% has values of 3.72%, 3.65%, and 5.02%, all of which are superior to GO. As a consequence of this, GNP causes a greater degree of hydration to be present. Another investigation (Qureshi and Panesar 2019) evaluated at the hydrated phases (after 1, 7, and 28 days) and found that the C-S-H and CH content in GO is higher than that in rGO composites.

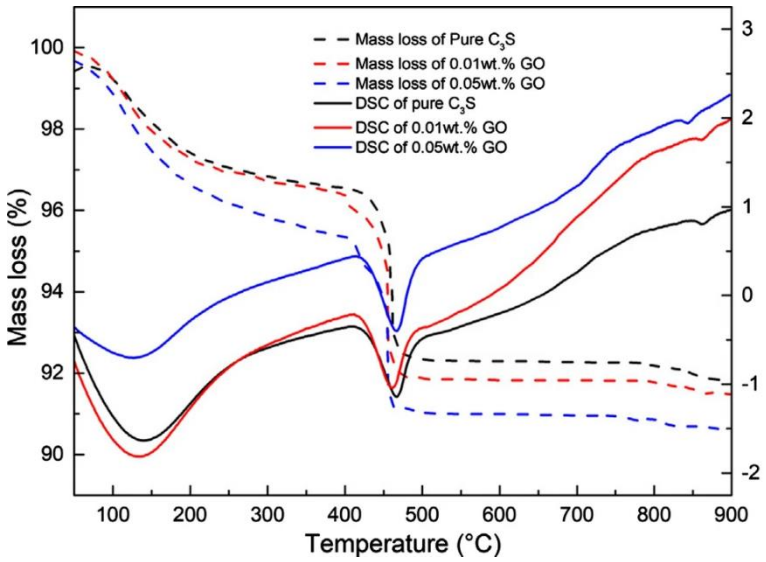

Figure 2.12 TGDTA plots of C_3S reinforced with GO at different dosages at 7 days curing period. (Kang et al. 2019)

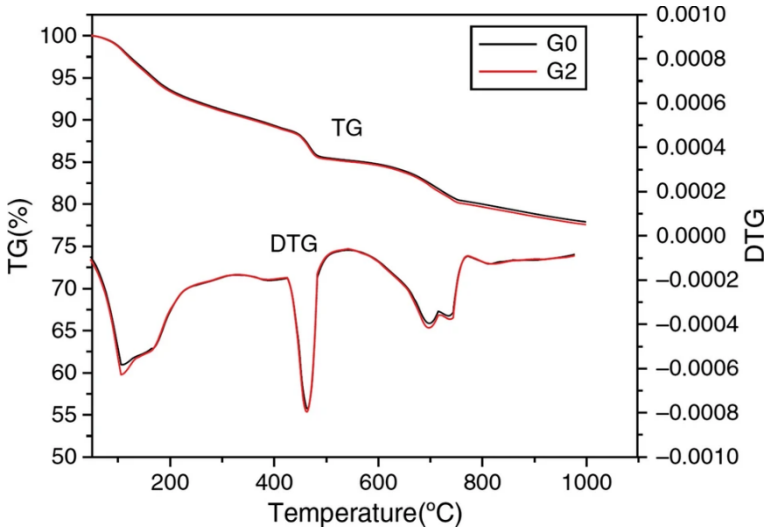

Figure 2.13 TGDTA plots of GNPs reinforced cement composites at 28 days curing period. (Qureshi and Panesar 2019)

2.6.5. Pore structure

Cement-based products have a large number of pores. Water is trapped within the pores of the cement mix due to porosity. Because they do not enable water to travel through them, pores with a small size have a lower porosity and a higher durability. The cementitious materials have a mechanical performance that is affected by the pore structure, which consists of holes and cracks. The effect of GO addition on the pore structure was studied by Lv et al. (2014), who found that incorporating GO in cement paste promotes the development of crystals in a rod-like shape. After that, these crystals develop a shape like a flower or polyhedron, and their arrangement becomes more regular and uniform. The expansion of hydrated crystals eventually occupy the available pore space, and this result the reduction of porosity of the material. Increased GO dosage in cement paste can substantially decrease average diameter, mean pore diameter, and total pore area. In addition, it is indicated that lowering the amount of larger pores (>100 nm) and increasing amount of small pores (<100 nm) can be achieved by increasing the GO dosage from 0.01 to 0.03%. If the dosage of GO in cement is higher than 0.03% by weight, then the majority of the pores shrink in size, and their dispersion become more uniform.

The CSH gel pores in GO and rGO composites are significantly larger than those in the control mix is identified by Qureshi and Panesar (2019). Based on the BET approach, in the results that they obtained for graphene-based cement composites are presented in Table 2.5. Graphene-based composites considerably enhance specific surface area and total pore volume values compared to the control mix. GO reinforced composites have specific area and total pore volume values greater than composites with rGO. Increased specific surface area facilitates higher nucleation and growth sites, resulting in the formation of more C-S-H gel.

A low dosage of GO indicated as percentage weight of cement advances the production of irregular hydration products, which results in decreased mechanical strength and increased porosity. However, results indicated that increase in the GO content to obtain regular hydration products further supports to develop dense microstructure in cement composites. Because of this, cracks and pores offer sufficient amount of space that allows the hydration products to start growing in the cement matrix. The size of the hole and the microcracks are diminished by forming the crystals (Lv et al. 2014). Employing mercury intrusion porosimetry (MIP), Mohammed et al. (2015) investigated the GO effects on pore size and demonstrated that the GO presence increased the number of gel pores. These findings indicate that nanomaterials based on graphene have the ability to lower the porosity of a material by simultaneously decreasing the pore diameter and the pore volume while maintaining a consistent pore size.

Table 2.5 Pore structure of graphene-based cement composites (Qureshi and Panesar 2019)

Pore dia range (0–22 nm)	Control	rGO 0.02%	rGO 0.04%	rGO 0.06%	GO 0.02%	GO 0.04%	GO 0.06%
Total volume of pore (cm^3/g)	21.42	24.34	24.65	24.74	23.89	24.57	25.91
Specific surface area (m^2/g)	60.45	68.68	68.56	69.80	67.40	69.30	73.10

2.7. Summary of literature

This chapter provides the review of literature on the role of graphene-based nanomaterials in cement composites. The mechanisms of microstructural analysis, cement hydration, pore structure, and characteristics of graphene-based cement composites have been systematically discussed. Based on a comprehensive review of the literature, the following observations are made:

- Nanomaterials, including Nano silica, CNTs, and GO, should be carefully dispersed and checked for a quality as they undergo agglomeration due to strong van der Waals bonds. Combination of sonication and admixture prevents agglomeration in the cement matrix. GO has more beneficial effect due to its oxygen functional groups compared to other nanomaterials.

- GO absorb free water, which reduces the workability of cement composites. The viable option for overcoming this issue is to employ a suitable admixture.

- GO can expedite the cement hydration by connecting C-S-H gel. The main benefit of GO is C-S-H gel seeding on their large surfaces. 2D nanosheet reinforcement strengthen cement through crack bridging. Pore refining by GO is very beneficial to improve strength and durability of composite.

- With regards to the cost of incorporating graphene-based nanomaterials, it is a less expensive material than CNTs, hence, attention has now been shifted to graphene materials. Also, cement composites have major benefits such as adding a small quantity of graphene-based nanomaterial results in the improvement of compressive, flexural, and tensile strengths.

- Among all the nanofillers listed, GO appears to have the most potential for improving the characteristics of cement-based composites. The 2D nanosheet, like CNTs, has great inherent characteristics that make it a good alternative for reinforcing cement matrix. In addition, oxygen-carrying functional groups are advantageous because they

facilitate uniform dispersion in cement, the nucleation of C-S-H, and densification of the microstructure.

The following are the research gaps identified from the extensive literature study:

- It is evident that GO has potential to modify the performance of cement composites. Most of the investigations are limited to the GO effect on cement paste or mortar, its application in concrete has not been studied. In the current situation, concrete is commonly used as a construction material, so its performance is primarily significant in the improving the service life of the major critical infrastructure.

- The GO incorporation in cement composites have been investigated in terms of microstructure and static mechanical properties. Comparatively, very less research available on the dynamic and durability properties of GO reinforced cement composites and hence need to be studied further.

- The combination of GO and SCM materials needs to be verified with regard to mechanical and long-term performance of cement concrete composites. It is worthwhile to develop the use of GO in associated with SCM materials in order to create composite with high mechanical and durability properties for the future generation of buildings and other infrastructure.

CHAPTER 3
SCOPE AND OBJECTIVES OF THE INVESTIGATION

3.1. Scope of the investigation

Cement concrete is commonly used as a construction material and its performance is paramount important in the construction of various engineering structures. In addition, the environmental issues associated with emission of greenhouse gas and depletion of natural resources, plays a major role in the sustainable development of concrete. Graphene oxide (GO) is a potential nanomaterial which can be utilised to modify the properties concrete composite. Significantly most of the studies have been investigated the influence of GO addition on microstructural and mechanical characteristics of cement composites such as cement paste and cement mortar. Also, very few investigations have been carried out on the dynamic mechanical characteristics and durability properties of the cement composites with the addition of GO. After going through the literature, it is observed that the necessity of performance and microstructural characteristics of concrete composite is need to be studied further. The present research is primarily focussed on the development of GO reinforced cement concrete (GCC) to determine the GO influence on performance and microstructural characteristics. Further the research is focused to verify the combined effect of GO and fly ash on the strength, performance and microstructural characteristics of concrete composite (GFC). It is worthwhile to develop the use of GO in associated with supplementary cementitious materials in order to create sustainable concrete composites with better mechanical and durability properties for the construction of civil infrastructure. Accordingly, a detailed experimental program has been planned. The static mechanical characteristics, mainly compressive strength, split tensile strength, flexural strength and elastic modulus of concrete composite have been evaluated. The

dynamic mechanical characteristics such as natural frequency and damping ratio, dynamic modulus of elasticity, dynamic rigidity modulus and dynamic poissons ratio were also determined. Microstructural and hydration characteristics of GCC and GFC were evaluated using characterization techniques, such as TGDTA, XRD, FTIR, SEM and EDAX. Finally, the durability properties such as water absorption, sorptivity, accelerated carbonation, rapid chloride penetration and resistance to acid attack were also investigated.

3.2. Objectives of the research work

The aim of present research work is to investigate the static mechanical, dynamic mechanical, durability and microstructural characteristics of GO reinforced cementitious concrete. Following are the objectives of the present investigation

- To determine the effect of GO on the static mechanical properties of concrete.
- To evaluate the effect of GO on the dynamic mechanical characteristics of concrete.
- To assess the effect of GO on the durability properties of concrete.
- To study the combined effect of GO and fly ash on the performance and microstructural characteristics of concrete.
- To validate the experimental results through numerical modelling.

3.3. Research methodology

To achieve the above-mentioned objectives, the present experimental investigation is planned and carried out in three different phases.

Phase-I: First phase of experimental program is planned to evaluate the static and dynamic mechanical characteristics, durability properties and microstructural characteristics of GO reinforced cement concrete. Two different grades of concrete mixes such as standard concrete (SC) and high strength concrete (HSC) with characteristic compressive strength of 30 MPa and 60 MPa respectively were designed in accordance

with IS:10262-2019. In this study, a range of GO content varied from 0% to 0.2% with an increment of 0.05% by weight of cement was considered. Phase-I is divided into two main parts. The first part focused on the evaluation of static mechanical characteristics such as compressive, split tensile, flexural strength and elastic modulus of GO reinforced concrete. In addition to that, dynamic properties such as natural frequencies, damping ratios and mode shapes were determined using impact hammer technique. The microstructural characterization was carried out using SEM, EDX, XRD, FTIR and TGDTA. The second part consists of assessment of durability performance of GO reinforced cement concrete was evaluated by performing water absorption, sorptivity, accelerated carbonation, rapid chloride penetration and acid attack tests. The performance of GO reinforced cement concrete is compared with the performance of control concrete.

Phase-II: Second phase of experimental program is aimed to evaluate the combined effect of GO and fly ash on static and dynamic mechanical properties, durability properties and microstructural characteristics of concrete. In this phase, the optimum dosage of GO attained from Phase-I and further replacement of cement with fly ash at 10%, 20%, and 30% by weight of cement was considered. Two different grades of concrete mixes with a compressive strength of 30 MPa and 60 MPa were investigated. Phase-II is also carried out in two different parts. The first part focused on the evaluation of static mechanical characteristics such as compressive, split tensile, flexural strength and elastic modulus. Dynamic properties have also been determined. The microstructural characterization has been carried out using SEM, EDX, XRD, FTIR and TGDTA. The second part consists of evaluation of durability performance of GO reinforced fly ash concrete was determined by conducting water absorption, sorptivity, accelerated carbonation, rapid chloride penetration and acid attack tests. The performance of GO reinforced fly ash concrete is compared with control concrete.

Phase-III: The third phase of the investigation consists of validation of experimental results with results obtained through finite element modelling (FEM). A FEM software ATENA was used to model 100x200mm cylinders in order to obtain the constitutive stress-strain curves analytically. The results of stress-strain curve obtained through modelling are compared with experimental results. Thereafter, a flexure specimen of

500x100x100mm was modelled and analysed using inputs from the 100x200mm cylindrical model. The results from flexure model are also validated with experimental findings.

CHAPTER 4
EXPERIMENTAL PROGRAM

4.1. General

This chapter consists of the information related to properties of materials, mix proportions, preparation process of GO solution and casting of specimens for the development of GO reinforced concrete composite specimens, GO reinforced fly ash based concrete composite specimens, and test methods used for assessment of static mechanical properties, dynamic mechanical properties, durability properties and microstructural characterization.

4.2. Materials

The materials used in this experimental study and its properties are as follows.

4.2.1. Cement

Ordinary Portland cement (OPC) of 53grade conforming to IS:269-2015 was used in this study. The chemical composition and physical properties of cement are given in Table 4.1 and Table 4.2, respectively.

4.2.2. Fly ash

Fly ash is a by-product obtained from the burning of pulverized coal in electric power generation plants. Fly ash is a fine powder which is finer than Portland cement and chemically reacts with the calcium hydroxide developed through the hydration of cement

and helps to improve the concrete properties. Fly ash having a specific gravity of 2.10 and class F according to IS:3812 (Part 1)-2003 was used in this investigation. The chemical composition of fly ash is given in Table 4.1.

Table 4.1 Chemical composition of cement and fly ash

Material	SiO_2	Al_2O_3	Fe_2O_3	CaO	SO_3	MgO	Na_2O	K_2O
Cement	20.265	4.31	3.315	64.38	3.46	1.355	0.1	0.91
Fly ash	61.97	29.63	3.29	2.57	0.13	0.94	0.33	0.83

Table 4.2 Cement physical properties

Fineness	Normal consistency	Specific gravity	Bulk density (kg/m^3)	setting time (min)		Compressive Strength (MPa)	
				Initial	Final	7 days	28 days
5%	32%	3.1	1440	55	186	46.1	54.2

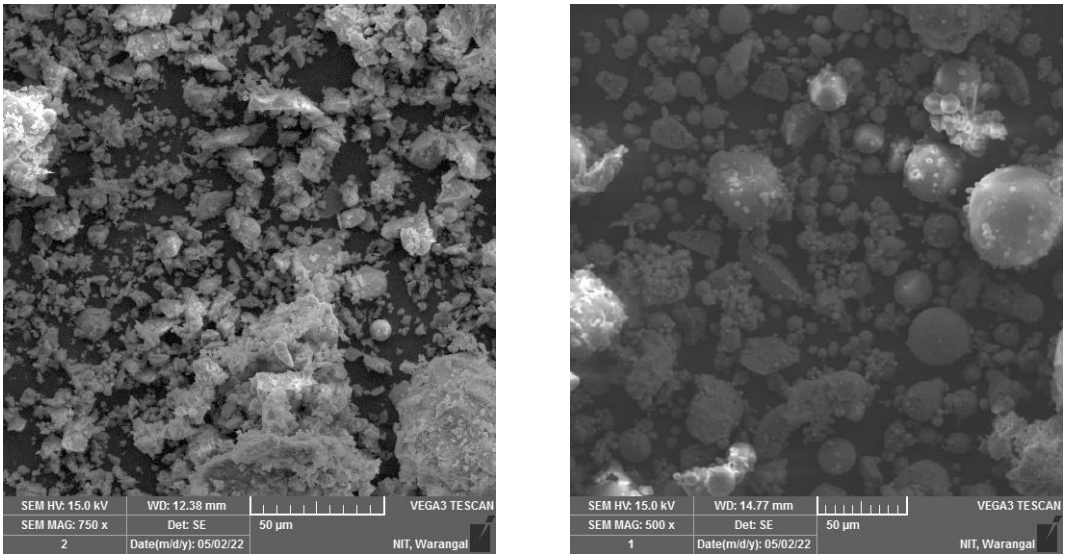

(a) **(b)**

Figure 4.1 SEM images of raw materials (a) Cement (b) Fly ash

4.2.3. Fine aggregate

Locally available river sand of zone-II conforming to IS:383-2016 was used as a fine aggregate (FA) in the investigation. Particle size distribution curve for fine aggregates is given in Figure 4.2. Physical properties of fine aggregate are shown in Table 4.3.

4.2.4. Coarse aggregate

Hard stone granite chips were used as a coarse aggregate (CA) conforming to IS:383-2016. The particle size distribution curve for coarse aggregates is shown in Figure 4.2 and physical properties of coarse aggregate are given in Table 4.3.

Table 4.3 Properties of aggregates

Physical properties	Specific gravity	Fineness modulus	Water absorption (%)	Unit weight, kg/m^3 (Dry compacted)
FA	2.51	2.96	1.28	1595
CA	2.85	6.78	0.51	1652

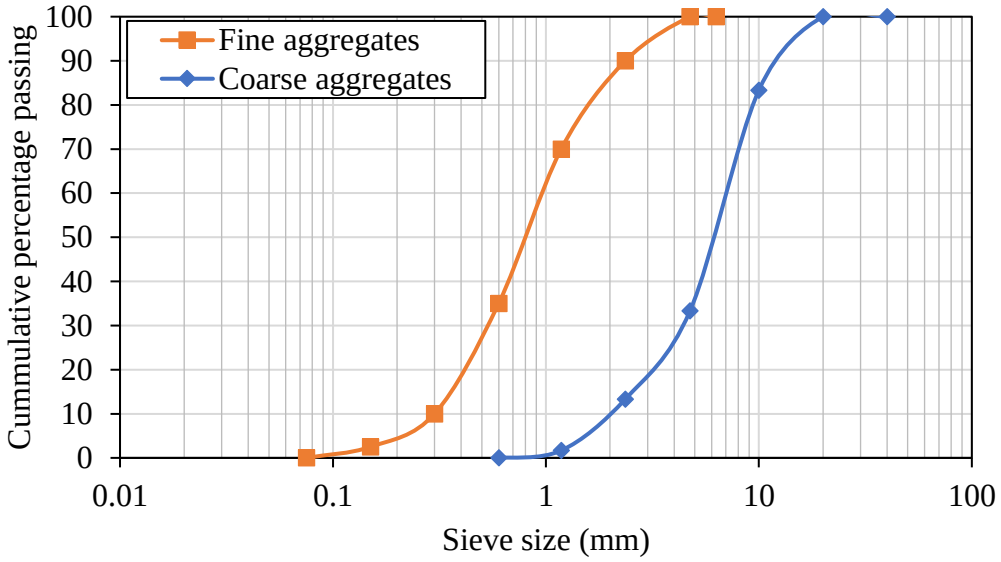

Figure 4.2 Particle size distribution for fine and coarse aggregates

4.2.5. Superplasticizer

In this experimental investigation, in order to attain the required workability of concrete, polycarboxylic ether-based superplasticizer (PCE) conforming to IS:9103-2018 was used.

4.2.6. Graphene oxide (GO)

Commercially available GO powder was used as nanomaterial in the present investigation. Physical properties of GO are shown in Table 4.4. An ultrasonication procedure was used to disperse GO in water with PC at 6 mg/mL concentration. SEM, EDX, FTIR and XRD techniques were performed to characterize GO and results are shown in Figure 4.3.

4.2.6.1. Microstructural characterization of GO

The structural characterization of GO was performed using SEM with EDX to obtain the morphology and composition of elements. The SEM image and the elemental weight percentages of GO are shown in Figure 4.3(a-b). Surface morphology of GO can be observed from the SEM image and the surface is wrinkled and folded form. The wrinkled morphology of GO refers to the large surface area interwoven with weak van der Waals bonds (Kang et al. 2019). The elemental percentage of GO indicates that it contains 73.02% of carbon (C) and 26.54% of oxygen (O), which represents the oxygenated functional groups attached to GO.

The XRD pattern of GO is presented in Figure 4.3(c). The pattern was attained using the PANalytical XPert-Pro diffractometer system with Cu Kα = 1.54060Å, range of scan 2θ=6°–80°, divergence slit with fixed value of 0.5°, size of step 0.008356 and time of step 12.7s, to determine the crystalline nature and interlayer spacing. The XRD pattern of the GO indicates the appearance of a single strong diffraction peak at 2θ=12.59° and its corresponding interlayer distance of 0.706 nm (Kang et al. 2019).

FT-IR spectra of GO given in Figure 4.3(d), represents the existence of functional groups on GO because of the disruption of oxygenated functionalities on the sp^2 hybridization. The pattern consists of hydroxyl (-OH) was observed at a peak of 3366 cm^{-1}, carbonyl group (C=O) was observed at peak of 1712 cm^{-1}, alkenic bonds (-C=C-) was observed at a peak of 1650 cm^{-1}, carboxyl (C–OH) was observed at a peak of 1116 cm^{-1} and epoxides (C–O–C) stretch was confirmed at a peak of 1184 cm^{-1} (Kang et al. 2019). The existence of these peaks confirms that GO comprises good hydrophilicity because of the existence of oxygenated functionalities such as hydroxyl, epoxy, carboxyl and carbonyl.

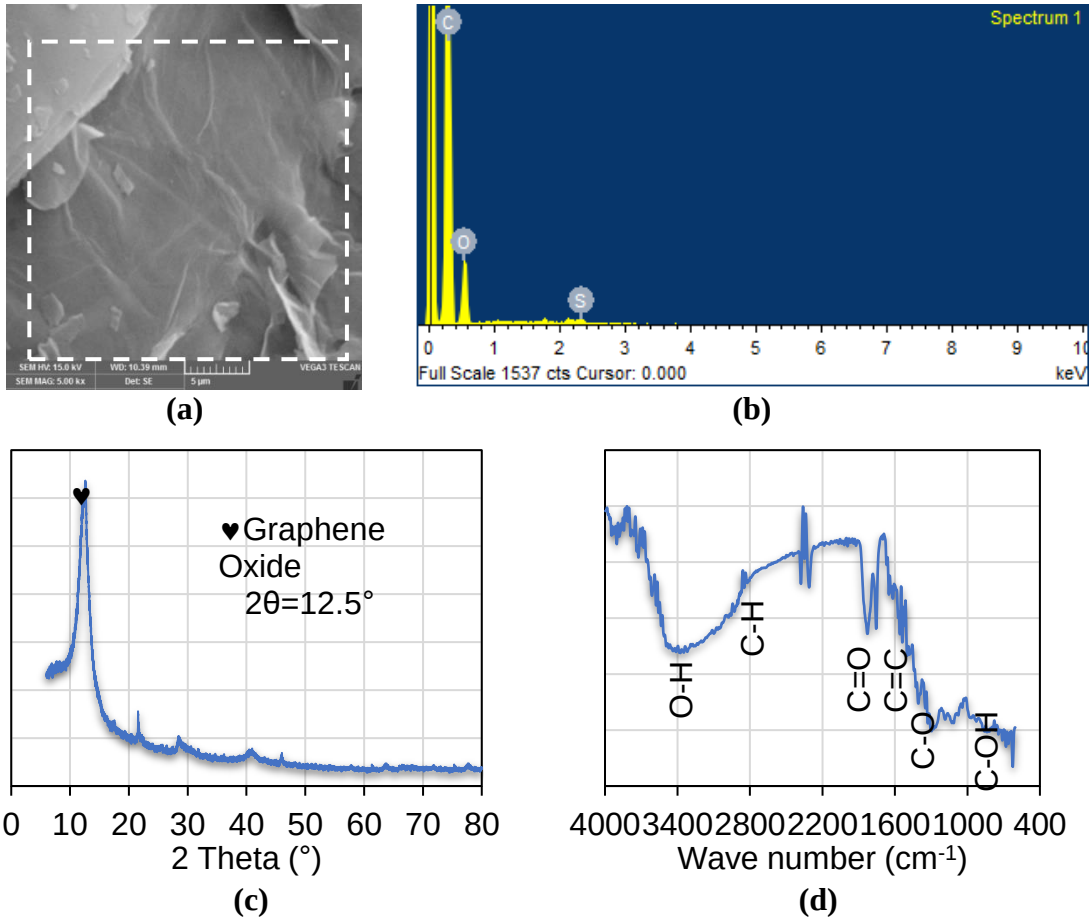

Figure 4.3 Microstructure characterization of GO (a) SEM, (b) EDX, (c) XRD, (d) FTIR

Table 4.4 Physical properties of GO

Average Lateral Dimension (X&Y)	Thickness (Z)	Number of Layers	Purity	Surface Area	Bulk Density
5-10 μm	0.8-2 nm	1-3	99%	110 - 250 m^2/g	0.122 g/cm^3

4.3. Mix proportions

The concrete mixes of standard concrete (SC) and high strength concrete (HSC) with characteristic compressive strength of 30 MPa and 60 MPa respectively were designed in accordance with IS:10262-2019. The high degree of workability with a slump value of 100 to150mm according to IS:456-2000 was considered in this study. Various trial mixes with varying superplasticizer dosages were tested, and the optimal dosage that produced required workability and strength was considered as control concrete. The mix proportions of different concrete grades considered are given in Table 4.5.

4.3.1. GO reinforced concrete

Literature shows that the low dosages of nanomaterials can remarkably enhances different characteristics of cement composite. Hence, the influence of GO addition on performance and microstructural characteristics of different grades of concrete were investigated in this study with a range of GO content varied from 0% to 0.2% with an increment of 0.05% by weight of cement.

4.3.2. GO reinforced fly ash concrete

In order to investigate the combined effect of GO addition and replacement of cement with fly ash on performance and microstructural characteristics of different grades of concrete. GO reinforced fly ash concrete was developed with optimum dosage of GO addition along with fly ash as a partial replacement of cement at low volumes such as 10%, 20% and 30% by weight.

Table 4.5 Mix proportions of various concrete mixes for 1m^3

S.No	Mix Designation	Water to cement ratio	OPC (kg)	FA (kg)	CA (kg)	PCE (%*)
1	SC	0.45	380	850	1046	0.5
2	HSC	0.30	450	788	1150	0.8

*Percentage by weight of cement

4.4. Preparation of concrete specimens

4.4.1. GO solution

GO solution was prepared in water along with polycarboxylic ether-based superplasticizer (functioning as a surfactant) through an ultrasonic process. The water used to prepare the solution of GO is obtained from the water quantity arrived from the mix proportion. A probe sonicator was employed for 60 minutes to produce uniform solution of GO, as shown in Figure 4.4. As a result, the concentration of GO dispersion at 6 g/L was obtained in an aqueous solution.

Figure 4.4 GO dispersion through ultrasonication

4.4.2. Concrete specimens

The following procedure is involved in the preparation of concrete specimens. Initially, uniform GO solution as a part of the water required for each mix along with the PCE was prepared. The various ingredients of concrete such as cement, fly ash, fine and coarse aggregate were mixed thoroughly. Then the water is added to the dry mix and mixed uniformly at low speed. Finally, the GO solution is added and thoroughly mixed, the entire mixing process continued for about 3 to 5 minutes. A power-driven mixer of 200 L capacity was used to achieve a uniform mix. Thereafter, fresh concrete mix was poured in moulds to prepare different types of specimens (cubes, cylinders and prisms) according to IS: 10086-2018. Followed by the moulds were wrapped with plastic sheets to prevent water loss. The specimens were extracted from the respective moulds after 24 hours and placed in water for curing under standard conditions.

(a)

(b)

(c)

Figure 4.5 Specimens preparation (a) Mixing, (b) casting and (c) curing

4.5. Test methods

4.5.1. Static mechanical properties

4.5.1.1. Workability

Workability of fresh concrete mixes were performed according to IS:1199-2018. The workability was evaluated by measuring the slump values using slump cone test. The fresh concrete is poured into the slump cone (300 mm height, 200 mm bottom diameter and 100 mm top diameter) in three different layers and tamped each layer 25 times with tamping rod, then the cone is removed in vertically upward direction carefully and the slump value was measured. Slump values for concrete mixes having different GO dosage were recorded and the effect of GO on fluidity of concrete was assessed.

4.5.1.2. Compressive strength

Compressive strength test was performed on cubes having size of 100x100x100mm at 7 and 28 days in accordance with IS:516 under direct compression using 200T capacity compression testing machine (CTM), as shown in Figure 4.6(a). The load was applied gradually at a uniform rate 14 N/mm^2/min. The maximum load carried by each specimen was noted down and the compressive strength is calculated as the average of three similar specimens. The compressive strength is arrived by the following equation:

$$f_c = \frac{F}{A_c} \quad \textbf{4.1}$$

Where 'f_c' is compressive strength in MPa, 'F' is maximum load in newtons, and 'A_c' is cross-sectional area in mm^2 of the specimen.

4.5.1.3. Split tensile strength

Split tensile strength test was performed according to IS:516 on cylindrical specimens 100mm diameter and 200mm height at 7 and 28 days, as shown in Figure 4.6(b). The rate

of loading was maintained at 1.2 N/mm^2/min to 2.4 N/mm^2/min. The maximum load taken by each sample was recorded. The splitting tensile strength of the specimen is calculated as follows:

$$f_t = \frac{2P}{\pi l d} \quad \textbf{4.2}$$

Where, 'f_t' is the split tensile strength of the specimen in MPa, 'P' is maximum load carried by specimen in N, 'l' is length of cylinder in mm, and 'd' is diameter of cylindrical specimen in mm. Split tensile strength is calculated as an average of three similar specimens.

4.5.1.4. Flexural strength

Prisms of size 100mm x 100mm x 500mm were used to obtain the flexural strength of different mixes for each curing age 7 and 28 days. The load was applied under four-point bending according to the IS:516 using universal testing machine, as shown in Figure 4.6(c). The rate of loading was maintained as 0.7 N/mm^2/min until the specimen fails. The flexural strength of the specimen is calculated as follows

$$F_b = \frac{P \times L}{b \times d^2} \quad \textbf{4.3}$$

in which 'a' is greater than 133 mm, or

$$F_b = \frac{3P \times a}{b \times d^2} \quad \textbf{4.4}$$

in which 'a' is less than 133 mm but greater than 110 mm. Where, 'F_b' is flexural strength in MPa, 'P' is failure load in newtons, 'a' is the distance measured on the tension side of the specimen between the line of fracture and the nearest support in mm, 'b', 'd' are the width and depth of the specimen in mm, and 'L' is length of span in mm. Flexural strength is calculated as the average of three similar specimens.

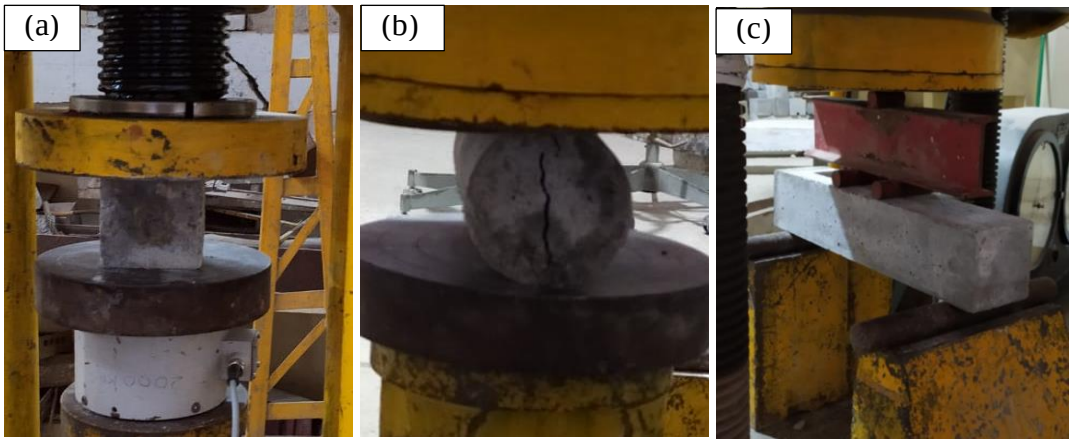

Figure 4.6 Test setup for strength properties a) Compressive strength, b) Split tensile strength, c) Flexural strength

4.5.1.5. Static modulus of elasticity

The static elastic modulus was evaluated in accordance with ASTM C469-14. This test method is meant for the evaluation of elastic chord modulus of moulded concrete cylinders subjected to longitudinal compressive stress. Experimental set up to determine static modulus of elasticity is shown in Figure 4.7. The load was applied monotonously without any shock at a rate of 250±50 kPa/s. Longitudinal deformations in cylindrical specimen corresponding to the load applied were recorded using data acquisition system (DAC) system connected with LVDTs and load cell. Elastic chord modulus has been calculated from the ratio of the change in compressive stress and longitudinal strain at two points. The first point is when the longitudinal strain is 0.000050 mm/mm and the second point is when the load is 40% of ultimate load. The average of at least three replicate specimens was considered. Modulus of elasticity is calculated as follows

$$\boldsymbol{E = \frac{(S_2 - S_1)}{(\varepsilon_2 - 0.000050)}} \qquad \textbf{4.5}$$

Where, 'E' is chord modulus of elasticity in MPa, 'S_1' is the stress in MPa corresponding to longitudinal strain ε_1 (0.000050), 'S_2' is stress at 40% of ultimate load, and ε_2 is longitudinal strain corresponding to stress S_2.

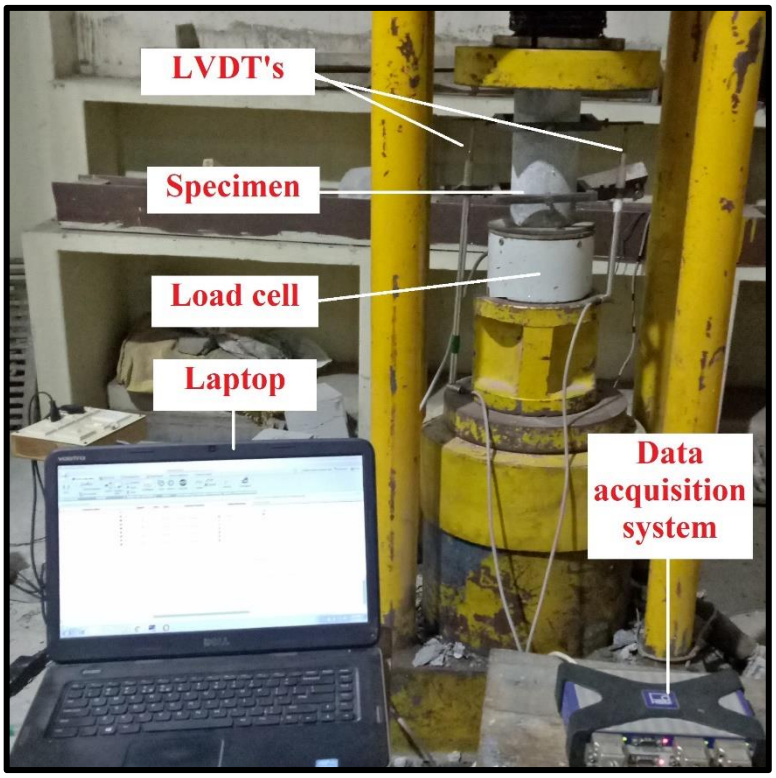

Figure 4.7 Experimental set up for static test

4.5.2. Dynamic mechanical properties

The prismatic beam specimens of size 100mm x 100mm x 500mm were cast for all percentage variations of GO for both the grades of concrete to investigate their fundamental natural frequency, damping ratio in free–free condition. Fundamental resonant frequencies were measured according to ASTM C215-19. In order to measure the dynamic characteristics of standard and high-grade concrete, 30 prisms were cast and tested.

All the prismatic beams were tested using impact hammer technique by using FFT dynamic analyser. The experimental set up for dynamic testing is shown in Figure 4.8. The basic test set-up and configuration consist of dynamic analyser connected with an impact hammer fitted with a forced transducer used to excite the specimen and piezoelectric accelerometer was used for measuring the response to the given excitation. The frequency response functions (FRFs) were obtained which is a ratio of output

response to the input excitation. All the data obtained from input and output devices was stored on the computer and can be accessed in required format for curve fitting. The FRFs were obtained in the frequency range of interest 0-10 kHz in the present study.

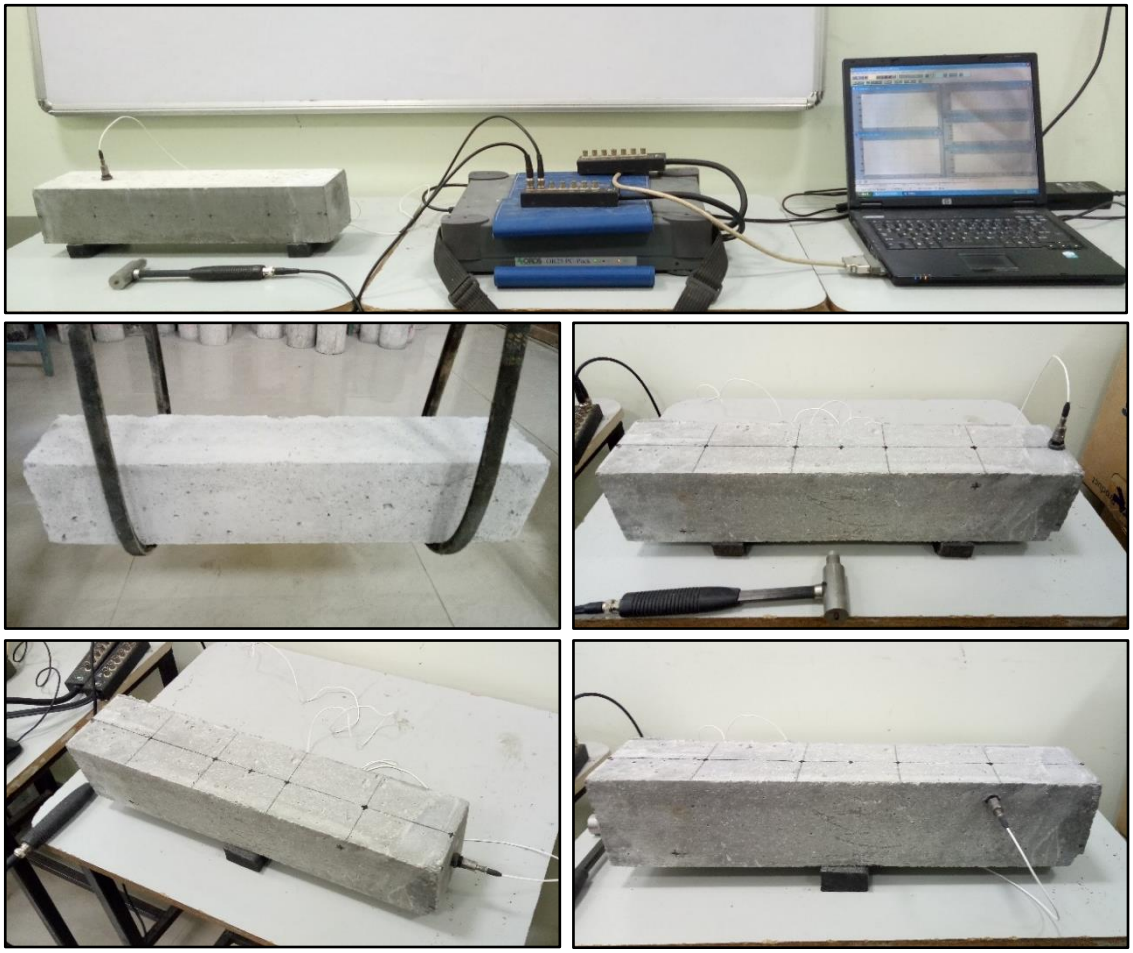

Figure 4.8 Experimental set up for dynamic test

4.5.2.1. Modal analysis

Modal analysis is a process of describing dynamic characteristics of the system and is carried out using impact hammer test with FFT dynamic analyser. Schematic representation of experimental set up for modal analysis is shown in Figure 4.10. All the beams were tested under free condition with excitation points marked on the surface of the test specimen, the accelerometer was placed at one of the points while the beam was excited at all the points using impact hammer, this is called roving hammer technique.

For curve fitting the FRFs received from the dynamic analyser, the data was transferred to the modal analysis smart office software. Modal parameters like natural frequency, damping ratio and mode shapes were extracted from the curve fitted FRFs, as shown in Figure 4.9.

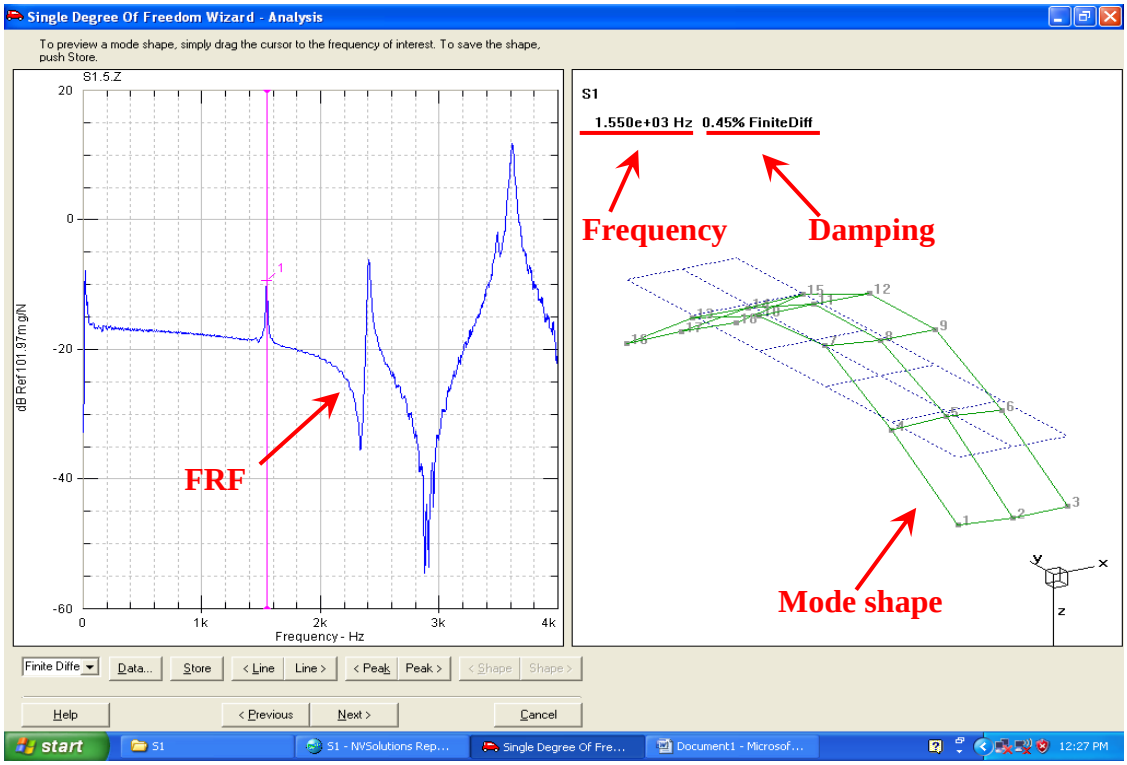

Figure 4.9 Typical frequency response function with first mode shape

4.5.2.2. Dynamic parameters

The dynamic parameters such as dynamic elastic modulus, rigidity modulus and poisson's ratio were evaluated by measuring the fundamental transverse, longitudinal and torsional resonant frequencies of test specimens in accordance with ASTM C215-19. In the impact or impulse resonance method, the fundamental resonant frequencies are measured using either the transverse, longitudinal or torsional mode of vibration, depending on the dimensions of the specimens and impact point on the specimen. The boundary conditions for the specimens changed depending on the mode of vibration. The various boundary conditions in each mode of vibration are shown in Figure 4.11. The position of impact

hammer and direction of striking are depending on the boundary conditions of the specimen and mode of vibration. The accelerometer was positioned on the specimen at one specified point to receive the response while vibrating the structure at the particular node, as shown in Figure 4.11. Dynamic elasticity modulus, rigidity modulus and poisson's ratio of concrete are evaluated from the following relationship

$$\textbf{Dynamic elasticity modulus, } E_d = CM(n)^2 \qquad \textbf{4.6}$$

$$\textbf{Dynamic rigidity modulus, } G_d = BM(n'')^2 \qquad \textbf{4.7}$$

$$\textbf{Dynamic poisson's ratio, } \mu = (E_d/2G_d)-1 \qquad \textbf{4.8}$$

Where 'M' is mass of the specimens in kg, 'n' is transverse mode of fundamental resonant frequency in Hz, 'n"' is torsional mode of fundamental resonant frequency in Hz, 'C' is $0.9464(L^3T/bt^3)$ in m^{-1}, 'B' is (4LR/A) in m^{-1}, 'L', 'b', 't' are length, width and depth of the specimens in m, 'T' is correction factor, 'R' is shape factor equal to 1.183, and 'A' is specimen cross-sectional area in m^2.

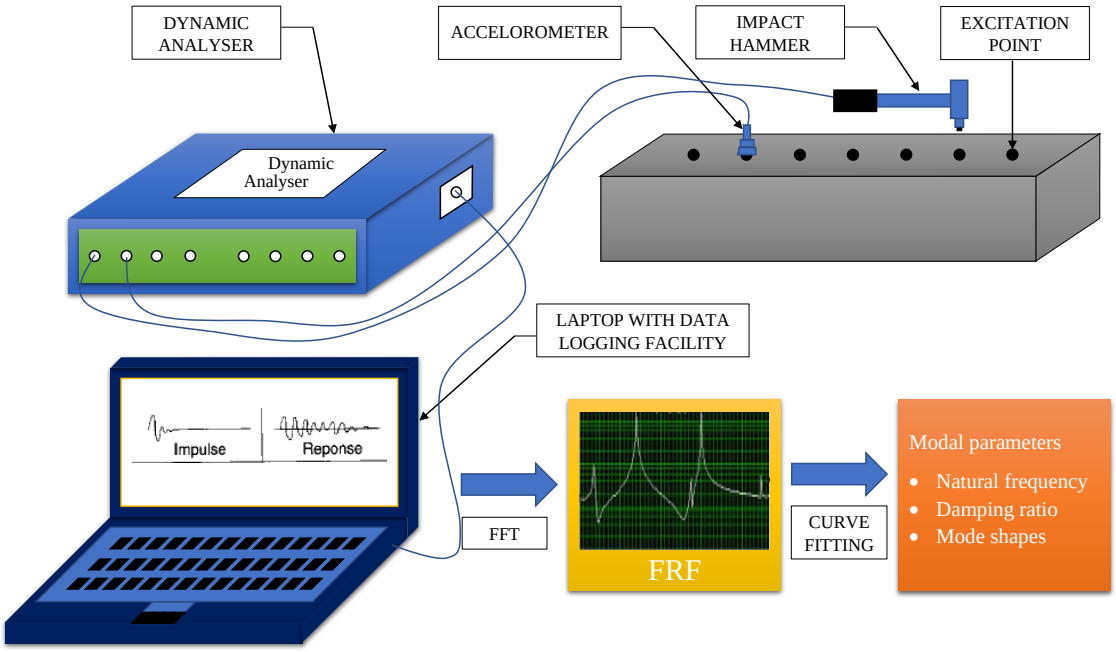

Figure 4.10 Schematic representation of experimental set up for dynamic testing

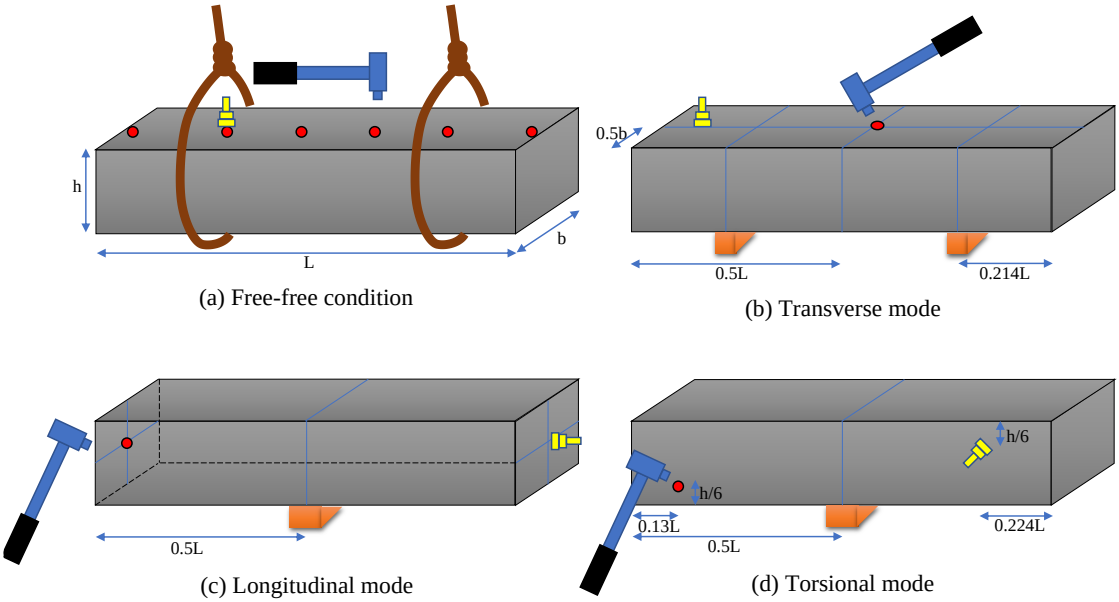

Figure 4.11 Boundary Conditions for Impact hammer test a) Free-free condition, b) Transverse mode, c) Longitudinal mode and d) Torsional mode

4.5.2.3. Ultrasonic pulse velocity (UPV) test

Ultrasonic pulse velocity test was conducted on a prismatic beam with dimensions 100 x 100 x 500mm in accordance with IS:13311(Part 1)-2018 at 28-day curing age. An electro-acoustical transducer generates the ultrasonic pulse, which was transmitted and received by the transducers placed on opposite side of the specimen. The principle of evaluating concrete quality in terms of homogeneity, uniformity and density is that greater velocities indicate good quality, but lower velocities may indicate concrete with more internal flaws or voids. In IS:13311(Part 1) standards, UPV ranges are specified for quality of concrete.

The dynamic elasticity modulus (E_d) of concrete is determined using following relation with the pulse velocity and dynamic Poisson's ratio (μ) given in IS:13311(Part 1) -2018.

$$E_d = \rho V^2 f(\mu) \quad \textbf{4.9}$$

$$f(\mu) = \frac{(1+\mu)(1-2\mu)}{(1-\mu)} \quad \textbf{4.10}$$

E_d is dynamic elastic modulus in MPa, ρ is density in kg/m^3 and V is pulse velocity in m/s. Dynamic Poisson's ratio value ranges between 0.20 to 0.35, with an average value of 0.24. Nevertheless, it is desired to measure it independently based on the type of concrete. The dynamic poisson's ratio can be evaluated by measuring the pulse velocity (V) of concrete beams along with the length (l) and fundamental resonant frequency (n) in longitudinal mode of vibration. The factor $f(\mu)$ is determined from these measurements using the relation:

$$f(\mu) = \frac{(2nl)^2}{V^2} \qquad \textbf{4.11}$$

4.5.3. Microstructural characterization

4.5.3.1. Scanning electron microscope (SEM) and Energy dispersive X-ray spectroscopy (EDX)

Morphology and elemental composition of the concrete mixes were acquired using a high-resolution SEM coupled with EDX equipment (Tescan, Vega 3 LMU), to understand the GO effect on microstructure. The samples of remanent pieces (about 10mm) were collected from the fracture surface of the concrete cubes tested under compression. A thin layer of gold-palladium was sputter-coated on sample prior to SEM imaging. As a result, multiple high-resolution images at various magnifications were attained. EDX patterns were obtained from the respective location in the SEM images to measure the elemental composition of hydrated products.

4.5.3.2. Xray diffraction analysis (XRD)

XRD was conducted using Panalytical X'Pert Pro X-ray diffractometer, at 45 kV in the range of $2\theta = 6°–80°$, CuKα radiation λ=1.54060 Å, divergence slit with fixed value 0.5°, size of step 0.008356 and time of step 10.8s, to identify the crystalline phases of the hydrated cement concrete with GO addition. The grounded samples passing through a 75-micron sieve of different concrete mixes prepared were used to investigate.

4.5.3.3. Fourier transform infrared spectroscopy (FTIR)

The formations of different hydration phases in the GO added cement concrete were determined through vibrational stretching modes of various molecular bonds by FTIR analysis using Bruker Alpha II compact FTIR spectrometer. with a spectral resolution of 4 cm^{-1}, 16 scans were recorded over the range of 4000–400 cm^{-1}. The grounded samples passing through a 75-micron sieve of different concrete mixes prepared were used to investigate.

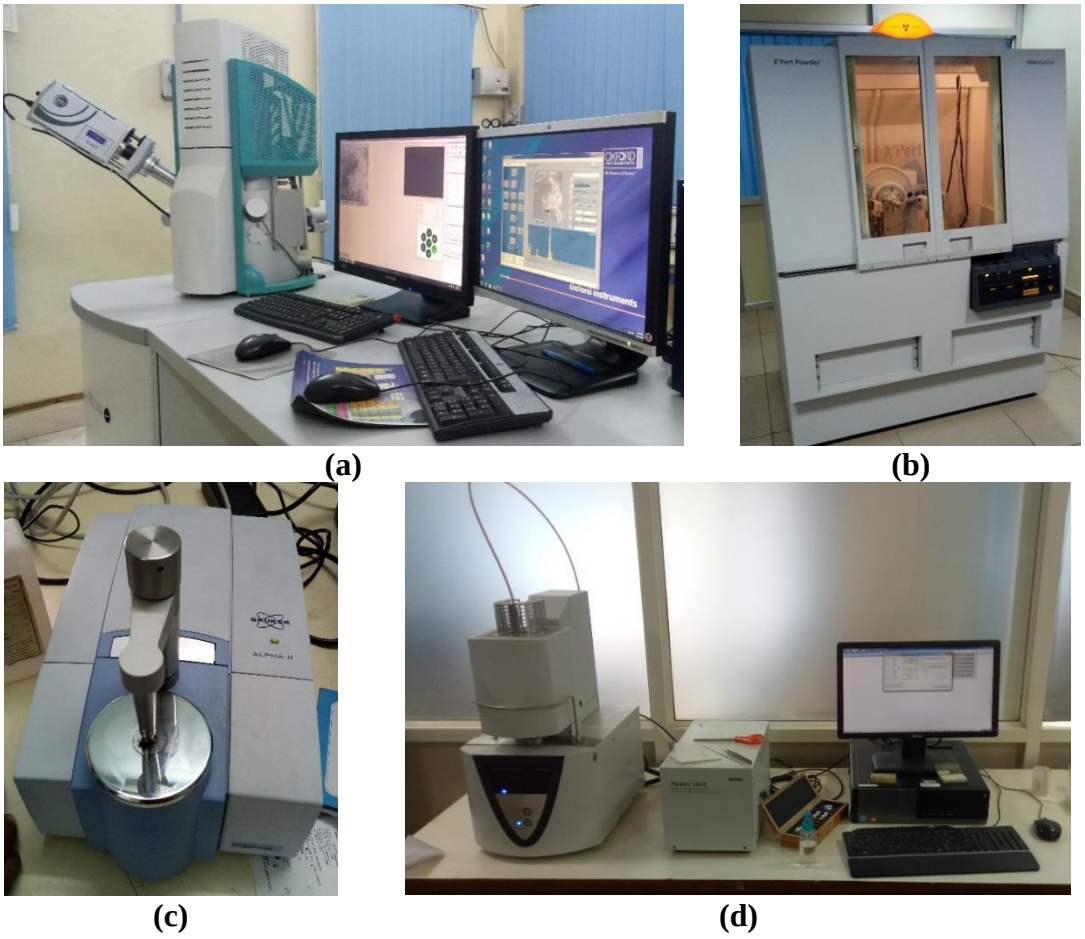

Figure 4.12 Microstructure characterization techniques (a) SEM & EDX, (b) XRD, (c) FTIR, (d) TGDTA

4.5.3.4. Thermogravimetric analysis (TGA)

A thermal gravimetric analyzer NETZSCH STA 2500 was employed for the analysis, to study the effect of GO addition on hydration characteristics of concrete matrix. Thermal analysis was conducted on the concrete powder samples passing through 75-micron sieve after 28 days of curing. About 30 mg of samples were heated from room temperature to 850 °C at a rate of 10 °C.min^{-1} under the nitrogen atmosphere for each test.

4.5.4. Durability characteristics

4.5.4.1. water absorption

Water absorption test was conducted in accordance with ASTM C642. Specimens used for the test were a disc of size 100mm dia and 50mm height cut from the cylindrical specimens of 100mm x 200mm. Three specimens from each concrete mix were tested at 28 days of curing and the mean values were considered.

4.5.4.2. Sorptivity

This test gives information on penetration of water by capillary pores from the surface of concrete that has been exposed to water. Disc specimen of size 100 mm dia and 50 mm thick were prepared and conditioned in accordance with ASTM C 1585 at a curing period of 28, 56, and 90 days. After drying the sample at 50±5 °C in the oven until mass difference between two consecutive readings of sample is less than 0.1%, it was placed on a desiccator to prevent atmospheric moisture absorption. To prevent evaporation from the surface not exposed, the circumference surface of disc was coated with epoxy and covered with polyethene sheets. Weight of the specimen was measured prior to immersing them in water, as shown in Figure 4.13. Weight of the specimen was measured using a stopwatch at intervals of 1, 5, 10, 20, 30, 60 minutes, and every hour up to 6 hours. Slope of the line drawn that is the best fit between water absorption and square root of time was used to calculate sorptivity (mm/√s) of concrete mixes. Initial rate of absorption is calculated as follows

$$I = \frac{m_t}{a \times d} \qquad \textbf{4.12}$$

Where, 'I' is initial rate of absorption in mm, 'm_t' is change in specimen weight in grams at the time 't', a is area of the specimen exposed to water in mm^2, and 'd' is water density in g/mm^3.

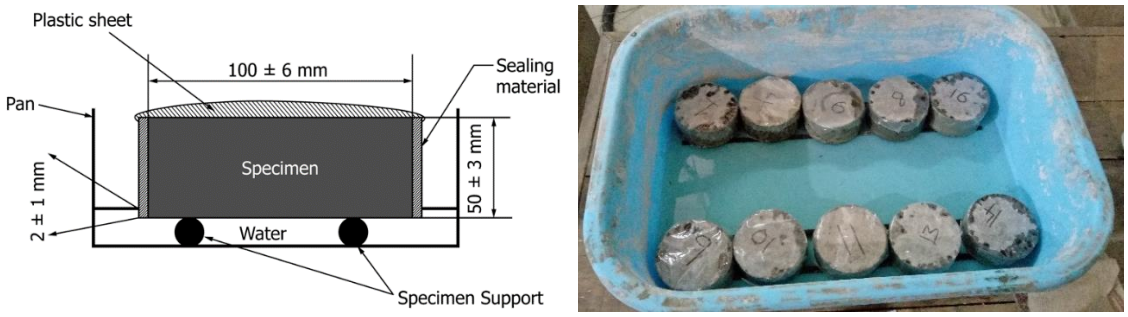

Figure 4.13 Sorptivity test setup

4.5.4.3. Accelerated carbonation

Three concrete cubes of size 100×100×100mm were cast for each concrete mix and cured for 28 days in water. After conditioning the concrete cubes in a ambient temperature for 14 days, the top, bottom, and two opposite side faces are sealed. The cubes are placed in a storage chamber once all but two faces have been sealed. In accelerated carbonation test, carbonation depth was determined after 500 hours of accelerated carbonation at 4 (V/V) % CO_2 at 27 °C temperature and 60% relative humidity. The test was carried out in accordance with ISO 1920-12:2015. To determine the carbonation depth, 1% phenolphthalein solution was sprayed on cut portions of specimen. Because of the phenolphthalein indicator, the carbonated portions retained colourless, whereas the uncarbonated areas coloured pink. After 24 hours of phenolphthalein spray, the carbonation depth was evaluated at ten different points and the average depth was determined using a measuring scale.

4.5.4.4. Acid attack

Resistance to acid attack was determined by casting the 100×100×100mm cubes for each concrete mix. In order to determine the acid attack resistance, cubes were placed in water curing for 28 days. Cubes were then immersed in sulfuric acid and hydrochloric acid solutions at 5% concentration by volume for 28, 56 and 90 days to continuously expose them to an acidic environment. The effect of acidic environment on specimens was generally evaluated by measuring change in size (specimens solid diagonals), weight, and compressive strength. The acidic resistance was measured by evaluating strength loss, weight loss and dimension loss of the specimens measured after they were submerged in acidic solution for 28, 56 and 90 days. The acid attack tests were carried out in accordance with ASTM C1898-20.

4.6. Concluding remarks

In this chapter, material properties and mix proportions for the development of GO reinforced concrete composite and GO reinforced fly ash based concrete composite were discussed. Dispersion of nanomaterial, procedures for casting of specimens and curing were also discussed. Testing methods used for the measurements of static and dynamic mechanical properties, durability properties and microstructural characterization were also discussed in detail.

CHAPTER 5
PHASE-I: GRAPHENE OXIDE REINFORCED CEMENT CONCRETE

5.1. General

The properties and performance of GO reinforced cement concrete under static and dynamic mechanical properties, microstructural characteristics and durability properties are presented in this chapter and the results are discussed in two parts. First part focused on evaluation of static mechanical characteristics such as compressive strength, split tensile strength, flexural strength and elastic modulus of GO reinforced concrete. In addition to that, dynamic properties such as natural frequency, damping ratio and mode shapes have also been determined. The microstructural characterization has been done using SEM, EDX, XRD, FTIR and TGDTA. The second part consists of assessment of durability performance of GO reinforced cement concrete by conducting water absorption, sorptivity, accelerated carbonation, rapid chloride penetration and acid attack tests. The results of GO reinforced cement concrete were compared with control concrete. The nomenclature of the mix ID's and Dosage of GO added in concrete are presented in Table 5.1.

Table 5.1 The nomenclature and GO dosages of concrete mixes

S. No.	GO (%)	Mix Designation	
		Standard concrete (SC)	High strength concrete (HSC)
1	0.00	SC-GO-0.00%	HSC-GO-0.00%
2	0.05	SC-GO-0.05%	HSC-GO-0.05%

S. No.	GO (%)	Mix Designation	
		Standard concrete (SC)	High strength concrete (HSC)
3	0.10	SC-GO-0.10%	HSC-GO-0.10%
4	0.15	SC-GO-0.15%	HSC-GO-0.15%
5	0.20	SC-GO-0.20%	HSC-GO-0.20%

5.2. Static mechanical properties

5.2.1. Workability

The slump values of concrete mixes with varying GO content are presented in Figure 5.1. It is observed that for both the grades of concrete mixes, slump values decreased with the GO addition and further decreased with the rise in GO dosage. The reduction in slump values with the addition of GO at 0.05%, 0.10%, 0.15% and 0.20% are recorded as 8%, 12%, 15% and 19% for standard concrete and 9%, 14%, 18% and 23% for high strength concrete, respectively, in comparison with the control concrete. Accordingly, the observations revealed that the GO addition to the concrete reduces the fluidity. Whereas the influence of GO on fluidity in standard concrete is less compared to high strength concrete. Comparable results were reported for cement paste incorporated with GO, showing an improvement in viscosity and a decrement in fluidity with the increase in GO content (Gong et al. 2015; Shang et al. 2015). This is attributed to the huge specific surface area of GO which absorbs more amount of water molecules and resorts in more water demand for cement composites with GO (Shang et al. 2015). The GO influence in the reduction of slump was less in standard concrete, as the quantity of water in standard concrete is more compared to high strength concrete. It is concluded that with an increase in GO content, the water demand rises tremendously, resulting in a negative impact on the fluidity of concrete mix.

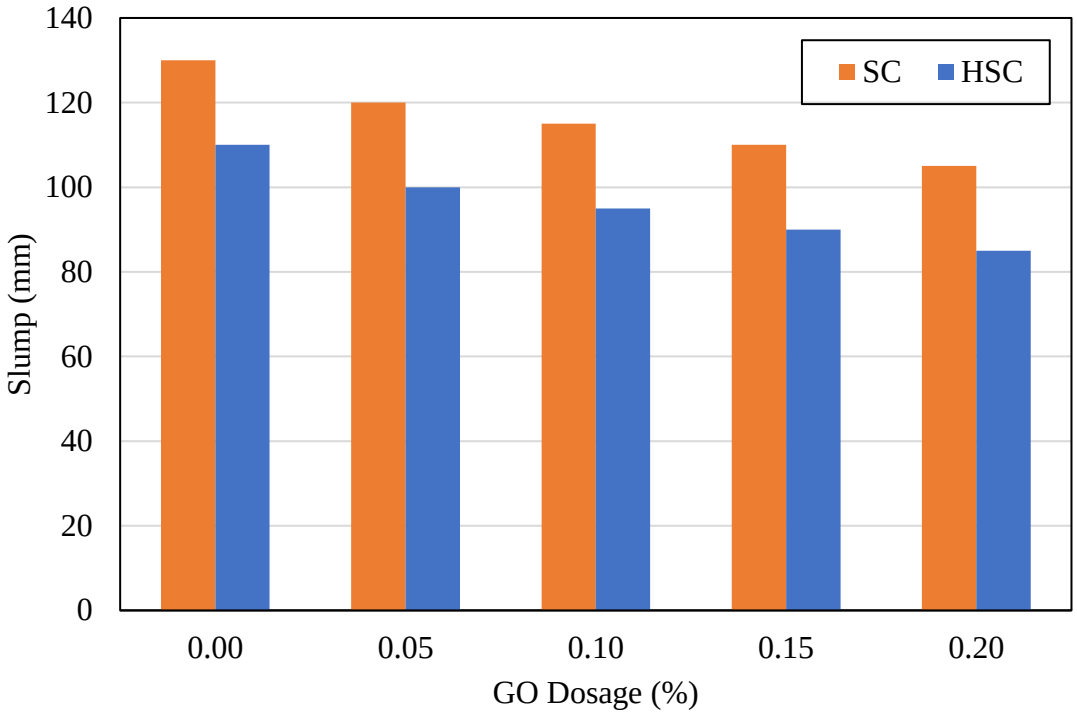

Figure 5.1 Slump values of GO-cement concrete

5.2.2. Strength properties

The variations in strength properties of concrete with varying GO contents for both grades of concrete are shown in Figure 5.2, 5.3, and 5.4. It is observed that the compressive, split tensile and flexural strength of the concrete are first increased and then decreased with reference to increase in GO content. This trend is observed for both standard concrete and high strength concrete, and for both curing ages. The most apparent compressive, split tensile and flexural strength values 60.5MPa, 3.52MPa and 8.10MPa for standard concrete and 86.0MPa, 5.41MPa and 10.80MPa for high strength concrete, respectively were observed at the age of 28 days for 0.15% GO content. The results also demonstrated that the incorporation of GO enhanced the strength properties of concrete. Highest values of the strength properties were found at a GO content of 0.15% for both grades of concrete. Increase in strength properties up to 0.15% GO content could be related to the GO influence on the hydration process, densification of microstructure and pore structure refinement of cement composites (Gong et al. 2015). The drop in the increase of strength

properties was observed with the increase in GO content in the range of 0.15%-0.20%, this may be associated with two reasons. First, the GO content is higher because the interlayer Van der Waals force of GO tends to agglomerate and GO dispersion within the concrete composite becomes difficult, thus leading to the degrading GO effect on the cement hydration process (Chuah et al. 2018). Second, GO consists of huge specific surface area and high surface energy, which has a great capacity to absorb greater amount of water, resulting in more demand for water content in GO–cement composites (Pan et al. 2015). Also, agglomerated GO absorbs more quantities of water, which leads to non-uniform w/c ratio, inhomogeneous dispersion of hydrated phases of cement, and less influence on the increase of strength properties of cement concrete.

It can be noticed that the influence of GO on the growth rate of strength properties is greater at early ages (7 days) compared to the later ages (28 days) for both grades of concrete. The increase rate in compressive, split tensile and flexural strength values for concrete with 0.15% GO was 60.6%, 31.1% and 26.3% at the age of 7days, 44.4%, 28.1% and 24.4% at the age of 28days, respectively for standard concrete, whereas for high strength concrete, 53.1%, 29.1% and 23.7% at the age of 7days, and 26.5%, 21.4% and 20.0% at the age of 28days, respectively. This may be associated with the hydration process and formation of more crystal structures of hydrate products takes place in concrete during the early-stage of hydration, so the rate of strength improvement of control concrete is higher at early ages (Lv et al. 2013). As GO expedites the hydration process, the growth of strength properties is more at early ages. When the hydration process of cement at its final stage, the rate of interaction decreases due to a reduction in oxygenated functionalities present on the GO. Therefore, the GO influence on growth rate of strength properties decreases with age. The associated concrete performance will be stable and the influence of GO will be less at later ages.

It can also be noticed that for standard concrete at 28 days, the highest values of compressive, split tensile and flexural strengths increased by 44.4%, 28.1% and 24.4%, respectively, for standard concrete compared to control concrete. Yet, it is worth noticing that for high strength concrete at 28 days, the maximum values of the compressive, split tensile and flexural strengths increased by 26.5%, 21.4% and 20.0%, respectively, the

percentage values being even lower than those of standard concrete. This could be due to more quantity of water absorbed by GO, which decreases the hydration process (Pan et al. 2015). The standard concrete consisting of a w/c ratio of 0.45 is higher compared to high strength concrete, which consists of a w/c ratio of 0.30. Thus, standard concrete with a more w/c ratio offers adequate free water and therefore, the GO effect is more in expediting the hydration process. Also, within the cement matrix to facilitate the dispersion of GO, a higher w/c ratio is required.

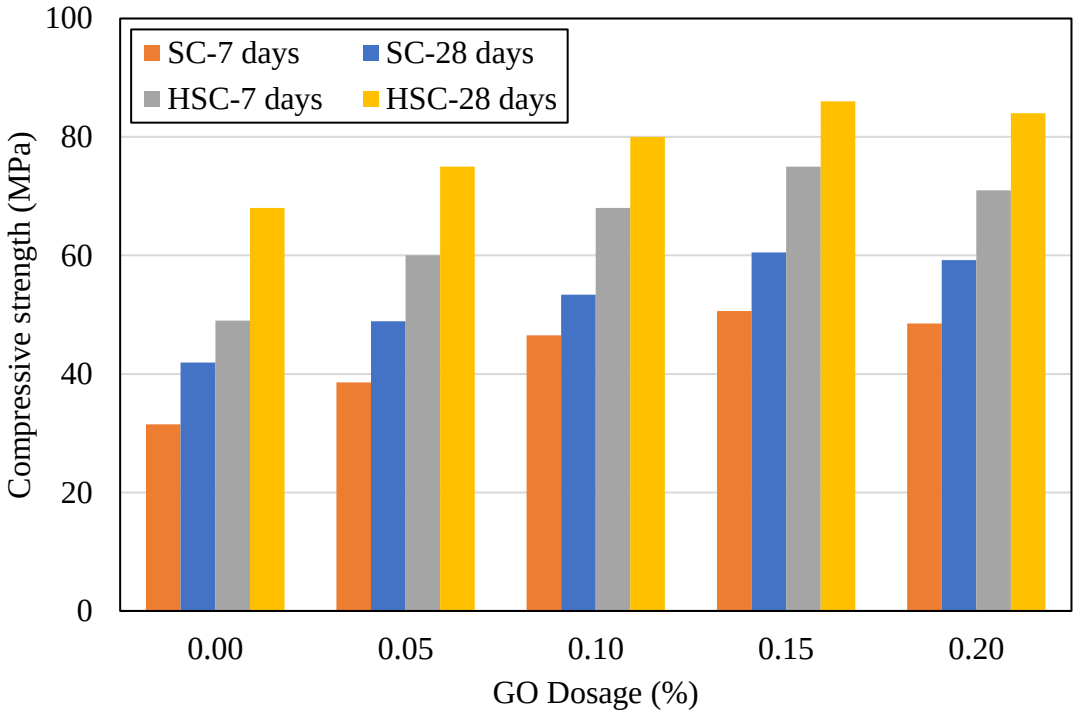

Figure 5.2 Compressive strength of GO-cement concrete

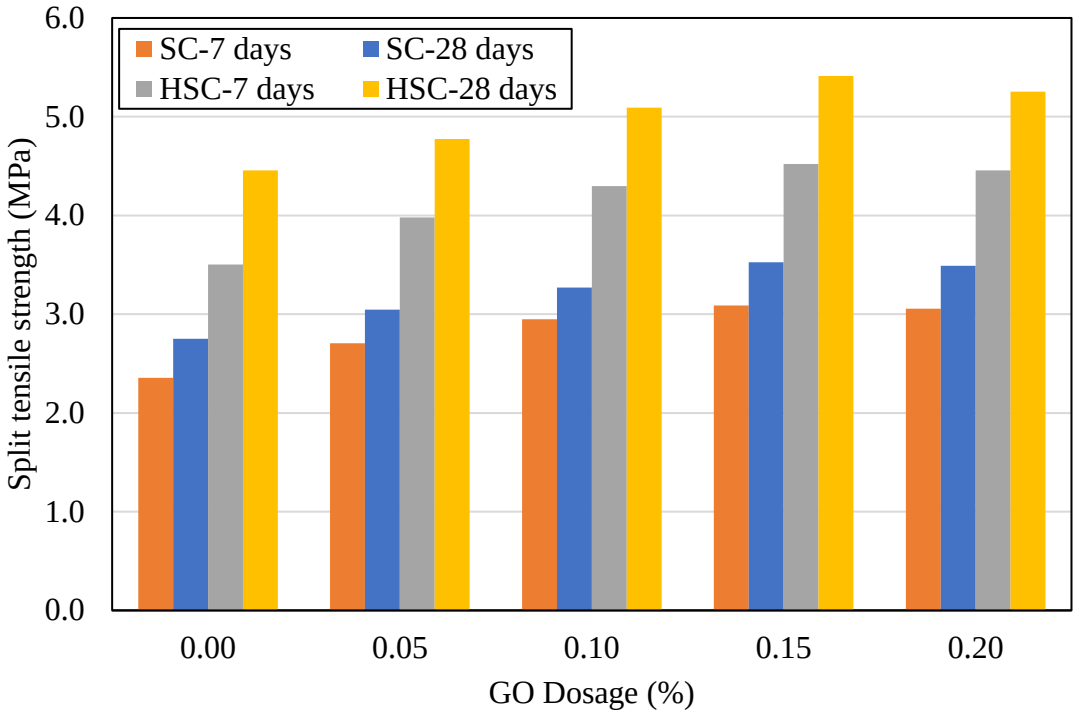

Figure 5.3 Split tensile strength of GO-cement concrete

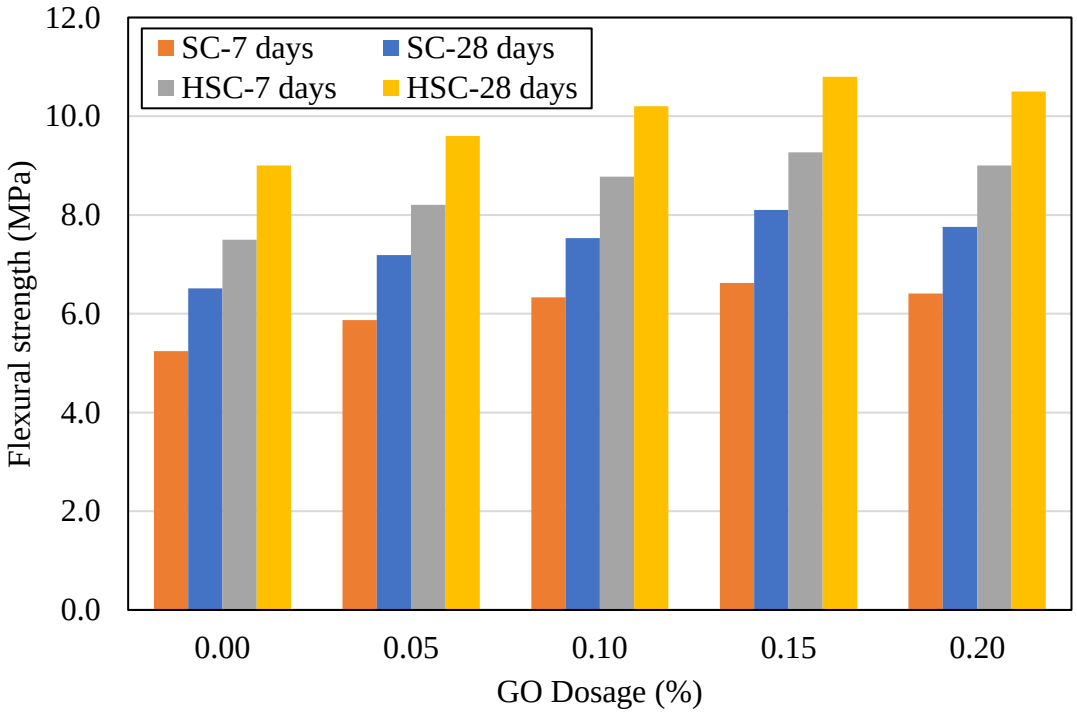

Figure 5.4 Flexural strength of GO-cement concrete

5.2.3. Static modulus of elasticity

The Stress-strain relationship of standard and high strength concrete with different GO dosages are shown in Figure 5.5 and 5.6. Elastic chord modulus of the standard concrete and high strength concrete containing various dosages of GO are shown in Figure 5.7. Elastic modulus of the concrete incorporated with GO was greater than the control concrete similar to the observations made for the compressive strength. This suggests that GO addition improved the elastic modulus of concrete. The concrete containing GO dosages 0%, 0.05%, 0.10%, 0.15% and 0.20%, the elastic modulus was 28.46, 30.95, 34.48, 36.63 and 35.90 GPa for standard concrete, and 37.48, 39.78, 41.86, 44.20 and 43.69 GPa for high strength concrete, respectively. The improvement in elastic modulus of concrete containing GO at a dosage of 0.05%, 0.10%, 0.15% and 0.20% was 8.75%, 21.13%, 28.69% and 26.13% for standard concrete, and 6.13%, 11.68%, 17.93% and 16.55% for high strength concrete, respectively, compared to that of concrete without GO. The addition of 0.15 % GO led to a substantial improvement in elastic modulus. As a result, GO addition is beneficial for improving the elastic modulus of concrete. However, with a GO dosage of 0.20%, elastic modulus of concrete decreased, which may be attributed to the high porosity and poor GO dispersion in concrete matrix. Based on the variation of the elastic modulus, the optimum content of GO in concrete is observed as 0.15%. The youngs modulus of concrete is mainly governed by three phases such as aggregate, cement paste and interfacial transition zone. The introduction of GO could amplify the hydration rate and improves the microstructure of cement composites (Long et al. 2018; Z. Lu et al. 2016). Additionally, the incorporation of GO to cementitious composites may produce a denser interfacial transition zone (Z. Lu et al. 2016). As a result, the incorporation of GO may improve resistance of concrete to elastic deformation.

According to the findings of static properties, incorporating GO into the concrete at a concentration of 0.20%, which is greater than the optimal GO dosage, resulted in a considerable reduction in mechanical characteristics when compared to the optimum concentration. This is consistent with the findings of Long et al. (2018). When GO is incorporated at higher dosage, it agglomerates owing to its huge specific surface area and

strong intermolecular interactions, such as the van der Waals force. As a result, the GO becomes less dispersed within the concrete mixture. Due to this, incorporating GO into concrete at a higher dosage than the optimal content considerably reduced the mechanical characteristics.

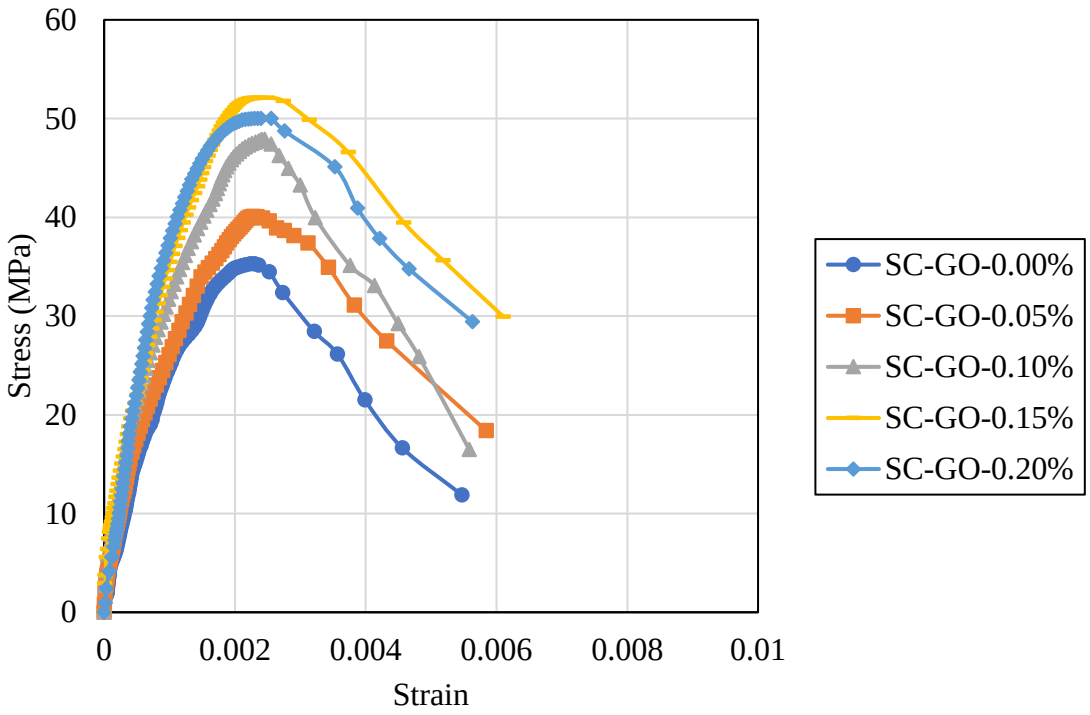

Figure 5.5 Stress-strain behaviour of standard concrete with different GO dosages

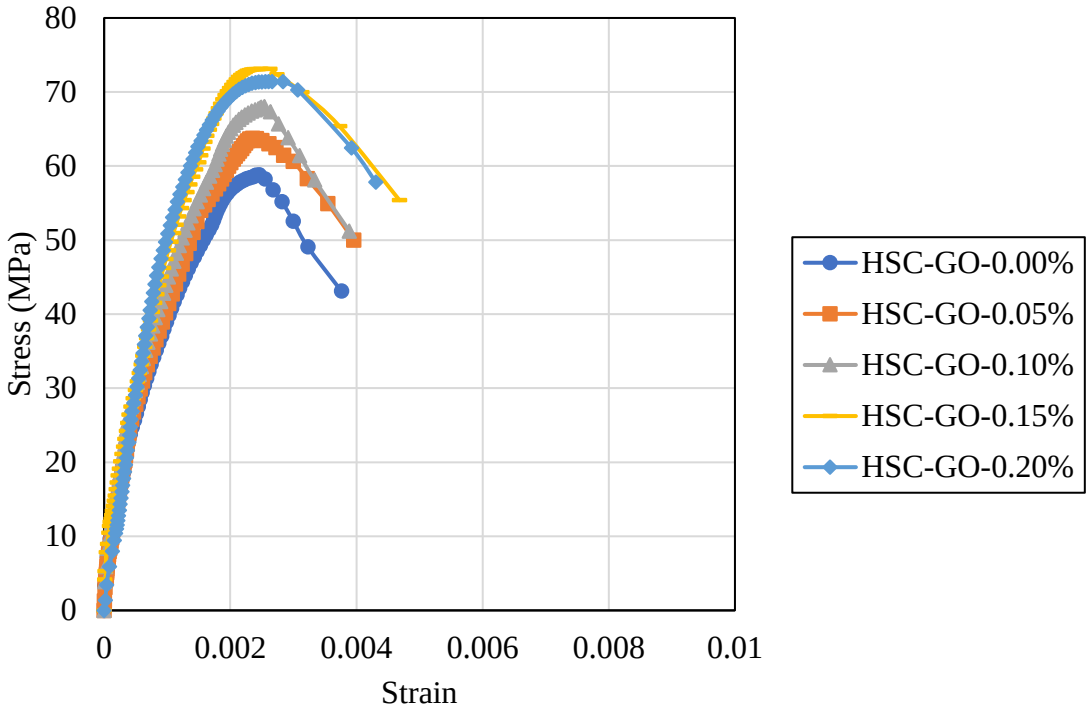

Figure 5.6 Stress-strain behaviour of high strength concrete with different GO dosages

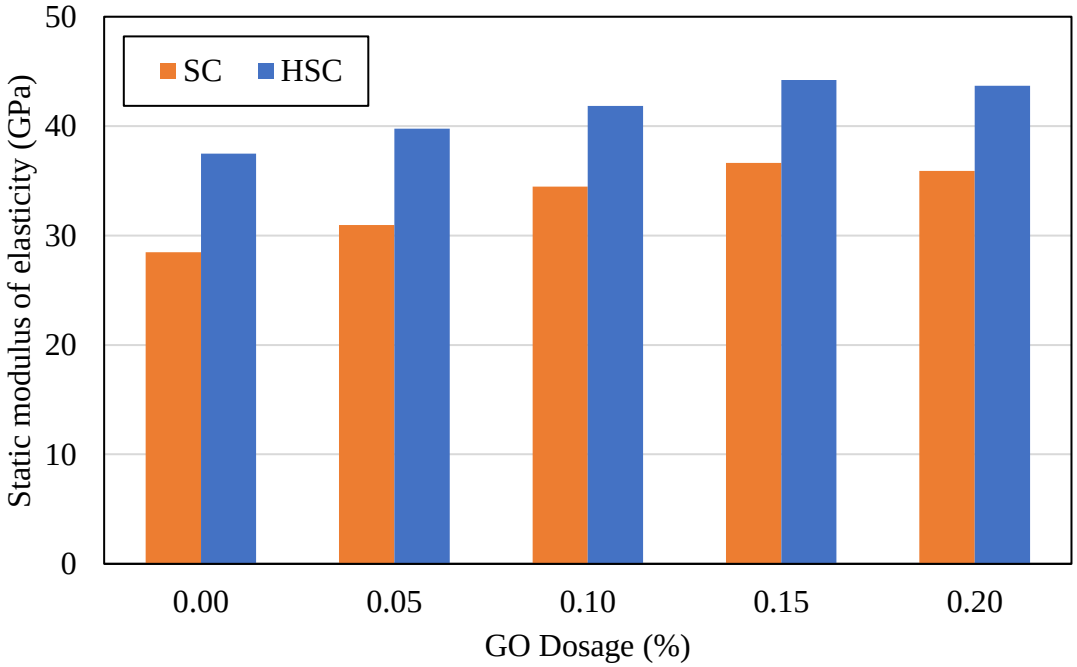

Figure 5.7 Static young's modulus of different cement concrete mixes

5.3. Dynamic mechanical properties

5.3.1. Natural frequencies (ω) and damping ratios (ζ)

Natural frequencies, damping ratios and different mode shapes of all concrete mixes were obtained from the frequency response functions using impact hammer technique and the results are shown in Table 5.2. Frequency response functions of standard concrete and high strength concrete with varying dosages of GO are shown in Figure 5.8 and 5.9. Different mode shapes for transverse vibration are shown in Figure 5.10. Typical acceleration time curves for different vibration modes are shown in Figure 5.11. From the results it is found that the fundamental natural frequencies of concrete prismatic specimens increased for both grades of concrete with the addition of GO content up to 0.15% compared to the control concrete, whereas the damping ratio was decreased. Thus, the GO addition is helpful for increasing the frequencies and decreasing the damping ratios of concrete. It was observed that the maximum increased fundamental natural frequencies were about 8.0% and 6.0% for the standard and high strength concrete with the GO dosage 0.15% compared to the fundamental natural frequency of control concrete. Maximum reduction in damping ratio was 29.1% and 26.3% for standard and high strength concrete with the GO dosage 0.15% compared to control concrete.

Concrete is a composite material comprises of several phases and non-uniform components such as numerous pores and irregularities in the phases at the microcosmic level, as well as numerous interfaces and pores within and between the elements at the meso-level. These imperfections and interfaces are the sources of damping energy. Under external force, there is non-uniform stress distribution not just among aggregates but also between cement paste and aggregates. Because of the non-uniform stress distribution, the composites may exceed the yield limit and experience plastic deformation. This cause relative motion between surfaces, which results in permanent energy loss. The elastic modulus of nano particles differs from that of the concrete matrix. Varying elastic moduli increase nonuniform stress distribution, which easily leads to plastic deformation to dissipate energy. The increase in total number of interfaces and enhancement of non-

uniform stress distribution both contribute to an increase in the damping (Zou, Liu, and Teng 2009).

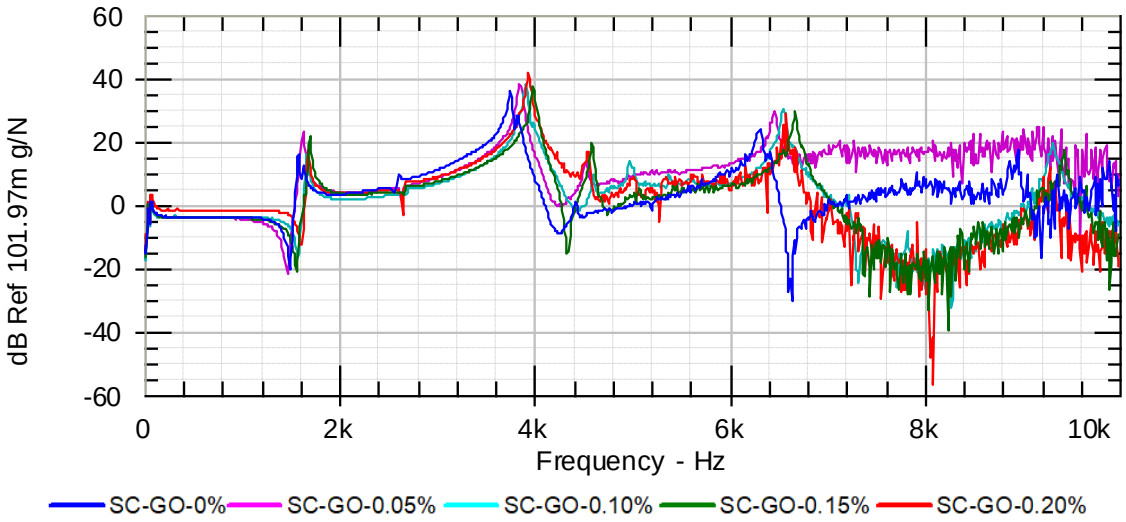

Figure 5.8 Frequency response function of standard concrete with different GO dosages

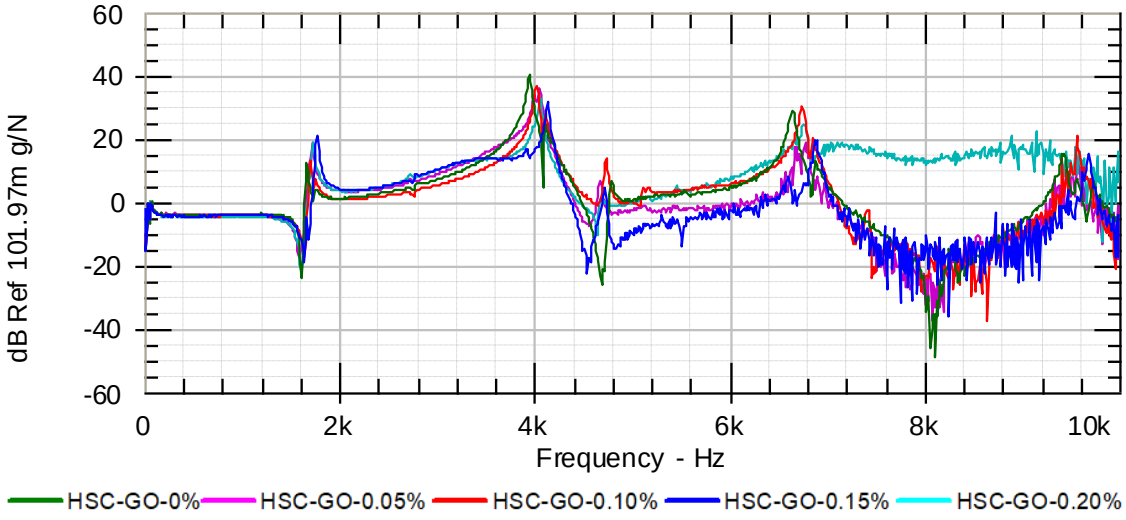

Figure 5.9 Frequency response function of high strength concrete with different GO dosages

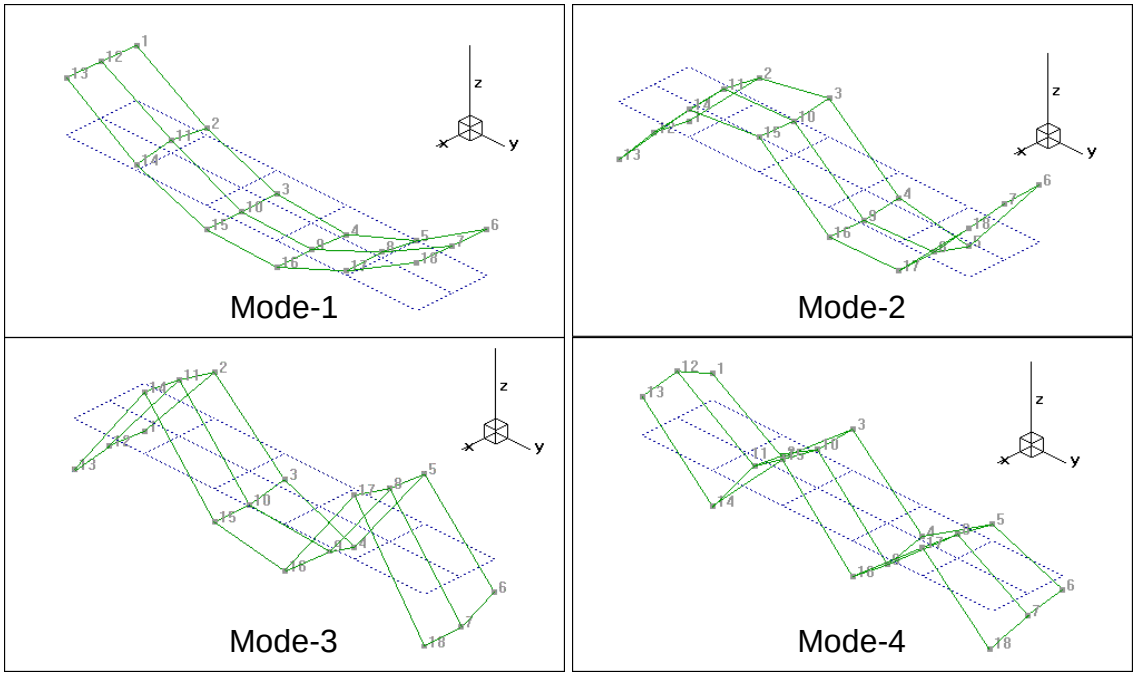

Figure 5.10 Typical mode shapes of transverse vibration

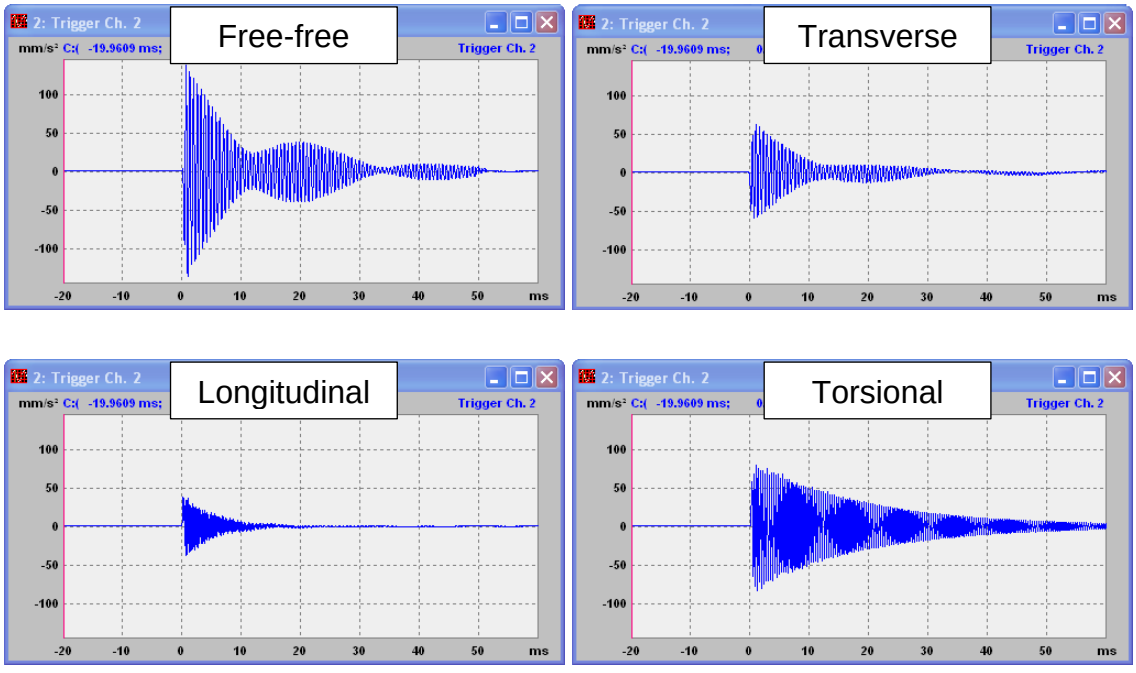

Figure 5.11 Typical acceleration time curves for different vibration modes

Table 5.2 Natural frequency (ω) and damping ratio (ζ) for first four modes of all concrete mixes

GO (%)	Frequency (Hz)				Damping ratio			
	Mode-1	Mode-2	Mode-3	Mode-4	Mode-1	Mode-2	Mode-3	Mode-4
Standard concrete (SC)								
0.00	1578	3746	6314	8956	0.86	0.53	0.43	0.32
0.05	1632	3858	6465	9177	0.81	0.47	0.41	0.3
0.10	1668	3914	6558	9291	0.76	0.44	0.35	0.29
0.15	1704	3995	6674	9425	0.61	0.41	0.34	0.26
0.20	1678	3946	6598	9320	0.68	0.43	0.34	0.28
High strength concrete (HSC)								
0.00	1663	3950	6648	9422	0.76	0.56	0.35	0.28
0.05	1703	4022	6745	9523	0.64	0.42	0.34	0.24
0.10	1721	4053	6780	9571	0.58	0.39	0.32	0.23
0.15	1763	4139	6890	9691	0.56	0.37	0.29	0.22
0.20	1732	4056	6774	9588	0.56	0.42	0.31	0.22

5.3.2. Dynamic elastic modulus and poissons ratio

Fundamental transverse, longitudinal and torsional resonant frequencies were determined for all concrete mixes in respective directions according to ASTM C215. The dynamic characteristic values attained for all concrete mixes are presented in Table 5.3. The experimental results shown that the fundamental resonant frequencies of all vibration modes are increased in concrete with the addition of GO up to 0.15% dosage compared to control concrete for both the grades of concrete. The values of dynamic elastic modulus

and rigidity modulus have been determined from the fundamental transverse frequencies and torsional frequencies. The dynamic poissons ratio was also calculated and presented in Table 5.3. From the results, it can be clearly noticed that dynamic elastic modulus, dynamic rigidity modulus and poissons ratio of concrete was enhanced with the addition of GO. It was noticed that the maximum increased dynamic elastic modulus in concrete with the addition of GO dosage 0.15% was 17.1% and 12.8% for the standard and high-grade concrete respectively compared to concrete without GO.

The dynamic modulus of cement composite is associated with the dynamic characteristics and volume fraction of its cement matrix, as well as the volume of voids (Long et al. 2018). GO incorporation could expedite the rate of hydration and improve the pore structure of cementitious composites (Lv et al. 2014). Additionally, by promoting hydration process, GO could improve the density of hydration products and have healing effects on pores and microcracks in cementitious composites. As a consequence, the incorporation of GO nanosheets reduces capillary pores while increasing volume fraction of solid hydrated phases in cement matrix. Nevertheless, poor dispersion of GO particles in cementitious matrix has a negative impact on its porosity. The elasticity modulus of porous materials is widely accepted to decrease with the improvement in porosity (Long et al. 2018). As a result, the dynamic modulus of samples with GO dosages up to 0.15% improved as the GO dosage increased, however beyond 0.15% of the GO reverse tendency is observed.

Table 5.3 Dynamic youngs modulus and poisons ratio of different concrete mixes from fundamental resonant frequencies according to ASTM C215

GO (%)	Transverse frequency (Hz)	Longitudinal frequency (Hz)	Torsional frequency (Hz)	Dynamic elastic modulus $E_{d,TR}$ (GPa)	Dynamic rigidity modulus G_d (Gpa)	Dynamic poissons ratio μ_d
Standard concrete (SC)						
0.00	1578	4338	2575	46.69	19.61	0.19
0.05	1632	4475	2658	49.74	20.81	0.20
0.10	1668	4572	2698	51.75	21.36	0.21
0.15	1704	4685	2748	54.66	22.42	0.22
0.20	1678	4585	2718	53.22	22.02	0.21
High strength concrete (HSC)						
0.00	1663	4562	2685	51.86	21.32	0.22
0.05	1703	4667	2732	54.16	21.99	0.23
0.10	1721	4726	2755	55.09	22.27	0.24
0.15	1763	4826	2808	58.51	23.41	0.25
0.20	1732	4765	2765	56.70	22.79	0.24

5.3.3. Ultrasonic pulse velocity

UPV test was conducted to evaluate uniformity and homogeneity of concrete with the incorporation of GO. The quality of concrete was evaluated at 28 days and categorized in accordance with IS:13311(Part 1)-2018. Table 5.4 shows the ultrasonic pulse velocities of standard and high strength concrete with and without GO. According to the UPV values, the inclusion of GO resulted in the formation of excellent quality concrete with greater uniformity. The pulse velocity of concrete with 0.15% GO is 4995 m/s for standard concrete and 5308 m/s for high strength concrete. The increase in concrete

quality might be attributed to nano filler effect of GO, which densifies the microstructure of concrete matrix. Therefore, improvement in uniformity and homogeneity of concrete indicates the development in strength characteristics of concrete.

Dynamic elasticity modulus (E_d) of the concrete is also calculated from the pulse velocity and dynamic Poisson's ratio (μ_d) using the Equation 4.9 and 4.10, the results are given in Table 5.4. The dynamic Poisson's ratio was assessed using ultrasonic pulse velocity measurements on concrete prisms and the fundamental resonant frequency in longitudinal mode of vibration determined by an impact resonance test. The trend of dynamic elastic modulus and poissons ratio is comparable to that of compressive strength for both the concrete grades. These findings are consistent with the impact resonance test.

Table 5.4 Dynamic youngs modulus and dynamic poisons ratio of different concrete mixes from UPV values according to IS:13311(Part-1)

GO (%)	UPV (m/s)	Longitudinal frequency (Hz)	Dynamic elastic modulus $E_{d,UPV}$ (GPa)	Dynamic poissons ratio µ
Standard concrete (SC)				
0.00	4554	4338	47.05	0.19
0.05	4708	4475	49.86	0.20
0.10	4850	4572	51.84	0.21
0.15	4995	4685	55.09	0.22
0.20	4864	4585	52.98	0.21
High strength concrete (HSC)				
0.00	4859	4562	52.03	0.22
0.05	5040	4667	54.23	0.23
0.10	5133	4726	55.39	0.24
0.15	5308	4826	58.46	0.25
0.20	5192	4765	57.22	0.24

5.4. Microstructural characterization

5.4.1. Scanning Electron Microscopy

The SEM images of standard concrete and high strength concrete specimens with varying GO contents (0, 0.05%, 0.10%, 0.15% and 0.20%) are depicted in Figure 5.12 and 5.13. The microstructure of standard concrete without addition of GO depicted in Figure 5.12(a), it can be revealed that the growth of calcium silicate hydrate, calcium hydroxide and ettringite crystals, with large number of micro cracks and pores, forming a loose and non-uniform network structure. The SEM images of standard concrete specimens with the incorporation of GO shown in Figure 5.12(b-e) clearly representing that in the presence of GO, the hydration products are strongly interweaved with each other, having lesser number of microcracks and pores. The rise in GO content shows the formation of compact, uniform and densified microstructure related to concrete without GO. High strength concrete specimen without the addition of GO is shown in Figure 5.13(a) indicates that the crystallinity of hydrated phases reduced with less number of large pores and cracks, forming dense network structure comparative to the standard concrete. Whereas high strength concrete specimens with GO shown in Figure 5.13(b-e), indicates that almost no isolated hydration phases, also the structure was compact, uniform and C–S–H phase interwoven with other hydration phases for the formation of dense structure. Based on the changes observed from SEM images, it is representing that GO presence in concrete expedite the hydration process to form larger hydrates and offers more nucleation sites for hydration process, it is reliable with other investigations (Kang et al. 2019). Resulted in the formation of uniform and densified structure at micro level with reduced pores and microcracks, which may be responsible for the enhanced strength properties.

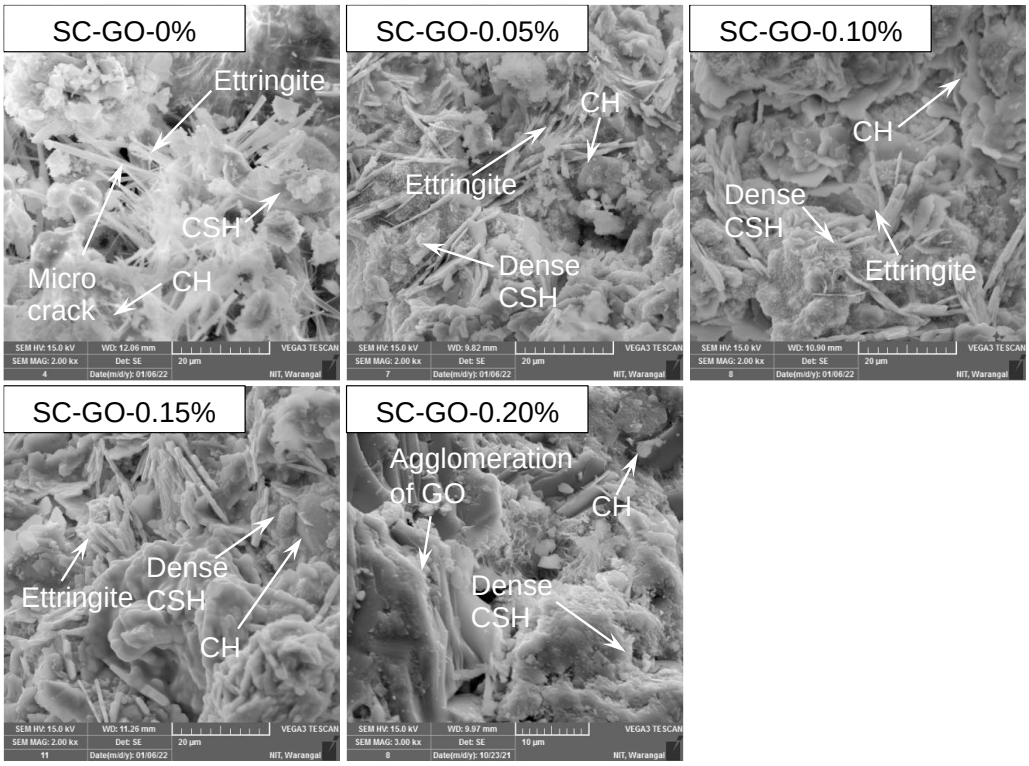

Figure 5.12 Microstructure of standard concrete with different GO content

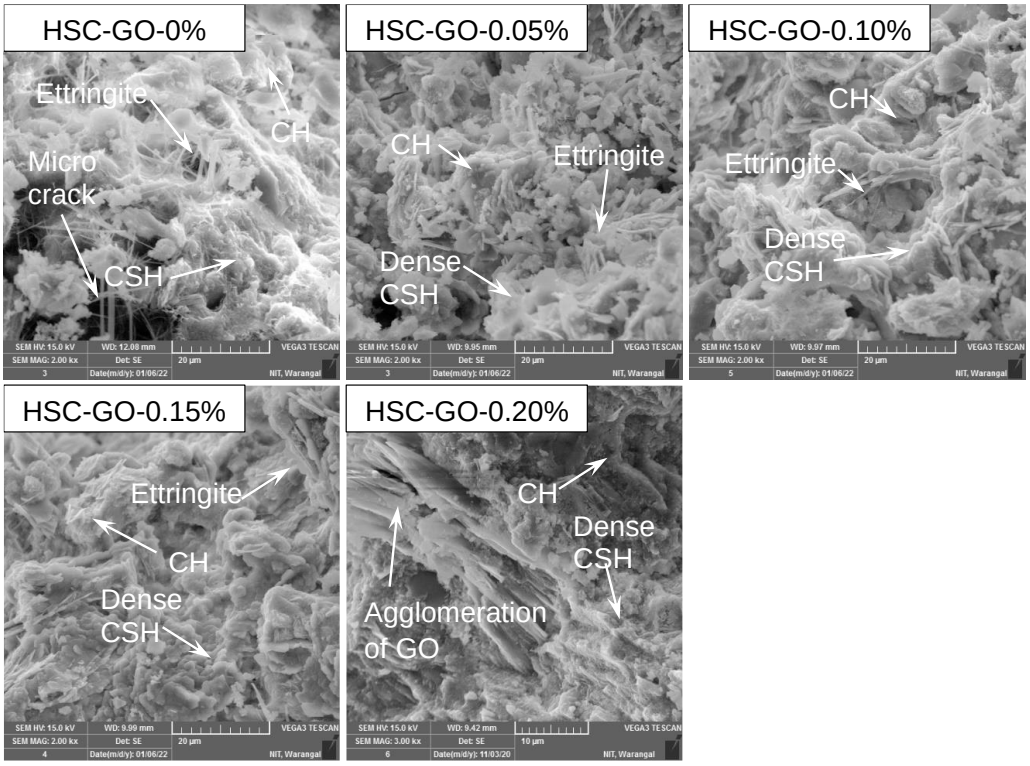

Figure 5.13 Microstructure of high strength concrete with different GO contents

5.4.2. Energy Dispersive X-Ray Spectroscopy

EDX method was used to analyse the elemental composition of hydration products from SEM images as shown in Figure 5.12 and 5.13. The following classification was used in this study so as to differentiate the hydrates with more amount of C-S-H phase from hydrates with more calcium hydroxide (CH) and monosulfates (AFm) (Kjellsen, Wallevik, and Fjällberg 1998).

$$\textbf{C-S-H: } 0.8 \leq Ca/Si \leq 2.5;\ (Al+Fe)/Ca \leq 0.2 \qquad \textbf{5.1}$$

$$\textbf{CH: } Ca/Si \geq 10;\ (Al+Fe)/Ca \leq 0.4;\ S/Ca \leq 0.04 \qquad \textbf{5.2}$$

$$\textbf{AFm: } Ca/Si \geq 4;\ (Al+Fe)/Ca > 0.4;\ S/Ca > 0.15 \qquad \textbf{5.3}$$

Analysis with compositions between these ranges were considered to represent hydrated phases of intermixed nature. The atomic ratio of Ca/Si, (Al+Fe)/Ca and S/Ca was analysed for all concrete mixes and presented in Table 5.5. In plain Portland cement pastes, the ratio of Ca/Si in C-S-H ranges from 1.2 to 2.3 with a mean of 1.75. The compact and densified microstructure is characterised by a low Ca/Si ratio due to formation of a stronger C-S-H network in cement matrix (Kunther, Ferreiro, and Skibsted 2017). Percentage atomic ratio of Ca/Si was quite high in control concrete, whereas incorporating GO in concrete decreased Ca/Si ratio and reduced with a rise in GO content. The same trend is observed for both the grades of concrete mixes. This indicates C-S-H and other hydration phases interwoven with each other and dense formation of phases during hydration of cement in the presence of GO (Kunther et al. 2017). This could be because of GO absorbs more quantity of water molecules, and turns into nucleation sites to hydrated phases, resulting in the formation of regulated and refined crystalline phases (Lv, Ma, Qiu, and Zhou 2013). This leads to tight mixture of GO and hydrated phases, and the development of a stable multiphase network structure, resulting improvement in microstructure and increase in strength properties of concrete (Lv et al. 2013).

Table 5.5 Percentage atomic ratios of different concrete mixes.

Mix	Standard concrete (SC)			High strength concrete (HSC)		
	Ca/Si	(Al+Fe)/Ca	S/Ca	Ca/Si	(Al+Fe)/Ca	S/Ca
GO-0.00%	2.44	0.16	0.15	1.77	0.14	0.13
GO-0.05%	2.14	0.17	0.07	1.42	0.19	0.02
GO-0.10%	2.10	0.18	0.06	1.26	0.20	0.02
GO-0.15%	1.70	0.21	0.02	1.05	0.21	0.01
GO-0.20%	1.94	0.20	0.07	1.12	0.24	0.01

5.4.3. X-Ray Diffraction Analysis

The XRD patterns of cement concrete with varying GO contents for different grades of concrete are shown in Figure 5.14 and 5.15. It can be observed that the most prominent peak indicated was crystalline phase of quartz positioned at 26.76° obtained from the sand. Besides, from the analysis of patterns the other peaks detected are calcium silicate hydrate (C-S-H), calcium hydroxide (CH) and trisulfoaluminate (AFt). According to the patterns, no appearance of change in peak positions of different GO contents in concrete mixes, suggesting that various GO contents in concrete exhibiting the identical crystals phases of hydrated products. The intensity of peak for C-S-H was positioned at 20.98°, 28.11° and 29.61°, CH was at 18.17°, 34.21°, 47.21° and 50.92° and AFt was positioned at 39.55°, 42.60°, 55.02° and 60.09° (Snehal, Das, and Akanksha 2020). The intensity of peak for C-S-H was observed to increase predominantly with the addition of GO and increased with rise in quantity of GO content compared to control concrete. Whereas, the intensity of peak for CH and Aft considerably increased with rise in GO content. The increase in intensity of peaks representing that GO addition has exhibited the increase in crystalline phases, which is confirming that the hydration process may be accelerated by GO and hence GO could support to generate more regular hydrated phases (Lv et al. 2013). Increase in peak intensity of high strength concrete samples is significantly lower

than the standard concrete may be due to the lower GO influence on the hydration process which was responsible for the lower rate of growth in strength properties. With the parameters outlined above, it can be concluded that GO expedited the hydration process, responsible for regulated and refined microstructure and hence improved the strength properties (Lv et al. 2013).

5.4.4. Fourier Transform Infrared Spectroscopy

The powder samples of different concrete mixes with varying GO dosages were also studied by the FTIR response, shown in Figure 5.16 and 5.17. The band region of 900–1100 cm^{-1} (Si-O asymmetric stretching vibration) characterizes the calcium silicate hydrate (C-S-H). It can be observed from IR spectra that the absorption peak of C-S-H shifts towards a higher wavenumber in GO presence with respect to the control concrete and observed to enhance with a rise in the GO content. This indicates the GO had influence on Ca/Si ratio and resulting in the formation of densified structure of hydrated products (Horgnies, Chen, and Bouillon 2013). This finding agrees well with the SEM, EDX, and XRD results. Further, it can be noted that the Calcium hydroxide was detected at a peak of 3643 cm^{-1} (O–H stretching vibration). The presence of trisulfoaluminate can be detected from the bands 857 cm^{-1} (Al-O stretching vibration), 1675 cm^{-1} and 3431 cm^{-1} (H_2O bending and stretching vibration) and monosulfate aluminates at 1400 cm^{-1} (asymmetric stretching of $[CO_3]^{2-}$) (Horgnies et al. 2013). The spectra of the standard concrete and high strength concrete samples with and without GO are identical patterns because of the similar formations of hydrated phases, apart from the positions of peaks and it might be due to incorporating GO into concrete expedite the hydration process and improves hydration products (Kang et al. 2019).

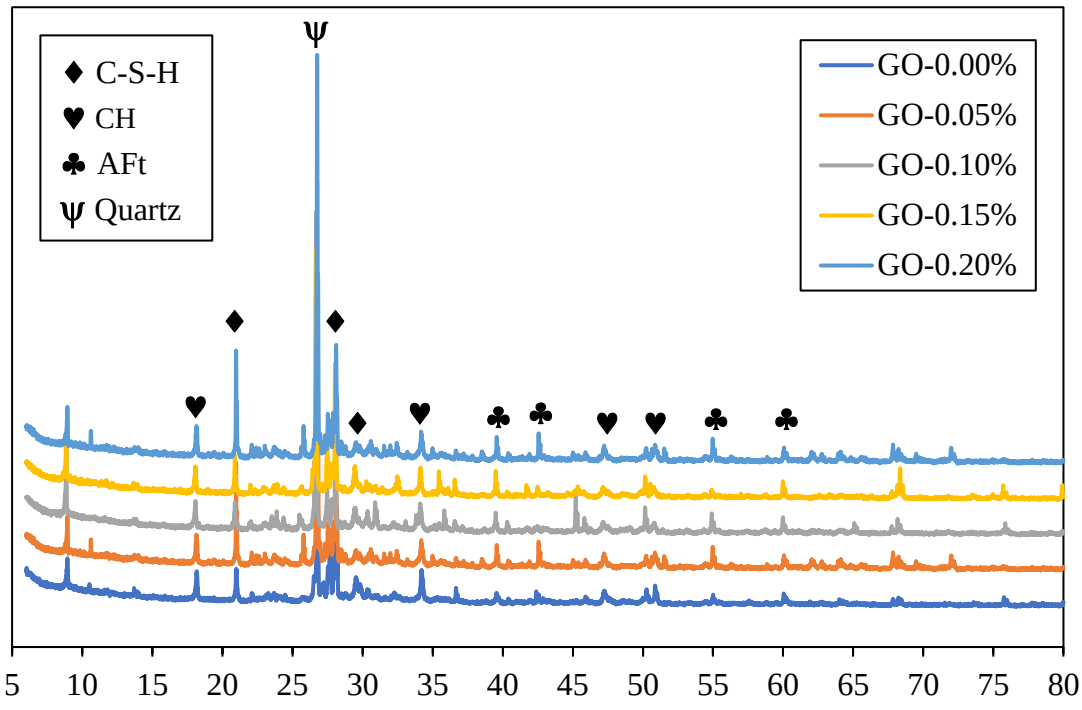

Figure 5.14 XRD patterns of standard concrete with different GO contents.

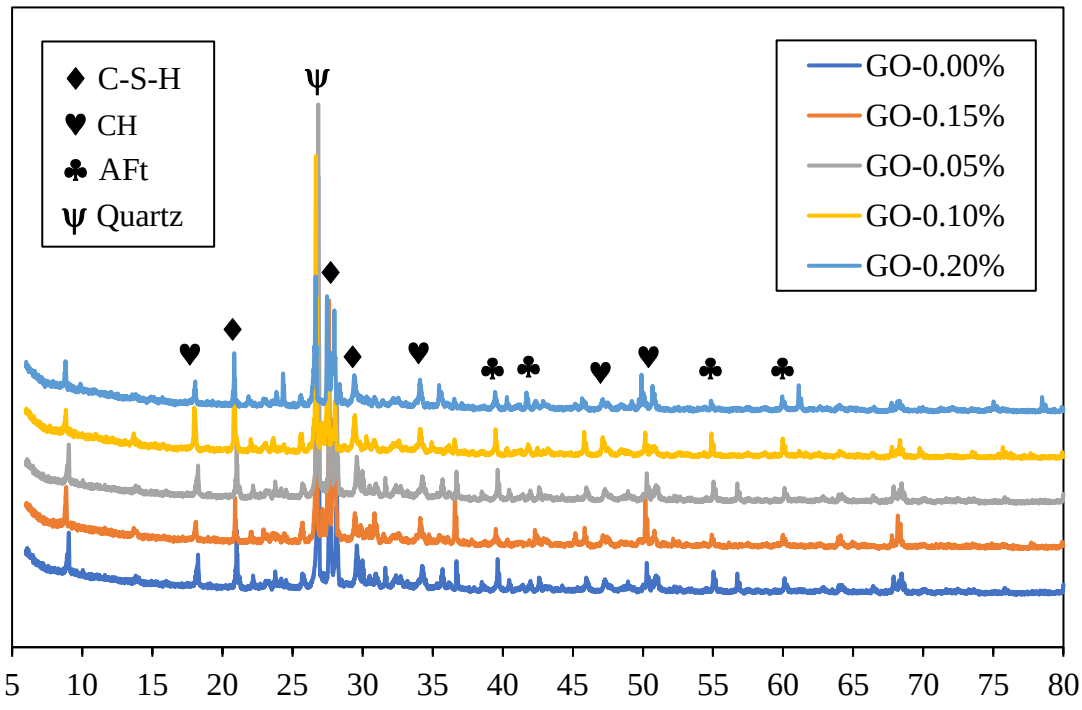

Figure 5.15 XRD patterns of high strength concrete with different GO contents.

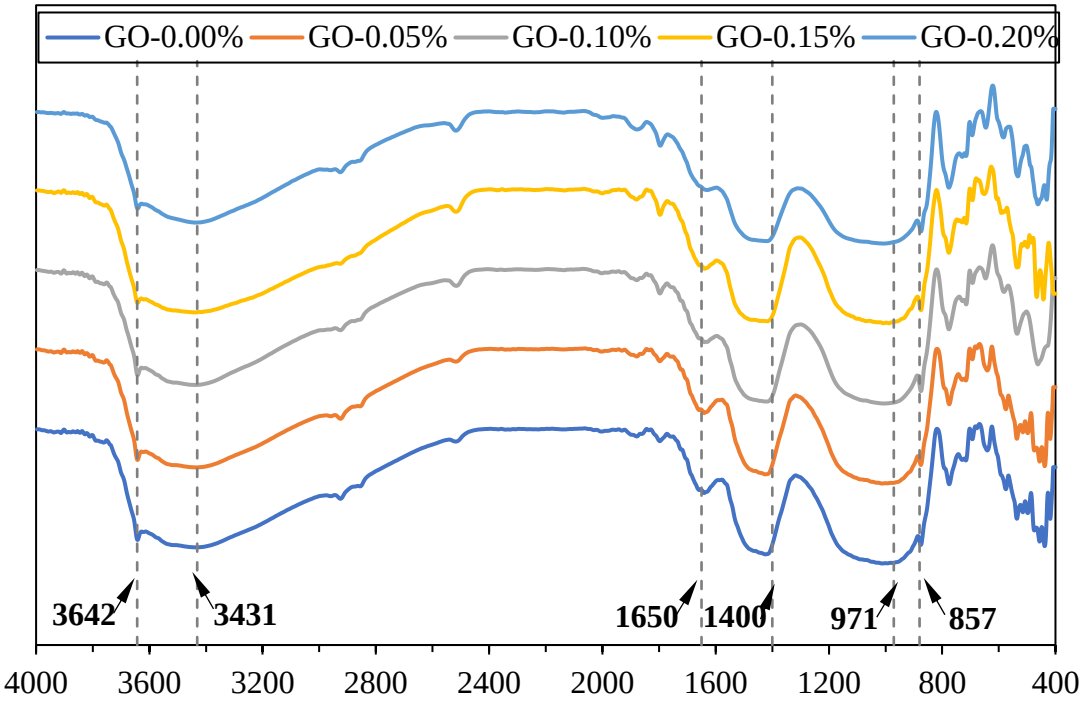

Figure 5.16 FTIR spectrum of standard concrete with different GO contents.

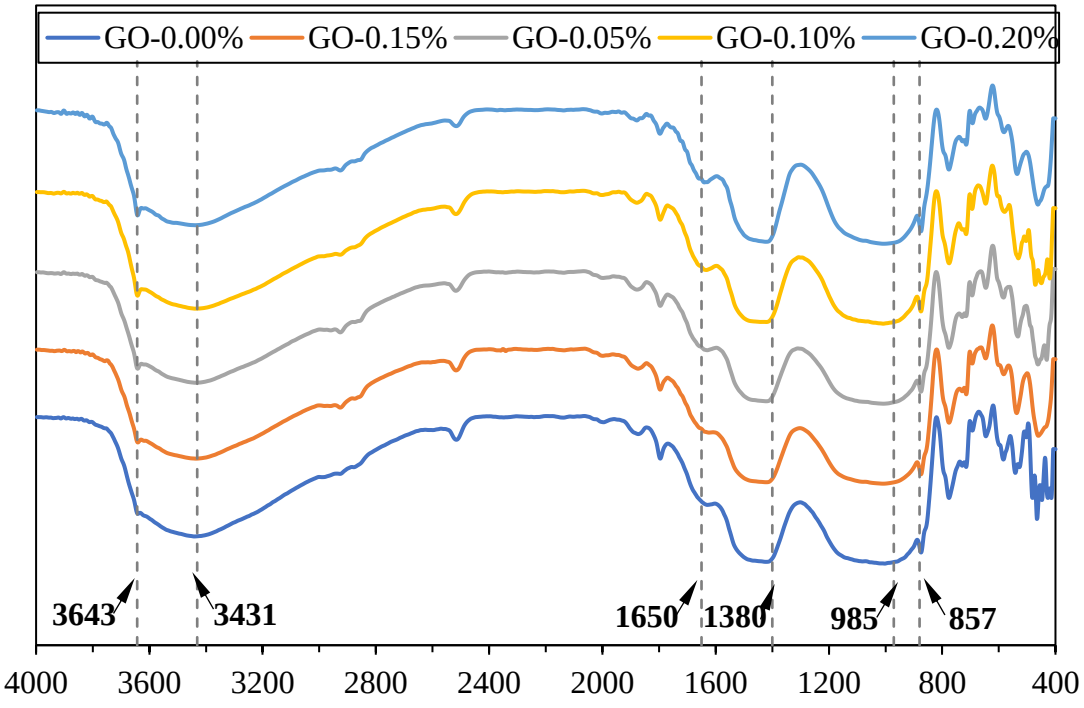

Figure 5.17 FTIR spectrum of high strength concrete with different GO contents.

5.4.5. Thermogravimetric Analysis

The thermal analysis test was conducted using NETZSCH STA 2500 to determine the thermogravimetric analysis (TGA) and the differential thermogravimetric (DTG) curves for all samples. The concrete specimens were grounded into powder at 28 days and the samples were heated at a heating rate of 10°C/min at temperatures ranges from 30°C to 850°C. The TGA and DTG results for standard and high strength concrete are shown in Figure 5.18 and 5.19. Furthermore, it is helpful to draw a DTG curve to understand the decomposition of each hydrated phase at specific temperature with the help of peaks. The temperature ranges of different phase transformations of the cement system considered in this study are as follow, the evaporable water at 30–105°C, the water loss from the decomposition of the C-S-H (dehydration, Ldh) at 105–400°C, dehydroxylation (Ldx) of the calcium hydroxide at 400–600°C, decarbonation (Ldc) of calcium carbonate at 600–850°C (Bhatty 1986; Deboucha et al. 2017).

Chemically bound water (CBW) and rate of hydration (α) are measured on the basis of mass losses noted in the TGA plots. The following equations were used for the calculations (Bhatty 1986; Deboucha et al. 2017) and presented in Table 5.6.

$$\mathbf{CBW = Ldh + Ldx + 0.41(Ldc)} \qquad \mathbf{5.4}$$

$$\mathbf{\alpha\ (\%) = CBW/0.24} \qquad \mathbf{5.5}$$

Mass loss caused by the decomposition of C-S-H gel was in the temperature range of 105°C–400°C (Deboucha et al. 2017). It can be noted that decomposition of C-S-H leads to an average mass loss of 9.28% and 12.48% for control concrete, whereas concrete with the incorporation of GO shows the mass loss of 9.55% and 13.13% at 0.05% GO dosage. As the dosage of GO gradually increased to 0.15%, loss of mass also increased to 9.94% and 13.53% for standard and high strength concrete, respectively. This representing a formation of C-S-H phase was increased in GO presence and increased with the rise in GO content. Hence, the concrete samples with GO were found to give a more strength compared to the control concrete. This finding agrees well with the SEM, EDX, and XRD results.

Similarly, the mass loss caused due to loss of water from calcium hydroxide (CH) was observed at 400°C–600°C. The calcium hydroxide phase quantification is evaluated using the Equation 5.6 (Kang et al. 2019) and shown in Table 5.6.

$$\boldsymbol{CH\ content}\ (\%) = \boldsymbol{mass\ loss\ of\ CH} \times \frac{\boldsymbol{molar\ mass\ of\ Ca(OH)_2}}{\boldsymbol{molar\ mass\ H_2O}} \qquad \textbf{5.6}$$

The values of rate of hydration and calcium hydroxide are shown in Figure 5.20. The measured quantity of the calcium hydroxide was 12.0% and 17.47% for control concrete, whereas concrete with the addition of GO at 0.05% was 12.49% and 17.90%. As the GO dosage increased to 0.15%, the quantity of calcium hydroxide was also increased to 12.99% and 18.50% for standard and high strength concrete, respectively. This is consistent with the observations of Yang et al. (2017) that the GO helps to produce more amount of hydration products. Therefore, the concrete with the incorporation of GO accelerates the degree of hydration.

Table 5.6 Chemically bound water (CBW), degrees of hydration (α) and calcium hydroxide (CH) for all concrete mixes.

Mix	Ldh (%)	Ldx (%)	Ldc (%)	CBW (%)	α (%)	CH (%)
SC-GO-0%	9.28	2.92	3.62	13.69	57.04	12.00
SC-GO-0.05%	9.55	3.04	3.90	14.19	59.14	12.49
SC-GO-0.10%	9.89	3.10	4.01	14.63	60.95	12.73
SC-GO-0.15%	9.94	3.16	4.20	14.82	61.76	12.99
SC-GO-0.20%	9.56	3.07	4.10	14.31	59.61	12.60
HSC-GO-0%	12.48	4.25	4.52	18.58	77.44	17.47
HSC-GO-0.05%	13.13	4.35	4.65	19.39	80.81	17.90
HSC-GO-0.10%	13.14	4.48	4.52	19.48	81.17	18.43
HSC-GO-0.15%	13.53	4.50	4.65	19.94	83.07	18.50
HSC-GO-0.20%	13.29	4.46	4.65	19.66	81.90	18.33

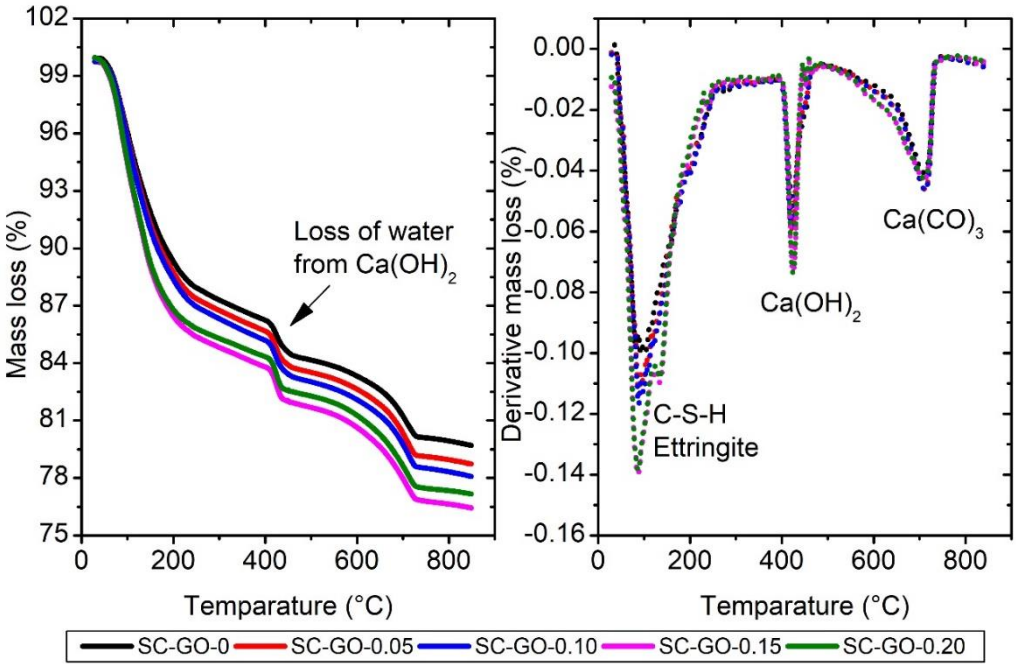

Figure 5.18 TGA and DTG analysis for standard concrete with different GO contents

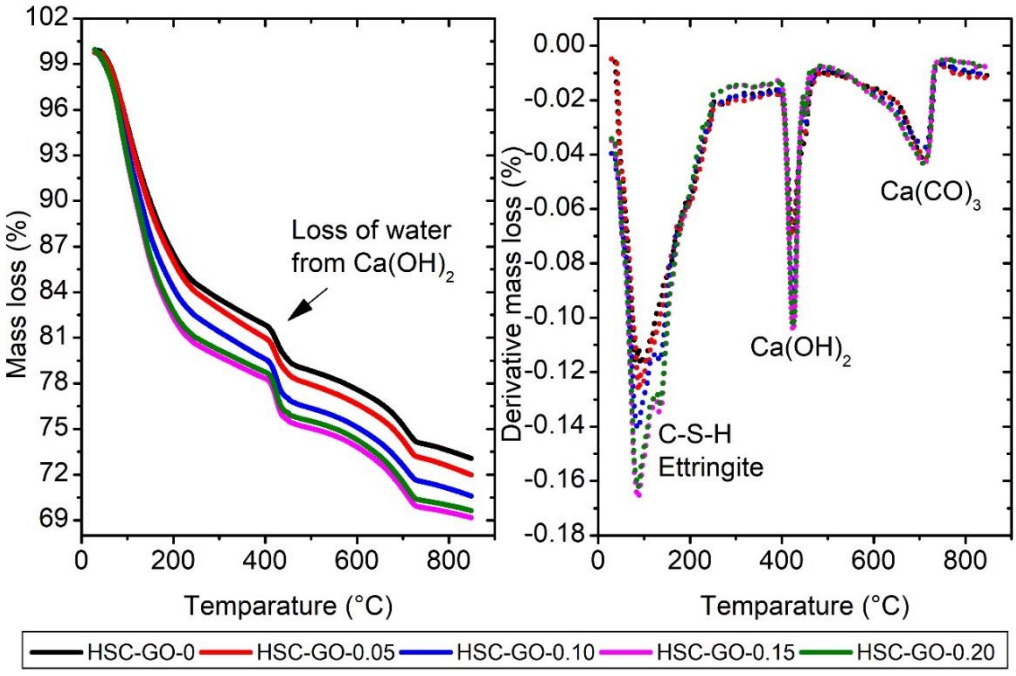

Figure 5.19 TGA and DTG analysis for high strength concrete with different GO contents

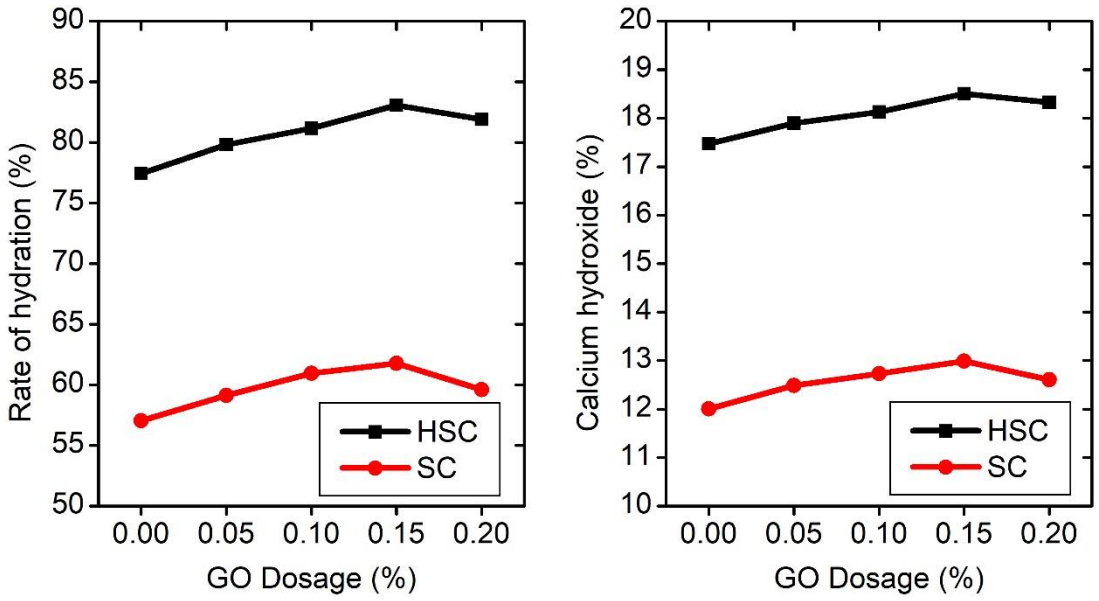

Figure 5.20 Rate of hydration and calcium hydroxide for standard and high strength concrete with different GO contents

5.5. Durability properties

5.5.1. Water absorption

Water absorption is an important test to assess concrete durability since it is an indirect indicator of water porosity. The water absorption test by immersion determines the difference in mass between a saturated surface dry sample and a dry sample. Water absorption by immersion in concrete mixes is primarily influenced by the parameters that govern concrete porosity. The water absorption values of concrete with varying GO contents for both the grades of concrete are shown in Figure 5.21. It is observed that GO incorporation in cement concrete was observed to be effective in resistance to water absorption mainly in concrete mixes with GO dosage up to 0.15%. The increase in GO dosage to 0.2% led to the decrease in resistance to water absorption. However, GO addition up to 0.2% exhibited a high resistance to the water absorption compared to control concrete. This trend is observed for both standard concrete and high strength concrete. The water absorption values with the addition of GO at 0%, 0.05%, 0.10%,

0.15% and 0.20% are recorded as 3.13%, 2.82%, 2.43%, 2.03% and 2.22% for standard concrete and 1.97%, 1.72%, 1.39%, 1.17% and 1.36% for high strength concrete, respectively. The enhanced resistance to water absorption may be attributable to broad barrier capabilities of GO and refinement of pore structure of the cement composites resulting from decrease in critical pore diameter. The decreased resistance to water absorption at 0.2% GO dosage can be due to GO sheets agglomeration in the cement composites.

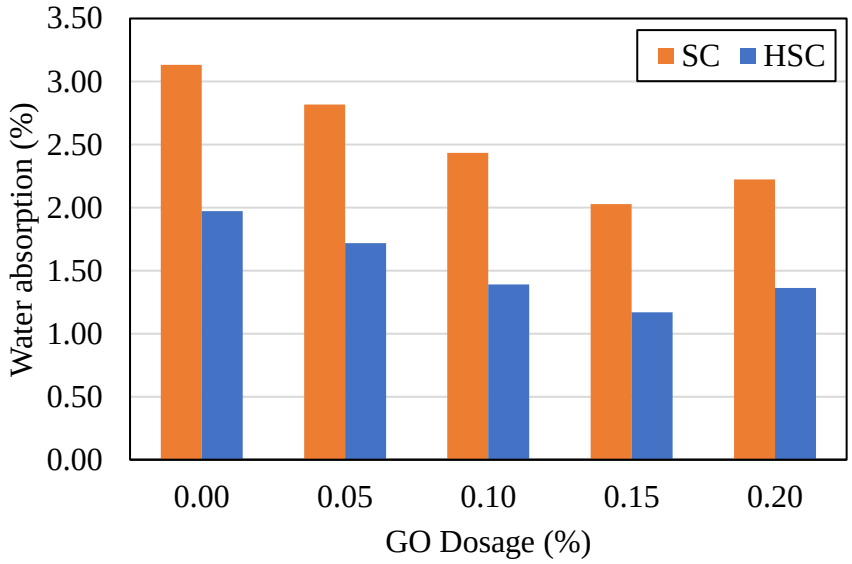

Figure 5.21 Water absorption of GO-cement concrete mixes

5.5.2. Water sorptivity

Water absorption by capillarity is one of the most important factors in understanding concrete's durability performance, because it may be exposed to severe environment during its service life that may influence its elements due to the permeability of the pore system that absorbs water or other harmful substances through capillarity action. Water absorption by capillarity refers to the penetration of a liquid into a porous substance caused by capillary surface stress. The water absorption via capillarity test of concrete determines its ability to absorb water through capillaries due to pressure differences between the water surface inside the capillaries and the ambient air. The water sorptivity

values of concrete with varying GO contents for both grades of concrete at 28, 56 and 90 days are shown in Figure 5.22. It is observed that the GO incorporation in cement concrete was found to be effective in resistance to the water sorptivity mainly in concrete mixes with GO dosage up to 0.15%. it is observed that the increase in GO dosage to 0.2% led to the decreased resistance to water sorptivity. However, GO addition up to 0.2% showed a greater resistance to the water sorptivity compared to control concrete. Similar trend is observed for both standard concrete and high strength concrete. The water sorptivity values with the addition of GO at 0%, 0.05%, 0.10%, 0.15% and 0.20% at 90 days were 0.0067, 0.0057, 0.0049, 0.0043, and 0.0048 mm/√s for standard concrete and 0.0032, 0.0022, 0.0014, 0.0008, and 0.0013 mm/√s for high strength concrete, respectively. The improved resistance to water sorptivity may be attributed to broad barrier capabilities of GO and refinement of pore structure of the cement composites resulting from decrease in critical pore diameter. The decreased resistance to water sorptivity at 0.2% GO dosage can be due to GO sheets agglomeration in the cement composites.

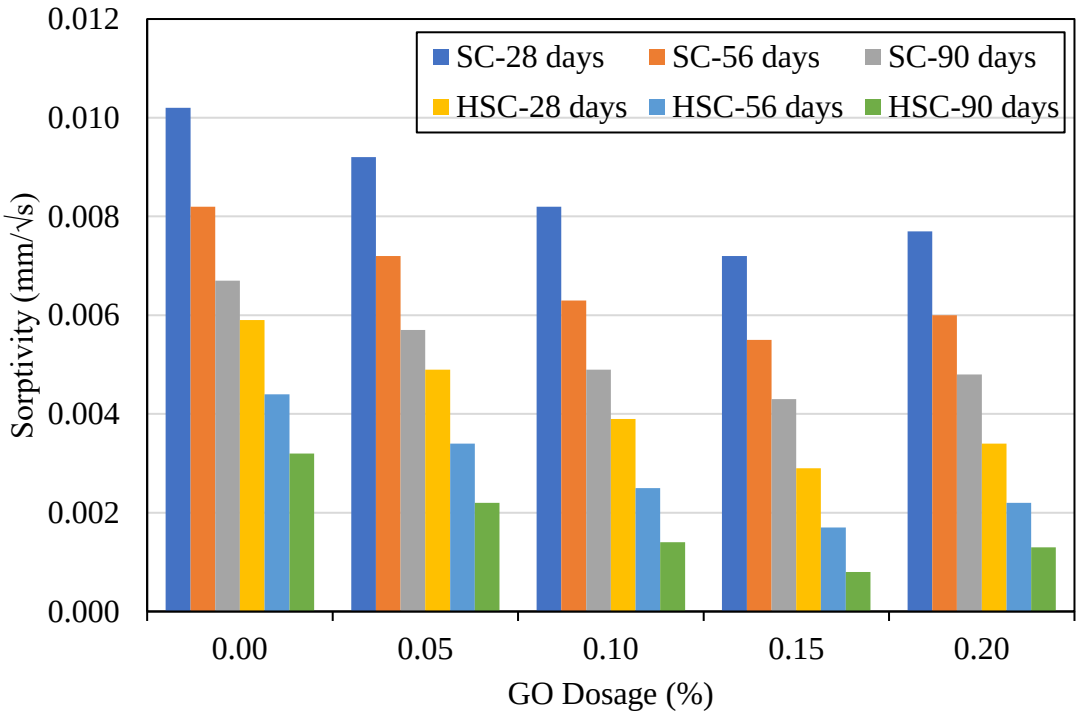

Figure 5.22 Water sorptivity of GO-cement concrete mixes

5.5.3. Accelerated Carbonation

To accomplish the satisfactorily service life, steel reinforced concrete buildings must be durable. Reinforcement corrosion due to carbonation can have a substantial impact on serviceability of structures. Hence carbonation resistance of concrete is a significant factor to evaluate. The carbonation depth values of concrete with varying GO contents for both grades of concrete are shown in Figure 5.23. Carbonation depth values of the various concrete mixes were observed to decrease with increase in GO dosage up to 0.15%. Concrete mix with 0.15% GO dosage was shown to have a minimum carbonation depth demonstrating that GO had more resistance to chemical intrusion by pore network structure. In contrast, carbonation depth of the concrete mix with 0.2% GO was recorded a less resistance to infused CO_2 ingression from the controlled environment compared to the concrete mixes with 0.15% GO. The carbonation depth values with the incorporation of GO at 0%, 0.05%, 0.10%, 0.15% and 0.20% were 19, 14, 12, 9, and 10 mm for standard concrete and 14, 10, 8, 6, and 7 mm for high strength concrete, respectively.

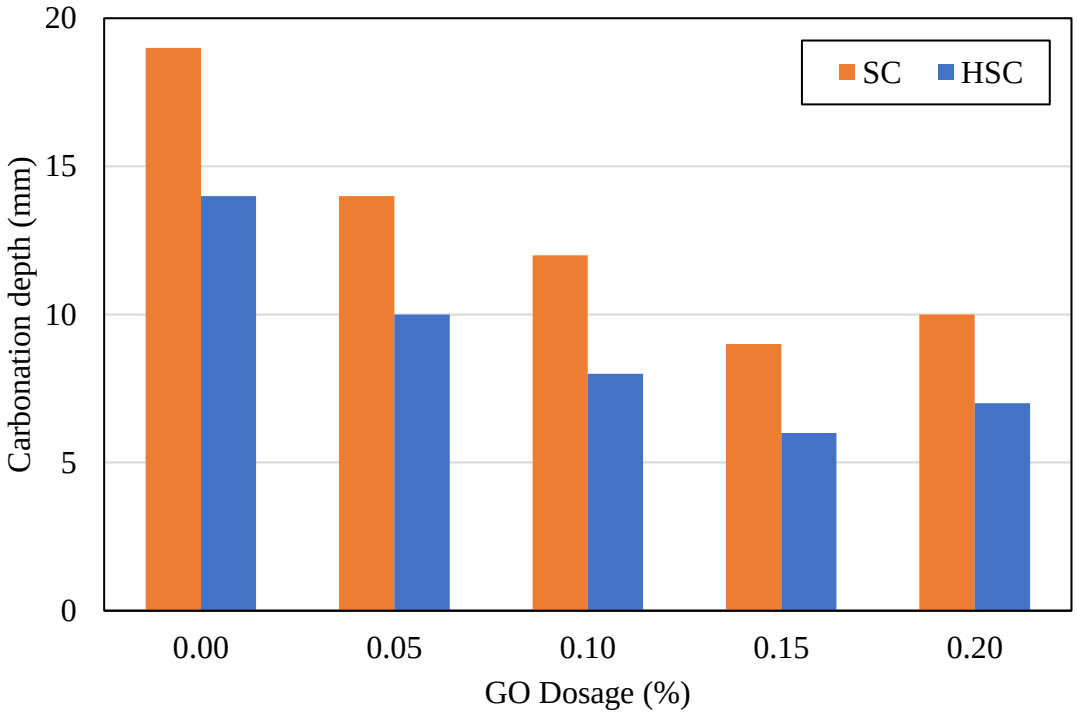

Figure 5.23 Carbonation depth of GO-cement concrete mixes

5.5.4. Rapid chloride penetration

According to ASTM C 1202, the findings of chloride ion penetration is determined by the charge passed. Figure 5.24 shows chloride ion permeability of concrete mixes with the addition of GO. Results demonstrated that increase in GO dosage had best to resistance against chloride ion permeability. The charge passed through concrete with GO addition up to 0.15% dosage was reduced compared with control concrete. However, for 0.2% dosage of GO addition in concrete had a better resistance to the chloride ion permeability compared to control concrete but resistance has been decreased compared to the concrete with 0.15% GO dosage. For the concrete mixes with the addition of GO at 0.15%, the charge passed was low, which could be attributable to the high dosage of GO. In contrast, the standard concrete mix without GO falls in high chloride ion-permeable class. Similarly, standard concrete and high strength concrete mixes were recorded greater resistance of chloride ion permeability with the increase in GO dosage up to 0.15%. Charge passed values of concrete mixes with GO at a dosage 0%, 0.05%, 0.10%, 0.15% and 0.20% were 2592, 2246, 1944, 1620, and 1706 coulombs for standard concrete and 1512, 1318, 1058, 821, and 886 coulombs for high strength concrete, respectively. However, the concrete mix containing 0.15% GO reported less chloride ion permeability in comparison to other mixes and the same mix also demonstrated pronounced increase in strength properties.

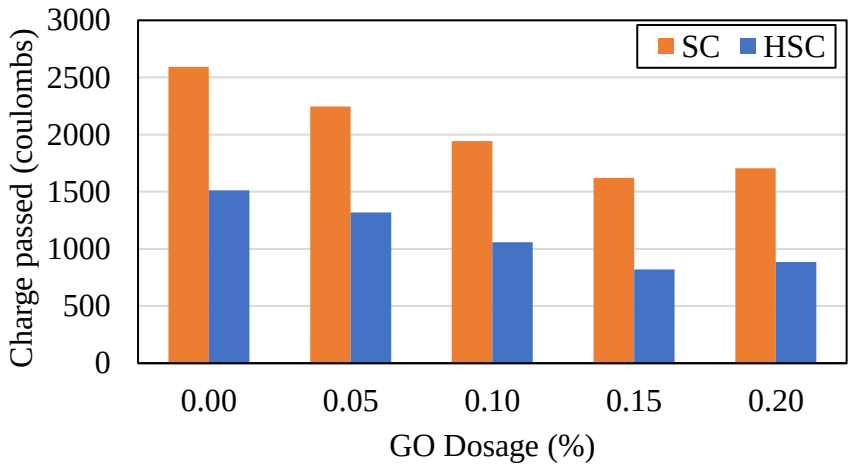

Figure 5.24 Charge passed of GO-cement concrete mixes

5.5.5. Acid attack

5.5.5.1. Dimension, weight and strength losses

The dimension, weight and strength losses in the concrete mixes at the 28, 56 and 90 days exposure of HCl and H_2SO_4 are shown in Figure 5.25 to 5.30. It is observed that the dimension, weight and strength losses of concrete mixes are increased with reference to increased age of the exposure and the degree of calcium leaching from concrete matrix was influenced by the type of acid. H_2SO_4 acidic environment resulted in pronounced influence in all concrete mixes, when compared to the HCL environment. The GO-reinforced cement concrete exhibited a greater resistance to acidic environment compared control concrete and the resistance to these losses are increased with an increasing GO dosage up to 0.15%. The average dimension, weight and strength losses in the concrete mixes without GO exposed to HCL attack at 90 days of exposure were 10.4%, 20.1%, and 42.9% for standard concrete and 8.05%, 15.5%, and 35.3% for high strength concrete, respectively. Whereas for concrete mixes with the addition of GO at 0.15% exposed to HCl acid for 90 days, these losses were decreased to 3.7%, 6.81%, and 18.34% for standard concrete and 3.53%, 5.72%, and 14.20% for high strength concrete, respectively. On the other hand, the average dimension, weight and strength losses in the concrete mixes without GO exposed to H_2SO_4 attack at 90 days of exposure were 42.2%, 53.8%, and 71.6% for standard concrete and 29.3%, 45.8%, and 66.2% for high strength concrete, respectively. Whereas for concrete mixes with the addition of GO at 0.15% exposed to H_2SO_4 acid for 90 days, these losses were decreased to 19.9%, 23.2%, and 30.3% for standard concrete and 13.3%, 18.4%, and 28.73% for high strength concrete, respectively. As a result, all test results demonstrated that increasing the GO content up to 0.15% reduced the degree of deterioration of concrete matrix in acid environment. The improved resistance of GO-reinforced concrete mixes was attributed to the incorporation of GO to concrete matrix, which provided a nano filler effect, preventing aggressive ions from surrounding environment to penetrate in to the concrete matrix. The incorporation of GO into the concrete matrix densified the microstructure. As a result, it prevented or retarded the migration of acid species from external solution. However, this reinforcing effect in

concrete matrix can prevent the development of chemical shrinkage cracks as a result of acid exposure, even though GO dispersion helps in the initial stages of the C-S-H gel self-desiccation by absorbing more free water.

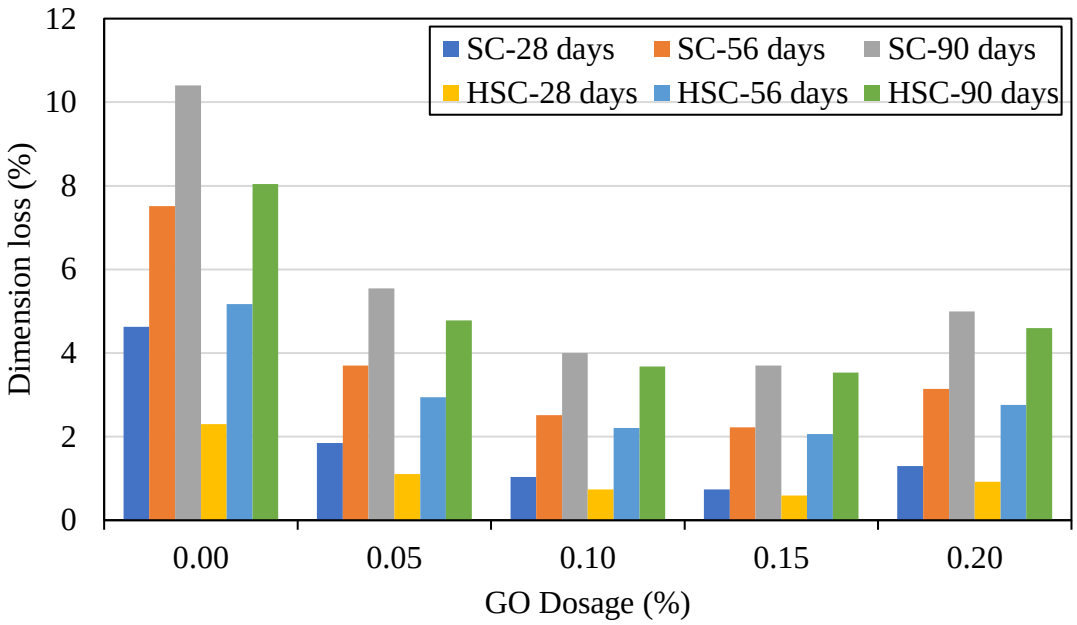

Figure 5.25 Dimension loss of GO-cement concrete mixes due to HCl attack

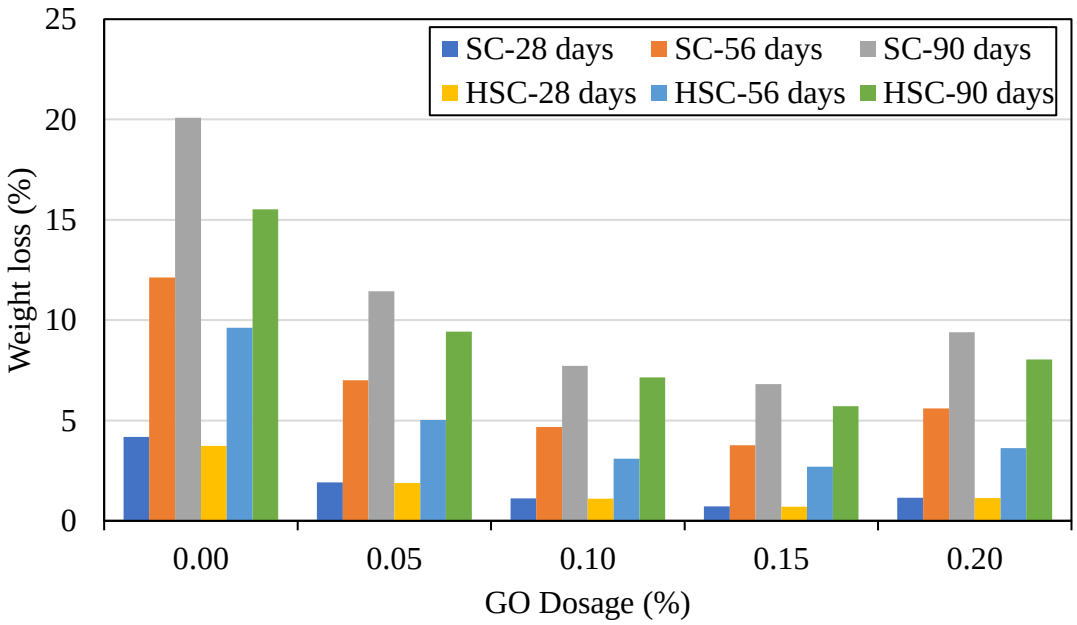

Figure 5.26 Weight loss of GO-cement concrete mixes due to HCl attack

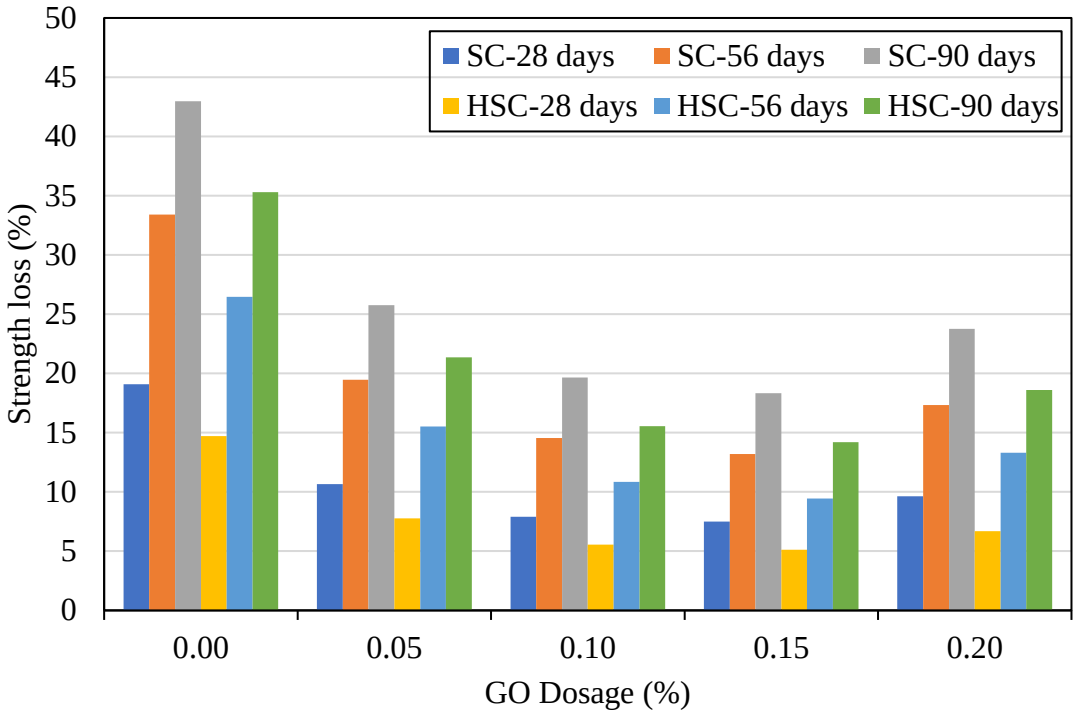

Figure 5.27 Strength loss of GO-cement concrete mixes due to HCl attack

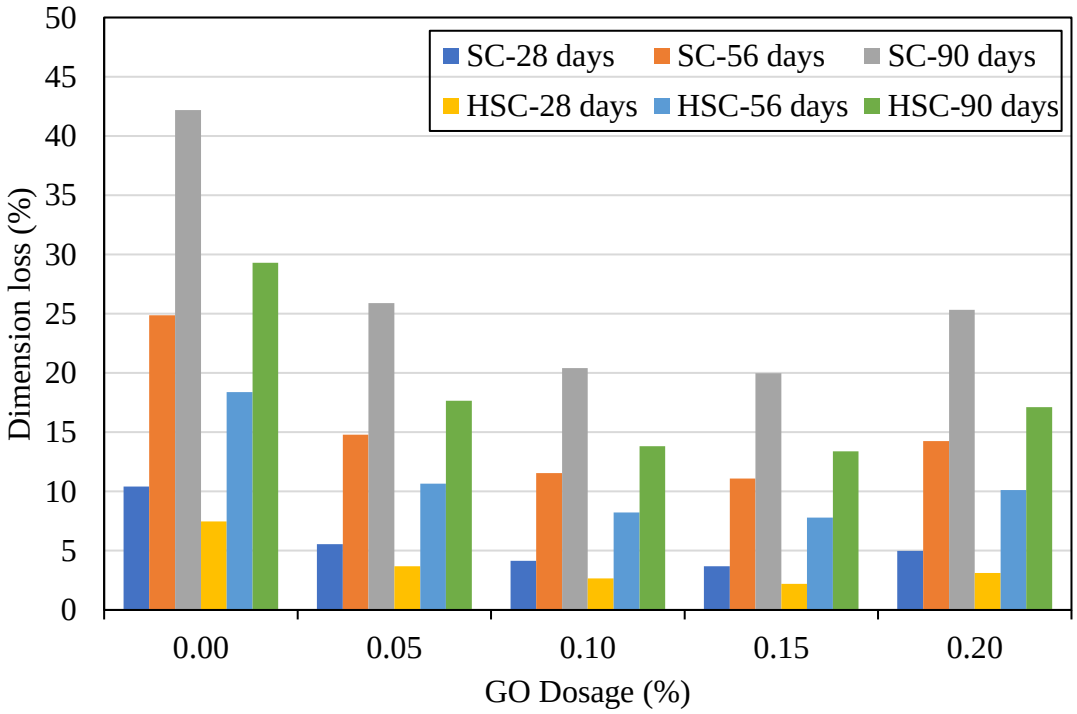

Figure 5.28 Dimension loss of GO-cement concrete mixes due to H_2SO_4 attack

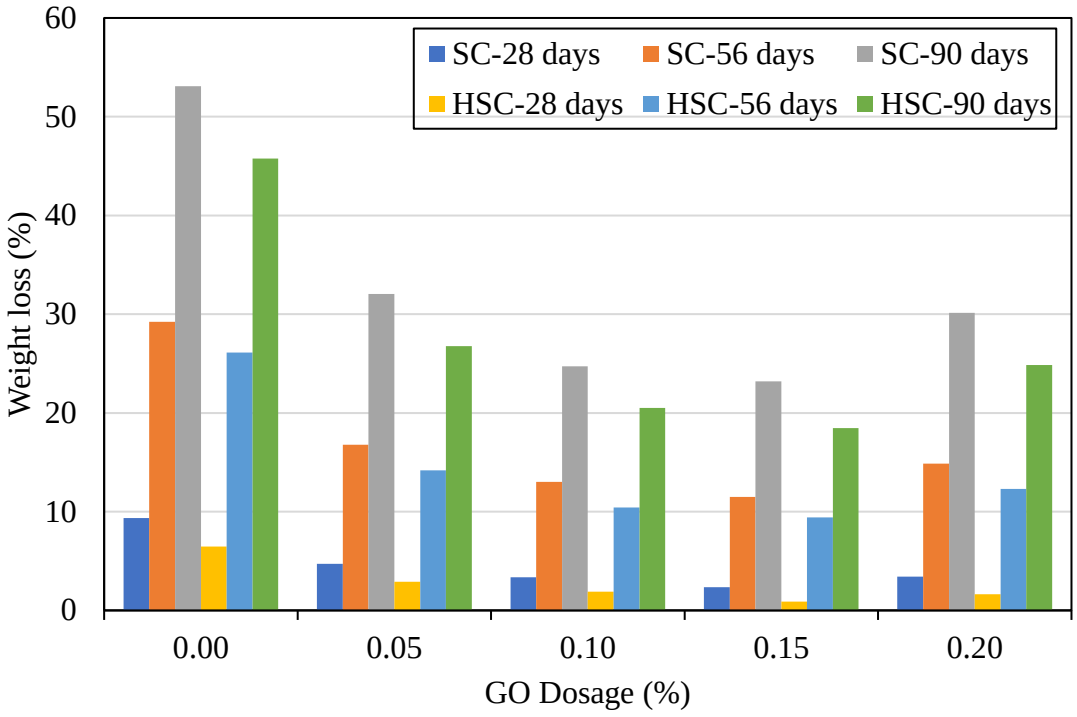

Figure 5.29 Weight loss of GO-cement concrete mixes due to H_2SO_4 attack

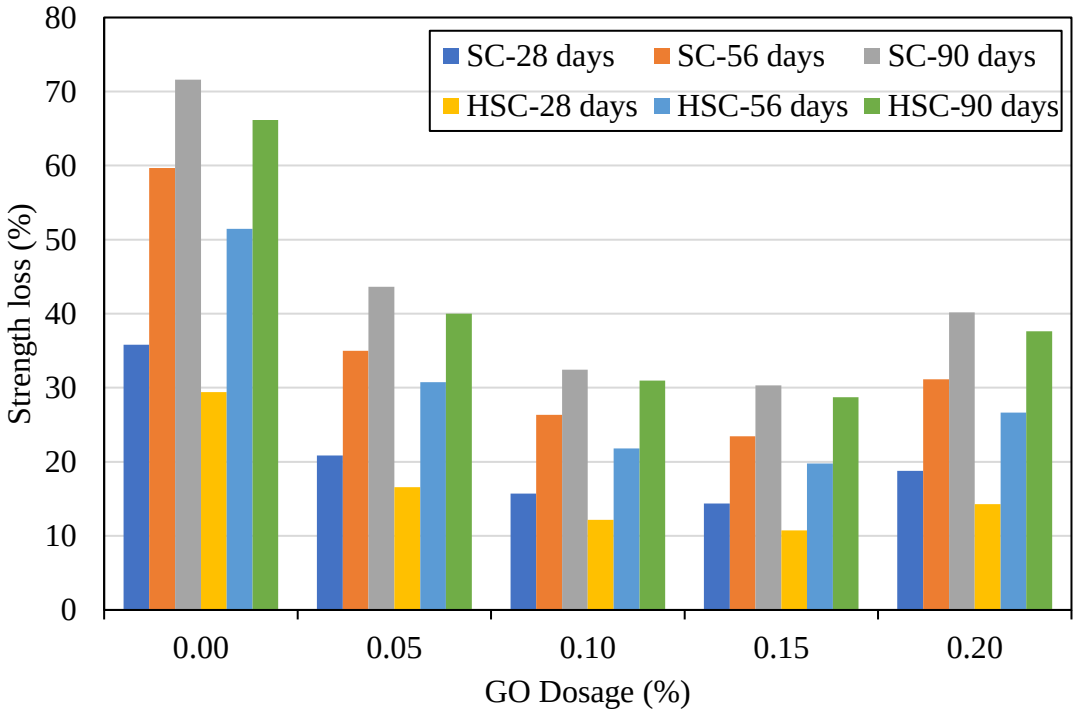

Figure 5.30 Strength loss of GO-cement concrete mixes due to H_2SO_4 attack

5.5.5.2. SEM

The morphology of GO-0 and GO-0.15 concrete mixes at the 90 days exposure of HCl and H_2SO_4 acid in both standard and high strength concrete is compared using SEM images shown in Figure 5.31 and 5.32. The fractured surface of concrete mixes containing GO-0% and GO-0.15% before acid attack is comprised of C-S-H gel (sheet morphology), calcium hydroxide (hexagonal plate morphology), and trisulfo aluminate (needle morphology). The acid attack has changed the shape and chemical composition of the hydration phases present in the concrete mixes significantly. The zone affected by acid attack can be completely filled with porous alumina-silica hydrogel after calcium leaching from the cement matrix. The acid exposed concrete mix containing GO-0.15% had traces of GO sheets interweaved inside the porous gel. While GO presence had an impact on the mineralogy of Ca-based ions that precipitated in the affected zone, it prevented ionic movement and mass transfer among cement matrix and acid solution.

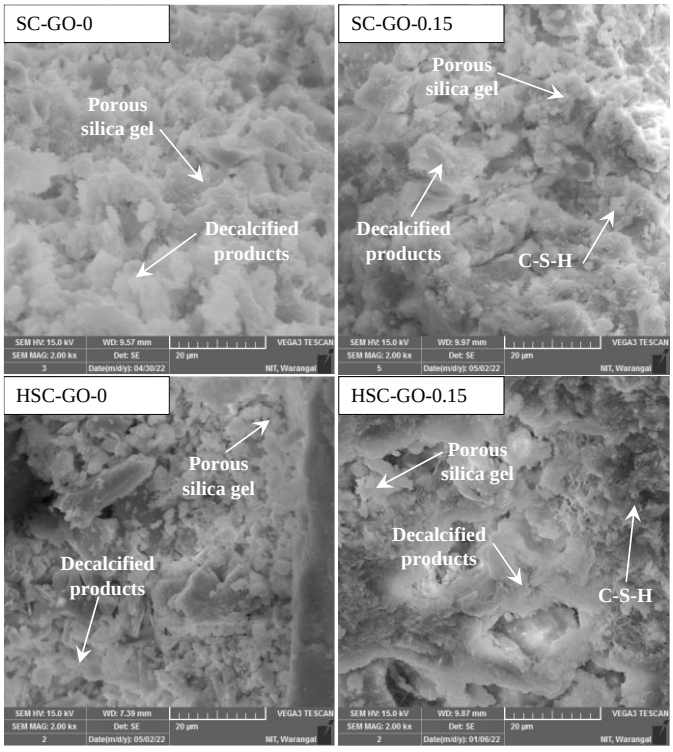

Figure 5.31 SEM images of GO-cement concrete mixes due to HCl attack

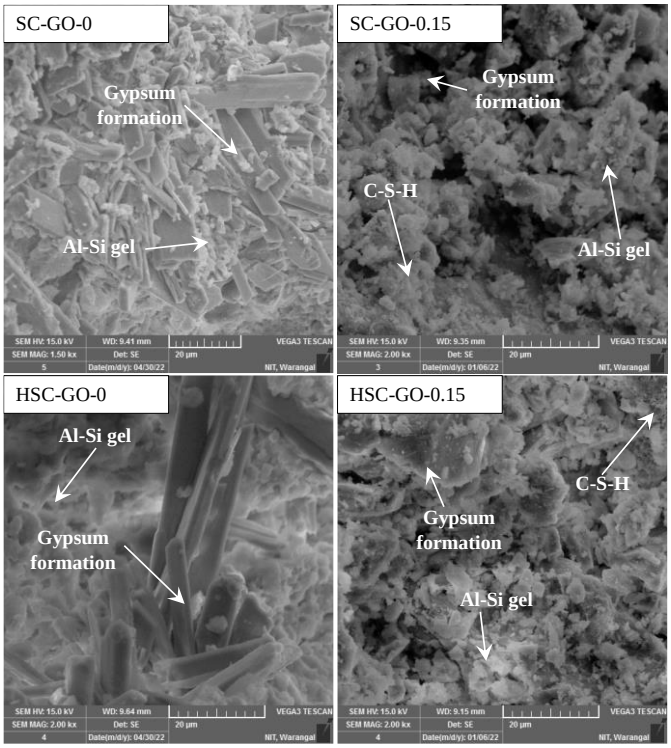

Figure 5.32 SEM images of GO-cement concrete mixes due to H_2SO_4 attack

5.5.5.3. EDX

The chemical composition of the affected zone in GO-0 and GO-0.15% concrete mixes of both the grades exposed to HCl and H_2SO_4 was assessed by an EDX values of calcium-to-silica ratio (Ca/Si ratio) and calcium-to-aluminium ratio (Ca/Al on Y-axis) and results are shown in Table 5.7. An EDS values of C-S-H gel, monosulfate, and calcium hydroxide areas were identified in concrete mixes containing GO-0% and GO-0.15% before acid attack was indicated in Table 5.5. Because of the HCl attack, these hydration products were decalcified and completely absent in the affected zone of GO-0 mixes. However, at the 90 days exposure of the acid attack, residues of C-S-H gel were still identified in the affected zone of concrete mixes containing GO-0.15%. It indicates that the GO inclusion functioned as a diffusion barrier, preventing leaching of C-S-H gel in acidic environment. Upon deterioration, affected area in two concrete mixes were filled by decalcified products with low calcium, high alumina and silica contents. This

demonstrates that GO incorporation in cement matrix prevented the leaching of Ca^{2+} ions from cement hydrates such as C-S-H, CH and ettringite into external solutions.

Table 5.7 EDX values of GO-cement concrete mixes due to acid attack

Mix	Before attack		After HCl attack		After H_2SO_4 attack	
	Si/Ca	Al/Ca	Si/Ca	Al/Ca	Si/Ca	Al/Ca
SC-GO-0.00	0.41	0.20	0.49	0.25	0.61	0.32
SC-GO-0.15	0.59	0.15	0.67	0.19	0.76	0.24
HSC-GO-0.00	0.56	0.20	0.68	0.25	0.85	0.29
HSC-GO-0.15	0.95	0.13	1.05	0.21	1.17	0.28

5.5.5.4. XRD

The XRD patterns of GO-0 and GO-0.15% concrete mixes after HCl and H_2SO_4 attack at the 90 days exposure in the affected area are shown in Figure 5.33 and 5.34. The findings were revealed by the XRD patterns of these mixes before HCl attack are given in Figure 5.14 and 5.15, the intensity of peak for C-S-H was positioned at 20.98°, 28.11° and 29.61°, CH was at 18.17°, 34.21°, 47.21° and 50.92° and AFt was positioned at 39.55°, 42.60°, 55.02° and 60.09°. HCl attack resulted in the considerable modification in chemical compositions of these samples, which were reflected in the change in their XRD patterns also. As a result, an amorphous peak at 2θ values of 23.8° was seen in the XRD pattern of all concrete mixes after acid attack, confirming the existence of gibbsite ($Al(OH)_3$) and quartz (SiO_2). These findings demonstrated that effect of strong acid environment on the complete dissolution of hydrated products as well as the presence of an amorphous alumina-silica hydrogel in concrete mixes exposed to acid attack. However, the presence of XRD peaks located at 2θ of 11.6°, 20.7°, 23.6°, 31.4°, 36.6° and 50.1° identifies the formation of gypsum ($CaSO4{\cdot}2H2O$) in the affected zones of concrete mixes exposed to H_2SO_4. Accordingly, recent investigations have shown the formation of gypsum in the affected zones of concrete matrix exposed to H_2SO_4.

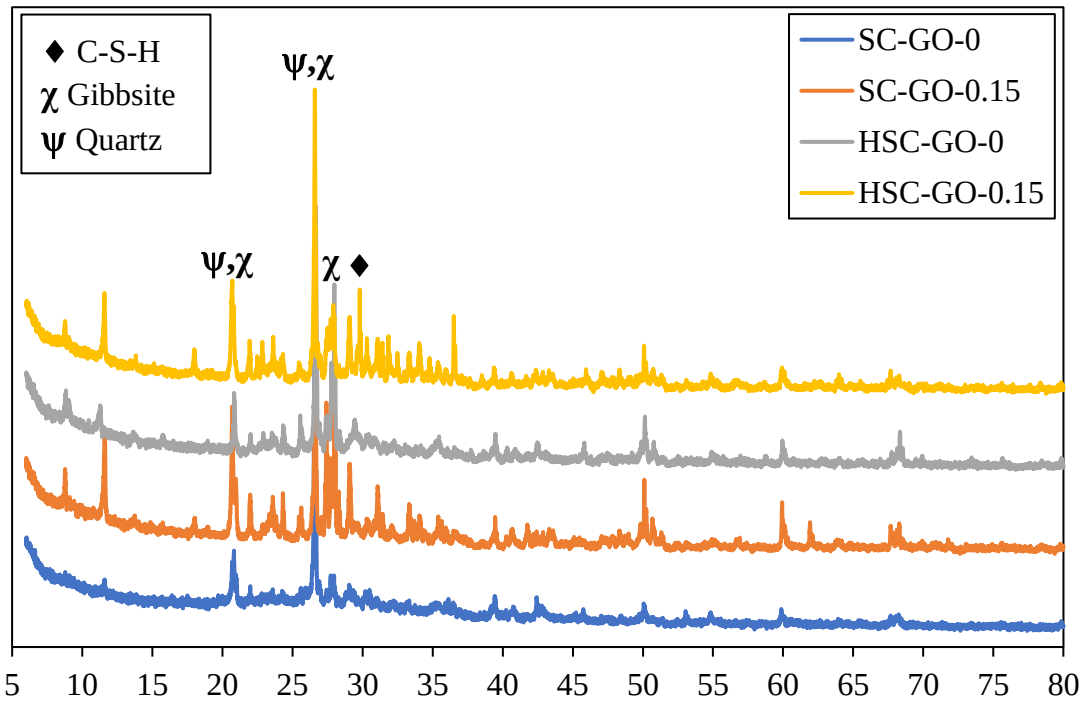

Figure 5.33 XRD patterns of GO-cement concrete mixes due to HCl attack

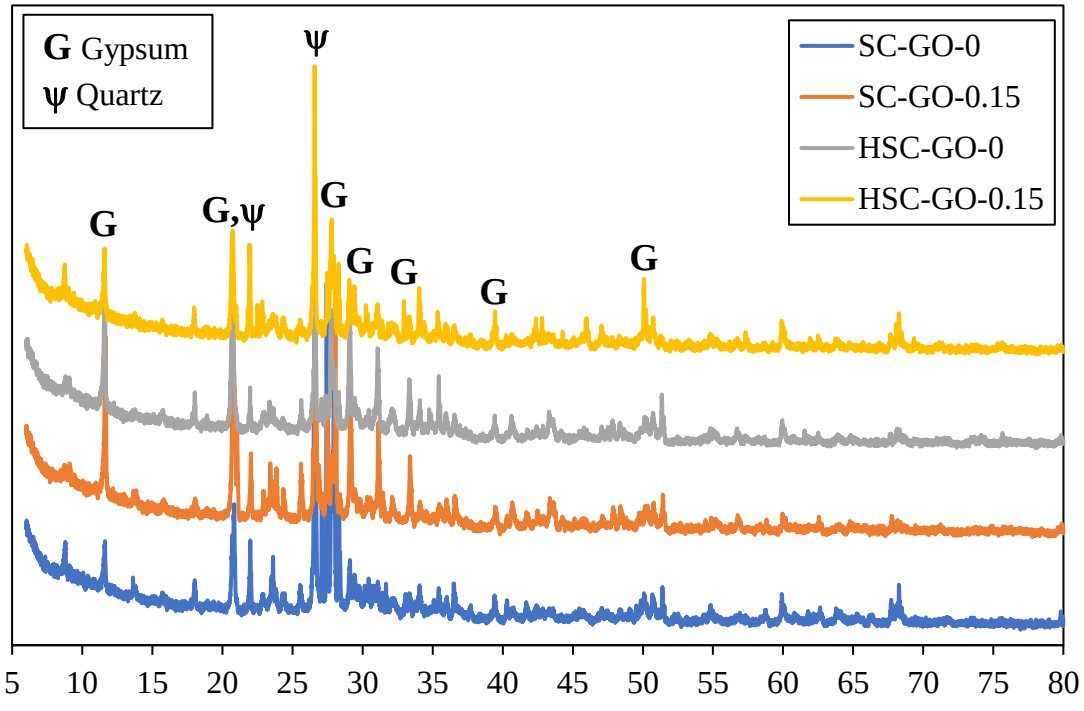

Figure 5.34 XRD patterns of GO-cement concrete mixes due to H_2SO_4 attack

5.5.5.5. FTIR

The FT-IR spectra of GO-0 and GO-0.15% concrete mixes after HCl and H_2SO_4 attack at the 90 days exposure in the affected area are shown in Figure 5.35 and 5.36. The findings were revealed by the FTIR patterns of these mixes before acid attack are shown in Figure 5.16 and 5.17, The band region of 900–1100 cm^{-1} (Si-O asymmetric stretching vibration) characterizes the calcium silicate hydrate (C-S-H), Calcium hydroxide was detected at a peak of 3643 cm^{-1} (O–H stretching vibration). The presence of trisulfoaluminate can be detected from the bands 857 cm-1 (Al-O stretching vibration), 1675 cm^{-1} and 3431 cm^{-1} (H_2O bending and stretching vibration) and monosulfate aluminates at 1400 cm^{-1} (asymmetric stretching of $[CO_3]^{2-}$). In respective FT-IR ranges, the IR bands associated with the C-O, Si(Al)-O, and O-H functional groups were observed. These findings demonstrated the effect of a strong acidic environment on the complete dissolution of hydrated products and development of an amorphous alumina-silica hydrogel in concrete mixes exposed to acid. On the other hand, the IR peaks related to S–O (1097 cm^{-1}) functional groups revealed that sulfate-bearing salt precipitated in concrete mixes when exposed to H_2SO_4 acid. These findings agreed with the SEM and XRD results.

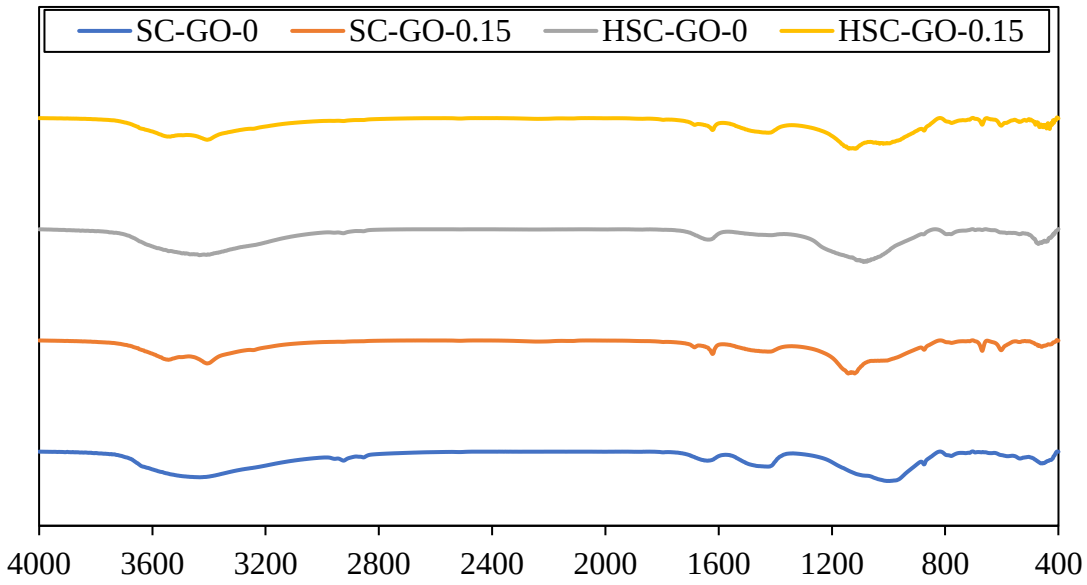

Figure 5.35 FT-IR spectra of GO-cement concrete mixes due to HCl attack

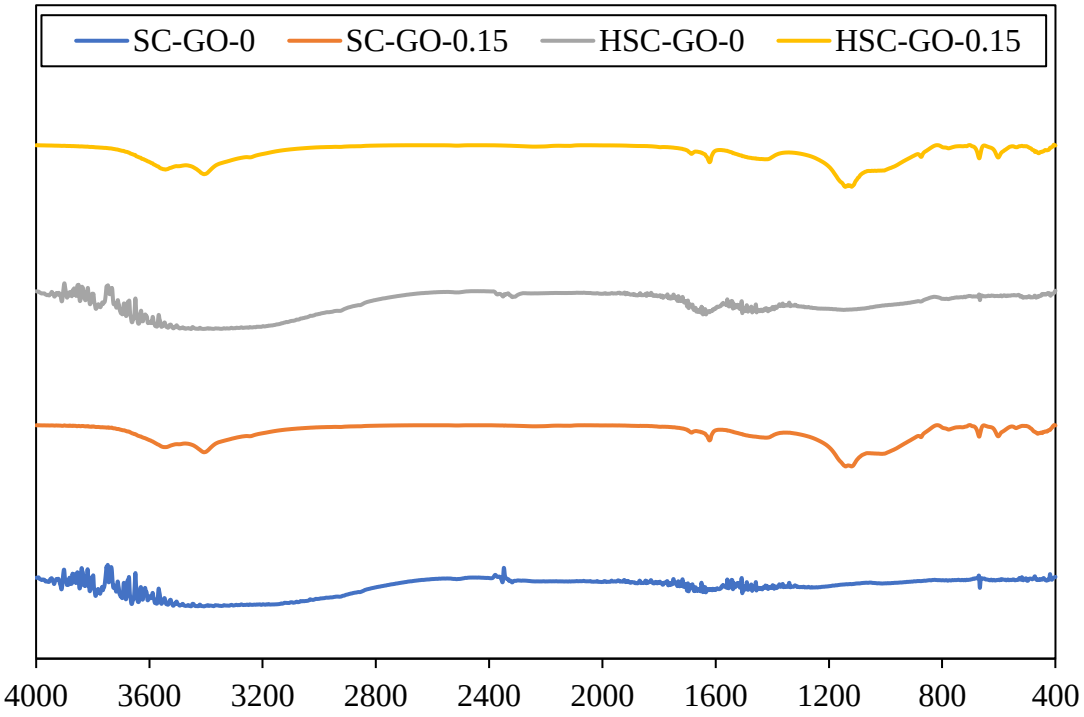

Figure 5.36 FT-IR spectra of GO-cement concrete mixes due to H_2SO_4 attack

5.5.5.6. TGDTA

The TGA pattern of the GO-0 and GO-0.15% concrete mixes for both the grades after the HCl and H_2SO_4 attack at the 90 days exposure, data collected from the affected area is shown in Figure 5.37 and 5.38. The temperature ranges of different phase transformations of the concrete matrix considered in this study are as follow, the evaporable water at 30–105°C, the water loss from the decomposition of the C-S-H (dehydration, Ldh) at 105–400°C, dihydroxylation (Ldx) of the calcium hydroxide at 400–600°C, decarbonation (Ldc) of calcium carbonate at 600–850°C were found in the GO-0 and GO-0.15% concrete mixes before acid attack are shown in Table 5.6. After the HCl and H_2SO_4 attack, the affected areas in these two concrete mixes were observed to have no evidence of hydration phases but to be substantially filled with alumina-silica hydrogel and gypsum, respectively. Weight loss caused by gypsum and hydrogel degradation was measured at temperatures ranging from 200 to 400 °C. The TGA analysis of total weight loss (TWL), gypsum and hydrogel present in the two concrete mixes is shown in Table 5.8. This

quantification of TGA analysis was calculated using the method suggested by Deboucha et al. (2017). The CBW content represents the degree of hydration in the concrete mixes. When 0.15% GO was added, the bound water levels increased by 8.25% and 7.32% for standard concrete and high-strength concrete, respectively, compared to control concrete. This shows that high dosage of GO influences the rate of hydration by attracting more free water to GO surface. On the other hand, the GO addition prevents carbonation of calcium hydroxide crystals and calcium oxide in concrete matrix. GO blocks diffusion pathways in concrete matrix that carbon dioxide gas needs to permeate from surrounding environment (Chu et al. 2020). Alumina-silica (Al-Si) hydrogel developed in the affected area of GO-0 and GO-0.15% concrete mixes was 25.51% and 24.58% for standard concrete and 24.10% and 22.79% for high strength concrete, respectively, at the 90 days exposure of HCl attack. Gypsum and alumina-silica (Al-Si) hydrogel developed in the affected area of GO-0 and GO-0.15% concrete mixes were 18.57% and 18.19% for standard concrete and 17.79% and 17.47% for high strength concrete, respectively, at the 90 days exposure of H_2SO_4 attack. It is possible that the GO addition acted as a diffusion barrier, reducing the amount of calcium leaching from the concrete matrix.

Table 5.8 Percentage mass loss from TGA analysis after acid attack

Mix	After HCl attack		After H_2SO_4 attack	
	Al–Si gel (%)	TWL (%)	Gypsum and Al–Si gel (%)	TWL (%)
SC-GO-0.00	25.51	28.07	18.57	21.09
SC-GO-0.15	24.58	26.59	18.19	19.93
HSC-GO-0.00	24.10	25.85	17.79	18.74
HSC-GO-0.15	22.79	24.04	17.47	18.41

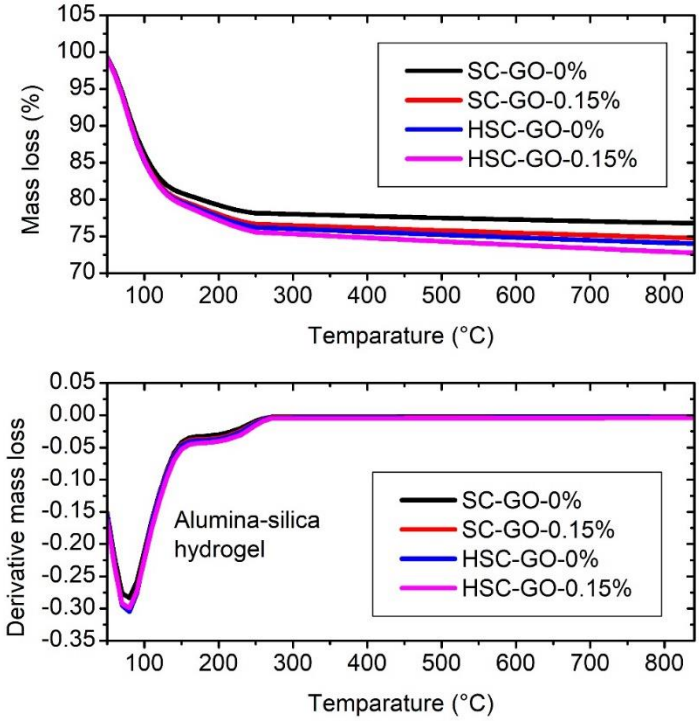

Figure 5.37 TGA and DTG plots of GO-cement concrete mixes due to HCl attack

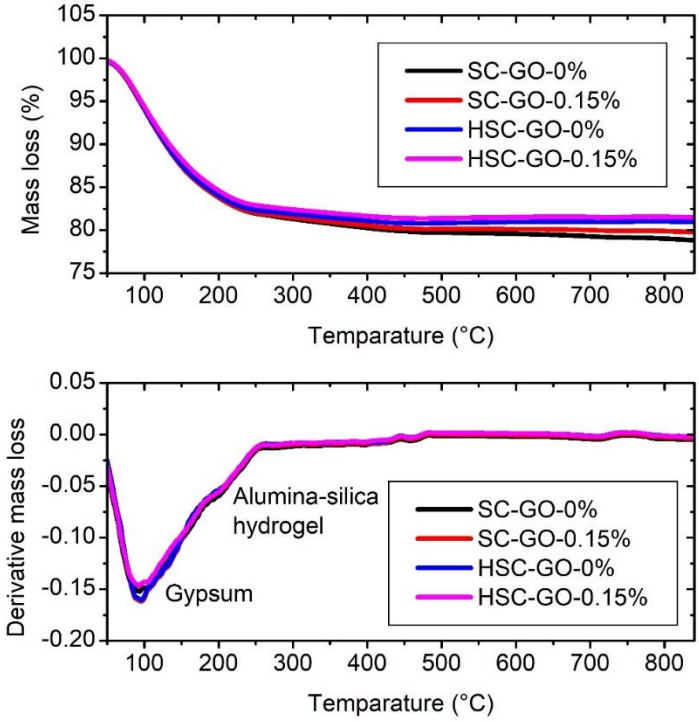

Figure 5.38 TGA and DTG plots of GO-cement concrete mixes due to H_2SO_4 attack

5.6. Concluding remarks from Phase-I

In this chapter GO effect on static & dynamic mechanical, and microstructural characteristics of concrete have been investigated. In addition, the durability performance of GO reinforced concrete composite have been determined and the results are compared with control concrete. The following conclusions are drawn from the experimental results.

(i) Static mechanical properties

- The reduction in slump values were observed with the addition of GO at varied dosages 0.05%, 0.10%, 0.15% and 0.20%. The percentage reduction was 7.7%, 11.5%, 15.4% and 19.2% for standard concrete and 9.1%, 13.6%, 18.2% and 22.7% for high strength concrete, respectively, compared to the control concrete.

- The workability of the concrete had greatly affected with the addition of GO. The results revealed that increase in GO dosage decreased the fluidity of concrete composite, this may be attributed to the large surface area of GO which absorbs more amount of free water.

- The most apparent compressive, split tensile and flexural strength values of 60.5MPa, 3.52MPa and 8.1MPa for standard concrete and 86.0MPa, 5.41MPa and 10.80MPa for high strength concrete, were observed respectively at the age of 28 days at 0.15% GO addition for both the grades of concrete.

- The rate of increase in compressive, split tensile and flexural strength values of concrete with 0.15% GO addition were 60.6%, 31.1% and 26.3% at 7days, 44.4%, 28.1% and 24.4% at 28days, respectively for standard concrete, whereas for high strength concrete the improvement was 53.1%, 29.1% and 23.7% at 7days, and 26.5%, 21.4% and 20.0% at 28days, respectively.

- The strength properties of cement concrete were remarkably improved with incorporation of GO at a dosage between 0.05% and 0.15%, this may be attributed to

the accelerated rate of hydration and formation of densified microstructure. While effect of 0.20% was lower than 0.15% which may be due to the GO agglomeration.

- The influence of GO on the growth rate of strength properties is more pronounced at early age compared to later age. Furthermore, the increasing rate of strength properties of standard concrete is more significant than high strength concrete. This can be attributed to more w/c ratio that can offer adequate free water, subsequently improved the process of hydration.

- The elastic modulus of GO incorporated concrete was increased by about 8.7–28.7% for standard concrete and 6.1–17.9% for high strength concrete at 28 days compared to control concrete, indicating the formation of a denser interfacial transition zone.

(ii) Dynamic mechanical properties

- Frequency response function of concrete with varying dosages of GO exhibited the improvement in natural frequencies and damping ratios up to 0.15% GO content. It was observed that the maximum increased fundamental natural frequencies were about 8.0% and 6.0% for the standard and high strength concrete at 0.15% GO dosage compared to control concrete.

- Maximum reduction in damping ratio was 29.1% and 26.3% for the standard and high strength concrete at 0.15% GO dosage compared to control concrete. The improvement in damping is attributed to the increase in total number of interfaces and enhancement of the non-uniform stress distribution both contribute to an increase in the damping ratio.

- The dynamic modulus of concrete with GO dosages up to 0.15% is improved, however beyond 0.15% of GO addition showed the reverse tendency. The maximum increased dynamic elastic modulus was 17.1% and 12.8% for the standard and high strength concrete respectively compared to control concrete.

- The UPV values exhibited that the incorporation of GO resulted in the formation of excellent quality concrete with improved homogeneity. The improvement in concrete

quality may be attributable to the nano filler effect of GO, which densifies the microstructure of cement matrix.

- The trend of dynamic elastic modulus is comparable to that of compressive strength for both concrete grades. The findings of UPV test results are complied with the impact resonance test results.

(iii) Microstructural characteristics

- The SEM images of concrete specimens representing that in presence of GO, the hydration products are strongly interweaved with each other, having lesser number of microcracks and pores. The GO content up to 0.15% shows the formation of compact, uniform and densified microstructure compared to control concrete.

- The percentage atomic ratio of Ca/Si was quite high in control concrete, whereas incorporating GO in concrete decreased the Ca/Si ratio and reduced with increase in GO content in both the grades of concrete mixes. This could be because of GO which absorbs more quantity of water molecules, and turn into nucleation sites to hydrated phases, resulting in the formation of regulated and refined crystalline phases.

- The increase in intensity of XRD peaks representing that GO addition has exhibited the increase in crystalline phases, which is confirming that the hydration process can be accelerated by the GO and hence GO could support to generate more regular hydrated phases.

- It is observed from the IR spectra that the absorption peak of C-S-H shifts towards a higher wavenumber in the presence of GO with respect to the control concrete and the trend continues with the increase in GO content up to 0.15% indicating that GO had influence on Ca/Si ratio and resulting in the formation of densified structure. These findings agree well with the SEM, EDX, and XRD results.

- The TGA analysis showed that the rate of hydration is improved with the addition of GO up to 0.15%. This could be because of graphene oxide which has oxygenated functional groups and a large specific surface area.

(iv) Durability properties

- The water absorption values with the addition of GO at 0%, 0.05%, 0.10%, 0.15% and 0.20% are recorded as 3.13%, 2.82%, 2.43%, 2.03% and 2.22% for standard concrete and 1.97%, 1.72%, 1.39%, 1.17% and 1.36% for high strength concrete, respectively.

- The water sorptivity values with the addition of GO at 0%, 0.05%, 0.10%, 0.15% and 0.20% at 90 days were 0.0067, 0.0057, 0.0049, 0.0043, and 0.0048 mm/√s for standard concrete and 0.0032, 0.0022, 0.0014, 0.0008, and 0.0013 mm/√s for high strength concrete, respectively.

- Enhanced resistance to water absorption may be attributed to the broad barrier capabilities of GO and refinement of pore structure of the concrete composite resulting from decrease in critical pore diameter.

- The carbonation depth values with the addition of GO at 0%, 0.05%, 0.10%, 0.15% and 0.20% were observed as 19, 14, 12, 9, and 10 mm for standard concrete and 14, 10, 8, 6, and 7 mm for high strength concrete, respectively.

- The results of RCPT in terms of Charge passed values of concrete mixes with GO at a dosage of 0%, 0.05%, 0.10%, 0.15% and 0.20% were observed as 2592, 2246, 1944, 1620, and 1706 coulombs for standard concrete and 1512, 1318, 1058, 821, and 886 coulombs for high strength concrete, respectively.

- The concrete mixes with 0.15% GO exposed to HCL acid for 90 days, the dimension, weight and strength losses were observed as 3.7%, 6.8%, and 18.3% for standard concrete and 3.5%, 5.7%, and 14.2% for high strength concrete, respectively.

- The concrete mixes with 0.15% GO exposed to H_2SO_4 acid for 90 days, the dimension, weight and strength losses were observed as 20.0%, 23.2%, and 30.3% for standard concrete and 13.4%, 18.5%, and 28.7% for high strength concrete, respectively.

- Microstructural characterization indicates that the GO inclusion acted as a diffusion barrier, and prevented the leaching of Ca^{2+} ions from cement hydrates such as C-S-H, CH and ettringite from the acidic environment.

CHAPTER 6
PHASE-II: GRAPHENE OXIDE AND FLY ASH BASED CEMENT CONCRETE

6.1. General

The performance of GO reinforced fly ash concrete under static and dynamic mechanical properties, microstructural characteristics and durability properties are presented in this chapter. This chapter is divided in two parts. First part focused on the evaluation of static mechanical properties such as compressive strength, split tensile strength, flexural strength and elastic modulus of GO reinforced fly ash concrete. In addition to that, dynamic properties such as natural frequency, damping ratio and mode shapes have also been evaluated. The microstructural characterization has been carried out using SEM, EDX, XRD FTIR and TGDTA. The second part consists of assessment of durability properties of GO reinforced fly ash concrete by conducting water absorption, sorptivity, accelerated carbonation, rapid chloride penetration and acid attack tests. The performance of GO reinforced fly ash concrete is compared with control concrete. Nomenclature of the mix ID's and Dosage of GO added and replacement of cement with fly ash in concrete are presented in Table 6.1.

Table 6.1 The nomenclature concrete mixes with GO additions and fly ash replacements

S. No.	GO (%)	Fly ash (%)	Mix Designation	
			Standard concrete (SC)	High strength concrete (HSC)
1	0.00	0	SC-GO-0, FA-0	HSC-GO-0, FA-0

S. No.	GO (%)	Fly ash (%)	Mix Designation	
			Standard concrete (SC)	High strength concrete (HSC)
2	0.15	0	SC-GO-0.15, FA-0	HSC-GO-0.15, FA-0
3	0.15	10	SC-GO-0.15, FA-10	HSC-GO-0.15, FA-10
4	0.15	20	SC-GO-0.15, FA-20	HSC-GO-0.15, FA-20
5	0.15	30	SC-GO-0.15, FA-30	HSC-GO-0.15, FA-30

6.2. Static mechanical properties

6.2.1. Workability

The combined effect of GO and fly ash on the fluidity of concrete with an optimized GO content 0.15% and varying fly ash replacements of 10%, 20%, 30% is shown in Figure 6.1. It is observed that for both the grades of concrete mixes, slump values decreased with the 10% replacement of cement with fly ash. The reduction in slump values with the addition of GO at 0.15% and fly ash replacement at 10% are recorded as 3.8% and 4.5% for standard and high strength concrete, respectively, in comparison with control concrete. It might be attributed to the more amount of free water is required to wet the particle surfaces owing to large specific surface area of GO. The formation of flocculation and agglomeration is caused because of electrostatic interaction among cement particles and GO, the hydrophilic oxygenated functions of GO absorbs the water molecules and remain entrapped (Shang et al. 2015). The fluidity of concrete improved efficiently with an increase in fly ash content above 10% in comparison with control concrete. The increase in slump values with the addition of GO at 0.15% and fly ash replacement at 20% and 30% are recorded as 3.8% and 11.5% for standard concrete and 4.5% and 13.6% for high strength concrete, respectively, in comparison with the control concrete. This shows that the formation of flocculation structures in concrete with GO can be decreased by cement replacement with fly ash. Therefore, fly ash counterbalanced the GO influence

on the decrease in fluidity. This might be ascribed to three reasons. First, because of the particle shape of fly ash which has a smooth spherical form having less water requirement. Second, the concrete fluidity improves because of the fly ash particles act as bouncing balls within the cement particles. Third, the fly ash can fill the voids within the cement particles, owing to fineness of fly ash is lesser than the cement, fly ash not only improves gradation of size but also fluidity of concrete (Han, Wang, and Yan 2014).

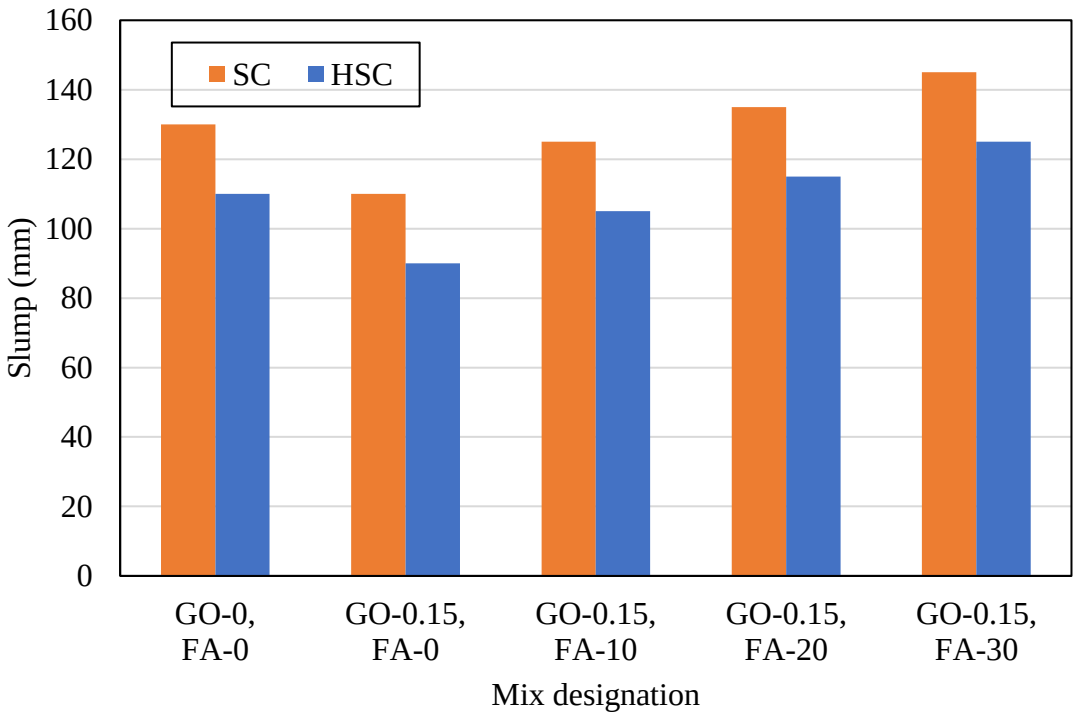

Figure 6.1 Slump values of GO-fly ash concrete

6.2.2. Strength properties

The variations of the strength properties of concrete with optimum GO content and varying replacements of fly ash at 10%, 20% and 30% for both grades of concrete are shown in Figure 6.2, 6.3, and 6.4. It can be seen that the compressive, split tensile and flexural strength of the concrete are decreased with reference to increment in fly ash replacement. Though, strength properties of concrete mixes with GO and fly ash replacement up to 30% are higher than that of the control concrete. This trend is observed

for both standard concrete and high-strength concrete, and for both curing ages. The most apparent compressive, split tensile and flexural strength values of 59.14MPa, 3.45MPa and 7.46MPa for standard concrete and 84.57MPa, 5.14MPa and 10.60MPa for high strength concrete, respectively, were observed at the age of 28 days for concrete with 0.15% GO content and 10% fly ash replacement.

Combined effect of GO and fly ash on growth rate of concrete is less at the early stages, although, strength properties of the concrete mixes with replacement of fly ash up to 30% are higher than control concrete at 7 days. At the age of 7 days, rate of increase in compressive, split tensile and flexural strength values for standard concrete were 31.43%, 24.32% and 13.88% for 10% fly ash replacement, 19.68%, 6.76% and 6.95% for 20% fly ash replacement, and 7.46%, 2.70% and 2.57% for 30% fly ash replacement, respectively compared to control concrete. Similarly, rate of increase in compressive, split tensile and flexural strength values for high strength concrete at the age of 7days were 22.86%, 14.55% and 8.06% for 10% fly ash replacement, 11.84%, 7.27% and 5.39% for 20% fly ash replacement, and 3.76%, 2.59% and 2.72% for 30% fly ash replacement, respectively compared to control concrete. This may be associated with the hydration process, the formation of more crystal structures of hydrated products takes place in concrete during the early-stage of hydration, so the rate of improvement of strength properties of control concrete is higher at early ages (Li et al. 2019). As GO expedites the hydration process, the growth of strength properties is higher at early ages. When the hydration process of cement reaches completion, the rate of interaction decreases due to a reduction in the oxygenated functionalities present on the GO sheets (Shang et al. 2015). Therefore, the drawback of fly ash on delaying early age development of strength was counterbalanced by GO.

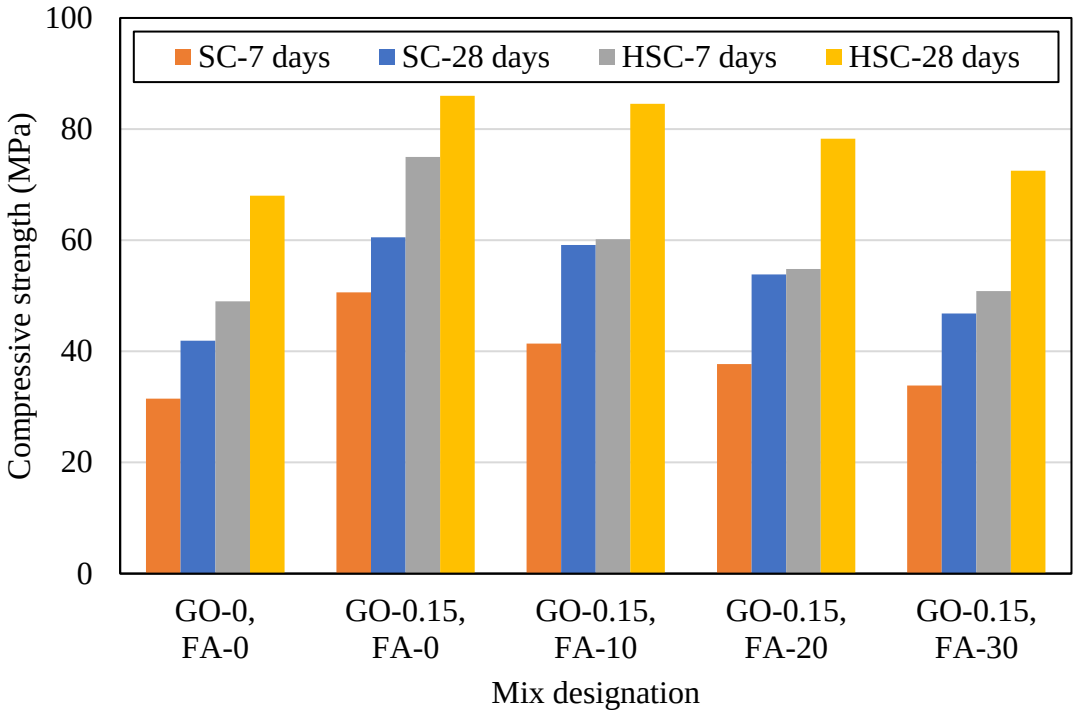

Figure 6.2 Compressive strength of GO-fly ash concrete

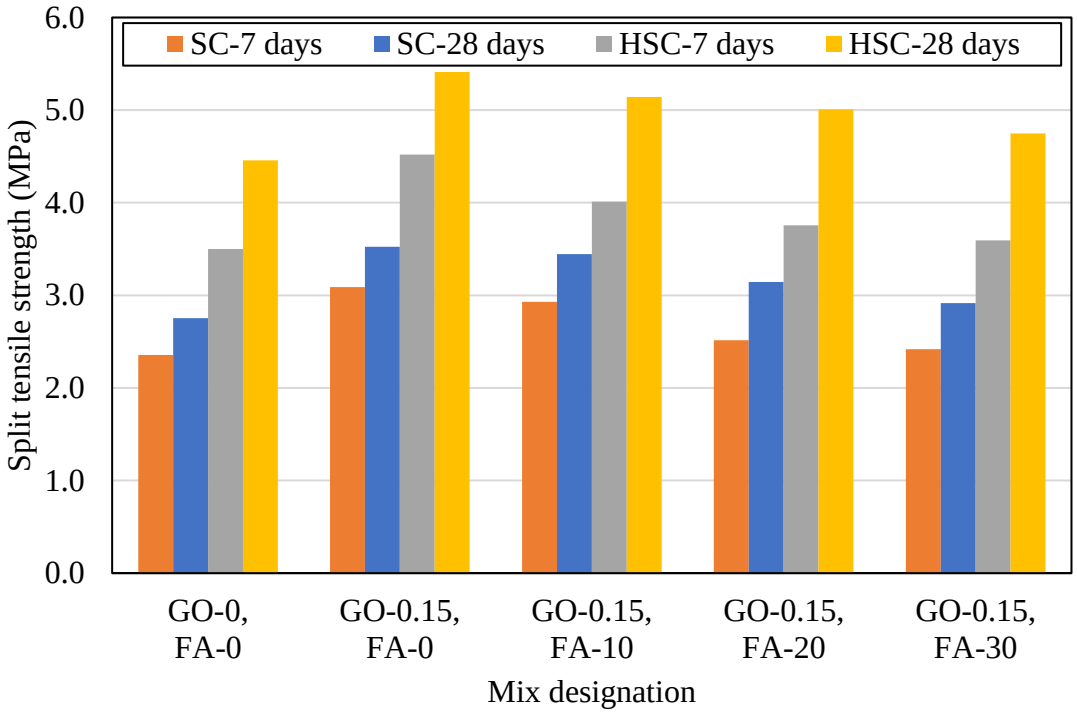

Figure 6.3 Split tensile strength of GO-fly ash concrete

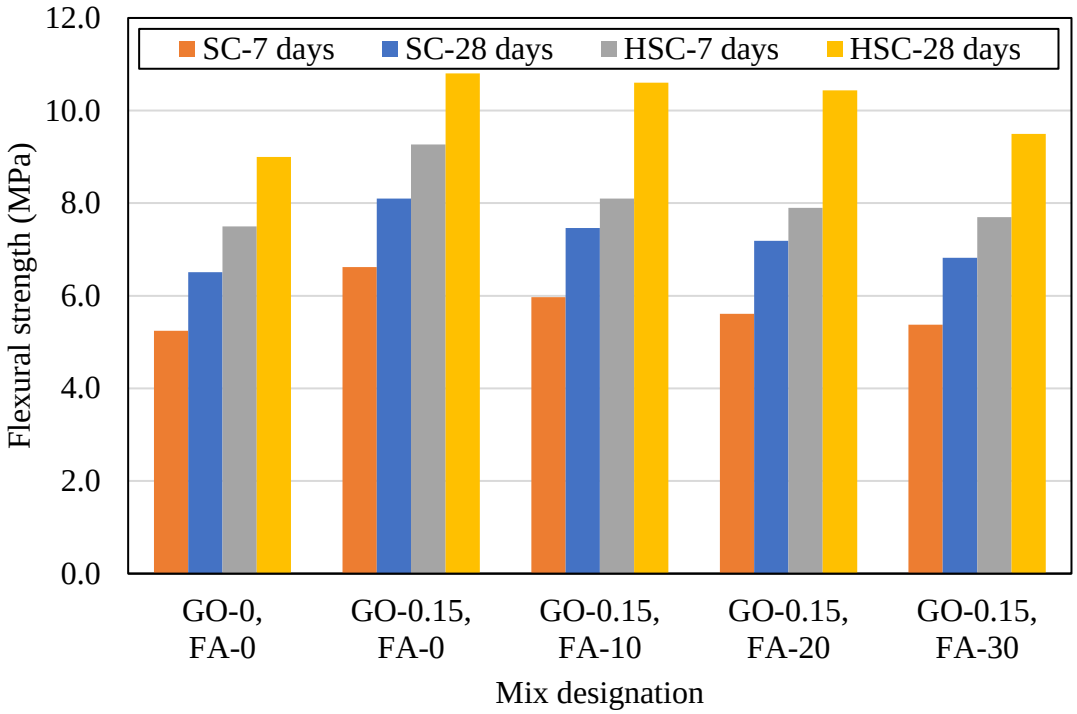

Figure 6.4 Flexural strength of GO-fly ash concrete

6.2.3. Static elastic modulus

The Stress-strain behaviour of standard and high strength concrete with different GO dosages are shown in Figure 6.5 and 6.6. Elastic chord modulus of standard concrete and high strength concrete containing various dosages of GO are shown in Figure 6.7. Elastic modulus of concrete incorporated with GO and fly ash was greater than control concrete similar to the observations made for the compressive strength. This suggests that GO addition and replacement of cement with fly ash improved elastic modulus of concrete. Elastic modulus of concrete containing GO at a dosage of 0.15% and replacement of cement with fly ash at 10%, 20% and 30% was 34.11, 31.07 and 28.86 GPa for standard concrete, and 43.47, 40.59 and 38.25 GPa for high strength concrete, respectively. The improvement in elastic modulus of concrete containing GO at 0.15% and fly ash at 10%, 20% and 30% was 19.86%, 9.15% and 1.39% for standard concrete, and 15.97%, 8.28% and 2.05% for high strength concrete, respectively, compared to that of concrete without GO and fly ash. The combined effect of GO and fly ash led to a substantial improvement

in elastic modulus. As a result, incorporation of GO and fly ash replacement is beneficial for improving the elastic modulus of concrete. Young's modulus of concrete is mainly governed by the three phases such as aggregates, cement paste and an interfacial transition zone (Chu et al. 2020). The introduction of GO could amplify the hydration rate and improve the microstructure of cementitious composites (Long et al. 2018; Z. Lu et al. 2016). Additionally, the incorporation of GO and fly ash to cementitious composites may produce a denser interfacial transition zone (Z. Lu et al. 2016). As a result, the incorporation of GO and fly ash may improve resistance of concrete to elastic deformation.

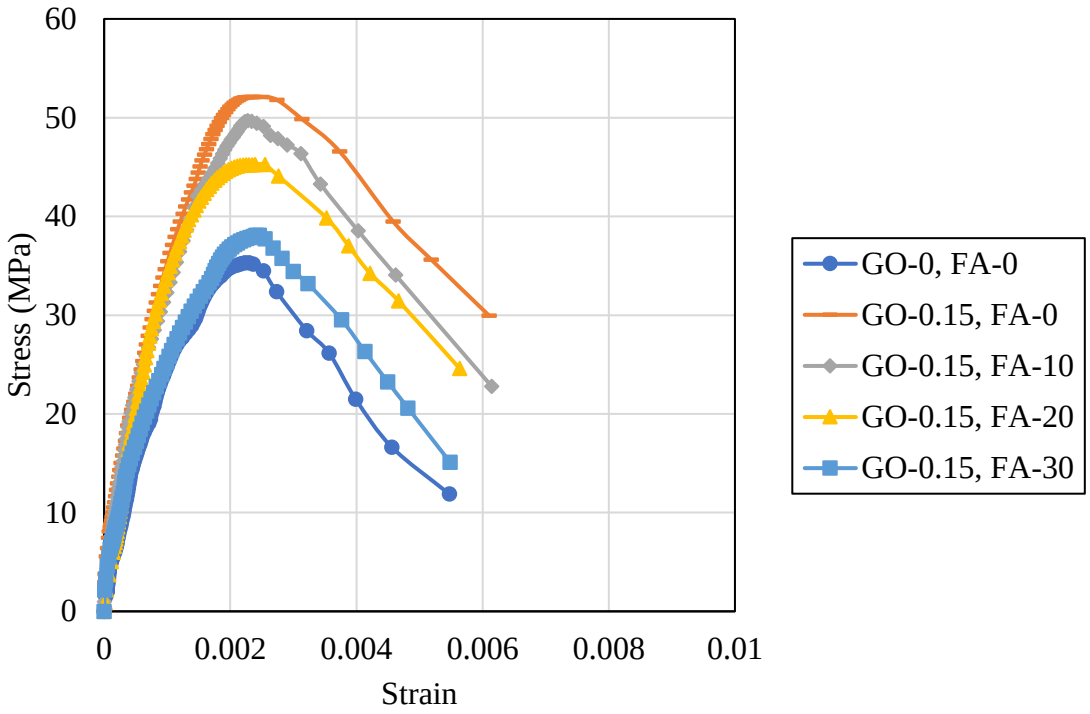

Figure 6.5 Stress-strain behaviour of standard concrete with GO and different fly ash replacements

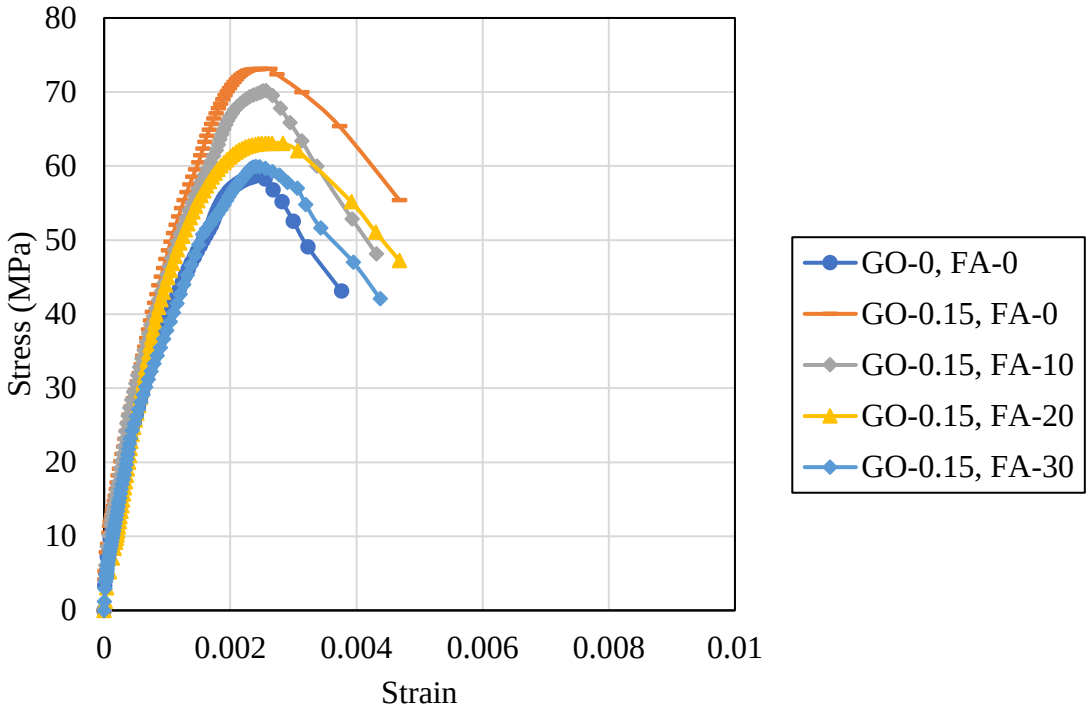

Figure 6.6 Stress-strain behaviour of high strength concrete with GO and different fly ash replacements

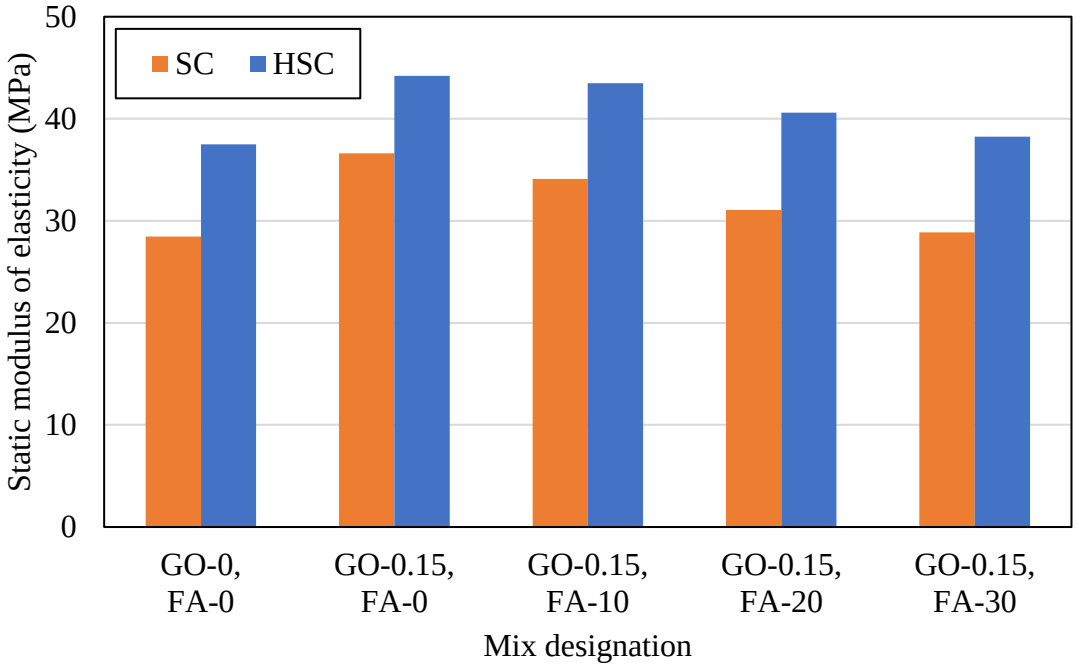

Figure 6.7 Static young's modulus of different GO-fly ash concrete mixes

6.3. Dynamic mechanical properties

6.3.1. Natural frequencies (ω) and damping ratios (ζ)

Natural frequencies, damping ratios and different mode shapes of all concrete mixes were obtained from the frequency response functions using impact hammer technique and the results are shown in Table 6.2. Frequency response functions of standard concrete and high strength concrete with varying dosages of GO are shown in Figure 6.8 and 6.9. Different mode shapes for transverse vibration are shown in Figure 6.10. Typical acceleration time curves for different vibration modes are shown in Figure 6.11. From the results it is found that fundamental natural frequencies of concrete prismatic beam specimens increased for both grades of concrete with the addition of GO and fly ash replacement compared to control concrete, whereas the damping ratio was decreased. Thus, the combined effect of GO and fly ash is helpful for increasing the frequencies and decreasing the damping ratios of concrete. The fundamental natural frequencies of concrete containing GO at a dosage of 0.15% and replacing cement with fly ash at 10%, 20% and 30% were 1676, 1632 and 1586 Hz for standard concrete, and 1728, 1712, and 1674 Hz for high strength concrete, respectively. The improvement in fundamental natural frequency of concrete containing GO at 0.15% and fly ash at 10%, 20% and 30% was 6.21%, 3.42% and 0.51% for standard concrete, and 3.91%, 2.95% and 0.66% for high strength concrete, respectively, compared to that of control concrete. Similarly, damping ratio of concrete containing GO at a dosage of 0.15% and replacing cement with fly ash at 10%, 20% and 30% were 0.65, 0.68 and 0.71 for standard concrete, and 0.58, 0.61, and 0.68 for high strength concrete, respectively. The decrease in damping ratio of concrete containing GO at 0.15% and fly ash at 10%, 20% and 30% was 24.42%, 20.93% and 17.44% for standard concrete, and 23.68%, 19.74% and 10.53% for high strength concrete, respectively, compared to that of control concrete.

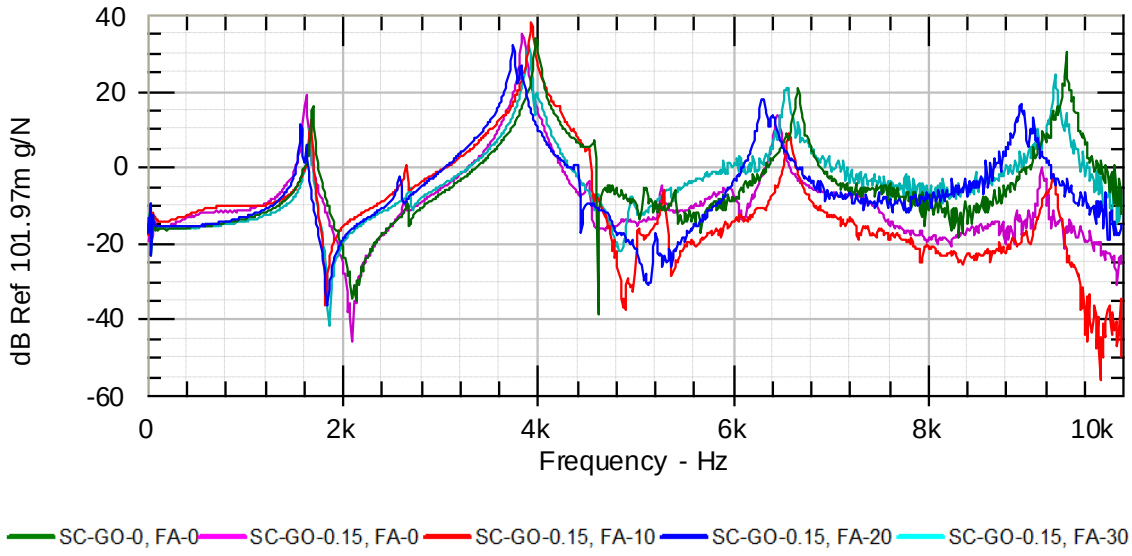

Figure 6.8 Frequency response function of standard concrete with GO and different fly ash replacements

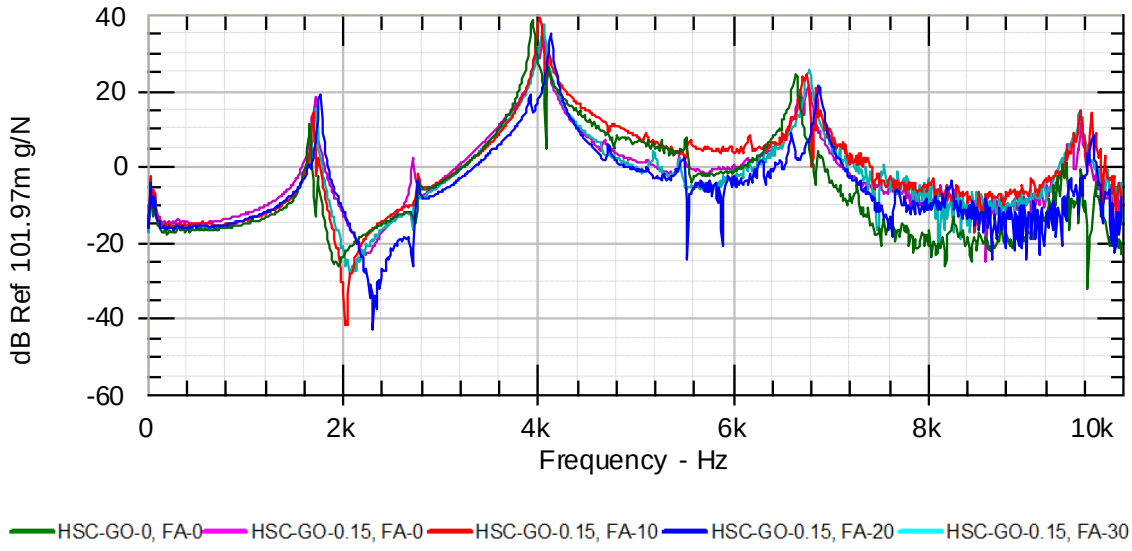

Figure 6.9 Frequency response function of high strength concrete with GO and different fly ash replacements

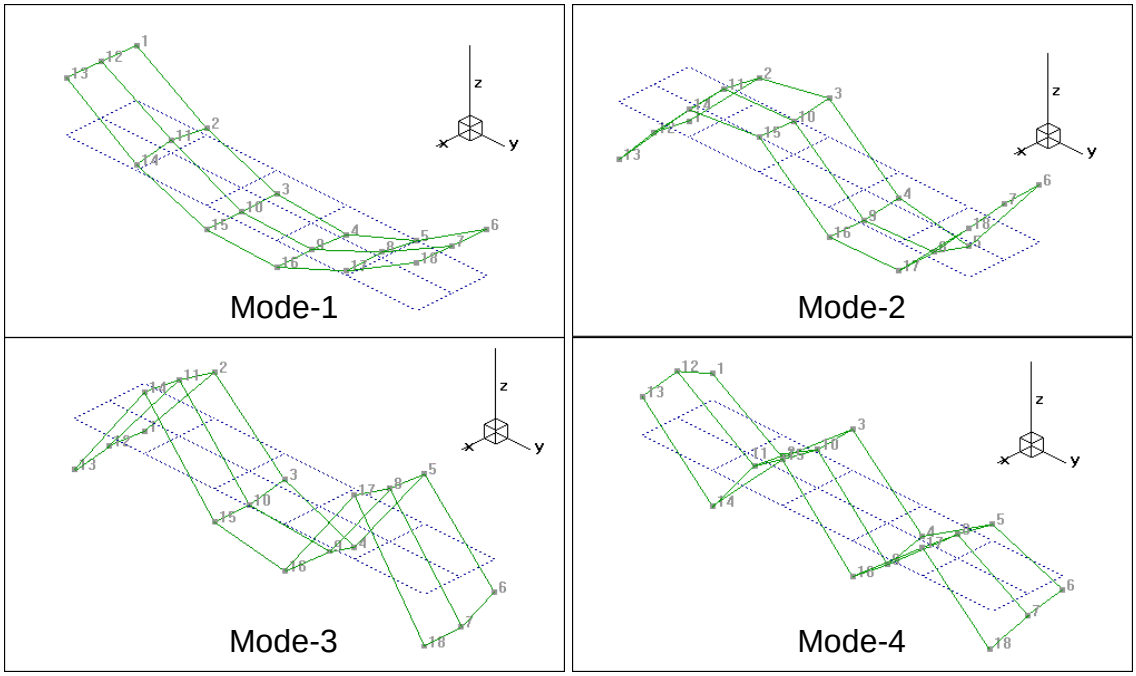

Figure 6.10 Typical mode shapes of transverse vibration

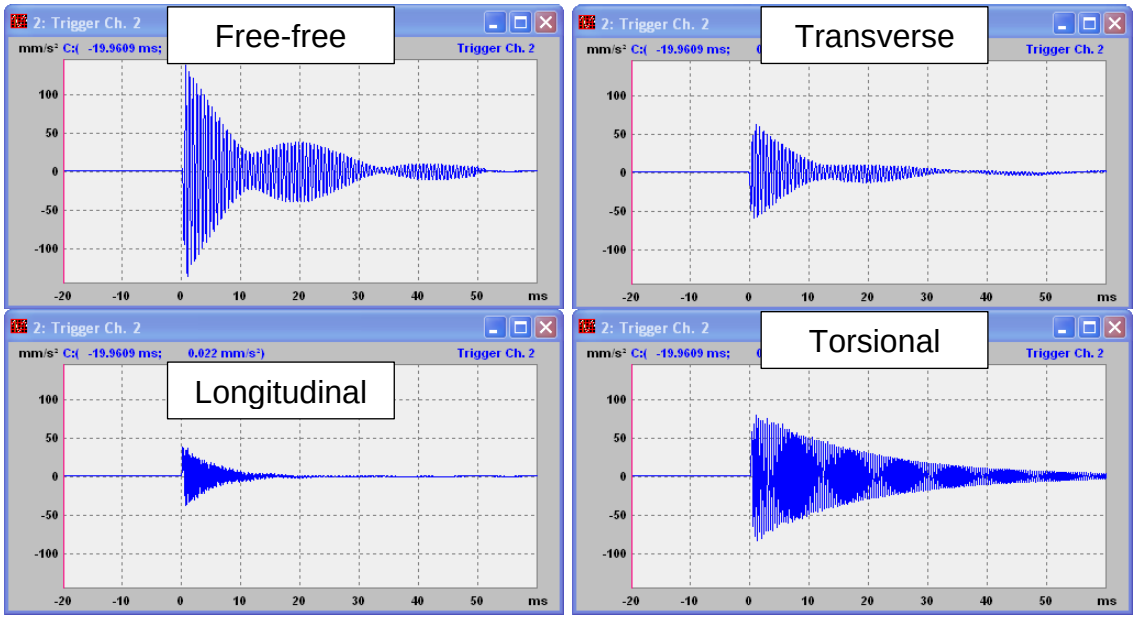

Figure 6.11 Typical acceleration time curves for different vibration modes

Table 6.2 Natural frequency (ω) and damping ratio (ζ) for first four modes of all concrete mixes

Mix	Frequency (Hz)				Damping ratio			
	Mode 1	Mode 2	Mode 3	Mode 4	Mode 1	Mode 2	Mode 3	Mode 4
Standard concrete (SC)								
GO-0, FA-0	1578	3746	6314	8956	0.86	0.53	0.43	0.32
GO-0.15, FA-0	1704	3995	6674	9425	0.61	0.41	0.34	0.26
GO-0.15, FA-30	1676	3937	6618	9315	0.65	0.43	0.35	0.27
GO-0.15, FA-30	1632	3901	6562	9208	0.68	0.45	0.39	0.29
GO-0.15, FA-30	1586	3842	6474	9168	0.71	0.48	0.41	0.31
High strength concrete (HSC)								
GO-0, FA-0	1663	3950	6648	9422	0.76	0.56	0.35	0.28
GO-0.15, FA-0	1763	4139	6890	9691	0.56	0.37	0.29	0.22
GO-0.15, FA-30	1728	4062	6810	9588	0.58	0.39	0.31	0.23
GO-0.15, FA-30	1712	4035	6764	9532	0.61	0.41	0.33	0.23
GO-0.15, FA-30	1674	3989	6684	9491	0.68	0.45	0.34	0.24

6.3.2. Dynamic elastic modulus and Poissons ratio

Fundamental transverse, longitudinal and torsional resonant frequencies were determined for all concrete mixes. The dynamic characteristic values attained for all concrete mixes are presented in Table 6.3. Experimental results shown that the fundamental resonant frequency of different vibration modes is increased in concrete with the addition of GO and replacement of fly ash up to 30% compared to control concrete for both grades of concrete. The values of dynamic elastic modulus and rigidity modulus have been determined from the fundamental transverse frequencies and torsional frequencies. The

dynamic poissons ratio was also calculated and presented in Table 6.3. From the results, it can be clearly noticed that dynamic elastic modulus, dynamic rigidity modulus and poissons ratio of concrete was improved with the addition GO and replacement of fly ash. The dynamic elastic modulus of concrete containing GO at a dosage of 0.15% and replacing cement with fly ash at 10%, 20% and 30% were 53.09, 50.14 and 47.54 GPa for standard concrete, and 56.44, 54.96, and 52.75 GPa for high strength concrete, respectively. The dynamic rigidity modulus was 22.02, 20.92 and 20.03 GPa for standard concrete, and 22.68, 22.35, and 21.68 GPa for high strength concrete, respectively. Similarly, the dynamic poissons ratio was 0.21, 0.20 and 0.19 for standard concrete, and 0.24, 0.23 and 0.22 for high strength concrete, respectively.

Table 6.3 Dynamic youngs modulus and poisons ratio of different concrete mixes from fundamental resonant frequencies according to ASTM C215

Mix	Transverse frequency (Hz)	Longitudinal frequency (Hz)	Torsional frequency (Hz)	Dynamic elastic modulus $E_{d,TR}$ (GPa)	Dynamic rigidity modulus G_d (Gpa)	Dynamic poissons ratio μ_d
Standard concrete (SC)						
GO-0, FA-0	1578	4338	2575	46.69	19.61	0.19
GO-0.15, FA-0	1704	4685	2748	54.66	22.42	0.22
GO-0.15, FA-10	1676	4595	2718	53.09	22.02	0.21
GO-0.15, FA-20	1632	4482	2654	50.14	20.92	0.20
GO-0.15, FA-30	1586	4416	2592	47.54	20.03	0.19

Mix	Transverse frequency (Hz)	Longitudinal frequency (Hz)	Torsional frequency (Hz)	Dynamic elastic modulus $E_{d,TR}$ (GPa)	Dynamic rigidity modulus G_d (Gpa)	Dynamic poissons ratio μ_d
High strength concrete (HSC)						
GO-0, FA-0	1663	4562	2685	51.86	21.32	0.22
GO-0.15, FA-0	1763	4826	2808	58.51	23.41	0.25
GO-0.15, FA-10	1728	4762	2758	56.44	22.68	0.24
GO-0.15, FA-20	1712	4661	2749	54.96	22.35	0.23
GO-0.15, FA-30	1674	4592	2702	52.75	21.68	0.22

6.3.3. Ultrasonic pulse velocity

UPV test was conducted to evaluate uniformity and homogeneity of concrete with the incorporation of GO and fly ash. The quality of concrete was evaluated at 28 days and categorized in accordance with IS:13311(Part 1)-2018. Table 6.4 shows ultrasonic pulse velocities of standard and high strength concrete with GO and fly ash and compared with control concrete. According to the UPV values, the combined effect of GO and fly ash on concrete resulted in formation of excellent quality concrete with greater uniformity. The pulse velocity of concrete with 0.15% GO and fly ash replacement at 10%, 20% and 30% was 4859, 4726, and 4625m/s for standard concrete and 5192, 5010, and 4897 m/s for high strength concrete. The increase in concrete quality might be attributed to nano filler effect of GO, which densifies microstructure of cement matrix. Therefore, improvement in the uniformity and homogeneity of cement concrete indicated the development in compressive strength of concrete.

Dynamic elasticity modulus (E_d) of the concrete was also evaluated from the pulse velocity and dynamic Poisson's ratio (μ_d) using Equation 4.9 and 4.10, the results are given in Table 6.4. The dynamic Poisson's ratio was measured using pulse velocity readings on concrete prisms and the fundamental resonant frequency in longitudinal mode of vibration determined by an impact hammer test. The trend of dynamic elastic modulus and poissons ratio is comparable to that of compressive strength for both concrete grades. These findings are consistent with the impact resonance test according to ASTM C215.

Table 6.4 Dynamic youngs modulus and dynamic poisons ratio of different concrete mixes from UPV values according to IS:13311(Part-1)

Mix	UPV (m/s)	Longitudinal frequency (Hz)	Dynamic elastic modulus, $E_{d,UPV}$ (GPa)	Dynamic poissons ratio, μ
Standard concrete (SC)				
GO-0, FA-0	4554	4338	47.05	0.19
GO-0.15, FA-0	4995	4685	55.09	0.22
GO-0.15, FA-30	4859	4595	53.21	0.21
GO-0.15, FA-30	4726	4482	50.42	0.20
GO-0.15, FA-30	4625	4416	49.14	0.19
High strength concrete (HSC)				
GO-0, FA-0	4859	4562	52.03	0.22
GO-0.15, FA-0	5308	4826	58.46	0.25
GO-0.15, FA-30	5192	4762	57.15	0.24
GO-0.15, FA-30	5010	4661	54.31	0.23
GO-0.15, FA-30	4897	4592	52.93	0.22

6.4. Microstructural characterization

6.4.1.1. SEM

The images of SEM of the different concrete mixes with GO content of 0.15% and different fly ash percentages of 10%, 20%, 30% are illustrated in Figure 6.12 and 6.13. Surface morphology of the control concrete sample is illustrated in Figure 6.12(a) and 6.13(a), it can be observed from the SEM image the development of CH, C-S-H, Afm and Aft have pores and micro-cracks lead to a loose and non-uniform structure. SEM image of GO-concrete is illustrated in Figure 6.12(b) and 6.13Figure 6.13(b), clearly indicating that concrete with GO addition, the crystallinity of hydration phases is closely interweaved with one another and have a less micro-cracks and pores. The surface of GO-concrete shows the formation of a compact, uniform and densified structure at micro-level compared with control concrete, which is responsible for the development of mechanical properties. SEM images are illustrated in Figure 6.12(c-e) and 6.13(c-e), structure of hydrated products of cement with the combination of fly ash and GO was improved compared to control concrete. Unreacted smooth spherical shape fly ash particles can also be noticed, which demonstrates hydration of fly ash is in progress, this is responsible for the improvement in strength properties of concrete with GO and fly ash.

6.4.1.2. EDX

EDX analysis was carried out to examine the elemental composition of hydration products from the images of SEM in Figure 6.12 and 6.13 and composition of elements percentage was given in Table 6.5. From the composition of elemental percentage, it is noticed that an increase in percentages of elements Ca, C and Si in comparison with control concrete for standard concrete and high strength concrete, and also substantial reduction in the element percentage of O was noticed. For control concrete, the Ca/Si elemental ratio was high and addition of GO decreased the Ca/Si ratio. This shows that process of hydration in presence of GO leads to the densified C-S-H formation and other hydration products interwoven with one another and improved the mechanical

characteristics of standard and high strength concrete with GO and fly ash (Kunther et al. 2017).

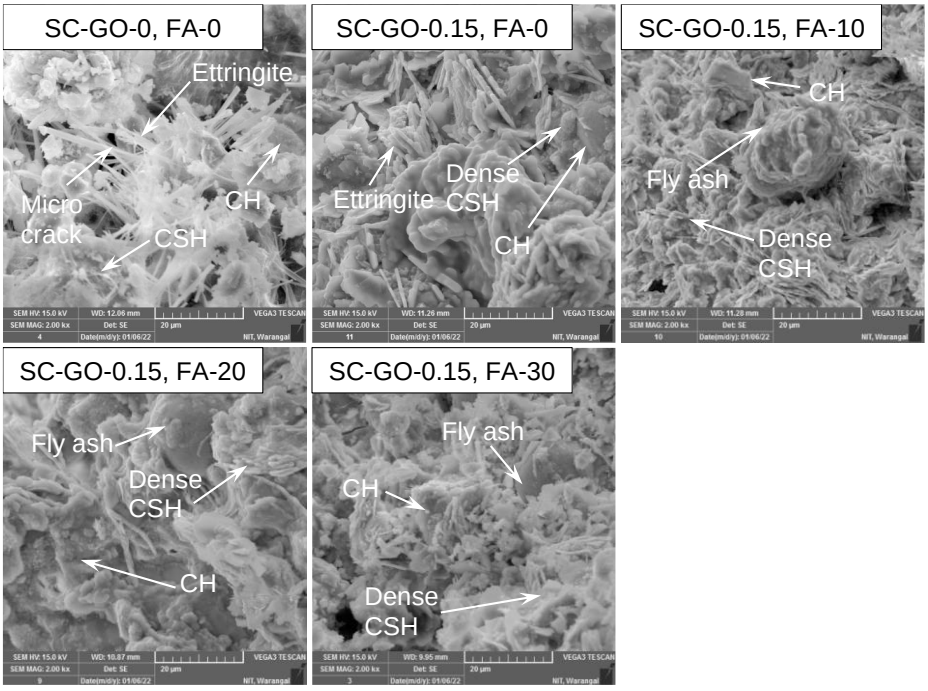

Figure 6.12 Microstructure of standard concrete with GO and fly ash

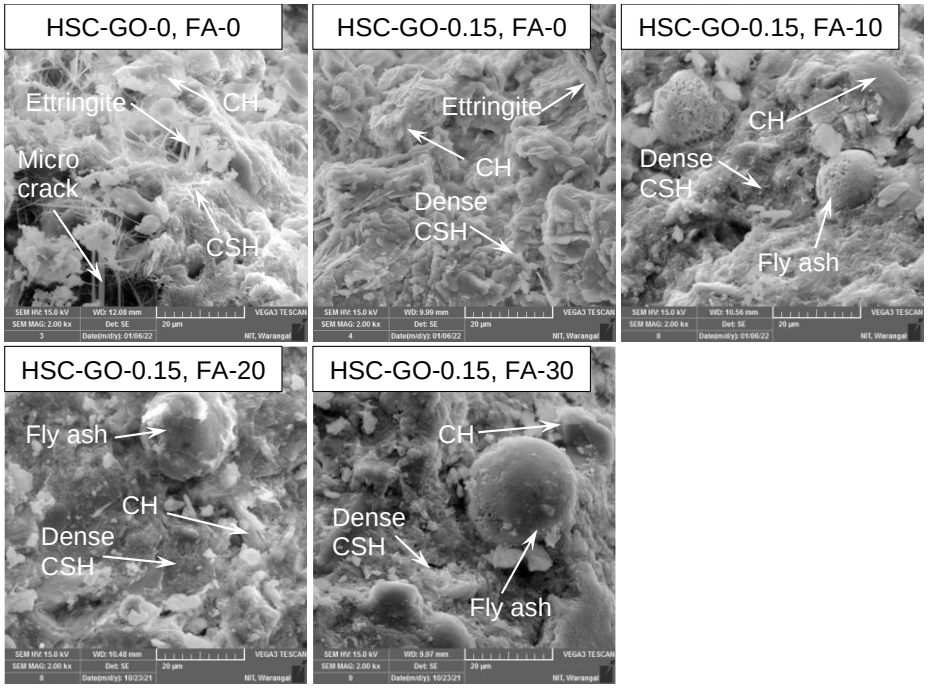

Figure 6.13 Microstructure of high strength concrete with GO and fly ash

Table 6.5 Percentage atomic ratios of different concrete mixes

Mix	Standard concrete (SC)			High strength concrete (HSC)		
	Ca/Si	(Al+Fe)/Ca	S/Ca	Ca/Si	(Al+Fe)/Ca	S/Ca
GO-0, FA-0	2.44	0.16	0.15	1.77	0.14	0.13
GO-0.15, FA-0	1.70	0.21	0.02	1.05	0.21	0.01
GO-0.15, FA-10	1.90	0.20	0.07	1.10	0.24	0.01
GO-0.15, FA-20	2.06	0.18	0.06	1.23	0.20	0.02
GO-0.15, FA-30	2.10	0.17	0.07	1.39	0.19	0.02

6.4.1.3. XRD

The XRD pattern of different concrete mixes are illustrated in Figure 6.14 and 6.15. The patterns demonstrate that no major difference in the positions of diffraction peaks (2θ = 18.12°, 20.83°, 34.07°, 39.73°, 42.50°, 50.76°, 54.86°, 60.25°) among the various concrete mixes, indicating that combination of fly ash and GO shows the identical crystals of hydration phases of CH, Aft and Afm (Snehal et al. 2020). Moreover, addition of GO and replacement of fly ash enhances the peaks intensity compared to control concrete, shows that the increase in crystallinity of hydration phases. Additionally, the reaction of cement and the oxygen functionalities of GO will help to increase the crystalline phase formation, the new crystalline phase formation contributed to enhancement of mechanical characteristics of standard and high strength concrete with GO and fly ash (Lv et al. 2013).

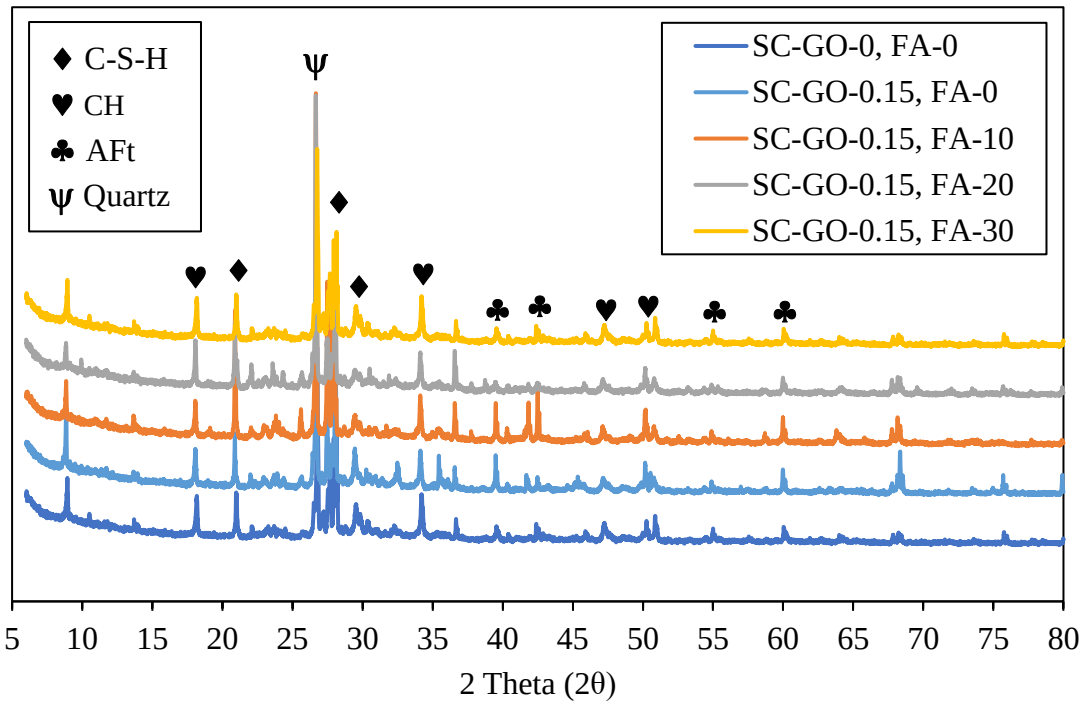

Figure 6.14 XRD patterns of standard concrete with GO and fly ash

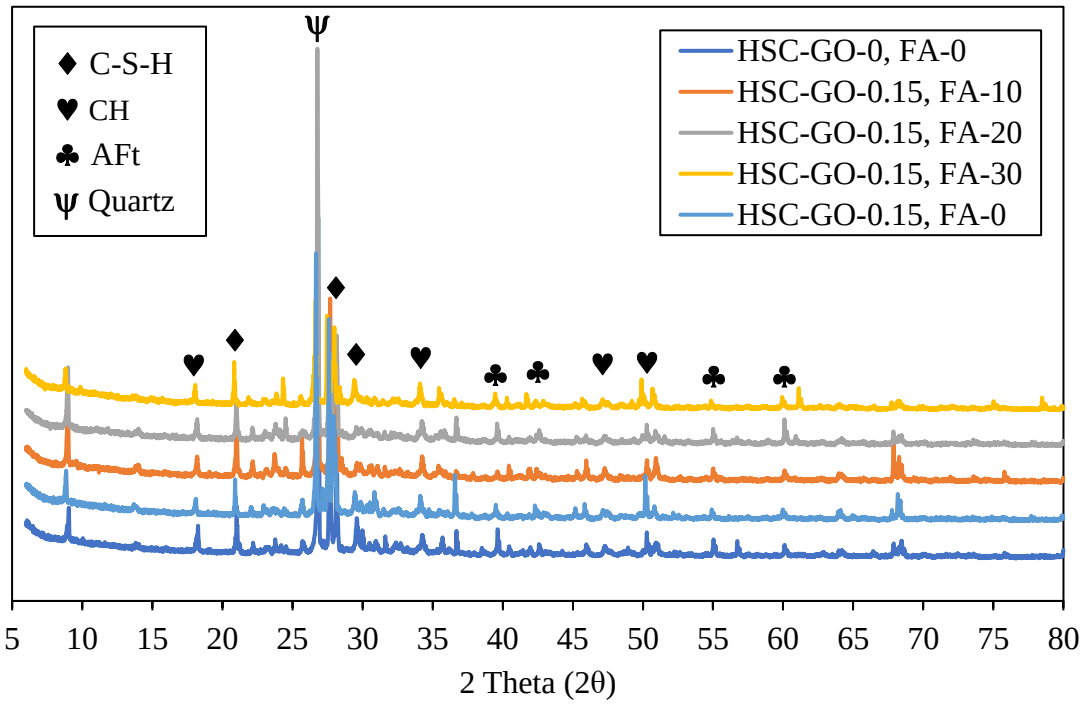

Figure 6.15 XRD patterns of high strength concrete with GO and fly ash

6.4.1.4. FTIR

The FTIR spectra for various mixes of concrete with GO and different replacements of fly ash are shown in Figure 6.16 and 6.17. It can be seen that the Calcium silicate hydrate in the band region of 950-1000 cm^{-1} and the GO addition increases the peak intensity. The absorption peak of calcium hydroxide can be noticed at 3643 cm^{-1}. It can also be demonstrated that the monosulfate aluminate peaks at the bands 1380 and 1665 cm^{-1} and strong trisulfate aluminate at 857, 1640-1680, and 3431 cm^{-1} (Horgnies et al. 2013). Because hydrated products are identical in all concrete mixes, the FTIR spectra is similar, except for differences in peaks between them. Additionally, when a GO is added, the absorption peak of Calcium silicate hydrate shifts to a higher wavenumber than that of control concrete. This demonstrates the addition of GO changes the Ca/Si ratio and formation of densified calcium silicate hydrate gels, because of this the strength characteristics were increased for standard and high strength concrete with GO and fly ash (Kang et al. 2019).

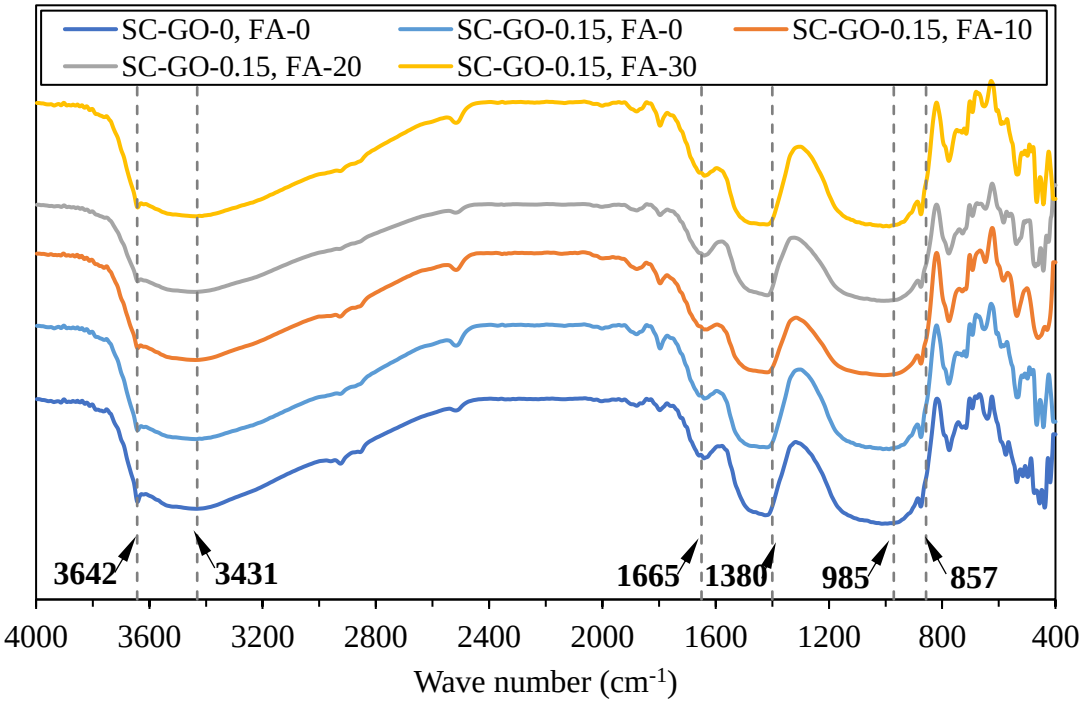

Figure 6.16 FTIR spectrum of standard concrete with GO and fly ash

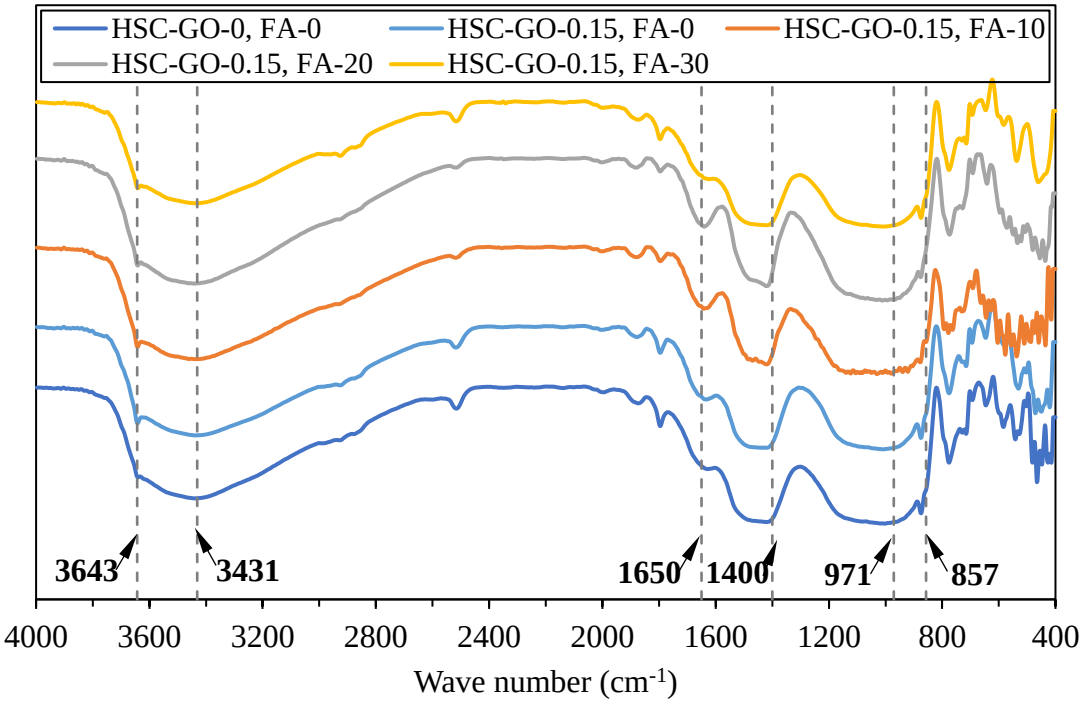

Figure 6.17 FTIR spectrum of high strength concrete with GO and fly ash

6.4.1.5. TGDTA

The values of non-evaporable water content at 28 days with GO and varying fly ash replacements are shown in Table 6.6. The values may be lower than the actual value since weakly bound water present in the certain hydrated products, including ettringites, starts to decompose at lower temperatures. The non-evaporable water content of concrete with GO and fly ash is greater than control concrete for standard and high strength concrete. With the increase in fly ash replacement, non-evaporable water content is steadily decreased, though it is greater than the concrete without GO. This is due to the substitution of fly ash reduces the quantity of cement content. This results in a decrease in quantity of hydrated products, especially prominent in the early phases. On the other hand, secondary hydration of fly ash increases non-evaporable water content. The rise in non-evaporable water content of concrete with GO and fly ash suggests that integration of GO has a role in improving the hydration of the concrete matrix with GO and fly ash at a later stage.

Because GO has a considerable influence on hydration degree, it may be expected that GO may have the influence on secondary hydration of fly ash.

The TGA and DTG results for standard and high strength concrete are shown in Figure 6.18 and 6.19. Combined effect of GO and fly ash on CH content of concrete mixes at 28 days of hydration is shown in Figure 6.20. The CH content of the concrete containing GO was lowered by 7.7% with the replacement of fly ash in comparison to control concrete. This can be due to the presence of fly ash, CH functions as a reactant and contributes to the secondary hydration process, which reduces the CH quantity. Because the secondary hydration process of fly ash begins in early ages, the first reaction is extremely slower, and the amount of CH used is considerably less than the amount produced by cement hydration, leads to gradual and constant increase in CH quantity. However, at 28 days, the quantity of CH generated in the system continues to decrease while the interaction between CH and fly ash increases. These two factors contribute to a reduction in CH. Provided that GO has a considerable impact on the CH content in the concrete matrix.

Table 6.6 Chemically bound water (CBW), degrees of hydration (α) and calcium hydroxide (CH) for all concrete mixes.

Mix	Ldh (%)	Ldx (%)	Ldc (%)	CBW (%)	α (%)	CH (%)
SC-GO-0, FA-0	9.28	2.92	3.62	13.69	57.04	12.00
SC-GO-0.15, FA-0	9.94	3.16	4.20	14.82	61.76	12.99
SC-GO-0.15, FA-10	9.98	3.09	4.20	14.75	61.47	12.70
SC-GO-0.15, FA-20	10.07	2.96	4.01	14.67	61.13	12.16
SC-GO-0.15, FA-30	9.55	2.87	3.90	14.02	58.42	11.78
HSC-GO-0, FA-0	12.48	4.25	4.52	18.58	77.44	17.47
HSC-GO-0.15, FA-0	13.53	4.50	4.65	19.94	83.07	18.50
HSC-GO-0.15, FA-10	13.43	4.41	4.65	19.84	82.68	18.12
HSC-GO-0.15, FA-20	13.14	4.32	4.52	19.32	80.50	17.76

Mix	Ldh (%)	Ldx (%)	Ldc (%)	CBW (%)	α (%)	CH (%)
HSC-GO-0.15, FA-30	13.13	4.13	4.66	19.17	79.87	16.97

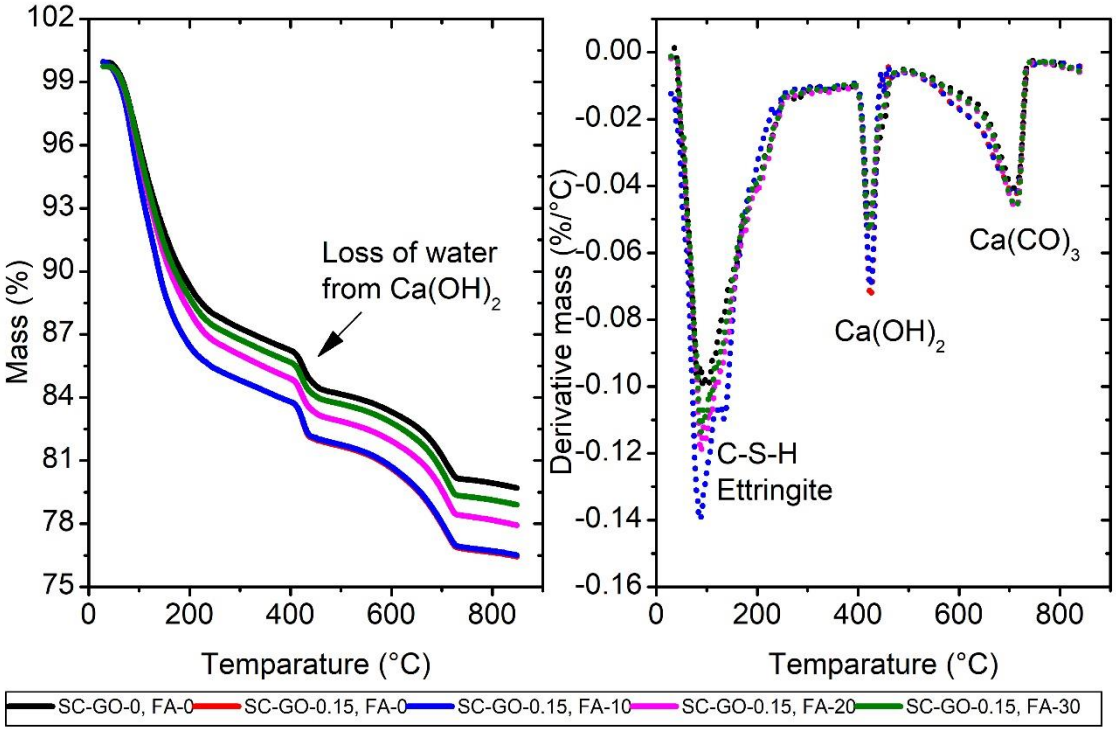

Figure 6.18 TGA and DTG analysis for standard concrete with GO and fly ash

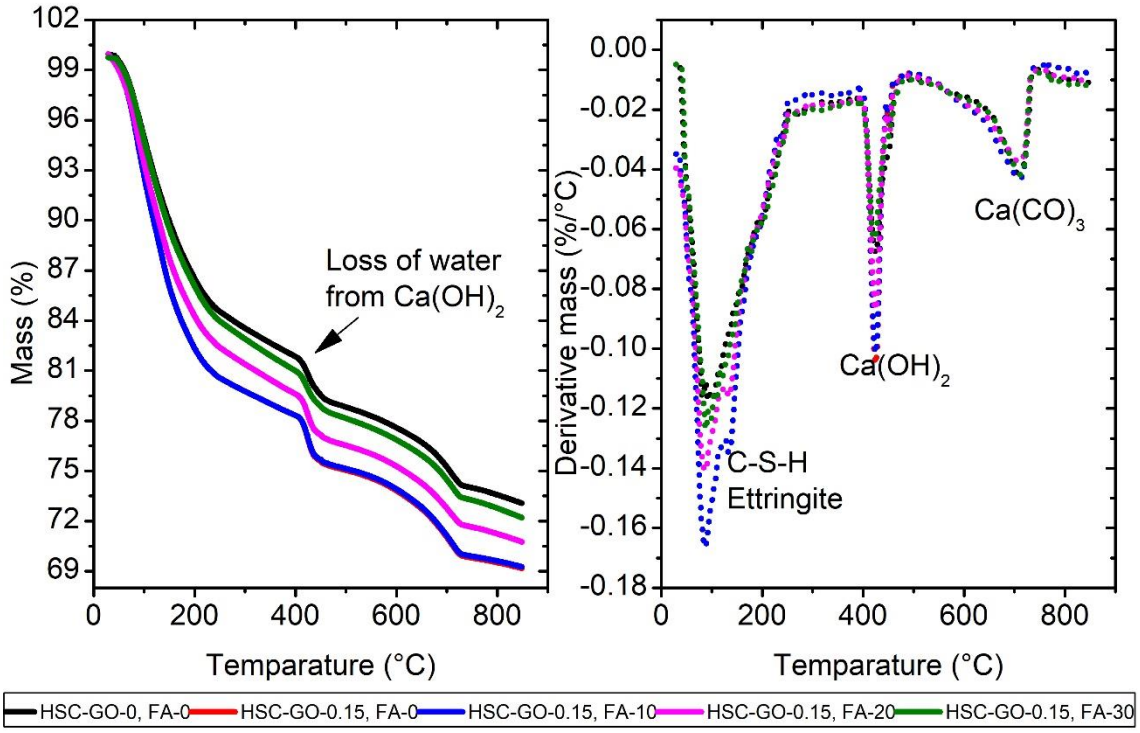

Figure 6.19 TGA and DTG analysis for high strength concrete with GO and fly ash

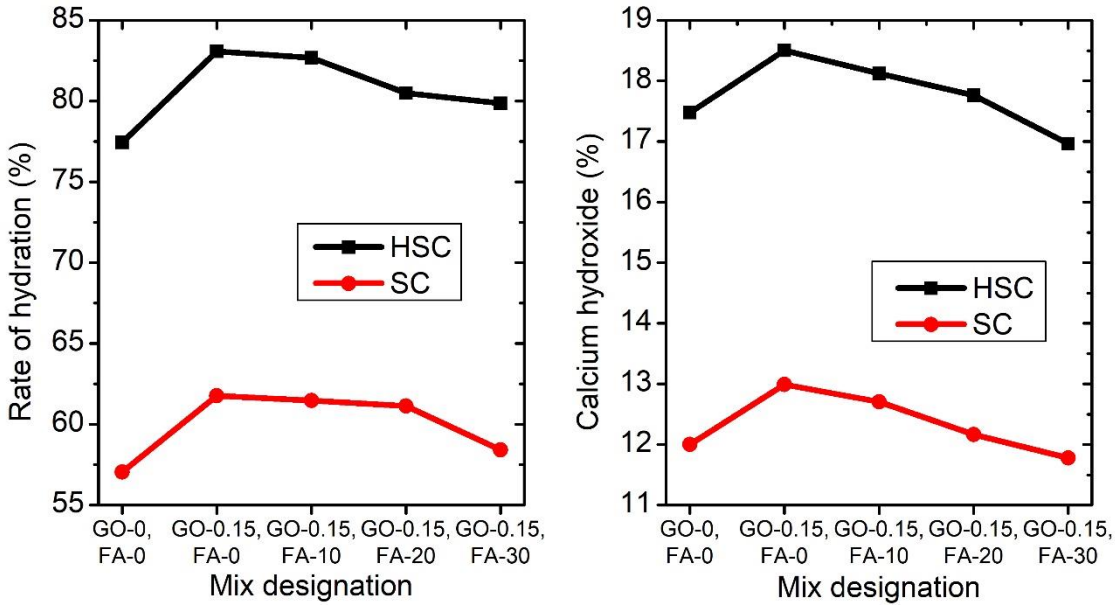

Figure 6.20 Rate of hydration and calcium hydroxide for standard and high strength concrete with GO and fly ash

6.5. Durability properties

6.5.1. Water absorption

Water absorption values of concrete with constant GO dosage and varying fly ash replacements for both grades of concrete are shown in Figure 6.21. It can be observed that combined effect of GO and fly ash in concrete was found to be effective in resistance to water absorption. Increase in fly ash replacements led to increased resistance to water absorption compared to control concrete. This trend is observed for both standard concrete and high strength concrete. Water absorption values of control concrete and concrete with constant GO dosage of 0.15% and varying fly ash replacements at 0%, 10%, 20%, and 30% are recorded as 2.03%, 1.74%, 1.64%, and 1.42% for standard concrete and 1.17%, 1.13%, 1.07%, and 0.98% for high strength concrete, respectively. Water absorption in concrete mixes is primarily influenced by the parameters that govern concrete porosity. The improved resistance to water absorption may be attributed to the extensive barrier properties of GO and fly ash, and refinement of pore structure of the cement composite resulting from decrease in critical pore diameter.

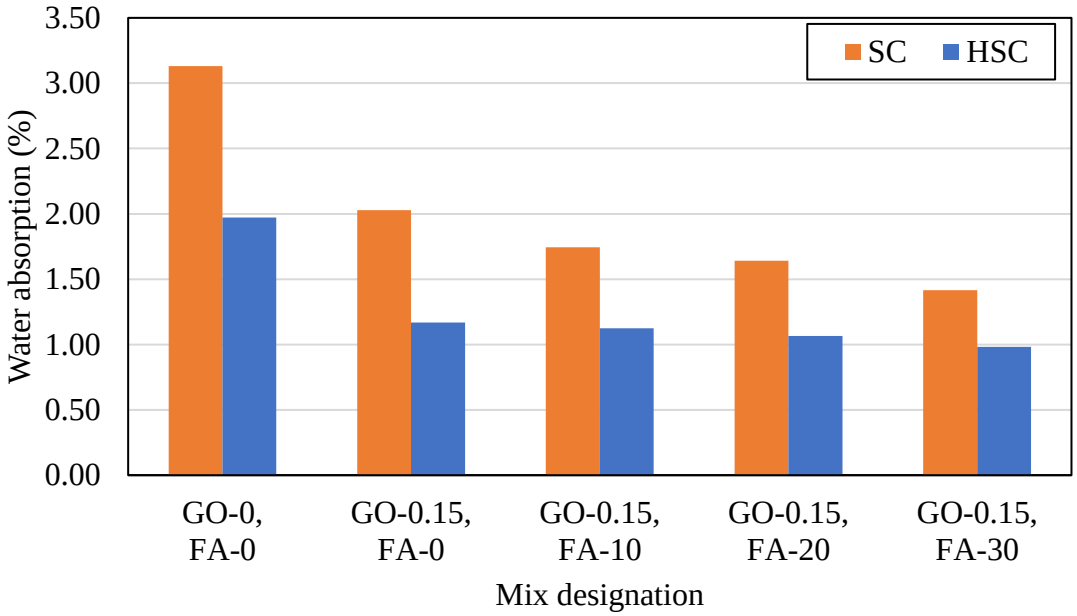

Figure 6.21 Water absorption of GO and fly ash based concrete mixes

6.5.2. Water sorptivity

The water sorptivity values of concrete with constant GO dosage and varying fly ash replacements for both grades of concrete at 28, 56 and 90 days are shown in Figure 6.22. It can be observed that GO and fly ash incorporation in concrete was found to be effective in resistance to the water sorptivity. Increase in fly ash replacements led to increased resistance to water sorptivity compared to control concrete. Similar trend is observed for both standard concrete and high strength concrete. Water sorptivity values of control concrete and concrete with constant GO dosage of 0.15% and varying fly ash replacements at 0%, 10%, 20%, and 30% at 90 days were 0.0067, 0.0043, 0.0041, 0.0039, and 0.0037 mm/√s for standard concrete and 0.0032, 0.00080, 0.00076 0.00072, and 0.00068 mm/√s for high strength concrete, respectively. Water sorptivity in concrete mixes is primarily influenced by the permeability of the pore system that absorbs water or other substances by increasing capillarity. The improved resistance to water sorptivity can be attributed to the micro filler and nano filler effect of fly ash and GO respectively.

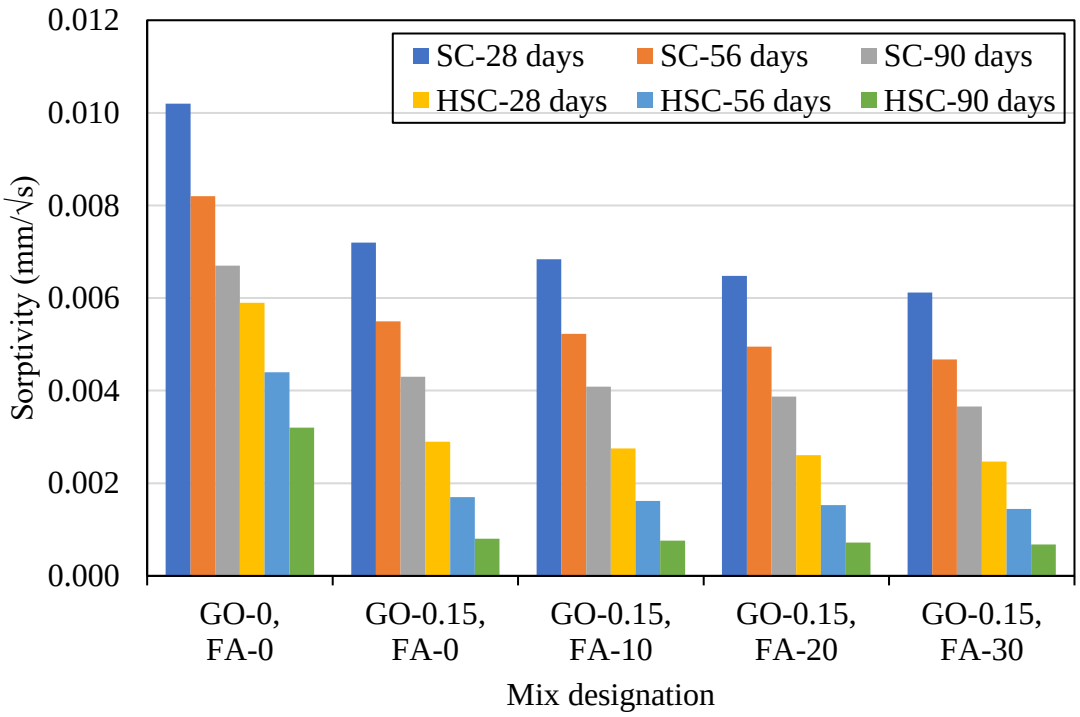

Figure 6.22 Water sorptivity of GO and fly ash based concrete mixes

6.5.3. Accelerated Carbonation

Carbonation depth values of concrete with constant GO dosage and varying fly ash replacements for both grades of concrete are shown in Figure 6.23. Carbonation depth of all concrete mixes was observed to decrease with increase in fly ash replacements. Carbonation depth of concrete mixes with 30% fly ash replacement was shown to have a minimum carbonation depth demonstrating that the combination of GO and fly ash has more resistance to chemical intrusion by pore network structure. This trend is observed for both standard concrete and high strength concrete. Carbonation depth values of control concrete and concrete with constant GO dosage of 0.15% and varying fly ash replacements at 0%, 10%, 20%, and 30% were 9, 8, 6, and 4 mm for standard concrete and 6, 5, 4, and 3 mm for high strength concrete, respectively.

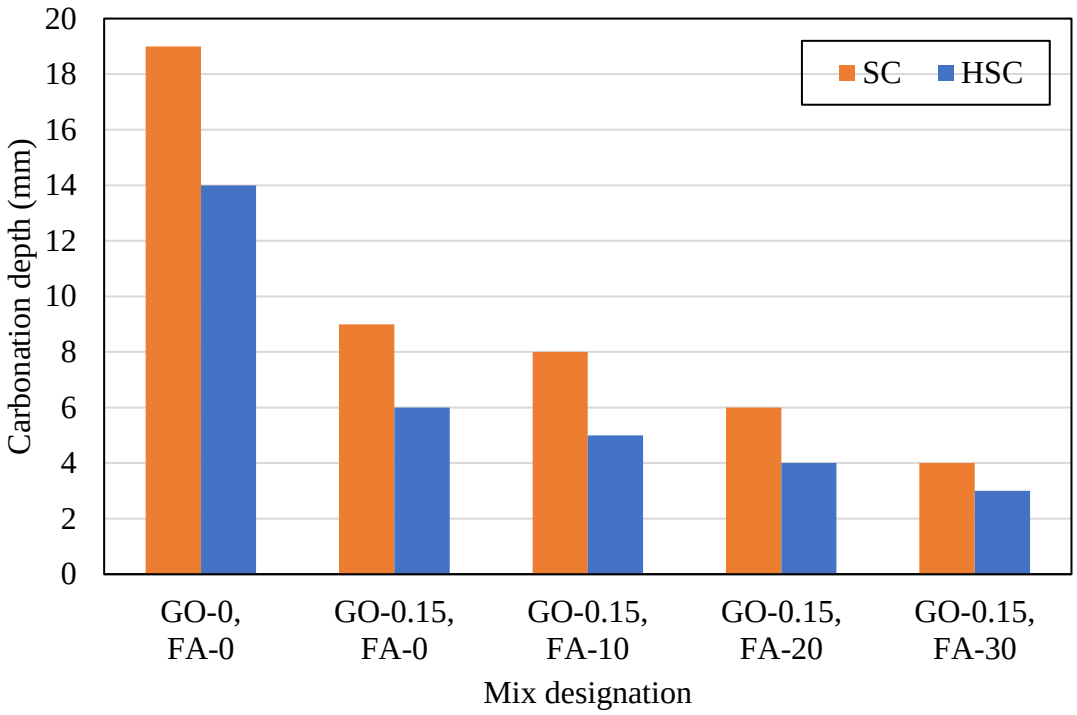

Figure 6.23 Carbonation depth of GO and fly ash based concrete mixes

6.5.4. Rapid chloride penetration

According to ASTM C 1202, the findings of chloride ion penetration is determined by the charge passed. Figure 6.24 shows the chloride ion permeability for the concrete mixes with constant GO dosage and varying fly ash replacements. It reveals that increase of fly ash replacements in concrete good to resist chloride ion permeability. For the concrete mixes with the addition of GO at 0.15% and fly ash replacement at 30%, the permeability was low, which could be attributable to the high dosage of GO and fly ash. In contrast, the standard concrete mix without GO falls in high chloride ion-permeable class. Similarly, standard concrete and high strength concrete mixes were exhibited increased resistance of chloride ion permeability with increase in fly ash replacement. Charge passed values of control concrete and concrete with constant GO dosage of 0.15% and varying fly ash replacements at 0%, 10%, 20%, and 30% were 1620, 1210, 1015, and 821 coulombs for standard concrete and 821, 648, 454, and 346 coulombs for high strength concrete, respectively. However, the concrete mix containing 0.15% GO and fly ash replacement at 30% exhibited less chloride ion permeability compared to all other mixes.

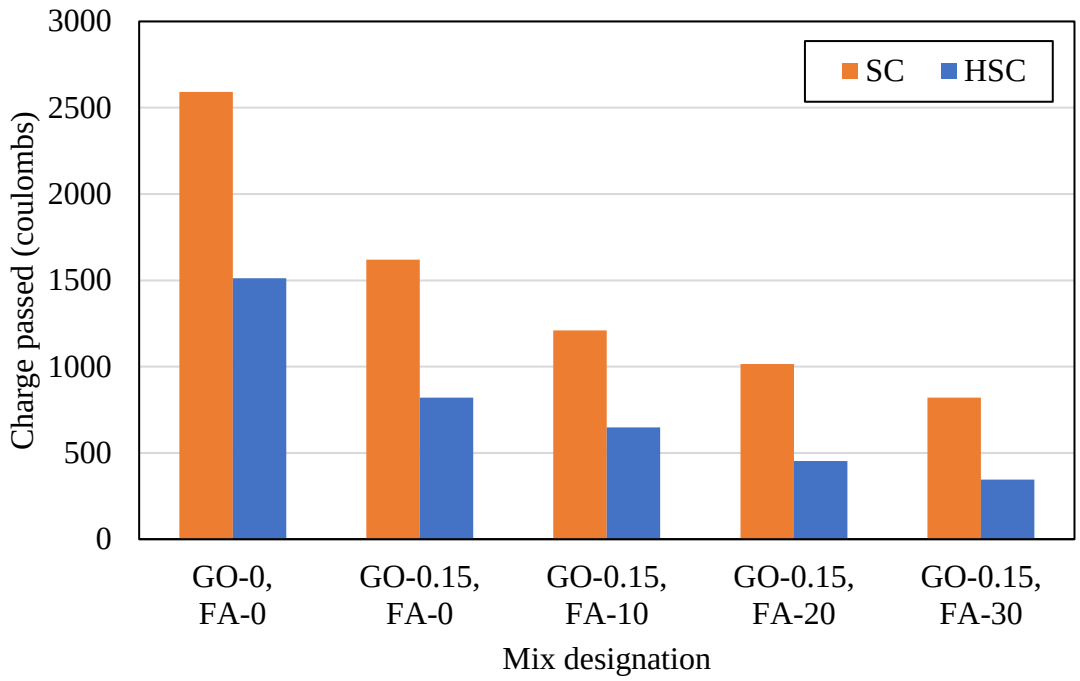

Figure 6.24 Charge passed of GO and fly ash based concrete mixes

6.5.5. ACID ATTACK

6.5.5.1. Dimension, weight and strength losses

The dimension, weight and strength losses in the concrete specimens at the 28, 56 and 90 days exposure of HCl and H_2SO_4 are shown in Figure 6.25 to 6.30. It can be observed that the dimension, weight and strength losses of all the specimens are increased with reference to increased age of the exposure and the degree of calcium leaching from concrete matrix was influenced by the type of acid. H_2SO_4 acidic environment resulted in higher losses of all concrete mixes, when compared to the HCL environment. The concrete with GO and fly ash exhibited a greater resistance to acidic environment compared control concrete and the resistance to these losses are increased with an increasing fly ash replacement. The average dimension, weight and strength losses in the concrete mixes without GO and fly ash exposed to HCL attack at 90 days of exposure were 10.4%, 20.1%, and 42.9% for standard concrete and 8.05%, 15.5%, and 35.3% for high strength concrete, respectively. Whereas for concrete mixes with the addition of GO at 0.15% and fly ash replacement at 30% exposed to HCl acid for 90 days, these losses were decreased to 2.52%, 4.38%, and 13.05% for standard concrete and 2.40%, 3.76%, and 9.82% for high strength concrete, respectively. On the other hand, the average dimension, weight and strength losses in the concrete mixes without GO and fly ash exposed to H_2SO_4 attack at 90 days of exposure were 42.2%, 53.1%, and 71.6% for standard concrete and 29.3%, 45.8%, and 66.2% for high strength concrete, respectively. Whereas for concrete mixes with the addition of GO at 0.15% and fly ash replacement at 30% exposed to H_2SO_4 acid for 90 days, these losses were decreased to 13.58%, 16.0%, and 20.46% for standard concrete and 9.10%, 12.25%, and 20.40% for high strength concrete, respectively. As a result, all test results demonstrated that increasing the fly ash replacement reduced the degree of deterioration of concrete matrix in acidic environments. The improved resistance of concrete mixes with GO and fly ash was attributed to the introduction of GO in to concrete matrix, which provided a filler effect, preventing the penetration of aggressive ions from acidic environment (Chu et al. 2020). The incorporation of GO into the concrete matrix densified the microstructure. As a result,

it prevented or retarded the migration of acid species from external solution. However, reinforcing effect in the concrete matrix can prevent development of chemical shrinkage cracks as a result of acid exposure, even though the GO dispersion helps in the initial stages of the C-S-H gel self-desiccation by absorbing more free water (Chu et al. 2020).

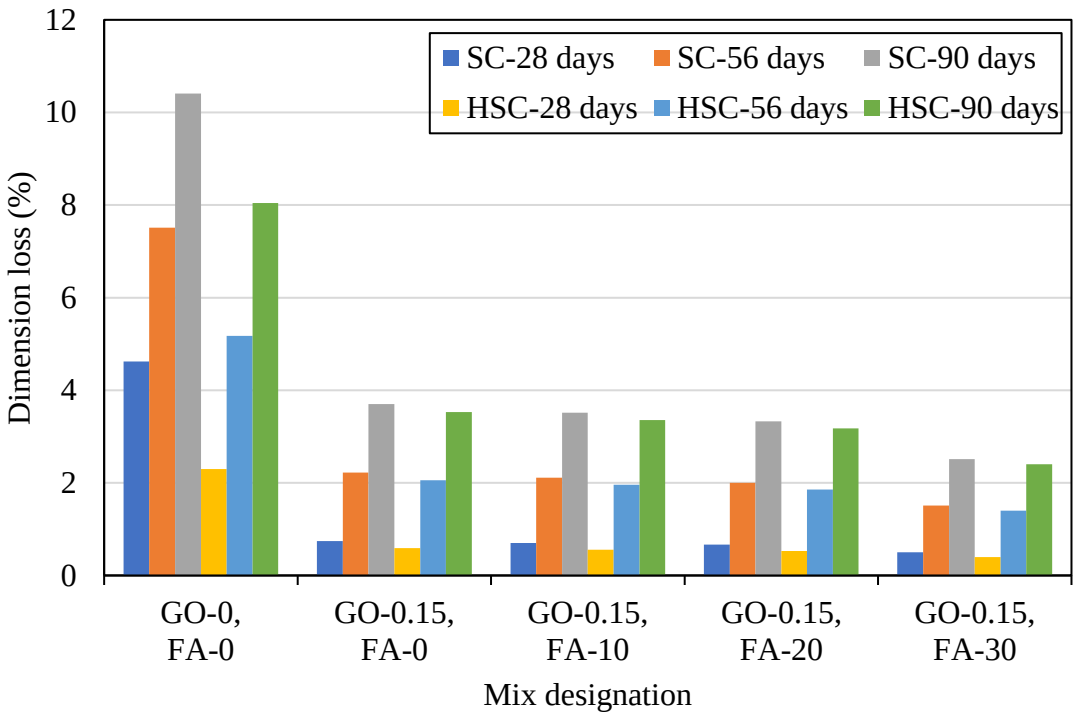

Figure 6.25 Dimension loss of GO and fly ash based concrete mixes due to HCl attack

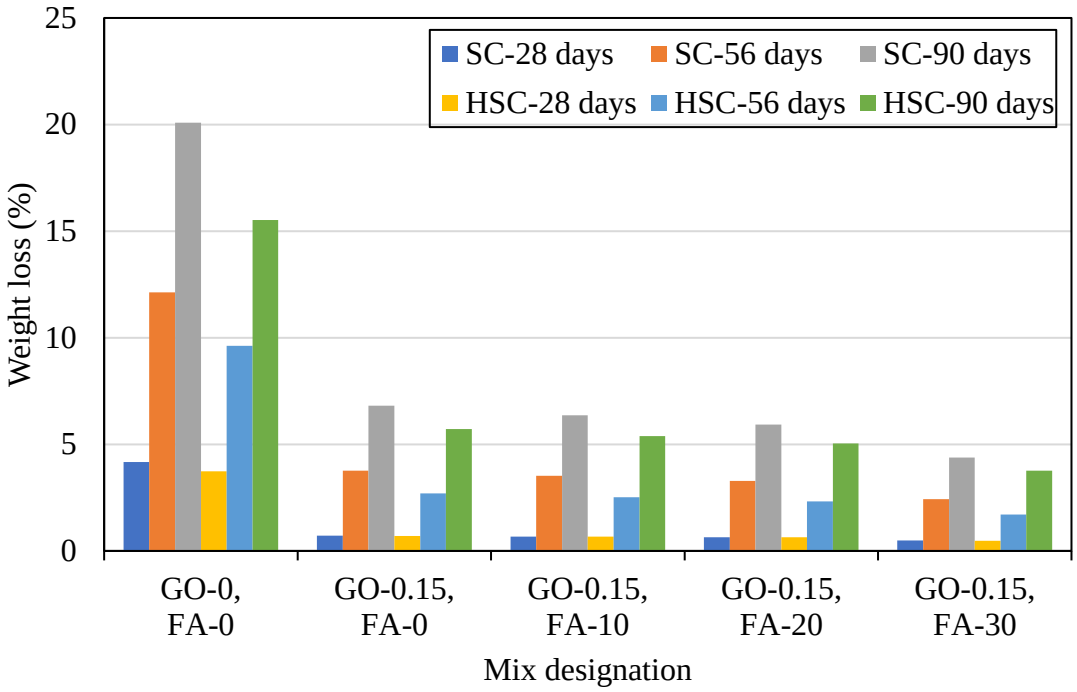

Figure 6.26 Weight loss of GO and fly ash based concrete mixes due to HCl attack

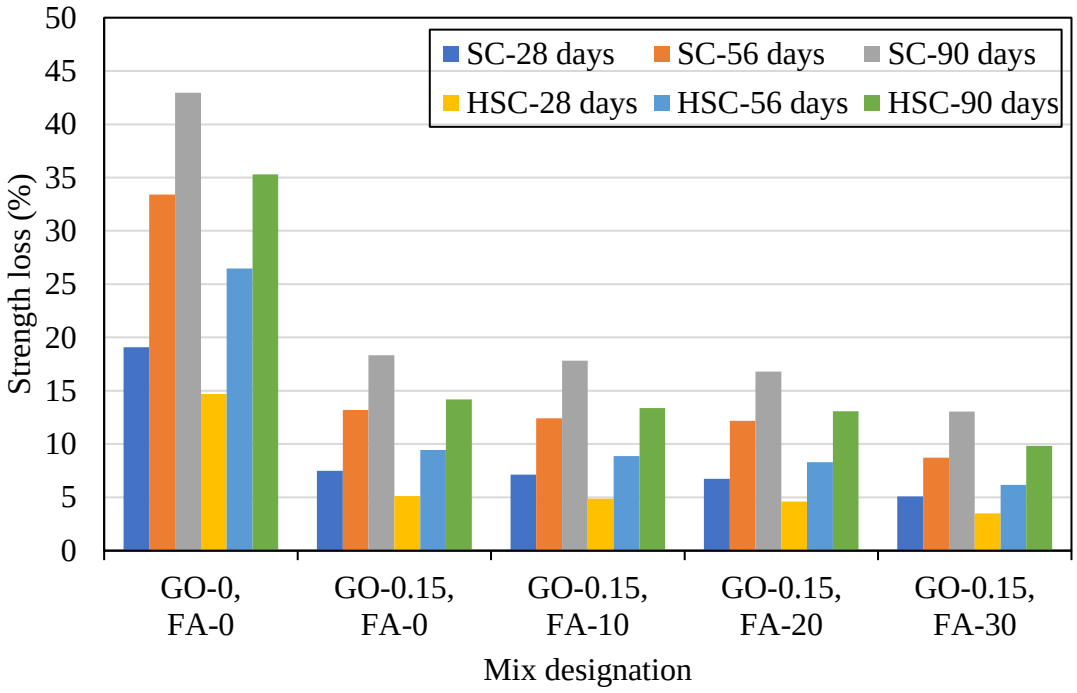

Figure 6.27 Strength loss of GO and fly ash based concrete mixes due to HCl attack

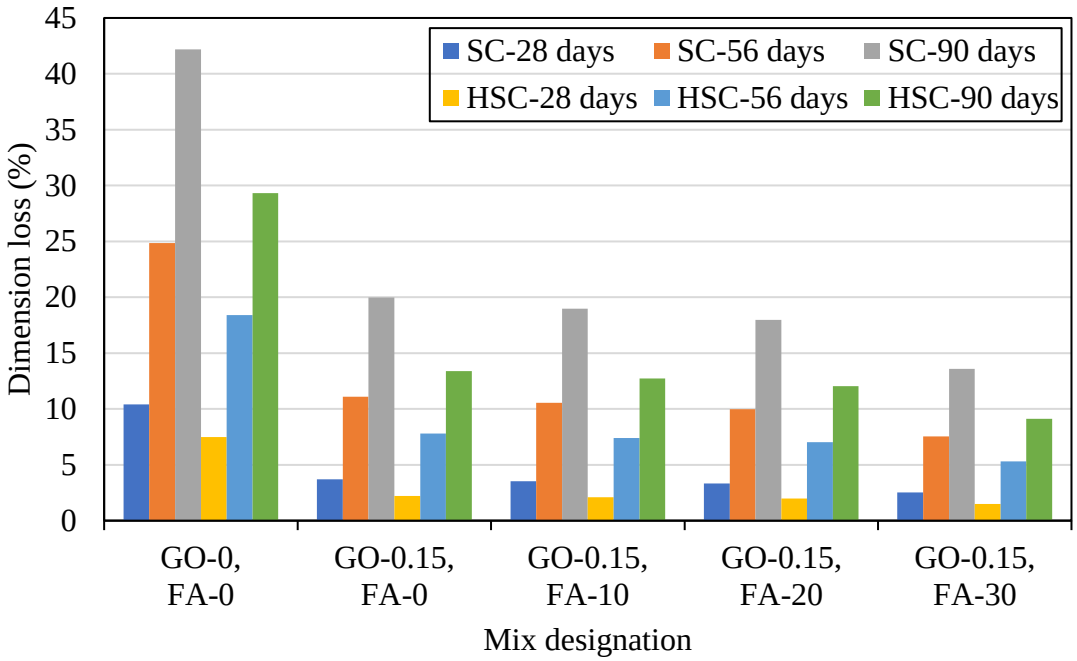

Figure 6.28 Dimension loss of GO and fly ash based concrete mixes due to H_2SO_4 attack

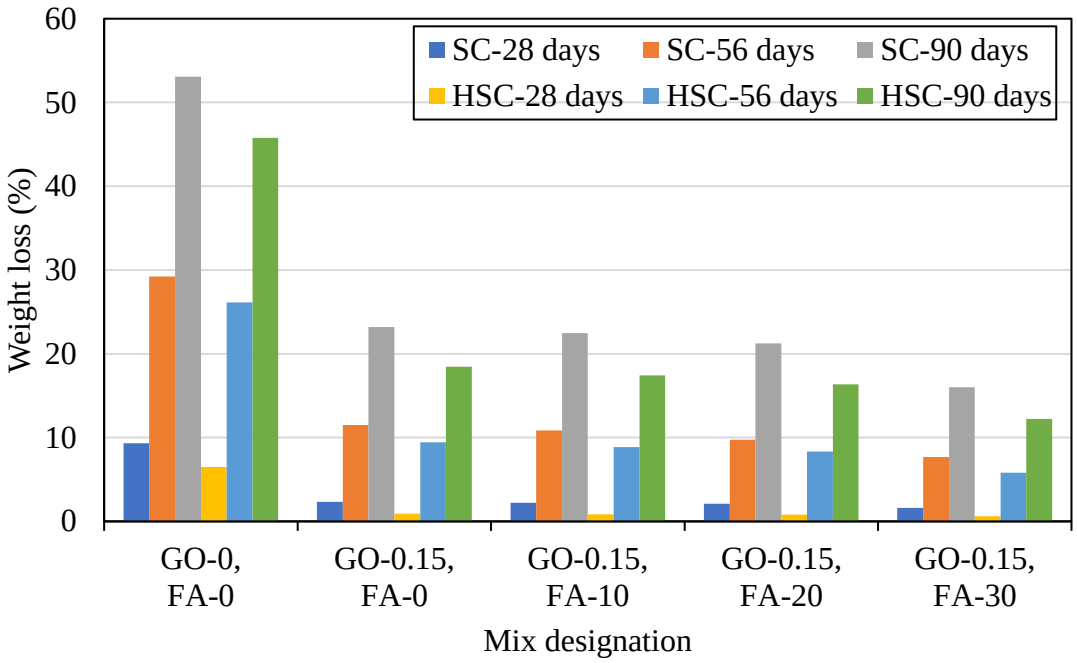

Figure 6.29 Weight loss of GO and fly ash based concrete mixes due to H_2SO_4 attack

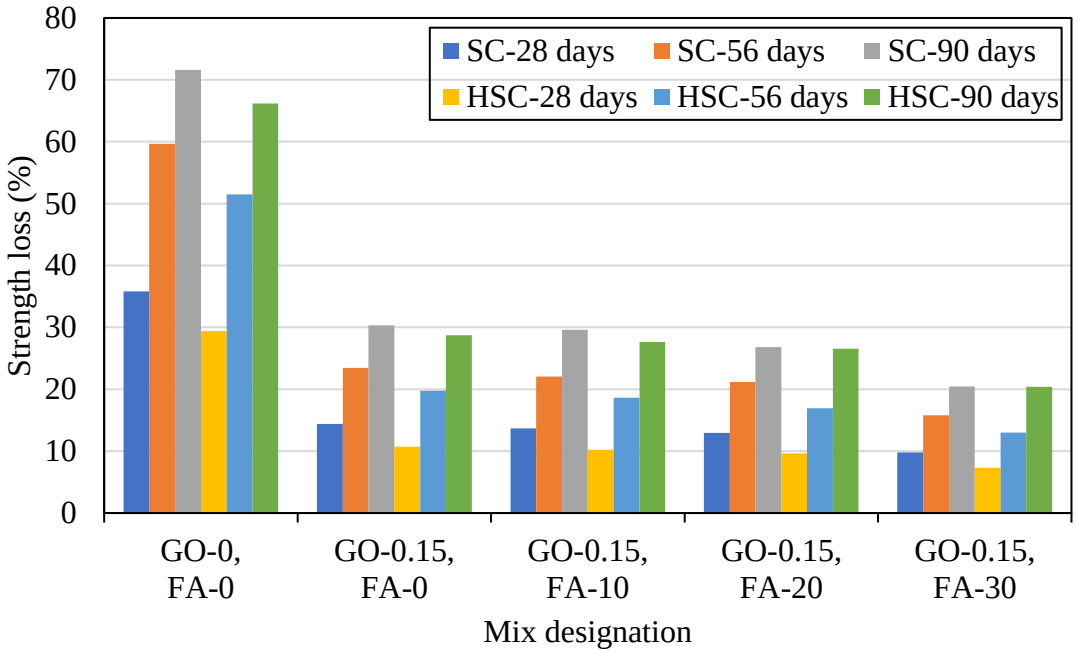

Figure 6.30 Strength loss of GO and fly ash based concrete mixes due to H_2SO_4 attack

6.5.5.2. SEM

The morphology of GO-0, FA-0 and GO-0.15, FA-30 concrete mixes at the 90 days exposure of HCl and H_2SO_4 acid in both standard and high strength concrete is compared using SEM images shown in Figure 6.31 and 6.32. The fractured surface of control concrete and concrete mixes containing GO-0.15% and fly ash 30% before acid attack is comprised of C-S-H gel (sheet morphology), calcium hydroxide (hexagonal plate morphology), and monosulfo aluminate (needle morphology). The acid attack has changed the shape and chemical composition of the hydration phases present in concrete mixes significantly. The area affected by acid attack can be completely filled with porous alumina-silica hydrogel after calcium leaching from the concrete matrix. The acid exposed concrete mix containing GO-0.15% and fly ash 30% had traces of GO sheets interlaced inside the porous gel. While presence of GO and fly ash had an impact on mineralogy of Ca-based ions that deposited in affected area, it prevented ionic movements and mass transfer among external solution and cement matrix.

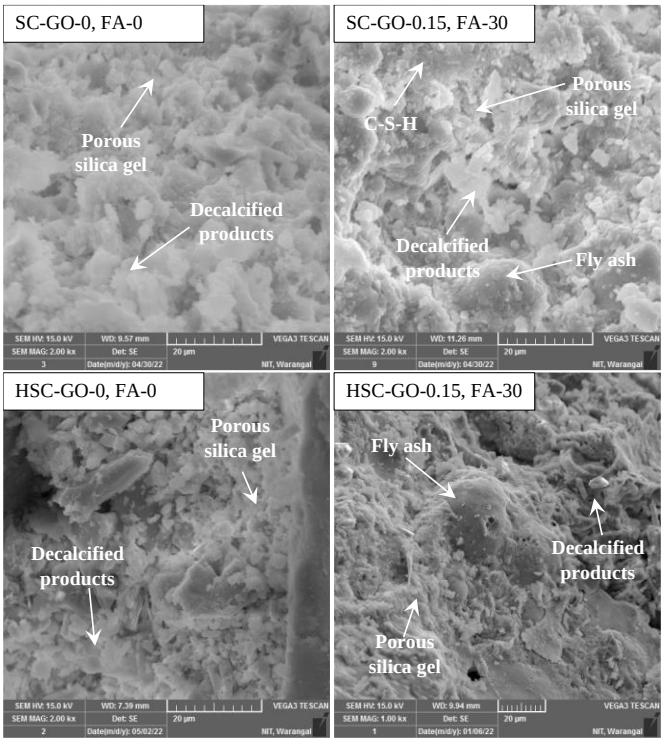

Figure 6.31 SEM images of GO and fly ash based concrete mixes due to HCl attack

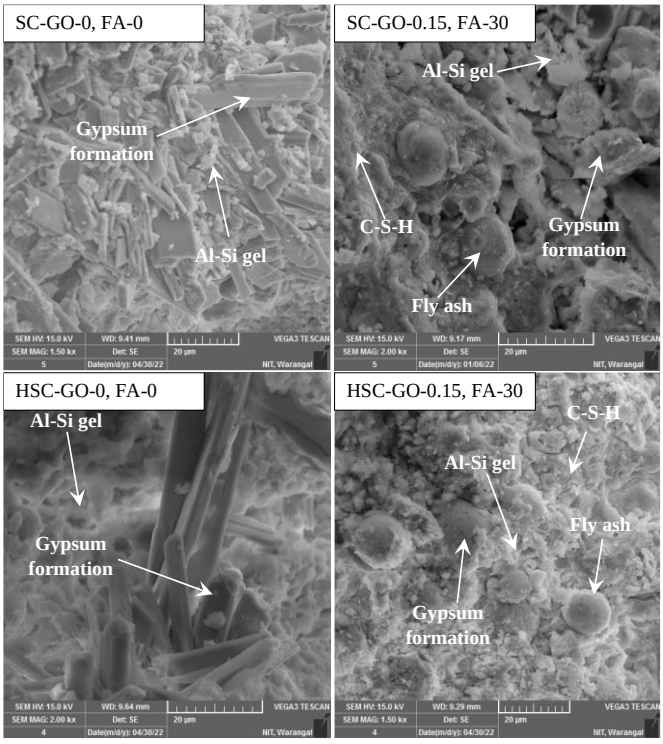

Figure 6.32 SEM images of GO and fly ash based concrete mixes due to H_2SO_4 attack

6.5.5.3. EDX

The chemical composition of the affected zone in GO-0, FA-0 and GO-0.15, FA-30 concrete mixes of both the grades exposed to HCl and H_2SO_4 was assessed by an EDX values of calcium-to-silica ratio (Ca/Si ratio) and calcium-to-aluminium ratio (Ca/Al ratio) and results are shown in Table 6.7. An EDX values of C-S-H gel, portlandite and monosulfate areas were identified in control concrete and concrete mixes containing GO-00.15% and fly ash 30% before acid attack was indicated in Table 6.5. Because of the HCl attack, these hydration products were decalcified and completely absent in the affected zone of control concrete mixes. However, at the 90 days exposure of the acid attack, residues of C-S-H gel were still identified in affected zones of concrete mixes containing GO-0.15% and fly ash 30%. It indicates that the GO inclusion functioned as a diffusion barrier, preventing leaching of C-S-H gel in acid environment. Upon deterioration, affected area in concrete mixes were filled by decalcified products with low calcium, high alumina and silica contents. This demonstrates that the incorporation of GO and fly ash replacement in concrete matrix prevented Ca_2^+ ions removal from hydration products such as C-S-H, CH and ettringite into external solutions.

Table 6.7 EDX values of GO and fly ash based concrete mixes due to acid attack

Mix	Before attack		After HCl attack		After H_2SO_4 attack	
	Si/Ca	Al/Ca	Si/Ca	Al/Ca	Si/Ca	Al/Ca
SC-GO-0, FA-0	0.41	0.15	0.49	0.19	0.61	0.26
SC-GO-0.15, FA-30	0.48	0.17	0.53	0.2	0.59	0.22
HSC-GO-0, FA-0	0.56	0.13	0.68	0.18	0.85	0.24
HSC-GO-0.15, FA-30	0.72	0.19	0.78	0.22	0.84	0.24

6.5.5.4. XRD

The XRD patterns of GO-0, FA-0 and GO-0.15, FA-30 concrete mixes after HCl and H_2SO_4 attack at the 90 days exposure in affected area are shown in Figure 6.33 and 6.34. The findings were revealed by the XRD patterns of these mixes before acid attack are shown in Figure 6.14 and 6.15, intensity of peak for C-S-H was positioned at 20.98°, 28.11° and 29.61°, CH was at 18.17°, 34.21°, 47.21° and 50.92° and AFt was positioned at 39.55°, 42.60°, 55.02° and 60.09°. HCl attack resulted in substantial modification in chemical compositions of these samples, which was reflected in change in their XRD patterns also. As a result, an amorphous peak at 2θ values of 23.8° was seen in the XRD pattern of all concrete mixes after acid attack, confirming the existence of gibbsite ($Al(OH)_3$) and quartz (SiO_2). These findings demonstrated that effect of a strong acidic environment on the complete dissolution of hydrated products as well as the presence of an amorphous alumina-silica hydrogel in concrete mixes exposed to acid attack. However, the presence of XRD peaks located at 2θ of 11.6°, 20.7°, 23.6°, 31.4°, 36.6° and 50.1° identified the formation of gypsum ($CaSO_4 \cdot 2H_2O$) in affected zones of concrete mixes exposed to H_2SO_4. Accordingly, recent investigations have shown the formation of gypsum (calcium sulfate dihydrate) in the affected zones of concrete matrix exposed to H_2SO_4.

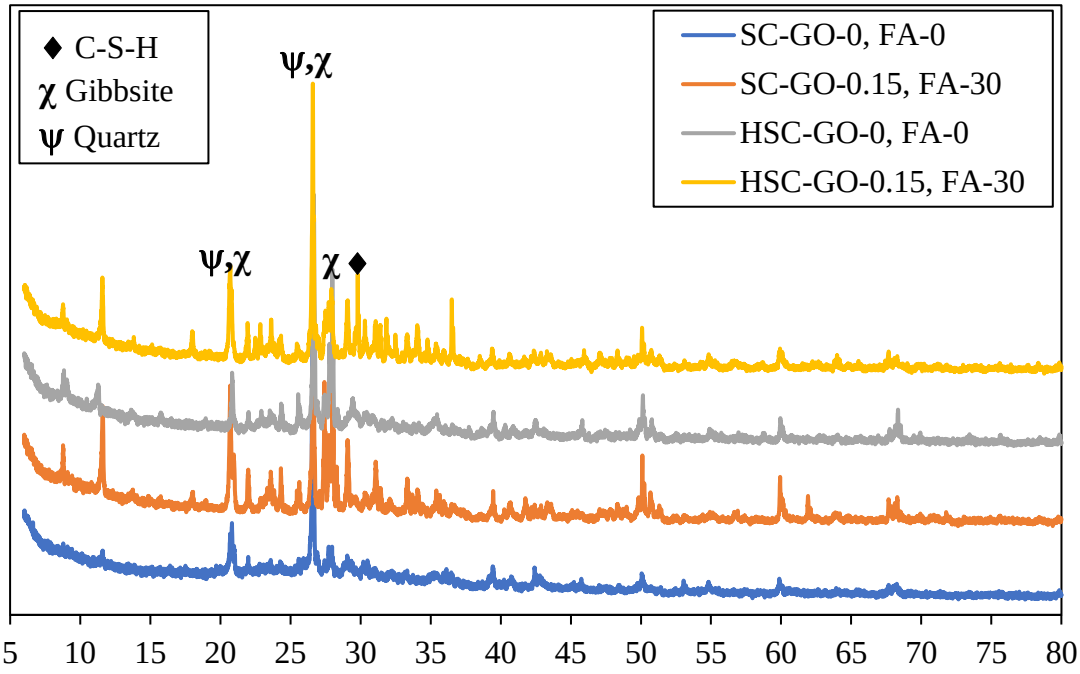

Figure 6.33 XRD patterns of GO and fly ash based concrete mixes due to HCl attack

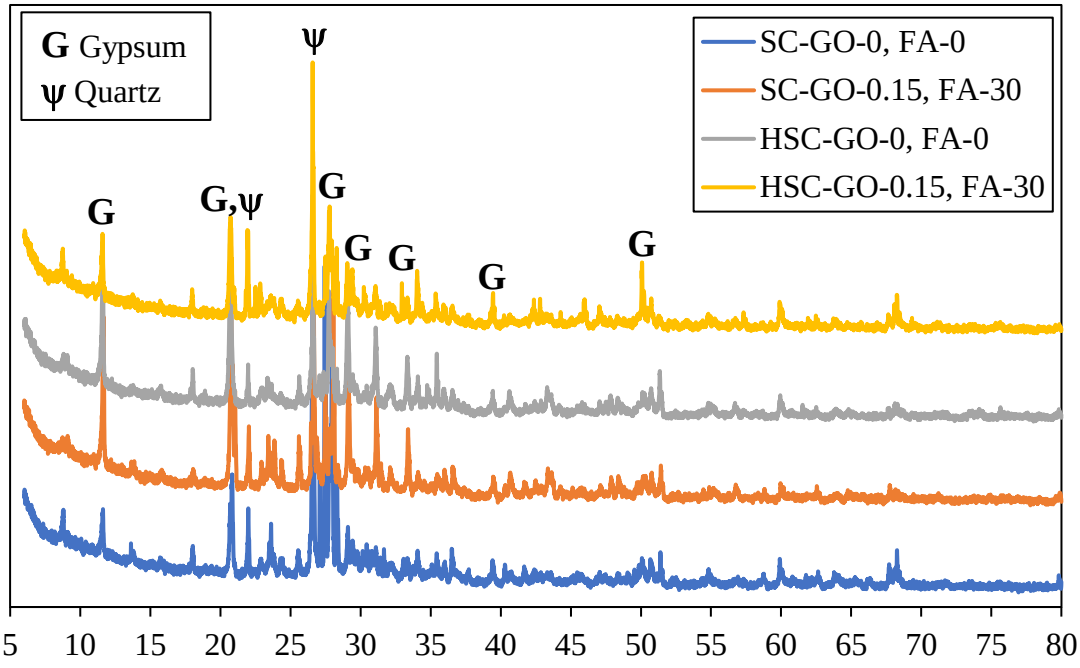

Figure 6.34 XRD patterns of GO and fly ash based concrete mixes due to H_2SO_4 attack

6.5.5.5. FTIR

The FT-IR spectra of GO-0, FA-0 and GO-0.15, FA-30 concrete mixes after HCl and H_2SO_4 attack at the 90 days exposure in affected areas is shown in Figure 6.35 and 6.36. The findings were revealed by the FTIR patterns of these mixes before acid attack are shown in Figure 6.16 and 6.17, The band region of 900–1100 cm^{-1} (Si-O asymmetric stretching vibration) characterizes C-S-H, CH was detected at a peak of 3643 cm^{-1} (O–H stretching vibration). The presence of trisulfoaluminate can be detected from the bands 857 cm^{-1} (Al-O stretching vibration), 1675 cm^{-1} and 3431 cm^{-1} (H_2O bending and stretching vibration) and monosulfate aluminates at 1400 cm^{-1} (asymmetric stretching of $[CO_3]^{2-}$). In respective FT-IR ranges, the IR bands related to the C-O, Si(Al)-O, and O-H functional groups were observed. These findings demonstrated that effect of strong acidic environment on the complete dissolution of hydrated products and development of an amorphous alumina-silica hydrogel in concrete mixes exposed to acid attack. On the other hand, the IR peaks related to S–O (1097 cm^{-1}) functional groups revealed that sulfate-bearing salt precipitated in concrete mixes when exposed to H_2SO_4 acid. These findings agreed with the SEM and XRD results.

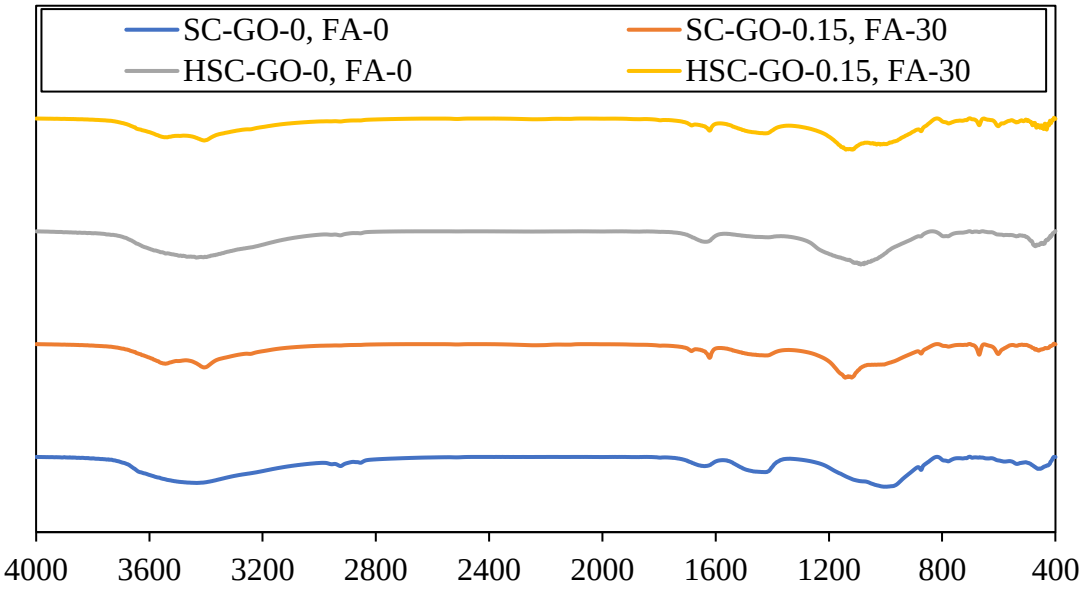

Figure 6.35 FT-IR spectra of GO and fly ash based concrete mixes due to HCl attack

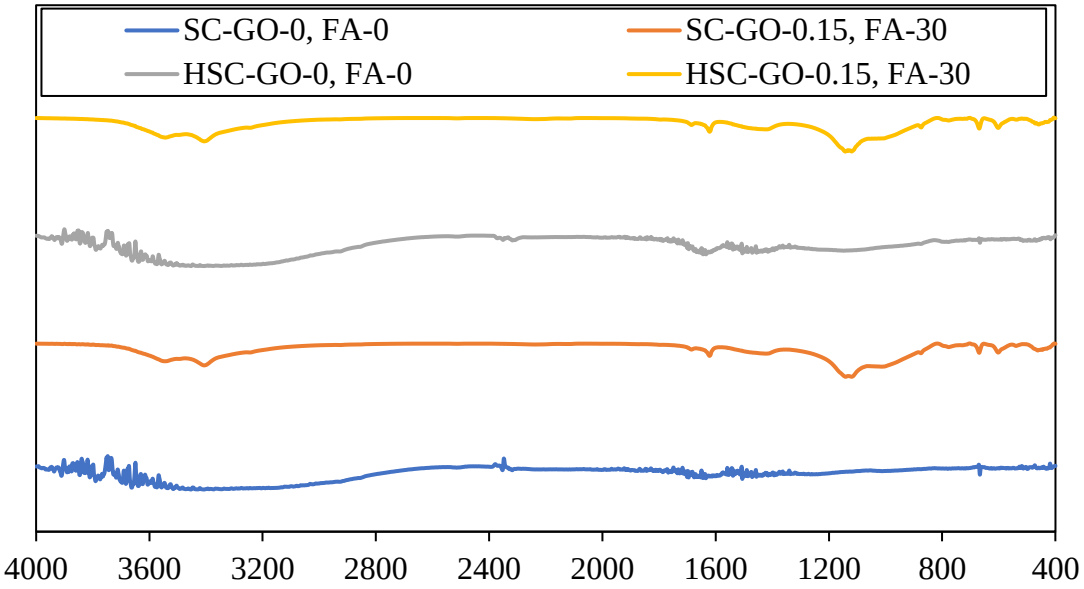

Figure 6.36 FT-IR spectra of GO and fly ash based concrete mixes due to H_2SO_4 attack

6.5.5.6. TGDTA

The TGA pattern of the GO-0, FA-0 and GO-0.15, FA-30 concrete mixes for both the grades after the HCl and H_2SO_4 attack at the 90 days exposure of data collected from the affected area are shown in Figure 6.37 and 6.38. The temperature ranges of different phase transformations of the concrete matrix considered in this study are as follows, the evaporable water at 30–105°C, the water loss from the decomposition of the C-S-H (dehydration, Ldh) at 105–400°C, dihydroxylation (Ldx) of the calcium hydroxide at 400–600°C, decarbonation (Ldc) of calcium carbonate at 600–850°C were found in the GO-0 and GO-0.15% concrete mixes before acid attack are shown in Table 6.6. After the HCl and H_2SO_4 attack, affected area in concrete mixes was observed to have no evidence of hydration phases, but to be substantially filled with alumina-silica hydrogel and gypsum, respectively. Weight loss caused by gypsum and hydrogel degradation was evaluated at temperatures ranging from 200 to 400 °C. The TGA analysis of total weight loss (TWL), alumina-silica hydrogel and gypsum present in the two concrete mixes is shown in Table 6.8. This quantification of TGA analysis was calculated using the method

suggested by Deboucha et al. (2017). The CBW content represents the degree of hydration in the concrete mixes. When 0.15% GO was added with 30% fly ash replacement, the bound water levels increased by 8.25% and 7.32% for standard concrete and high-strength concrete, respectively, compared to control concrete. This shows that high dosage of GO influences the rate of hydration by absorbing more free water. On the other hand, the GO addition and fly ash replacement prevents carbonation of CH crystals and calcium oxide in concrete matrix. GO and fly ash blocks the diffusion pathways in the concrete matrix that carbon dioxide gas needs to permeate from surrounding environment (Chu et al. 2020). Alumina-silica (Al-Si) hydrogel developed in affected area of GO-0, FA-0 and GO-0.15, FA-30 concrete mixes was 25.51% and 24.33% for standard concrete, and 24.10% and 22.53% for high strength concrete, respectively, at the 90 days exposure of HCl acid. Gypsum and alumina-silica (Al-Si) hydrogel developed in affected area of GO-0, FA-0 and GO-0.15, FA-30 concrete mixes were 18.57% and 17.92% for standard concrete, and 17.79% and 17.20% for high strength concrete, respectively, at the 90 days exposure of H_2SO_4 acid. It can be observed that GO addition and fly ash replacement acted as a diffusion barrier, reducing the amount of calcium leaching from the concrete matrix.

Table 6.8 Percentage mass loss from TGA analysis after acid attack

Mix	After HCl attack		After H_2SO_4 attack	
	Al–Si gel (%)	TWL (%)	Gypsum and Al–Si gel (%)	TWL (%)
SC-GO-0, FA-0	25.51	28.07	18.57	21.09
SC-GO-0.15, FA-30	24.33	25.85	17.92	19.13
HSC-GO-0, FA-0	24.10	25.85	17.79	18.74
HSC-GO-0.15, FA-30	22.53	23.27	17.20	17.60

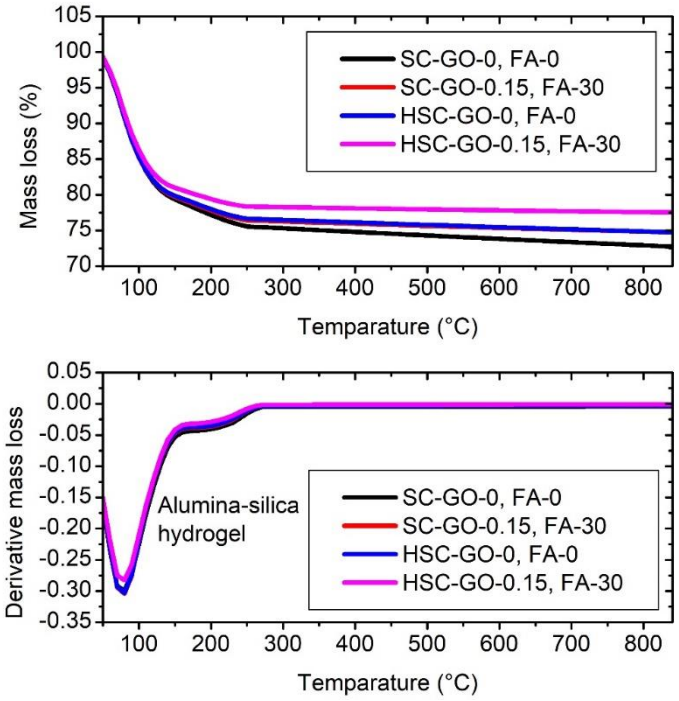

Figure 6.37 TGA and DTG plots of GO and fly ash based concrete mixes due to HCl attack

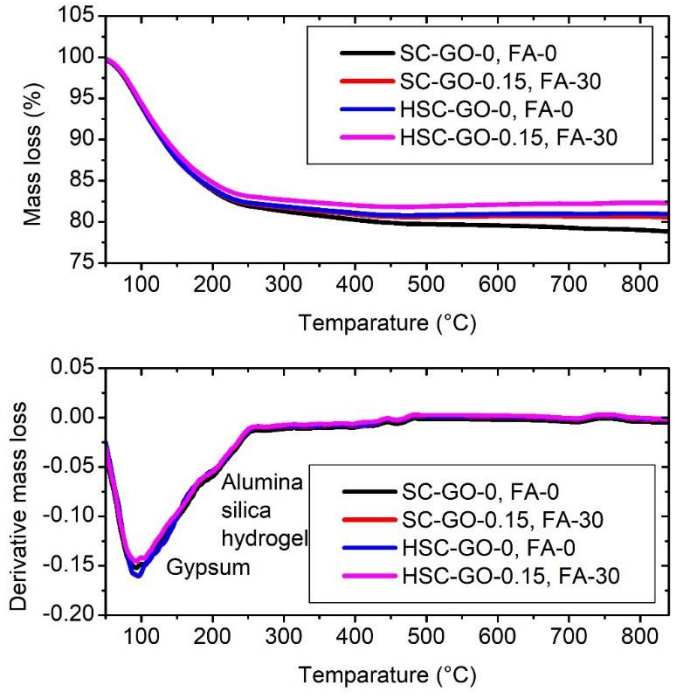

Figure 6.38 TGA and DTG plots of GO and fly ash based concrete mixes due to H_2SO_4 attack

6.6. Concluding remarks from Phase-II

In this chapter the combined effect of GO and fly ash on static & dynamic mechanical, and microstructural characteristics of concrete have been investigated and the results are compared with control concrete. In addition, the durability properties of GO and fly ash based concrete have been determined. The following conclusions are drawn from the experimental investigations.

(i) Static mechanical properties

- The increase in slump values with the addition of GO at 0.15% and fly ash replacement at 20% and 30% are recorded as 3.8% and 11.5% for standard concrete and 4.5% and 13.6% for high strength concrete, respectively, compared to the control concrete.

- The decrease in the fluidity with the addition of GO is counterbalanced by fly ash, this could be because of less water requirement, size gradation and ball effect.

- The rate of increase in compressive, split tensile and flexural strength values at 7days for standard concrete was 31.43%, 24.32% and 13.88% for 10% fly ash replacement, 19.68%, 6.76% and 6.95% for 20% fly ash replacement, and 7.5%, 2.70% and 2.57% for 30% fly ash replacement, respectively compared to control concrete.

- The rate of increase in compressive, split tensile and flexural strength values for high strength concrete at the age of 7days was 22.86%, 14.55% and 8.06% for 10% fly ash replacement, 11.84%, 7.27% and 5.39% for 20% fly ash replacement, and 3.76%, 2.59% and 2.72% for 30% fly ash replacement, respectively compared to control concrete.

- The combined effect of GO and fly ash on strength improvement of concrete is less at early stages, though, the strength properties of the GO reinforced concrete mixes with replacement of fly ash up to 30% are higher than control concrete at 7 days.

Therefore, the drawback of fly ash in delaying the early age strength development was counterbalanced by GO.

- The growth rate of concrete strength properties is more at the later age (at 28 days) compared to the early age (at 7 days) may be attributed to the secondary hydration process of fly ash.

- The improvement in elastic modulus of concrete containing GO at 0.15% and fly ash at 10%, 20% and 30% was 19.86%, 9.15% and 1.39% for standard concrete, and 15.97%, 8.28% and 2.05% for high strength concrete, respectively, compared to control concrete.

(ii) Dynamic mechanical properties

- The improvement in fundamental natural frequency of concrete containing GO at 0.15% and fly ash at 10%, 20% and 30% was 6.21%, 3.42% and 0.51% for standard concrete, and 3.91%, 2.95% and 0.66% for high strength concrete, respectively, compared to control concrete.

- The percentage decrease in damping ratio of concrete containing GO at 0.15% and fly ash at 10%, 20% and 30% was 24.42%, 20.93% and 17.44% for standard concrete, and 23.68%, 19.74% and 10.53% for high strength concrete, respectively, compared to that of control concrete.

- The dynamic elastic modulus of concrete containing GO at a dosage of 0.15% and replacing cement with fly ash at 10%, 20% and 30% was 53.09, 50.14 and 47.54 GPa for standard concrete, and 56.44, 54.96 and 52.75 GPa for high strength concrete, respectively.

- According to the UPV test results, it is inferred that the quality of concrete is excellent according to IS-13311, this is evident from the combined effect of GO and fly ash which has greater uniformity and might be attributed to nano filler effect of GO and size gradation of fly ash, which densifies the microstructure of the concrete matrix.

(iii) Microstructural characteristics

- The surface of concrete with GO and fly ash shows formation of a compact, uniform and densified structure at micro-level compared with control concrete, and unreacted smooth spherical shape fly ash particles demonstrates secondary hydration of fly ash which is in progress.

- The Ca/Si elemental ratio was high for control concrete and the GO addition and fly ash replacement decreases Ca/Si ratio in concrete matrix which densifies C-S-H phase.

- GO addition and replacement of fly ash enhanced the peaks intensity compared to control concrete, reveals that increase in crystallinity of hydration phases.

- The presence of GO and fly ash, the absorption peak of Calcium silicate hydrate shifts to a higher wavenumber than that of control concrete, demonstrating that the addition of GO changes the Ca/Si ratio and formation of densified calcium silicate hydrate gels.

- TGA analysis showed the increase in non-evaporable water content of concrete with GO and fly ash suggesting that the integration of GO and fly ash has definitely a role in improving the secondary hydration of the concrete matrix at a later stage.

(iv) Durability properties

- Water absorption values of control concrete and concrete with constant GO dosage of 0.15% and varying fly ash replacements at 0%, 10%, 20%, and 30% are recorded as 2.03%, 1.74%, 1.64% and 1.42% for standard concrete and 1.17%, 1.13%, 1.07% and 0.98% for high strength concrete, respectively.

- Water sorptivity values of control concrete and concrete with constant GO dosage of 0.15% and varying fly ash replacements at 0%, 10%, 20%, and 30% at 90 days were 0.0043, 0.0041, 0.0039, and 0.0037 mm/√s for standard concrete and 0.00080, 0.00076, 0.00072, and 0.00068 mm/√s for high strength concrete, respectively.

- Enhanced resistance to water absorption may be due to the extensive barrier capacities of GO and refinement of pore structure of the cement composites resulting from decrease in critical pore diameter.

- Carbonation depth values of control concrete and concrete with GO dosage 0.15% and fly ash replacements 0%, 10%, 20%, and 30% were 9, 8, 6, and 4 mm for standard concrete and 6, 5, 4, and 3 mm for high strength concrete, respectively.

- The results of RCPT test in terms of Charge passed values of control concrete and concrete with GO dosage 0.15% and fly ash replacements 0%, 10%, 20%, and 30% were 1620, 1210, 1015, and 821 coulombs for standard concrete and 821, 648, 454, and 346 coulombs for high strength concrete, respectively.

- The concrete mixes with the addition of GO at 0.15% and fly ash replacement at 30% exposed to HCL acid for 90 days, the dimension, weight and strength losses were observed as 2.52%, 4.38%, and 13.05% for standard concrete and 2.4%, 3.76%, and 9.82% for high strength concrete, respectively.

- The concrete mixes with the addition of GO at 0.15% and fly ash replacement at 30% exposed to H_2SO_4 acid for 90 days, the percentage losses in dimension, weight and strength were 13.6%, 16.0%, and 20.5% for standard concrete and 9.1%, 12.2%, and 20.4% for high strength concrete, respectively.

- Microstructural characterization indicates that the GO inclusion and fly ash replacement acts as a diffusion barrier, and prevented the leaching of Ca^{2+} ions from cement hydrates such as C-S-H, CH and ettringite from the acidic environment.

CHAPTER 7
PHASE-III: NUMERICAL MODELLING

7.1. General

In chapters 5 and 6, the performance and microstructural characteristics of GO-cement concrete and GO and fly ash based concrete were thoroughly discussed. To develop GO-based concrete composite, more number of combinations and trials are performed, it is time incentive and more energy required for comprehensive experimentation. To avoid the time consuming and cumbersome experimentation process, non-linear analysis is required for reinforced concrete structures because of its relatively low tensile strength, low strain capacities, and serviceability limits of the concrete. ATENA is a user-friendly software designed specifically for non-linear analysis of reinforced concrete structures. In this chapter, the experimental results are compared with the results obtained from finite element modelling using ATENA.

7.2. Finite Element Modelling using ATENA-GiD

This section outlines the pre-processing required to create a complete geometry and then a finite element model for non-linear finite element analysis. The objective of the geometric model is to represent the geometry, material characteristics, and boundary conditions of the structure. The automated mesh generation is done in pre-processing to construct the analytical model for the finite element analysis. The creation of geometrical points is the first step in defining geometry. These points are later connected to create boundary lines. The surfaces are created by selecting suitable boundary lines. The formation of volumes can be accomplished either by the extrusion of surfaces or by manually selecting all surfaces that are bounded by the volume. In GiD, volumes are used

to model regions that have a three-dimensional structure. After the geometry has been created, the properties of the materials should be defined and then assigned to the different volumes. Supports and loads are often defined with the use of boundary conditions. "Intervals" are used in GiD to establish the loads and boundary conditions. A series of loads and boundary conditions that are applied in a specified number of steps is represented by an interval. A detailed loading history can be specified using an appropriate specification of intervals. It is always beneficial to establish monitoring points in ATENA analysis. During the analysis, the monitoring points are utilized to observe the history of specific quantities. i.e., to monitor the history of deflection or loads at specific points. The monitoring points are particular conditions that must be defined in the first interval.

7.3. Material models used in ATENA

The ATENA software system provides number of material models for various materials and purposes. Von Mises plasticity can be utilized for metals, Drucker Prager plasticity with associated or non-associated flow rule is available for rock and soil, and steel reinforcement can be determined using a multilinear uniaxial model with cycling. Non-linear and constant springs can be used for supports, while Mohr-columb friction is available for interfaces. The use of isotropic elastic material law can be advantageous in some cases. Nonetheless, the material models for concrete are the most important in ATENA. These advanced models account for all of the important characteristics of actual material behaviour in compression and tension. ATENA includes three nonlinear material models for concrete: a crack band model based on fracture energy, a fracture plastic model with non-associated plasticity, and a micro plane material model.

Various fracture plastic models available in ATENA are CC3DCementitious, CC3DNonLinCementitious, CC3DNonLinCementitious2, and CC3DNonLinCementitious2User, with the following differences: CC3DCementitious is based on the assumption that the material has a linear response up to the point where it reaches the failure envelope under compression and tension. This implies that no

hardening regime exists. On the other hand, the material CC3DNonLinCementitious undergoes a hardening regime before it reaches its compressive strength. The material CC3DNonLinCementitious2 is the same as CC3DNonLinCementitious, but it uses a purely incremental formulation for the fracturing part of the model, while CC3DNonLinCementitious uses a total formulation. This material can be used in creep calculations or when the properties of the material need to be changed during the analysis. The CC3DNonLinCementitious2User material has user-defined laws for a group of material laws, including tensile and softening behaviour diagrams, a shear retention factor, and the influence of lateral compression on tensile strength.

The material type cementitious2 was used for the plain concrete, which is suitable for materials that are similar to concrete. CC3DNonLinCementitious2 is the ATENA name for this nonlinear cementitious material. The best solution is commonly to generate all parameters for the relevant concrete grade or cube strength if there are no comprehensive experimental data available. When experimental results for some of the parameters are available, such as tensile strength or elastic modulus from an experiment, the suggested method is to generate material properties for the corresponding concrete grade or compressive strength first and then modify the properties for which experimental results are available. The cube strength is given as an input to automatically generate the material parameters for standard concrete and high-strength concrete, which are updated with the available experimental results and are presented in Table 7.1.

7.4. FE model generation

To determine the stress-strain behaviour of concrete under uniaxial compression, 100x200mm cylinder was modelled and then a flexure specimen with dimensions of 100x100x500 mm prismatic beam was analysed for validation in ATENA-GiD software. In the present study, the element used in creating the model is a hexahedron for concrete specimen and a tetrahedron for supporting steel plates. The boundary conditions employed in this study were identical to those used in the analysis of the simply supported beam. The following steps are followed to analyse the model in ATENA-Gid.

Table 7.1 Modified input data for standard concrete and high strength concrete without GO

Input Format	Property type	SC	HSC
Basic	Youngs modulus	28462.79 MPa	37481.75 MPa
	Poissons ratio	0.15	0.15
	Direct tensile strength	2.75 MPa	4.46 MPa
	Compressive strength	41.9 MPa	68.0 MPa
Tensile	Fracture energy	0.000129	0.000129
	Fixed crack	1	1
	Activate aggregate interlock	20mm	20mm
Compressive	Plastic strain	0.002	0.002
	Onset of crushing	0	0
	Fc reduction	0.6	0.6

7.4.1. Modelling of cylinder under uniaxial compression

A cylindrical model was created using ATENA-GiD. The experimental findings of compressive strength and stress-strain results were used as input parameters. To estimate the stress-strain behaviour under compression, a cylindrical specimen having a size of 100 mm diameter and 200mm height was analysed to confirm the accuracy of model. Figure 7.1 shows the steps followed in modelling the 100x200mm cylindrical specimen. Figure 7.2 to 7.5 shows the stress-strain behaviour from the experimental and FEM model using ATENA under uniaxial compression, respectively. Table 7.2 shows the findings of peak stress from the experimental and FEM model for standard concrete and high strength concrete, respectively. The results obtained from model using ATENA software are higher side compared to the experimental results. It is also observed that the results generated by the numerical model are in good agreement with the experimental values, the percentage error in peak-stress is less than 15%.

Table 7.2 Comparison of peak stress results from experimental and ATENA

Mix	Standard concrete (SC)			High strength concrete (HSC)		
	Exp.	ATENA	Error (%)	Exp.	ATENA	Error (%)
GO-0.00	35.30	39.39	11.58%	58.80	64.96	10.48%
GO-0.05	40.10	43.38	8.18%	63.75	69.48	8.99%
GO-0.10	47.89	52.23	9.06%	68.00	75.64	11.23%
GO-0.15	52.10	56.87	9.15%	73.10	78.87	7.89%
GO-0.20	50.00	55.26	10.52%	71.40	78.74	10.28%
GO-0.15, FA-10	49.68	54.12	8.94%	70.19	76.89	9.54%
GO-0.15, FA-20	45.24	48.97	8.24%	63.06	69.67	10.48%
GO-0.15, FA-30	38.10	42.14	10.59%	59.95	66.93	11.64%

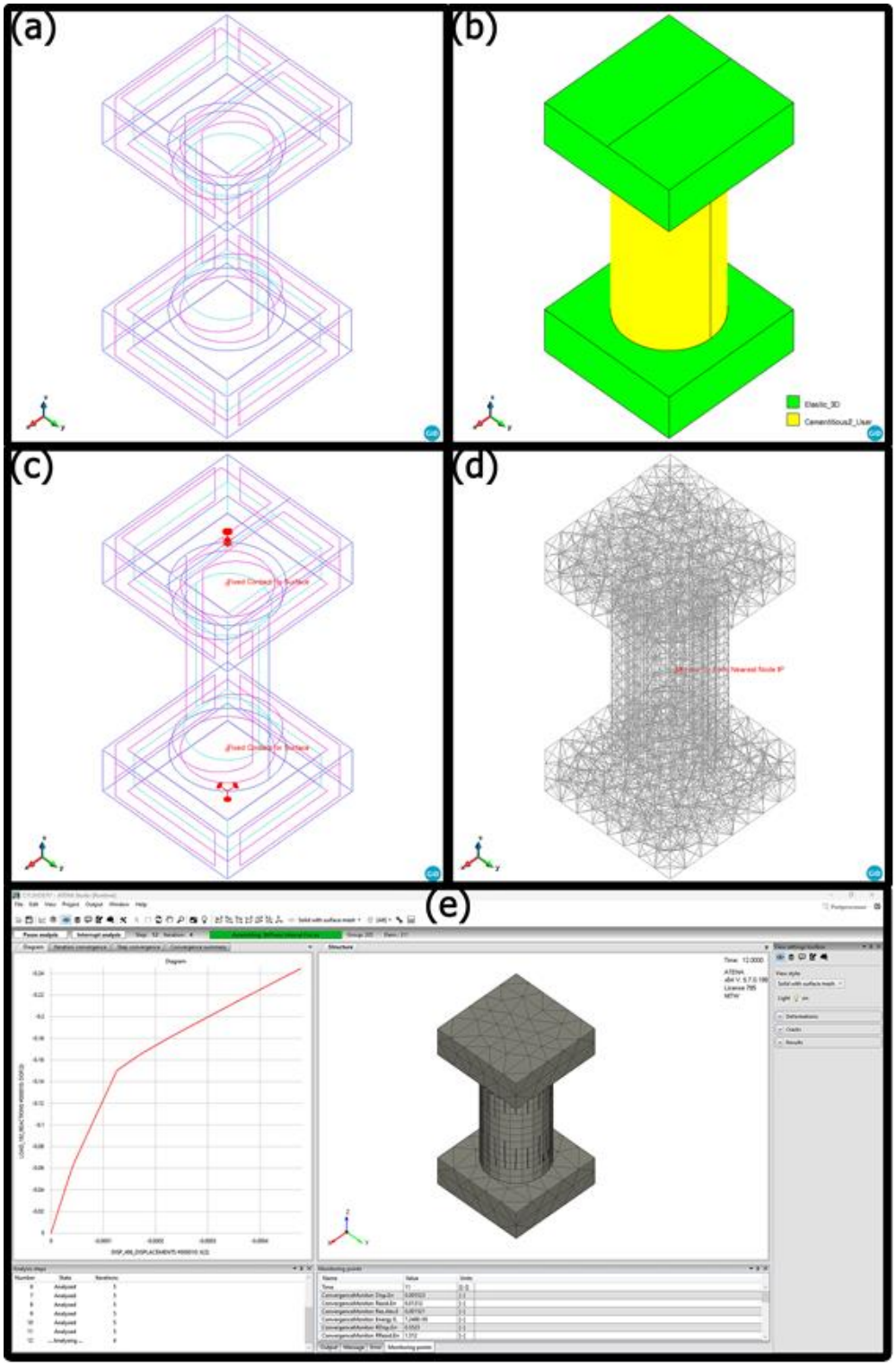

Figure 7.1 Modelling steps followed in ATENA-GiD software for cylinder. (a) Geometric model (b) Boundary conditions (c) Material properties (d) Meshing properties (e) ATENA analysis

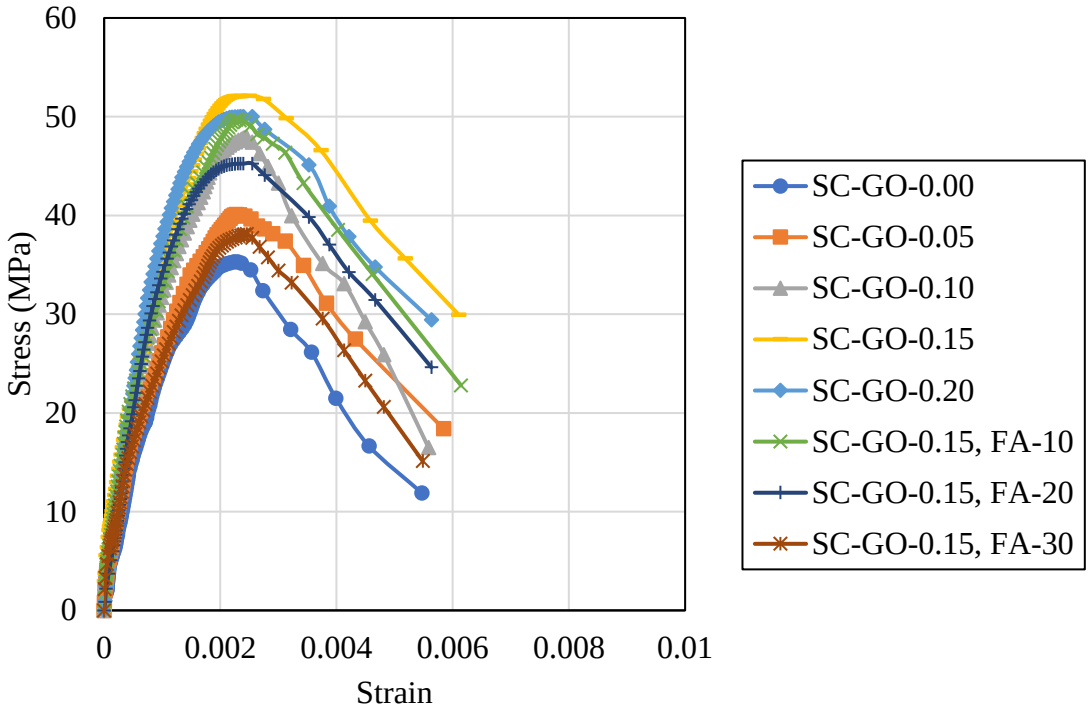

Figure 7.2 Experimental stress strain curves for standard concrete

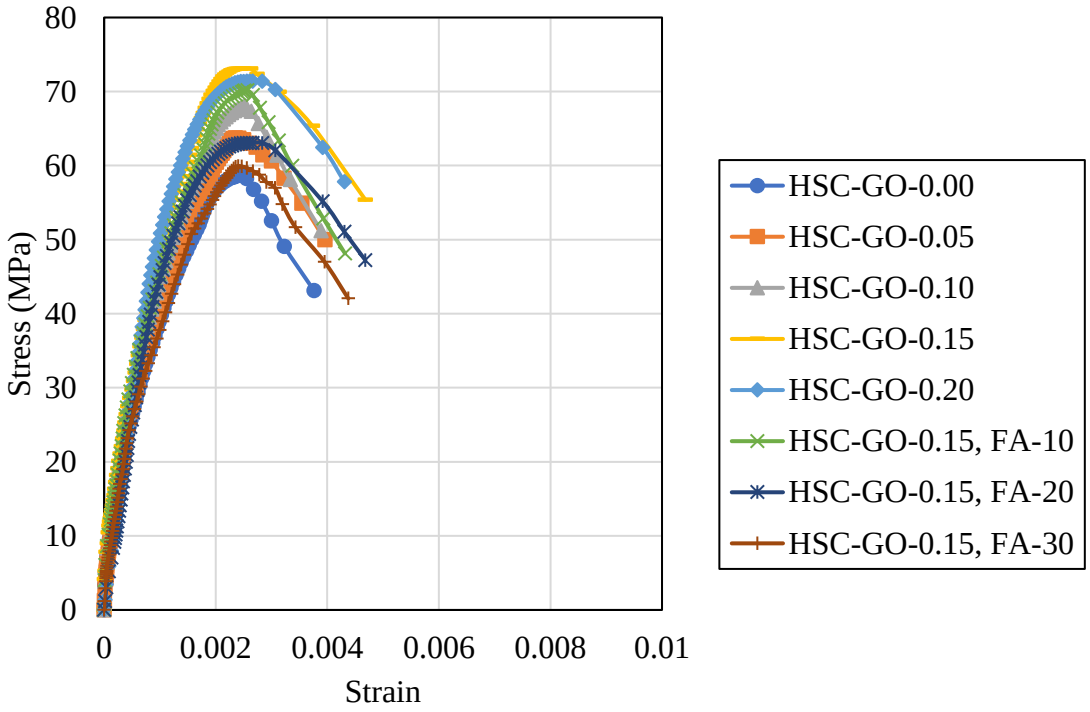

Figure 7.3 Experimental stress strain curves for high strength concrete

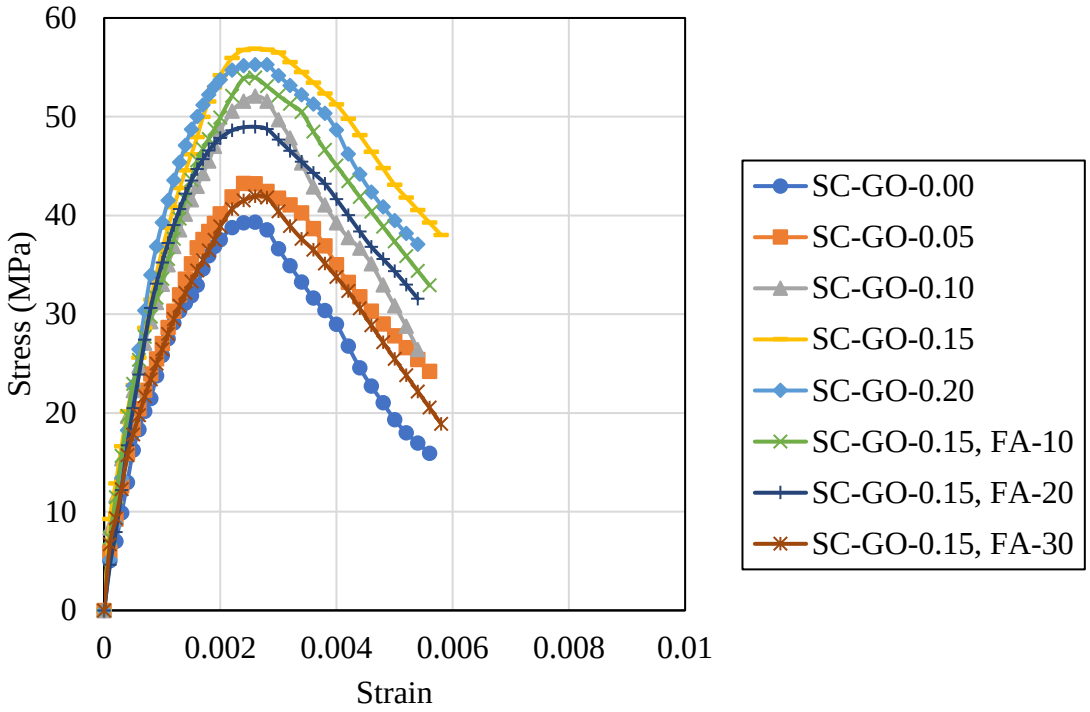

Figure 7.4 ATENA stress strain curves for standard concrete

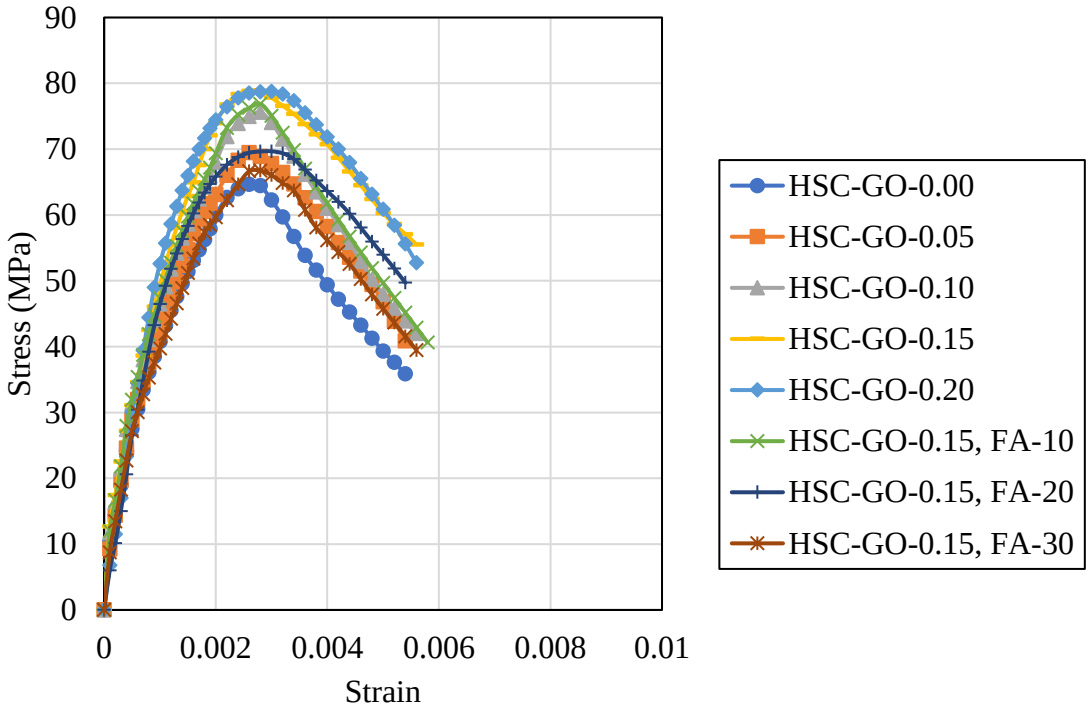

Figure 7.5 ATENA stress strain curves for high strength concrete

7.4.2. Modelling of prism for flexure

A flexural model of a prismatic beam of size 100x100x500 mm was modelled with the properties obtained from the cylindrical model under uniaxial compression. Modelling has performed to validate the results obtained with experimental data and the values determined from the numerical modelling under flexure. Since the model considered for flexure is symmetric about the centre of the specimen, only half of it was examined and analysed with ATENA. Figure 7.6 shows the steps involved in developing a prismatic beam model under flexure. The experimental concrete stress-strain curve under uniaxial load is manually provided to create a numerical model under flexure. Table 7.3 demonstrates a comparison of the flexural strength obtained through numerical modelling and experimental results for standard concrete and high strength concrete, respectively. The predicted flexural strength results are in good agreement with the experimental values with the margin of error less than 15%.

Table 7.3 Comparison of flexural strength results from experimental and ATENA

Mix	Standard concrete (SC)			High strength concrete (HSC)		
	Exp.	ATENA	Error (%)	Exp.	ATENA	Error (%)
GO-0.00	6.51	7.20	10.60%	9.00	10.05	11.67%
GO-0.05	7.19	7.77	8.14%	9.60	10.38	8.13%
GO-0.10	7.53	8.57	13.81%	10.20	11.28	10.59%
GO-0.15	8.10	8.64	6.67%	10.80	11.79	9.17%
GO-0.20	7.76	8.48	9.26%	10.50	11.75	11.90%
GO-0.15, FA-10	7.46	8.41	12.70%	10.60	11.62	9.62%
GO-0.15, FA-20	7.19	8.06	12.12%	10.43	11.54	10.60%
GO-0.15, FA-30	6.82	7.54	10.59%	9.50	10.78	13.51%

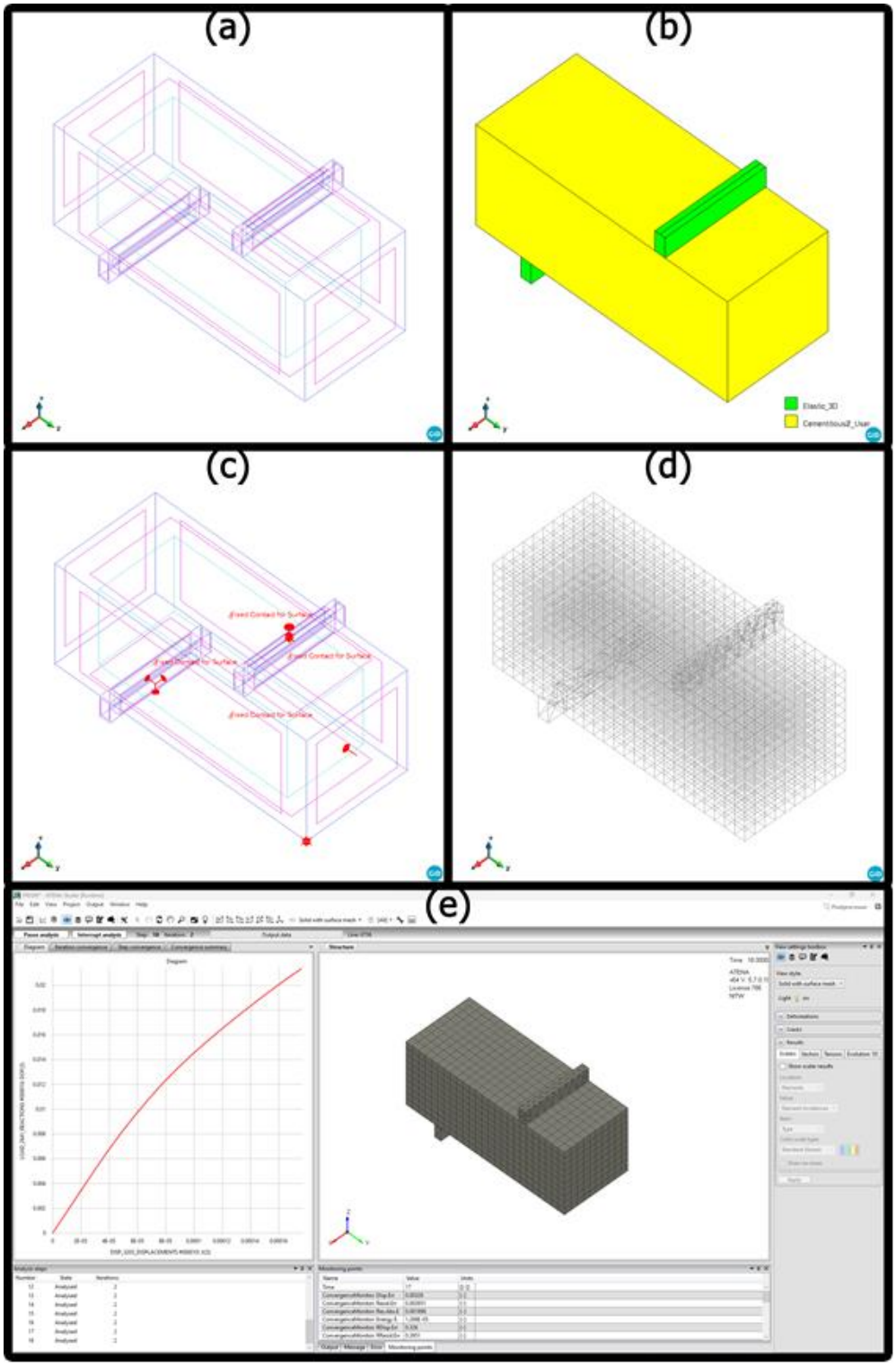

Figure 7.6 Modelling steps followed in ATENA-GiD software for prism. (a) Geometric model (b) Boundary conditions (c) Material properties (d) Meshing properties (e) ATENA analysis

7.5. Concluding remarks from Phase-III

- Experimental results of GO-cement concrete and GO-fly ash concrete are in good agreement with the values obtained by the finite element modelling of cylinders and prismatic beams.

- Peak stress values of GCC and GFC under uniaxial compression are compared with peak stress values obtained through FEM modelling. The percentage variation is observed between experimental results and analytical results are less than 15%.

- Experimental flexural strength results are compared with results obtained by the FEM model and are in good agreement.

- The developed FEM model can be used for different GO dosages and different loading conditions in order to avoid comprehensive and time consuming experimentation.

CHAPTER 8
OVERALL CONCLUSIONS

8.1. General

This chapter presents the overall conclusions of the present investigation which is aimed to evaluate the performance and microstructural characteristics of GO reinforced cement concrete and GO reinforced fly ash concrete. In addition, finite element modelling has been done to validate the experimental results. The following conclusions have been drawn from the present investigation:

8.2. Conclusions on effect of GO on cement concrete

- The reduction in slump values were observed with the addition of GO at varied dosages 0.05%, 0.10%, 0.15% and 0.20%. The percentage reduction was 7.7%, 11.5%, 15.4% and 19.2% for standard concrete and 9.1%, 13.6%, 18.2% and 22.7% for high strength concrete, respectively, compared to the control concrete.

- The workability of the concrete had greatly affected with the addition of GO. The results revealed that increasing in GO dosage decreased the fluidity of concrete composite, this may be attributed to the large surface area of GO which absorbs more free water.

- The most apparent compressive, split tensile and flexural strength values of 60.5MPa, 3.52MPa and 8.1MPa for standard concrete and 86.0MPa, 5.41MPa and 10.80MPa for high strength concrete, were observed respectively at the age of 28 days at 0.15% GO addition for both the grades of concrete.

- The rate of increase in compressive, split tensile and flexural strength values of concrete with 0.15% GO addition were 60.6%, 31.1% and 26.3% at 7days, 44.4%, 28.1% and 24.4% at 28days, respectively for standard concrete, whereas for high strength concrete the improvement was 53.1%, 29.1% and 23.7% at 7days, and 26.5%, 21.4% and 20.0% at 28days, respectively.

- The strength properties of cement concrete were remarkably improved with incorporation of GO at a dosage between 0.05% and 0.15%, this may be attributed to the accelerated hydration rate and densified microstructure. While effect of 0.20% was lower than 0.15% which may be due to the GO agglomeration.

- The influence of GO on the growth rate of strength properties is more pronounced at early age compared to later age. Furthermore, the increasing rate of strength properties of standard concrete is more significant than high strength concrete. This can be attributed to more w/c ratio that can offer adequate free water, subsequently improves the hydration process.

- The elastic modulus of GO incorporated concrete was increased by about 8.7–28.7% for standard concrete and 6.1–17.9% for high strength concrete at 28 days compared to control concrete, indicating the formation of a denser interfacial transition zone.

- Frequency response function of concrete with varying dosages of GO exhibited the improvement in natural frequencies and damping ratios up to 0.15% GO content. It was observed that the maximum increased fundamental natural frequencies were about 8.0% and 6.0% for the standard and high strength concrete at 0.15% GO dosage compared to control concrete.

- Maximum reduction in damping ratio was 29.1% and 26.3% for the standard and high strength concrete at 0.15% GO dosage compared to control concrete. The improvement in damping is attributed to the increase in total number of interfaces and enhancement of the non-uniform stress distribution both contribute to an increase in the damping ratio.

- The dynamic modulus of concrete with GO dosages up to 0.15% is improved, however beyond 0.15% of GO addition showed the reverse tendency. The maximum increased dynamic elastic modulus was 17.1% and 12.8% for the standard and high strength concrete respectively compared to control concrete.

- The UPV values exhibited that the incorporation of GO resulted in the formation of excellent quality concrete with improved homogeneity. The improvement in concrete quality may be attributable to the nano filler effect of GO, which densifies the microstructure of cement matrix.

- The trend of dynamic elastic modulus is comparable to that of compressive strength for both concrete grades. The findings of UPV test results are complied with the impact resonance test results.

- The SEM images of concrete specimens representing that in presence of GO, the hydration products are strongly interweaved with each other, having lesser number of microcracks and pores. The GO content up to 0.15% shows the formation of compact, uniform and densified microstructure compared to control concrete.

- The percentage atomic ratio of Ca/Si was quite high in control concrete, whereas incorporating GO in concrete decreased the Ca/Si ratio and reduced with increase in GO content in both the grades of concrete mixes. This could be because of GO which absorbs more quantity of water molecules, and turn into nucleation sites to hydrated phases, resulting in the formation of regulated and refined crystalline phases.

- The increase in intensity of XRD peaks representing that GO addition has exhibited the increase in crystalline phases, which is confirming that the hydration process can be accelerated by the GO and hence GO could support to generate more regular hydrated phases.

- It is observed from the IR spectra that the absorption peak of C-S-H shifts towards a higher wavenumber in the presence of GO with respect to the control concrete and the trend continues with the increase in GO content up to 0.15%indicating that GO

had influence on Ca/Si ratio and resulting in the formation of densified structure. These findings agree well with the SEM, EDX, and XRD results.

- The TGA analysis showed that the rate of hydration is improved with the addition of GO up to 0.15%. This could be because of graphene oxide which has oxygenated functional groups and a large specific surface area.

- The water absorption values with the addition of GO at 0%, 0.05%, 0.10%, 0.15% and 0.20% are recorded as 3.13%, 2.82%, 2.43%, 2.03% and 2.22% for standard concrete and 1.97%, 1.72%, 1.39%, 1.17% and 1.36% for high strength concrete, respectively.

- The water sorptivity values with the addition of GO at 0%, 0.05%, 0.10%, 0.15% and 0.20% at 90 days were 0.0067, 0.0057, 0.0049, 0.0043, and 0.0048 mm/√s for standard concrete and 0.0032, 0.0022, 0.0014, 0.0008, and 0.0013 mm/√s for high strength concrete, respectively.

- Enhanced resistance to water absorption may be attributed to the broad barrier capabilities of GO and refinement of pore structure of the cement composite resulting from decrease in critical pore diameter.

- The carbonation depth values with the addition of GO at 0%, 0.05%, 0.10%, 0.15% and 0.20% were observed as 19, 14, 12, 9, and 10 mm for standard concrete and 14, 10, 8, 6, and 7 mm for high strength concrete, respectively.

- The results of RCPT test in terms of Charge passed values of concrete mixes with GO at a dosage of 0%, 0.05%, 0.10%, 0.15% and 0.20% were observed as 2592, 2246, 1944, 1620, and 1706 coulombs for standard concrete and 1512, 1318, 1058, 821, and 886 coulombs for high strength concrete, respectively.

- The concrete mixes with 0.15% GO exposed to HCL acid for 90 days, the dimension, weight and strength losses were observed as 3.7%, 6.8%, and 18.3% for standard concrete and 3.5%, 5.7%, and 14.2% for high strength concrete, respectively.

- The concrete mixes with 0.15% GO exposed to H2SO4 acid for 90 days, the dimension, weight and strength losses were observed as 20.0%, 23.2%, and 30.3% for standard concrete and 13.4%, 18.5%, and 28.7% for high strength concrete, respectively.

- Microstructural characterization indicates that the GO inclusion acted as a diffusion barrier, and prevented the leaching of Ca2+ ions from cement hydrates such as C-S-H, CH and ettringite from the acidic environment.

8.3. Conclusions on combined effect of GO and fly ash on concrete

- The increase in slump values with the addition of GO at 0.15% and fly ash replacement at 20% and 30% are recorded as 2.31% and 6.92% for standard concrete and 1.82% and 7.27% for high strength concrete, respectively, in comparison with the control concrete.

- The fly ash counterbalances the GO influence on the decrease in fluidity because of less water requirement, size gradation and ball effect.

- At the age of 7days, the increase rate in compressive, split tensile and flexural strength values for standard concrete were 31.43%, 24.32% and 13.88% for 10% fly ash replacement, 19.68%, 6.76% and 6.95% for 20% fly ash replacement, and 4.29%, 2.70% and 2.57% for 30% fly ash replacement, respectively compared to control concrete.

- Increase rate in compressive, split tensile and flexural strength values for high strength concrete at the age of 7days were 20.82%, 14.55% and 16.66% for 10% fly ash replacement, 9.80%, 7.27% and 11.78% for 20% fly ash replacement, and 4.57%, 2.59% and 2.40% for 30% fly ash replacement, respectively compared to control concrete.

- The combined effect of GO and fly ash on growth rate concrete is less at the early stages, although, strength properties of the GO reinforced concrete mixes with replacement of fly ash up to 30% are higher than control concrete at 7 days. Therefore, the drawback of fly ash on delaying the early age development of strength was counterbalanced by GO.

- The growth rate of concrete strength properties is more at the later age (at 28 days) compared to the early age (at 7 days) could be owing to the secondary hydration of fly ash.

- The improvement in elastic modulus of concrete containing GO at 0.15% and fly ash at 10%, 20% and 30% was 19.86%, 9.15% and 1.39% for standard concrete, and 15.97%, 8.28% and 2.05% for high strength concrete, respectively, compared to control concrete.

- The improvement in fundamental natural frequency of concrete containing GO at 0.15% and fly ash at 10%, 20% and 30% was 6.21%, 3.42% and 0.51% for standard concrete, and 3.91%, 2.95% and 0.66% for high strength concrete, respectively, compared to control concrete.

- The decrease in fundamental damping ratios of concrete containing GO at 0.15% and fly ash at 10%, 20% and 30% was 24.42%, 20.93% and 17.44% for standard concrete, and 23.68%, 19.74% and 10.53% for high strength concrete, respectively, compared to that of control concrete.

- The dynamic elastic modulus of concrete containing GO at a dosage of 0.15% and replacing cement with fly ash at 10%, 20% and 30% were 53.09, 50.14 and 47.54 GPa for standard concrete, and 56.44, 54.96, and 52.75 GPa for high strength concrete, respectively.

- Similarly, the dynamic poissons ratio of concrete containing GO at a dosage of 0.15% and replacing cement with fly ash at 10%, 20% and 30% were 0.21, 0.20 and 0.19 for standard concrete, and 0.24, 0.23 and 0.22 for high strength concrete, respectively.

- According to the UPV test results, combined effect of GO and fly ash on concrete resulted in formation of excellent quality concrete with greater uniformity which might be attributed to nano filler effect of GO and size gradation of fly ash, which densifies the microstructure of the concrete matrix.

- The surface of concrete with GO and fly ash shows formation of a compact, uniform and densified structure at micro-level compared with control concrete, and unreacted smooth spherical shape fly ash particles demonstrates secondary hydration of fly ash is in progress.

- The Ca/Si elemental ratio was high for control concrete, and addition of GO and replacement of fly ash decreases the Ca/Si ratio in concrete matrix which densifies C-S-H phase.

- GO addition and replacement of fly ash enhances the peaks intensity compared to control concrete, shows that increase in crystallinity of hydration phases.

- In the presence of GO and fly ash the absorption peak of Calcium silicate hydrate shifts to a higher wavenumber than that of control concrete, demonstrating that the addition of GO changes the Ca/Si ratio and formation of densified calcium silicate hydrate gels.

- TGA analysis showed the increase in non-evaporable water content of concrete with GO and fly ash suggesting that the integration of GO and fly ash has a role in improving the secondary hydration of the concrete matrix at a later stage.

- Water absorption values of control concrete and concrete with constant GO dosage of 0.15% and varying fly ash replacements at 0%, 10%, 20%, and 30% are recorded as 2.03%, 1.74%, 1.64% and 1.42% for standard concrete and 1.17%, 1.13%, 1.07% and 0.98% for high strength concrete, respectively.

- Water sorptivity values of control concrete and concrete with constant GO dosage of 0.15% and varying fly ash replacements at 0%, 10%, 20%, and 30% at 90 days were

0.0043, 0.0041, 0.0039, and 0.0037 mm/√s for standard concrete and 0.00080, 0.00076, 0.00072, and 0.00068 mm/√s for high strength concrete, respectively.

- Enhanced resistance to water absorption may be attributed to the extensive barrier capacities of GO and refinement of pore structure of the cement composites resulting from decrease in critical pore diameter.

- Carbonation depth values of control concrete and concrete with GO dosage 0.15% and fly ash replacements 0%, 10%, 20%, and 30% were 9, 8, 6, and 4 mm for standard concrete and 6, 5, 4, and 3 mm for high strength concrete, respectively.

- The results of RCPT test in terms of Charge passed values of control concrete and concrete with GO dosage 0.15% and fly ash replacements 0%, 10%, 20%, and 30% were 1620, 1210, 1015, and 821 coulombs for standard concrete and 821, 648, 454, and 346 coulombs for high strength concrete, respectively.

- The concrete mixes with the addition of GO at 0.15% and fly ash replacement at 30% exposed to HCl acid for 90 days, dimension, weight and strength losses were decreased to 6.1%, 10.7%, and 31.8% for standard concrete and 5.9%, 9.2%, and 23.9% for high strength concrete, respectively.

- The concrete mixes with the addition of GO at 0.15% and fly ash replacement at 30% exposed to H2SO4 acid for 90 days, dimension, weight and strength losses were decreased to 33.2%, 39.1%, and 49.9% for standard concrete and 22.2%, 29.9%, and 49.8% for high strength concrete, respectively.

- Microstructural characterization indicates that the GO inclusion and fly ash replacement functioned as a diffusion barrier, and prevented the leaching of Ca2+ ions from cement hydrates such as C-S-H, CH and ettringite from the acidic environment.

8.4. Conclusions on validation of experimental results with numerical modelling

- Experimental results of GO-cement concrete and GO-fly ash concrete are in good agreement with the values obtained by the finite element modelling of cylinders and prismatic beams.
- Peak stress values of GCC and GFC under uniaxial compression are compared with peak stress values of FEM model. The percentage variation is observed between experimental results and analytical results are less than 15%.
- Experimental flexural strength results are compared with results obtained by the FEM model and the results are in good agreement.
- The developed FEM model can be used and for different GO dosages and different loading conditions in order to avoid comprehensive experimentation.

8.5. Specific contribution made in this work

- The optimum influence of GO on static and dynamic mechanical properties, microstructural characteristics and durability performance of cement concrete has been assessed.
- The combined effect of GO and fly ash on static and dynamic mechanical properties, microstructural characteristics and durability performance of cement concrete has been determined.
- Finite element modelling has been done using ATENA-GiD software to avoid comprehensive experimentation.

8.6. Scope for the further study

- The effect of GO on long term durability of concrete such as creep and shrinkage.
- The effect of GO on the structural behavior of concrete members such as flexure, shear and bond.
- The combined effect of GO and other SCMs such as GGBS, silica fume, metakaolin etc on the performance of concrete.

REFERENCES

Abrishami, M. Ebrahimizadeh, and V. Zahabi. 2016. “Reinforcing Graphene Oxide/Cement Composite with NH2 Functionalizing Group.” *Bulletin of Materials Science* 39(4):1073–78. doi: 10.1007/s12034-016-1250-7.

Abu Al-Rub, Rashid K., Bryan M. Tyson, Ardavan Yazdanbakhsh, and Zachary Grasley. 2012. “Mechanical Properties of Nanocomposite Cement Incorporating Surface-Treated and Untreated Carbon Nanotubes and Carbon Nanofibers.” *Journal of Nanomechanics and Micromechanics* 2(1):1–6. doi: 10.1061/(ASCE)NM.2153-5477.0000041.

Alkhateb, Hunain, Ahmed Al-Ostaz, Alexander H. D. Cheng, and Xiaobing Li. 2013. “Materials Genome for Graphene-Cement Nanocomposites.” *Journal of Nanomechanics and Micromechanics* 3(3):67–77. doi: 10.1061/(ASCE)NM.2153-5477.0000055.

Alotaibi, Faisal, Tran T. Tung, Md J. Nine, Shervin Kabiri, Mahmoud Moussa, Diana N. H. Tran, and Dusan Losic. 2018. “Scanning Atmospheric Plasma for Ultrafast Reduction of Graphene Oxide and Fabrication of Highly Conductive Graphene Films and Patterns.” *Carbon* 127:113–21. doi: 10.1016/j.carbon.2017.10.075.

Ariffin, M. A. M., M. A. R. Bhutta, M. W. Hussin, M. Mohd Tahir, and Nor Aziah. 2013. “Sulfuric Acid Resistance of Blended Ash Geopolymer Concrete.” *Construction and Building Materials* 43:80–86. doi: 10.1016/j.conbuildmat.2013.01.018.

Babak, Fakhim, Hassani Abolfazl, Rashidi Alimorad, and Ghodousi Parviz. 2014. “Preparation and Mechanical Properties of Graphene Oxide: Cement

Nanocomposites." *The Scientific World Journal* 2014:1–10. doi: 10.1155/2014/276323.

Bentur, A., A. Peled, and D. Yankelevsky. 1997. "Enhanced Bonding of Low Modulus Polymer Fibers-Cement Matrix by Means of Crimped Geometry." *Cement and Concrete Research* 27(7):1099–1111. doi: 10.1016/S0008-8846(97)00088-4.

Bhatty, Javed I. 1986. "Hydration versus Strength in a Portland Cement Developed from Domestic Mineral Wastes — a Comparative Study." *Thermochimica Acta* 106:93–103. doi: 10.1016/0040-6031(86)85120-6.

Brandt, Andrzej M. 2008. "Fibre Reinforced Cement-Based (FRC) Composites after over 40 Years of Development in Building and Civil Engineering." *Composite Structures* 86(1–3):3–9. doi: 10.1016/j.compstruct.2008.03.006.

Cao, Ming-li, Hui-xia Zhang, and Cong Zhang. 2016. "Effect of Graphene on Mechanical Properties of Cement Mortars." *Journal of Central South University* 23(4):919–25. doi: 10.1007/s11771-016-3139-4.

Choi, Wonbong, Indranil Lahiri, Raghunandan Seelaboyina, and Yong Soo Kang. 2010. "Synthesis of Graphene and Its Applications: A Review." *Critical Reviews in Solid State and Materials Sciences* 35(1):52–71. doi: 10.1080/10408430903505036.

Chu, Hongyan, Yu Zhang, Fengjuan Wang, Taotao Feng, Liguo Wang, and Danqian Wang. 2020. "Effect of Graphene Oxide on Mechanical Properties and Durability of Ultra-High-Performance Concrete Prepared from Recycled Sand." *Nanomaterials* 10(9):1718. doi: 10.3390/nano10091718.

Chuah, Samuel, Wengui Li, Shu Jian Chen, Jay G. Sanjayan, and Wen Hui Duan. 2018. "Investigation on Dispersion of Graphene Oxide in Cement Composite Using Different Surfactant Treatments." *Construction and Building Materials* 161:519–27. doi: 10.1016/j.conbuildmat.2017.11.154.

Chuah, Samuel, Zhu Pan, Jay G. Sanjayan, Chien Ming Wang, and Wen Hui Duan. 2014. “Nano Reinforced Cement and Concrete Composites and New Perspective from Graphene Oxide.” *Construction and Building Materials* 73:113–24. doi: 10.1016/j.conbuildmat.2014.09.040.

Collins, Frank, John Lambert, and Wen Hui Duan. 2012. “The Influences of Admixtures on the Dispersion, Workability, and Strength of Carbon Nanotube–OPC Paste Mixtures.” *Cement and Concrete Composites* 34(2):201–7. doi: 10.1016/j.cemconcomp.2011.09.013.

Cwirzen, A., K. Habermehl-Cwirzen, A. G. Nasibulin, E. I. Kaupinen, P. R. Mudimela, and V. Penttala. 2009. “SEM/AFM Studies of Cementitious Binder Modified by MWCNT and Nano-Sized Fe Needles.” *Materials Characterization* 60(7):735–40. doi: 10.1016/j.matchar.2008.11.001.

Davalos, Julio F. 2012. “Advanced Materials for Civil Infrastructure Rehabilitation and Protection.” in *Seminar at The Citty College of New York, New York*.

Deboucha, Walid, Nordine Leklou, Abdelhafid Khelidj, and Mohamed N. Oudjit. 2017. “Hydration Development of Mineral Additives Blended Cement Using Thermogravimetric Analysis (TGA): Methodology of Calculating the Degree of Hydration.” *Construction and Building Materials* 146:687–701. doi: 10.1016/j.conbuildmat.2017.04.132.

Emiru, Tarko Fentaw, and Delele Worku Ayele. 2017. “Controlled Synthesis, Characterization and Reduction of Graphene Oxide: A Convenient Method for Large Scale Production.” *Egyptian Journal of Basic and Applied Sciences* 4(1):74–79. doi: 10.1016/j.ejbas.2016.11.002.

Geim, A. K., and K. S. Novoselov. 2007. “The Rise of Graphene.” *Nature Materials* 6(3):183–91. doi: 10.1038/nmat1849.

Geng, Yan, Shu Jun Wang, and Jang-Kyo Kim. 2009. “Preparation of Graphite Nanoplatelets and Graphene Sheets.” *Journal of Colloid and Interface Science* 336(2):592–98. doi: 10.1016/j.jcis.2009.04.005.

Gengler, Régis Y. N., Daniel S. Badali, Dongfang Zhang, Konstantinos Dimos, Konstantinos Spyrou, Dimitrios Gournis, and R. J. Dwayne Miller. 2013. “Revealing the Ultrafast Process behind the Photoreduction of Graphene Oxide.” *Nature Communications* 4(1):2560. doi: 10.1038/ncomms3560.

Gholampour, Aliakbar, Meisam Valizadeh Kiamahalleh, Diana N. H. Tran, Togay Ozbakkaloglu, and Dusan Losic. 2017. “Revealing the Dependence of the Physiochemical and Mechanical Properties of Cement Composites on Graphene Oxide Concentration.” *RSC Advances* 7(87):55148–56. doi: 10.1039/C7RA10066C.

Gong, Kai, Zhu Pan, Asghar H. Korayem, Ling Qiu, Dan Li, Frank Collins, Chien Ming Wang, and Wen Hui Duan. 2015. “Reinforcing Effects of Graphene Oxide on Portland Cement Paste.” *Journal of Materials in Civil Engineering* 27(2). doi: 10.1061/(ASCE)MT.1943-5533.0001125.

Grubb, J. A., J. Blunt, C. P. Ostertag, and T. M. Devine. 2007. “Effect of Steel Microfibers on Corrosion of Steel Reinforcing Bars.” *Cement and Concrete Research* 37(7):1115–26. doi: 10.1016/j.cemconres.2007.04.012.

Hamoush, Sameer, Taher Abu-Lebdeh, and Toney Cummins. 2010. “Deflection Behavior of Concrete Beams Reinforced with PVA Micro-Fibers.” *Construction and Building Materials* 24(11):2285–93. doi: 10.1016/j.conbuildmat.2010.04.027.

Han, Fanghui, Dongmin Wang, and Peiyu Yan. 2014. “Hydration Kinetics of Composite Binder Containing Different Content of Slag or Fly Ash.” *Journal of the Chinese Ceramic Society* 42(5):613–20.

Hilding, Jenny, Eric A. Grulke, Z. George Zhang, and Fran Lockwood. 2003. "Dispersion of Carbon Nanotubes in Liquids." *Journal of Dispersion Science and Technology* 24(1):1–41. doi: 10.1081/DIS-120017941.

Horgnies, M., J. J. Chen, and C. Bouillon. 2013. "Overview about the Use of Fourier Transform Infrared Spectroscopy to Study Cementitious Materials." Pp. 251–62 in.

Horszczaruk, Elżbieta, Ewa Mijowska, Ryszard J. Kalenczuk, Małgorzata Aleksandrzak, and Sylwia Mijowska. 2015. "Nanocomposite of Cement/Graphene Oxide – Impact on Hydration Kinetics and Young's Modulus." *Construction and Building Materials* 78:234–42. doi: 10.1016/j.conbuildmat.2014.12.009.

Hu, Miaomiao, Jintang Guo, Jinjie Fan, Pengpeng li, and Di Chen. 2019. "Dispersion of Triethanolamine-Functionalized Graphene Oxide (TEA-GO) in Pore Solution and Its Influence on Hydration, Mechanical Behavior of Cement Composite." *Construction and Building Materials* 216:128–36. doi: 10.1016/j.conbuildmat.2019.04.180.

Kaneto, K., M. Tsuruta, G. Sakai, W. Y. Cho, and Y. Ando. 1999. "Electrical Conductivities of Multi-Wall Carbon Nano Tubes." *Synthetic Metals* 103(1–3):2543–46. doi: 10.1016/S0379-6779(98)00221-5.

Kang, Donghoon, Kang Seok Seo, HeeYoung Lee, and Wonseok Chung. 2017. "Experimental Study on Mechanical Strength of GO-Cement Composites." *Construction and Building Materials* 131:303–8. doi: 10.1016/j.conbuildmat.2016.11.083.

Kang, Xiaojuan, Xiaohong Zhu, Jueshi Qian, Jiaping Liu, and Yongbo Huang. 2019. "Effect of Graphene Oxide (GO) on Hydration of Tricalcium Silicate (C3S)." *Construction and Building Materials* 203:514–24. doi: 10.1016/j.conbuildmat.2019.01.117.

Kawashima, Shiho, Pengkun Hou, David J. Corr, and Surendra P. Shah. 2013. "Modification of Cement-Based Materials with Nanoparticles." *Cement and Concrete Composites* 36:8–15. doi: 10.1016/j.cemconcomp.2012.06.012.

Kim, Hyunwoo, Ahmed A. Abdala, and Christopher W. Macosko. 2010. "Graphene/Polymer Nanocomposites." *Macromolecules* 43(16):6515–30. doi: 10.1021/ma100572e.

Kjellsen, K. O., O. H. Wallevik, and L. Fjällberg. 1998. "Microstructure and Microchemistry of the Paste—Aggregate Interfacial Transition Zone of High-Performance Concrete." *Advances in Cement Research* 10(1):33–40. doi: 10.1680/adcr.1998.10.1.33.

Kunther, Wolfgang, Sergio Ferreiro, and Jørgen Skibsted. 2017. "Influence of the Ca/Si Ratio on the Compressive Strength of Cementitious Calcium–Silicate–Hydrate Binders." *Journal of Materials Chemistry A* 5(33):17401–12. doi: 10.1039/C7TA06104H.

Labroo, Pratima, and Yue Cui. 2013. "Flexible Graphene Bio-Nanosensor for Lactate." *Biosensors and Bioelectronics* 41:852–56. doi: 10.1016/j.bios.2012.08.024.

Lee, Seung Whan, Cecilia Mattevi, Manish Chhowalla, and R. Mohan Sankaran. 2012. "Plasma-Assisted Reduction of Graphene Oxide at Low Temperature and Atmospheric Pressure for Flexible Conductor Applications." *The Journal of Physical Chemistry Letters* 3(6):772–77. doi: 10.1021/jz300080p.

Li, Dan, Marc B. Müller, Scott Gilje, Richard B. Kaner, and Gordon G. Wallace. 2008. "Processable Aqueous Dispersions of Graphene Nanosheets." *Nature Nanotechnology* 3(2):101–5. doi: 10.1038/nnano.2007.451.

Li, Dong-Bo, Hong-Chi Zhang, Peng-Bo Lei, Jia-Ping Liu, and Dong Zhao. 2019. "Synergistic Effects of Fly Ash and Graphene Oxide on Workability, Mechanical Property of Cement-Based Materials." *Science of Advanced Materials* 11(11):1647–55.

Li, Geng Ying, Pei Ming Wang, and Xiaohua Zhao. 2005. “Mechanical Behavior and Microstructure of Cement Composites Incorporating Surface-Treated Multi-Walled Carbon Nanotubes.” *Carbon* 43(6):1239–45. doi: 10.1016/j.carbon.2004.12.017.

Li, Geng Ying, Pei Ming Wang, and Xiaohua Zhao. 2007. “Pressure-Sensitive Properties and Microstructure of Carbon Nanotube Reinforced Cement Composites.” *Cement and Concrete Composites* 29(5):377–82. doi: 10.1016/j.cemconcomp.2006.12.011.

Li, Hui, Hui-gang Xiao, Jie Yuan, and Jinping Ou. 2004. “Microstructure of Cement Mortar with Nano-Particles.” *Composites Part B: Engineering* 35(2):185–89. doi: 10.1016/S1359-8368(03)00052-0.

Li, Wengui, Xiangyu Li, Shu Jian Chen, Yan Ming Liu, Wen Hui Duan, and Surendra P. Shah. 2017. “Effects of Graphene Oxide on Early-Age Hydration and Electrical Resistivity of Portland Cement Paste.” *Construction and Building Materials* 136:506–14. doi: 10.1016/j.conbuildmat.2017.01.066.

Li, Wengui, Xiangyu Li, Shu Jian Chen, Guangcheng Long, Yan Ming Liu, and Wen Hui Duan. 2017. “Effects of Nanoalumina and Graphene Oxide on Early-Age Hydration and Mechanical Properties of Cement Paste.” *Journal of Materials in Civil Engineering* 29(9). doi: 10.1061/(ASCE)MT.1943-5533.0001926.

Li, Xiangyu, Asghar Habibnejad Korayem, Chenyang Li, Yanming Liu, Hongsen He, Jay G. Sanjayan, and Wen Hui Duan. 2016. “Incorporation of Graphene Oxide and Silica Fume into Cement Paste: A Study of Dispersion and Compressive Strength.” *Construction and Building Materials* 123:327–35. doi: 10.1016/j.conbuildmat.2016.07.022.

Li, Xiangyu, Yan Ming Liu, Wen Gui Li, Chen Yang Li, Jay G. Sanjayan, Wen Hui Duan, and Zongjin Li. 2017. “Effects of Graphene Oxide Agglomerates on Workability, Hydration, Microstructure and Compressive Strength of Cement

Paste." *Construction and Building Materials* 145:402–10. doi: 10.1016/j.conbuildmat.2017.04.058.

Li, Xiangyu, Zeyu Lu, Samuel Chuah, Wengui Li, Yanming Liu, Wen Hui Duan, and Zongjin Li. 2017. "Effects of Graphene Oxide Aggregates on Hydration Degree, Sorptivity, and Tensile Splitting Strength of Cement Paste." *Composites Part A: Applied Science and Manufacturing* 100:1–8. doi: 10.1016/j.compositesa.2017.05.002.

Li, Xueguang, Wei Wei, Hao Qin, and Yun Hang Hu. 2015. "Co-Effects of Graphene Oxide Sheets and Single Wall Carbon Nanotubes on Mechanical Properties of Cement." *Journal of Physics and Chemistry of Solids* 85:39–43. doi: 10.1016/j.jpcs.2015.04.018.

Lin, Li, and Zhongfan Liu. 2016. "On-the-Spot Growth." *Nature Materials* 15(1):9–10. doi: 10.1038/nmat4498.

Long, Wu-Jian, Yu-cun Gu, Feng Xing, and Kamal H. Khayat. 2018. "Microstructure Development and Mechanism of Hardened Cement Paste Incorporating Graphene Oxide during Carbonation." *Cement and Concrete Composites* 94:72–84. doi: 10.1016/j.cemconcomp.2018.08.016.

Long, Wu-Jian, Hao-Dao Li, Chang-Le Fang, and Feng Xing. 2018. "Uniformly Dispersed and Re-Agglomerated Graphene Oxide-Based Cement Pastes: A Comparison of Rheological Properties, Mechanical Properties and Microstructure." *Nanomaterials* 8(1):31. doi: 10.3390/nano8010031.

Long, Wu-Jian, Jing-Jie Wei, Hongyan Ma, and Feng Xing. 2017. "Dynamic Mechanical Properties and Microstructure of Graphene Oxide Nanosheets Reinforced Cement Composites." *Nanomaterials* 7(12):407. doi: 10.3390/nano7120407.

Long, Wu-Jian, Jing-Jie Wei, Feng Xing, and Kamal H. Khayat. 2018. "Enhanced Dynamic Mechanical Properties of Cement Paste Modified with Graphene Oxide

Nanosheets and Its Reinforcing Mechanism." *Cement and Concrete Composites* 93:127–39. doi: 10.1016/j.cemconcomp.2018.07.001.

Long, Wu-Jian, Dan Zheng, Hua-bo Duan, Ningxu Han, and Feng Xing. 2018. "Performance Enhancement and Environmental Impact of Cement Composites Containing Graphene Oxide with Recycled Fine Aggregates." *Journal of Cleaner Production* 194:193–202. doi: 10.1016/j.jclepro.2018.05.108.

Lowe, Sean E., and Yu Lin Zhong. 2016. "Challenges of Industrial-Scale Graphene Oxide Production." Pp. 410–31 in *Graphene Oxide*. Chichester, UK: John Wiley & Sons, Ltd.

Lu, Cong, Zeyu Lu, Zongjin Li, and Christopher K. Y. Leung. 2016. "Effect of Graphene Oxide on the Mechanical Behavior of Strain Hardening Cementitious Composites." *Construction and Building Materials* 120:457–64. doi: 10.1016/j.conbuildmat.2016.05.122.

Lu, Lingchao, Piqi Zhao, and Zeyu Lu. 2018. "A Short Discussion on How to Effectively Use Graphene Oxide to Reinforce Cementitious Composites." *Construction and Building Materials* 189:33–41. doi: 10.1016/j.conbuildmat.2018.08.170.

Lu, Liulei, and Dong Ouyang. 2017. "Properties of Cement Mortar and Ultra-High Strength Concrete Incorporating Graphene Oxide Nanosheets." *Nanomaterials* 7(7):187. doi: 10.3390/nano7070187.

Lu, Zeyu, Binmeng Chen, ChristopherK. Y. Leung, Zongjin Li, and Guoxing Sun. 2019. "Aggregation Size Effect of Graphene Oxide on Its Reinforcing Efficiency to Cement-Based Materials." *Cement and Concrete Composites* 100:85–91. doi: 10.1016/j.cemconcomp.2019.04.005.

Lu, Zeyu, Dongshuai Hou, Hongyan Ma, Tianyuan Fan, and Zongjin Li. 2016. "Effects of Graphene Oxide on the Properties and Microstructures of the Magnesium

Potassium Phosphate Cement Paste." *Construction and Building Materials* 119:107–12. doi: 10.1016/j.conbuildmat.2016.05.060.

Lu, Zeyu, Xiangyu Li, Asad Hanif, Binmeng Chen, Pavithra Parthasarathy, Jinguang Yu, and Zongjin Li. 2017. "Early-Age Interaction Mechanism between the Graphene Oxide and Cement Hydrates." *Construction and Building Materials* 152:232–39. doi: 10.1016/j.conbuildmat.2017.06.176.

Lv, S. H., L. J. Deng, W. Q. Yang, Q. F. Zhou, and Y. Y. Cui. 2016. "Fabrication of Polycarboxylate/Graphene Oxide Nanosheet Composites by Copolymerization for Reinforcing and Toughening Cement Composites." *Cement and Concrete Composites* 66:1–9. doi: 10.1016/j.cemconcomp.2015.11.007.

Lv, Shenghua, Haoyan Hu, Jia Zhang, Xiaoqian Luo, Ying Lei, and Li Sun. 2017. "Fabrication of GO/Cement Composites by Incorporation of Few-Layered GO Nanosheets and Characterization of Their Crystal/Chemical Structure and Properties." *Nanomaterials* 7(12):457. doi: 10.3390/nano7120457.

Lv, Shenghua, Jingjing Liu, Ting Sun, Yujuan Ma, and Qingfang Zhou. 2014. "Effect of GO Nanosheets on Shapes of Cement Hydration Crystals and Their Formation Process." *Construction and Building Materials* 64:231–39. doi: 10.1016/j.conbuildmat.2014.04.061.

Lv, Shenghua, Yujuan Ma, Chaochao Qiu, Ting Sun, Jingjing Liu, and Qingfang Zhou. 2013. "Effect of Graphene Oxide Nanosheets of Microstructure and Mechanical Properties of Cement Composites." *Construction and Building Materials* 49:121–27. doi: 10.1016/j.conbuildmat.2013.08.022.

Lv, Shenghua, Yujuan Ma, Chaochao Qiu, and Qingfang Zhou. 2013. "Regulation of GO on Cement Hydration Crystals and Its Toughening Effect." *Magazine of Concrete Research* 65(20):1246–54. doi: 10.1680/macr.13.00190.

Lv, Shenghua, Sun Ting, Jingjing Liu, and Qingfang Zhou. 2014. "Use of Graphene Oxide Nanosheets to Regulate the Microstructure of Hardened Cement Paste to

Increase Its Strength and Toughness." *CrystEngComm* 16(36):8508. doi: 10.1039/C4CE00684D.

Ma, Peng-Cheng, Naveed A. Siddiqui, Gad Marom, and Jang-Kyo Kim. 2010. "Dispersion and Functionalization of Carbon Nanotubes for Polymer-Based Nanocomposites: A Review." *Composites Part A: Applied Science and Manufacturing* 41(10):1345–67. doi: 10.1016/j.compositesa.2010.07.003.

Marcano, Daniela C., Dmitry v. Kosynkin, Jacob M. Berlin, Alexander Sinitskii, Zhengzong Sun, Alexander Slesarev, Lawrence B. Alemany, Wei Lu, and James M. Tour. 2010. "Improved Synthesis of Graphene Oxide." *ACS Nano* 4(8):4806–14. doi: 10.1021/nn1006368.

Marikunte, Shashidhara, Corina Aldea, and Surendra P. Shah. 1997. "Durability of Glass Fiber Reinforced Cement Composites:" *Advanced Cement Based Materials* 5(3–4):100–108. doi: 10.1016/S1065-7355(97)00003-5.

Mehta, P. Kumar, and Paulo J. M. Monteiro. 2014. *Concrete: Microstructure, Properties, and Materials*. 4th Edition. New York: McGraw-Hill Education.

Mohammed, A., N. T. K. Al-Saadi, and R. Al-Mahaidi. 2017. "Utilization of Graphene Oxide to Synthesize High-Strength Cement-Based Adhesive." *Journal of Materials in Civil Engineering* 29(4). doi: 10.1061/(ASCE)MT.1943-5533.0001705.

Mohammed, A., J. G. Sanjayan, W. H. Duan, and A. Nazari. 2015. "Incorporating Graphene Oxide in Cement Composites: A Study of Transport Properties." *Construction and Building Materials* 84:341–47. doi: 10.1016/j.conbuildmat.2015.01.083.

Mohammed, A., J. G. Sanjayan, W. H. Duan, and A. Nazari. 2016. "Graphene Oxide Impact on Hardened Cement Expressed in Enhanced Freeze–Thaw Resistance." *Journal of Materials in Civil Engineering* 28(9). doi: 10.1061/(ASCE)MT.1943-5533.0001586.

Naseri, Farzad, Mohammad Irani, and Masoud Dehkhodarajabi. 2016. “Effect of Graphene Oxide Nanosheets on the Geotechnical Properties of Cemented Silty Soil.” *Archives of Civil and Mechanical Engineering* 16(4):695–701. doi: 10.1016/j.acme.2016.04.008.

Nasibulin, Albert G., Tatyana Koltsova, Larisa I. Nasibulina, Ilya V. Anoshkin, Alexandr Semencha, Oleg V. Tolochko, and Esko I. Kauppinen. 2013. “A Novel Approach to Composite Preparation by Direct Synthesis of Carbon Nanomaterial on Matrix or Filler Particles.” *Acta Materialia* 61(6):1862–71. doi: 10.1016/j.actamat.2012.12.007.

Novoselov, K. S., A. K. Geim, S. V. Morozov, D. Jiang, Y. Zhang, S. V. Dubonos, I. V. Grigorieva, and A. A. Firsov. 2004. “Electric Field Effect in Atomically Thin Carbon Films.” *Science* 306(5696):666–69. doi: 10.1126/science.1102896.

Oltulu, Meral, and Remzi Şahin. 2013. “Effect of Nano-SiO2, Nano-Al2O3 and Nano-Fe2O3 Powders on Compressive Strengths and Capillary Water Absorption of Cement Mortar Containing Fly Ash: A Comparative Study.” *Energy and Buildings* 58:292–301. doi: 10.1016/j.enbuild.2012.12.014.

Pan, Zhu, Li He, Ling Qiu, Asghar Habibnejad Korayem, Gang Li, Jun Wu Zhu, Frank Collins, Dan Li, Wen Hui Duan, and Ming Chien Wang. 2015. “Mechanical Properties and Microstructure of a Graphene Oxide–Cement Composite.” *Cement and Concrete Composites* 58:140–47. doi: 10.1016/j.cemconcomp.2015.02.001.

Patil, Avinash J., Jemma L. Vickery, Thomas B. Scott, and Stephen Mann. 2009. “Aqueous Stabilization and Self-Assembly of Graphene Sheets into Layered Bio-Nanocomposites Using DNA.” *Advanced Materials* 21(31):3159–64. doi: 10.1002/adma.200803633.

Peng, Hui, Yaping Ge, C. S. Cai, Yongxing Zhang, and Zhen Liu. 2019. “Mechanical Properties and Microstructure of Graphene Oxide Cement-Based Composites.”

Construction and Building Materials 194:102–9. doi: 10.1016/j.conbuildmat.2018.10.234.

Peng, Li, Zhen Xu, Zheng Liu, Yangyang Wei, Haiyan Sun, Zheng Li, Xiaoli Zhao, and Chao Gao. 2015. "An Iron-Based Green Approach to 1-h Production of Single-Layer Graphene Oxide." *Nature Communications* 6(1):5716. doi: 10.1038/ncomms6716.

Porwal, H., S. Grasso, and M. J. Reece. 2013. "Review of Graphene–Ceramic Matrix Composites." *Advances in Applied Ceramics* 112(8):443–54. doi: 10.1179/174367613X13764308970581.

Proctor, B. A., D. R. Oakley, and K. L. Litherland. 1982. "Developments in the Assessment and Performance of Grc over 10 Years." *Composites* 13(2):173–79. doi: 10.1016/0010-4361(82)90056-8.

Qian, C. X., and P. Stroeven. 2000. "Development of Hybrid Polypropylene-Steel Fibre-Reinforced Concrete." *Cement and Concrete Research* 30(1):63–69. doi: 10.1016/S0008-8846(99)00202-1.

Qin, Hao, Wei Wei, and Yun Hang Hu. 2017. "Synergistic Effect of Graphene-Oxide-Doping and Microwave-Curing on Mechanical Strength of Cement." *Journal of Physics and Chemistry of Solids* 103:67–72. doi: 10.1016/j.jpcs.2016.12.009.

Qing, Ye, Zhang Zenan, Kong Deyu, and Chen Rongshen. 2007. "Influence of Nano-SiO2 Addition on Properties of Hardened Cement Paste as Compared with Silica Fume." *Construction and Building Materials* 21(3):539–45. doi: 10.1016/j.conbuildmat.2005.09.001.

Qiu, Ling, Xuehua Zhang, Wenrong Yang, Yufei Wang, George P. Simon, and Dan Li. 2011. "Controllable Corrugation of Chemically Converted Graphene Sheets in Water and Potential Application for Nanofiltration." *Chemical Communications* 47(20):5810. doi: 10.1039/c1cc10720h.

Qureshi, Tanvir S., and Daman K. Panesar. 2019. “Impact of Graphene Oxide and Highly Reduced Graphene Oxide on Cement Based Composites.” *Construction and Building Materials* 206:71–83. doi: 10.1016/j.conbuildmat.2019.01.176.

Roy, Rahul, Ananda Mitra, Ajay T. Ganesh, and V. Sairam. 2018. “Effect of Graphene Oxide Nanosheets Dispersion in Cement Mortar Composites Incorporating Metakaolin and Silica Fume.” *Construction and Building Materials* 186:514–24. doi: 10.1016/j.conbuildmat.2018.07.135.

Said, A. M., M. S. Zeidan, M. T. Bassuoni, and Y. Tian. 2012. “Properties of Concrete Incorporating Nano-Silica.” *Construction and Building Materials* 36:838–44. doi: 10.1016/j.conbuildmat.2012.06.044.

Saleem, Hareema, Mobeen Haneef, and Hina Y. Abbasi. 2018. “Synthesis Route of Reduced Graphene Oxide via Thermal Reduction of Chemically Exfoliated Graphene Oxide.” *Materials Chemistry and Physics* 204:1–7. doi: 10.1016/j.matchemphys.2017.10.020.

Scrivener, Karen L., and R. James Kirkpatrick. 2008. “Innovation in Use and Research on Cementitious Material.” *Cement and Concrete Research* 38(2):128–36. doi: 10.1016/j.cemconres.2007.09.025.

See, Chee Howe, and Andrew T. Harris. 2007. “A Review of Carbon Nanotube Synthesis via Fluidized-Bed Chemical Vapor Deposition.” *Industrial & Engineering Chemistry Research* 46(4):997–1012. doi: 10.1021/ie060955b.

Shamsaei, Ezzatollah, Felipe Basquiroto de Souza, Xupei Yao, Emad Benhelal, Abozar Akbari, and Wenhui Duan. 2018. “Graphene-Based Nanosheets for Stronger and More Durable Concrete: A Review.” *Construction and Building Materials* 183:642–60. doi: 10.1016/j.conbuildmat.2018.06.201.

Shang, Yu, Dong Zhang, Chao Yang, Yanyun Liu, and Yong Liu. 2015. “Effect of Graphene Oxide on the Rheological Properties of Cement Pastes.” *Construction and Building Materials* 96:20–28. doi: 10.1016/j.conbuildmat.2015.07.181.

Sharma, Snigdha, and N. C. Kothiyal. 2016. “Comparative Effects of Pristine and Ball-Milled Graphene Oxide on Physico-Chemical Characteristics of Cement Mortar Nanocomposites.” *Construction and Building Materials* 115:256–68. doi: 10.1016/j.conbuildmat.2016.04.019.

Sharma, Snigdha, Divya Susan, N. C. Kothiyal, and Ramanjit Kaur. 2018. “Graphene Oxide Prepared from Mechanically Milled Graphite: Effect on Strength of Novel Fly-Ash Based Cementitious Matrix.” *Construction and Building Materials* 177:10–22. doi: 10.1016/j.conbuildmat.2018.05.051.

Si, Yongchao, and Edward T. Samulski. 2008. “Synthesis of Water Soluble Graphene.” *Nano Letters* 8(6):1679–82. doi: 10.1021/nl080604h.

Snehal, K., B. B. Das, and M. Akanksha. 2020. “Early Age, Hydration, Mechanical and Microstructure Properties of Nano-Silica Blended Cementitious Composites.” *Construction and Building Materials* 233:117212. doi: 10.1016/j.conbuildmat.2019.117212.

Soldano, Caterina, Ather Mahmood, and Erik Dujardin. 2010. “Production, Properties and Potential of Graphene.” *Carbon* 48(8):2127–50. doi: 10.1016/j.carbon.2010.01.058.

Stankovich, Sasha, Dmitriy A. Dikin, Richard D. Piner, Kevin A. Kohlhaas, Alfred Kleinhammes, Yuanyuan Jia, Yue Wu, SonBinh T. Nguyen, and Rodney S. Ruoff. 2007. “Synthesis of Graphene-Based Nanosheets via Chemical Reduction of Exfoliated Graphite Oxide.” *Carbon* 45(7):1558–65. doi: 10.1016/j.carbon.2007.02.034.

Stephens, Catherine, Lesa Brown, and Florence Sanchez. 2016. “Quantification of the Re-Agglomeration of Carbon Nanofiber Aqueous Dispersion in Cement Pastes and Effect on the Early Age Flexural Response.” *Carbon* 107:482–500. doi: 10.1016/j.carbon.2016.05.076.

Strano, Michael S., Valerie C. Moore, Michael K. Miller, Mathew J. Allen, Erik H. Haroz, Carter Kittrell, Robert H. Hauge, and R. E. Smalley. 2003. "The Role of Surfactant Adsorption during Ultrasonication in the Dispersion of Single-Walled Carbon Nanotubes." *Journal of Nanoscience and Nanotechnology* 3(1):81–86. doi: 10.1166/jnn.2003.194.

Sun, Ling, and Bunshi Fugetsu. 2013. "Mass Production of Graphene Oxide from Expanded Graphite." *Materials Letters* 109:207–10. doi: 10.1016/j.matlet.2013.07.072.

Tapasztó, Orsolya, Levente Tapasztó, Márton Markó, Frank Kern, Rainer Gadow, and Csaba Balázsi. 2011. "Dispersion Patterns of Graphene and Carbon Nanotubes in Ceramic Matrix Composites." *Chemical Physics Letters* 511(4–6):340–43. doi: 10.1016/j.cplett.2011.06.047.

Tong, Teng, Zhou Fan, Qiong Liu, Sen Wang, Susheng Tan, and Qiang Yu. 2016. "Investigation of the Effects of Graphene and Graphene Oxide Nanoplatelets on the Micro- and Macro-Properties of Cementitious Materials." *Construction and Building Materials* 106:102–14. doi: 10.1016/j.conbuildmat.2015.12.092.

Tung, Vincent C., Matthew J. Allen, Yang Yang, and Richard B. Kaner. 2009. "High-Throughput Solution Processing of Large-Scale Graphene." *Nature Nanotechnology* 4(1):25–29. doi: 10.1038/nnano.2008.329.

Tyson, Bryan M., Rashid K. Abu Al-Rub, Ardavan Yazdanbakhsh, and Zachary Grasley. 2011. "Carbon Nanotubes and Carbon Nanofibers for Enhancing the Mechanical Properties of Nanocomposite Cementitious Materials." *Journal of Materials in Civil Engineering* 23(7):1028–35. doi: 10.1061/(ASCE)MT.1943-5533.0000266.

Walters, D. A., L. M. Ericson, M. J. Casavant, J. Liu, D. T. Colbert, K. A. Smith, and R. E. Smalley. 1999. "Elastic Strain of Freely Suspended Single-Wall Carbon Nanotube Ropes." *Applied Physics Letters* 74(25):3803–5. doi: 10.1063/1.124185.

Wang, Baomin, Ruishuang Jiang, and Zhenlin Wu. 2016. “Investigation of the Mechanical Properties and Microstructure of Graphene Nanoplatelet-Cement Composite.” *Nanomaterials* 6(11):200. doi: 10.3390/nano6110200.

Wang, Guoxiu, Bei Wang, Jinsoo Park, Ying Wang, Bing Sun, and Jane Yao. 2009. “Highly Efficient and Large-Scale Synthesis of Graphene by Electrolytic Exfoliation.” *Carbon* 47(14):3242–46. doi: 10.1016/j.carbon.2009.07.040.

Wang, Howard. 2009. “Dispersing Carbon Nanotubes Using Surfactants.” *Current Opinion in Colloid & Interface Science* 14(5):364–71. doi: 10.1016/j.cocis.2009.06.004.

Wang, Liguo, Shupeng Zhang, Dapeng Zheng, Haibin Yang, Hongzhi Cui, Waiching Tang, and Dongxu Li. 2017. “Effect of Graphene Oxide (GO) on the Morphology and Microstructure of Cement Hydration Products.” *Nanomaterials* 7(12):429. doi: 10.3390/nano7120429.

Wang, Min, Rumin Wang, Hao Yao, Shameel Farhan, Shuirong Zheng, and Congcong Du. 2016. “Study on the Three Dimensional Mechanism of Graphene Oxide Nanosheets Modified Cement.” *Construction and Building Materials* 126:730–39. doi: 10.1016/j.conbuildmat.2016.09.092.

Wang, Min, Hao Yao, Rumin Wang, and Shuirong Zheng. 2017. “Chemically Functionalized Graphene Oxide as the Additive for Cement–Matrix Composite with Enhanced Fluidity and Toughness.” *Construction and Building Materials* 150:150–56. doi: 10.1016/j.conbuildmat.2017.05.217.

Wang, Qin, Xinyou Cui, Jian Wang, Shiyu Li, Chunxiang Lv, and Yichen Dong. 2017. “Effect of Fly Ash on Rheological Properties of Graphene Oxide Cement Paste.” *Construction and Building Materials* 138:35–44. doi: 10.1016/j.conbuildmat.2017.01.126.

Wang, Qin, Jian Wang, Chun-xiang Lu, Bo-wei Liu, Kun Zhang, and Chong-zhi Li. 2015. “Influence of Graphene Oxide Additions on the Microstructure and

Mechanical Strength of Cement." *New Carbon Materials* 30(4):349–56. doi: 10.1016/S1872-5805(15)60194-9.

Wang, Qin, Jian Wang, Chun-xiang Lv, Xi-you Cui, Shi-yu Li, and Xi Wang. 2016. "Rheological Behavior of Fresh Cement Pastes with a Graphene Oxide Additive." *New Carbon Materials* 31(6):574–84. doi: 10.1016/S1872-5805(16)60033-1.

Wei, Jing, Yan Liang, Yaoxin Hu, Biao Kong, Jin Zhang, Qinfen Gu, Yuping Tong, Xianbiao Wang, San Ping Jiang, and Huanting Wang. 2016. "Hydrothermal Synthesis of Metal–Polyphenol Coordination Crystals and Their Derived Metal/N-doped Carbon Composites for Oxygen Electrocatalysis." *Angewandte Chemie* 128(40):12658–62. doi: 10.1002/ange.201606327.

Wichmann, Malte H. G., Karl Schulte, and H. Daniel Wagner. 2008. "On Nanocomposite Toughness." *Composites Science and Technology* 68(1):329–31. doi: 10.1016/j.compscitech.2007.06.027.

Yang, Haibin, Hongzhi Cui, Waiching Tang, Zongjin Li, Ningxu Han, and Feng Xing. 2017. "A Critical Review on Research Progress of Graphene/Cement Based Composites." *Composites Part A: Applied Science and Manufacturing* 102:273–96. doi: 10.1016/j.compositesa.2017.07.019.

Yang, Haibin, Manuel Monasterio, Hongzhi Cui, and Ningxu Han. 2017. "Experimental Study of the Effects of Graphene Oxide on Microstructure and Properties of Cement Paste Composite." *Composites Part A: Applied Science and Manufacturing* 102:263–72. doi: 10.1016/j.compositesa.2017.07.022.

Yang, Xiaowei, Junwu Zhu, Ling Qiu, and Dan Li. 2011. "Bioinspired Effective Prevention of Restacking in Multilayered Graphene Films: Towards the Next Generation of High-Performance Supercapacitors." *Advanced Materials* 23(25):2833–38. doi: 10.1002/adma.201100261.

Zhang, Long, Xuan Li, Yi Huang, Yanfeng Ma, Xiangjian Wan, and Yongsheng Chen. 2010. "Controlled Synthesis of Few-Layered Graphene Sheets on a Large Scale

Using Chemical Exfoliation." *Carbon* 48(8):2367–71. doi: 10.1016/j.carbon.2010.02.035.

Zhao, Li, Xinli Guo, Chuang Ge, Qi Li, Liping Guo, Xin Shu, and Jiaping Liu. 2016. "Investigation of the Effectiveness of PC@GO on the Reinforcement for Cement Composites." *Construction and Building Materials* 113:470–78. doi: 10.1016/j.conbuildmat.2016.03.090.

Zhao, Li, Xinli Guo, Chuang Ge, Qi Li, Liping Guo, Xin Shu, and Jiaping Liu. 2017. "Mechanical Behavior and Toughening Mechanism of Polycarboxylate Superplasticizer Modified Graphene Oxide Reinforced Cement Composites." *Composites Part B: Engineering* 113:308–16. doi: 10.1016/j.compositesb.2017.01.056.

Zhao, Xiao-Ling, and Lei Zhang. 2007. "State-of-the-Art Review on FRP Strengthened Steel Structures." *Engineering Structures* 29(8):1808–23. doi: 10.1016/j.engstruct.2006.10.006.

Zheng, Qiaofeng, Baoguo Han, Xia Cui, Xun Yu, and Jinping Ou. 2017. "Graphene-Engineered Cementitious Composites." *Nanomaterials and Nanotechnology* 7:184798041774230. doi: 10.1177/1847980417742304.

Zhou, Cheng, Fangxian Li, Jie Hu, Mengmeng Ren, Jiangxiong Wei, and Qijun Yu. 2017. "Enhanced Mechanical Properties of Cement Paste by Hybrid Graphene Oxide/Carbon Nanotubes." *Construction and Building Materials* 134:336–45. doi: 10.1016/j.conbuildmat.2016.12.147.

Zou, Dujian, Tiejun Liu, and Jun Teng. 2009. "Improving the Damping Ability by the Addition of Nano SiO 2 to the Concrete Materials." P. 74933C in, edited by J. Leng, A. K. Asundi, and W. Ecke.

PUBLICATIONS RELATED TO THE WORK

Journals

1. P.V.R.K. Reddy, D.R. Prasad, (2023). The role of graphene oxide in the strength and vibration characteristics of standard and high-grade cement concrete. ***Journal of Building Engineering, Elsevier***, 63(A), 105481. https://doi.org/10.1016/j.jobe.2022.105481 (**SCIE, IF:7.14**)

2. P.V.R.K. Reddy, D.R. Prasad, (2022). Graphene oxide reinforced cement concrete – a study on mechanical, durability and microstructure characteristics. ***Fullerenes, Nanotubes and Carbon Nanostructures, Taylor and Francis,*** *31(3), 255-265*. https://doi.org/10.1080/1536383X.2022.2141231 (**SCIE, IF:2.06**)

3. P.V.R.K. Reddy, D.R. Prasad, (2022). Synergetic effect of graphene oxide and fly ash on workability, mechanical and microstructural properties of high strength concrete. ***Jordan journal of civil engineering, JUST***, 16(3), 507-517. (**ESCI**)

4. P.V.R.K. Reddy, D.R. Prasad, (2022). A study on workability, strength and microstructure characteristics of graphene oxide and fly ash based concrete. ***Materials Today: Proceedings, Elsevier***, 62(6), 2919-2925. https://doi.org/10.1016/j.matpr.2022.02.495 (**SCOPUS**)

5. P.V.R.K. Reddy, D.R. Prasad, (2022). Investigation on the impact of graphene oxide on microstructure and mechanical behaviour of concrete. ***Journal of Building Pathology and Rehabilitation, Springer***, 7(1), 1-10. https://doi.org/10.1007/s41024-022-00166-1 (**SCOPUS**)

Book Chapters

1. P.V.R.K. Reddy, D.R. Prasad, (2023). Static and dynamic mechanical properties of graphene oxide and fly ash based concrete. In: Singh, S.B., Gopalarathnam, M., Kodur, V.K.R. and Matsagar, V.A. (eds) Fiber Reinforced Polymeric Materials and Sustainable Structures. ***Composites Science and Technology, Springer***. https://doi.org/10.1007/978-981-19-8979-7_34

Conferences

1. P.V.R.K. Reddy, D.R. Prasad, (2023). Experimental and Numerical Investigation on Stress-Strain Relationship of Graphene Oxide and Fly ash-based Concrete under Axial Compression. International Conference on Cement and Building Koncrete for a sustainable and Resilient infrastructure (CBKR 2023), March 28–29. ***NIT Warangal,*** India.

2. P.V.R.K. Reddy, D.R. Prasad, (2022). Influence of graphene oxide on static and dynamic characteristics of fly ash based high strength concrete. International Conference on Recent Developments in Civil Engineering (RDC-2022), October 20–21. ***MNNIT Allahabad***, India.

3. P.V.R.K. Reddy, D.R. Prasad, (2022). A study on workability, strength and microstructure characteristics of graphene oxide and fly ash based concrete. 13th International Conference on Materials, Processing & Characterization - (ICMPC 2022), April 22nd – 24th. ***GRIET, Hyderabad***, India.

4. P.V.R.K. Reddy, D.R. Prasad, (2022). Static and dynamic mechanical properties of graphene oxide and fly ash based concrete. US2020 partnership workshop on FRP Materials and sustainable structures, March 4th. ***BITS Pilani, Pilani***, India.